UNIVERSIDADE ESTADUAL DE CAMPINAS

INSTITUTO DE QUÍMICA

GUILHERME AUGUSTO FERREIRA

BLOCK COPOLYMER-SURFACTANT COMPLEX SALTS: FROM DILUTE PARTICLE DISPERSIONS TO CONCENTRATED PHASES AND APPLICATIONS

SAIS COMPLEXOS DE COPOLÍMEROS EM BLOCO E SURFACTANTES: DE DISPERSÕES DE PARTÍCULAS A FASES CONCENTRADAS E APLICAÇÕES

CAMPINAS
2018

GUILHERME AUGUSTO FERREIRA

BLOCK COPOLYMER-SURFACTANT COMPLEX SALTS: FROM DILUTE PARTICLE DISPERSIONS TO CONCENTRATED PHASES AND APPLICATIONS

SAIS COMPLEXOS DE COPOLÍMEROS EM BLOCO E SURFACTANTES: DE DISPERSÕES DE PARTÍCULAS A FASES CONCENTRADAS E APLICAÇÕES

Tese de Doutorado apresentada ao Instituto de Química da Universidade Estadual de Campinas como parte dos requisitos exigidos para a obtenção do título de Doutor em Ciências

Doctor´s Thesis presented to the Institute of Chemistry of the University of Campinas as part of the requirements to obtain the title of Doctor in Sciences.

Supervisor: Prof. Dr. Watson Loh

O arquivo digital corresponde à versão final da Tese defendida pelo aluno Guilherme Augusto Ferreira e orientada pelo Prof. Dr. Watson Loh.

CAMPINAS
2018

Informações para Biblioteca Digital

Título em outro idioma: Sais complexos de copolímeros em bloco e surfactantes : de dispersões de partículas a fases concentradas e aplicações
Palavras-chave em inglês:
Surfactants
Block copolymers
Electrostatic interaction
Colloidal nanoparticles
Structural characterization
Área de concentração: Físico-Química
Titulação: Doutor em Ciências
Banca examinadora:
Watson Loh [Orientador]
Nadya Pesce da Silveira
Rosângela Itri
Rene Alfonso Nome Silva
Daniela Zanchet
Data de defesa: 11-12-2018
Programa de Pós-Graduação: Química

BANCA EXAMINADORA

Prof. Dr. Watson Loh (Orientador)

Profa. Dra. Nadya Pesce da Silveira (Universidade Federal do Rio Grande do Sul)

Profa. Dra. Rosângela Itri (Instituo de Fisica-USP)

Prof. Dr. Rene Alfonso Nome Silva (IQ-UNICAMP)

Profa. Dra. Daniela Zanchet (IQ-UNICAMP)

A Ata da defesa assinada pelos membros da Comissão Examinadora, consta no SIGA/Sistema de Fluxo de Dissertação/Tese e na Secretaria do Programa da Unidade.

Este exemplar corresponde à redação final da Tese de Doutorado defendida pelo(a) aluno(a) **GUILHERME AUGUSTO FERREIRA,** aprovada pela Comissão Julgadora em 11 de dezembro de 2018.

Dedication

I dedicate this thesis to my mother, Vilma, whose examples and dedication guided my life and will guide forever.

This work is also dedicated to the memory of my aunt Benedita Beatriz and my uncle Joaquim.

Dedico esta tese à minha mãe, Vilma, cujos exemplos e dedicação guiaram minha vida e guiarão para sempre.

Esse trabalho também é dedicado à memória da minha tia Benedita Beatriz e do meu tio Joaquim.

"Life need not be easy, provided only that it is not empty"

<div align="right">

Lise Meitner (1878-1968)

Austrian-Swedish Physicist.

</div>

"And if I ever lose my way
And if I ever go astray
Show me direction, direction
Take me to the darkest hour
Show to me the strength and power
Give me the key"

<div align="right">

Dolores O'Riordan of The Cranberries (1971-2018)

Irish Singer and Songwriter.

</div>

Acknowledgements

Resumo

"Sais complexos" de copolímeros em bloco e surfactantes ($BCPCS$), contendo um bloco neutro e hidrossolúvel e um bloco iônico complexado com íons surfactante, foram preparados a partir de copolímeros em bloco de poli(acrilamida)-*bloco*-poli(ácido acrílico), onde o bloco acrilato foi neutralizado por contra-íons surfactantes de dodecil ou hexadeciltrimetilamônio através de interações eletrostáticas. A combinação de Espalhamento de Luz Dinâmico (DLS) e Estático (SLS), Espalhamento de Raios-X em Baixos Ângulos (SAXS), Potencial Zeta, Microscopia Eletrônica de Transmissão Criogênica (Cryo-TEM), Calorimetria Diferencial de Varredura (DSC) e Ressonância Magnética Nuclear com Campo de Gradiente Pulsado (PFG NMR) foi empregada para estudar os $BCPCS$ em solução aquosa em uma ampla faixa de concentração.

A dispersão dos $BCPCS$ em solução originou partículas com uma coroa estabilizadora de bloco neutro e hidrossolúvel do copolímero rodeando um núcleo hidratado consistindo nas unidades de carga oposta complexadas. Utilizando os $BCPCS$, partículas com um núcleo líquido-cristalino são obtidas de maneira reprodutível e comportam-se de maneira diferente daquelas obtidas convencionalmente misturando-se soluções aquosas individuais do copolímero em bloco e do surfactante com seus respectivos contra-íons simples. Em ambos os casos, as partículas são estruturas metaestáveis, com propriedades físico-químicas, como tamanho e presença ou ausência de estrutura interna, fortemente dependentes do procedimento de preparo.

Medidas de PFG NMR revelaram que as partículas dispersas de $BCPCS$ coexistem com pequenos agregados e uma baixa quantidade de íons surfactantes dissociados. Tanto o núcleo das partículas quanto a coroa foram investigados sob diferentes abordagens. A adição de quantidades adequadas de álcoois de cadeia longa às partículas dispersas de $BCPCS$ levou à variação do seu arranjo interno, produzindo uma variedade de estruturas líquido-cristalinas adicionais. Nanopartículas de metal (prata e ouro) foram seletivamente ligadas à superfície de partículas de $BCPCS$, formando nanoestruturas do tipo planeta-satélite com potenciais aplicações em catálise interfacial.

Os sais complexos foram também estudados em amostras com diferentes concentrações contendo 20-99% em massa de água. Os resultados de SAXS revelaram pela primeira vez, para amostras hidratadas, a formação de estruturas hierárquicas ordenadas em ambas as escalas de tamanho do copolímero em bloco e do surfactante, análogas às

estruturas que foram previamente reportadas para complexos de copolímero em bloco-surfactante no estado sólido ou fundidos.

Abstract

Block copolymer-surfactant "complex salts" ($BCPCS$), containing one neutral water soluble block and one polyion/surfactant-ion block, were prepared from poly(acrylamide)-*block*-poly(acrylic acid) block copolymers by neutralizing the acrylate charges with cationic dodecyl- or hexadecyltrimethylammonium surfactant counterions through electrostatic interactions. A combination of Dynamic (DLS) and Static (SLS) Light Scattering, Small Angle X-ray Scattering (SAXS), Zeta Potential, Cryogenic Transmission Electron Microscopy (Cryo-TEM), Differential Scanning Calorimetry (DSC) and Pulse-Field Gradient Nuclear Magnetic Resonance (PFG NMR) were employed to study hydrated $BCPCS$ in a wide range of concentration.

The dispersion of $BCPCS$ originated particles with a stabilizing corona of neutral water-soluble blocks of the copolymer surrounding a hydrated core consisting of complexed oppositely charged units. By using $BCPCS$, particles with a liquid crystalline core are reproducible obtained and behave different from those conventionally by mixing individual aqueous solutions of the block copolymer and surfactant with their respective simple counterions. In both cases, the particles are metastable structures, with physicochemical properties, like size and presence or absence of core structure, strongly dependent on the preparation procedure.

Additionally, PFG NMR studies revealed that $BCPCS$ dispersed particles coexist with small aggregates and a small amount of dissociated surfactant ions. Both particle core and corona were investigated under different approaches. The addition of suitable amounts of long-chain alcohols to the $BCPCS$ dispersed particles led to the variation of their core arrangement, producing a variety of additional liquid crystalline structures. Metal (silver and gold) nanoparticles were selectively attached to the surface of $BCPCS$ particles, forming planet-satellite nanostructures with potential applications in interfacial catalysis.

The $BCPCS$ were also studied in samples at different concentrations containing 20-99 wt% water. The SAXS results revealed for the first time, for hydrated samples, the formation of ordered hierarchical structures on both block copolymer and surfactant length scales, analogous to structures that have previously been reported for solvent-free block copolymer-surfactant complexes in the solid or melt state.

List of Figures

Abbreviations

BCP	Block Copolymer
$BCPCS$	Block Copolymer Complex Salt
cmc	Critical Micellar Concentration
CPP	Critical Packing Parameter
Cryo-TEM	Cryogenic Transmission Electron Microscopy
CP	Conventionally Prepared
CS	Complex Salt
$C_{12}TABr$	Dodecyltrimethylammonium Bromide
$C_{16}TABr$	Hexadecyltrimethylammonium Bromide
$C3Ms$	Complex Coacervate Core Micelles
DLS	Dynamic Light Scattering
DNA	Deoxyribonucleic Acid
DSC	Differential Scanning Calorimetry
L_α	Lamellar Fluid Phase
L_β	Lamellar Gel Phase
PAA	Poly(Acrylic Acid)
$PAAm - b - PAA$	Poly(Acrylamide)-*block*-Poly(Acrylic Acid)
PEC	Polyelectrolyte Complex
PIC	Polyion Complex Micelles
PFG NMR	Pulse-Field Gradient Nuclear Magnetic Resonance
R	Long-chain alcohol/CS mass ratio
RNA	Ribonucleic Acid
SAXS	Small Angle X-ray Scattering
SLS	Static Light Scattering

Summary

Introduction

Complex formation through electrostatic interaction between oppositely charged (macro)species is a process that takes place everywhere, under different conditions. In our body, proteins are attracted to peptides,[1] RNA[2], and other proteins[3] of different charge, forming complexes that play an important role in many vital functions (Figure 1A). In health science, DNA-lipid complexes, the lipoplexes, have shown a great potential in gene therapy (Figure 1B).[4]

In food formulation, the complexation of proteins and polysaccharides of opposite charges originates good emulsion stabilizers and carrier agents that deliver flavor and aroma (Figure 1C).[5,6] In material science, electrostatic complexation between oppositely charged polymers are used to create chemically and thermally stable fibers (Figure 1D).[7] In nature, underwater adhesives used by marine animals are based on oppositely charged polyelectrolytic components, like poly(phosphates), poly(sulfates), and poly(amines) (Figure 1E).[8]
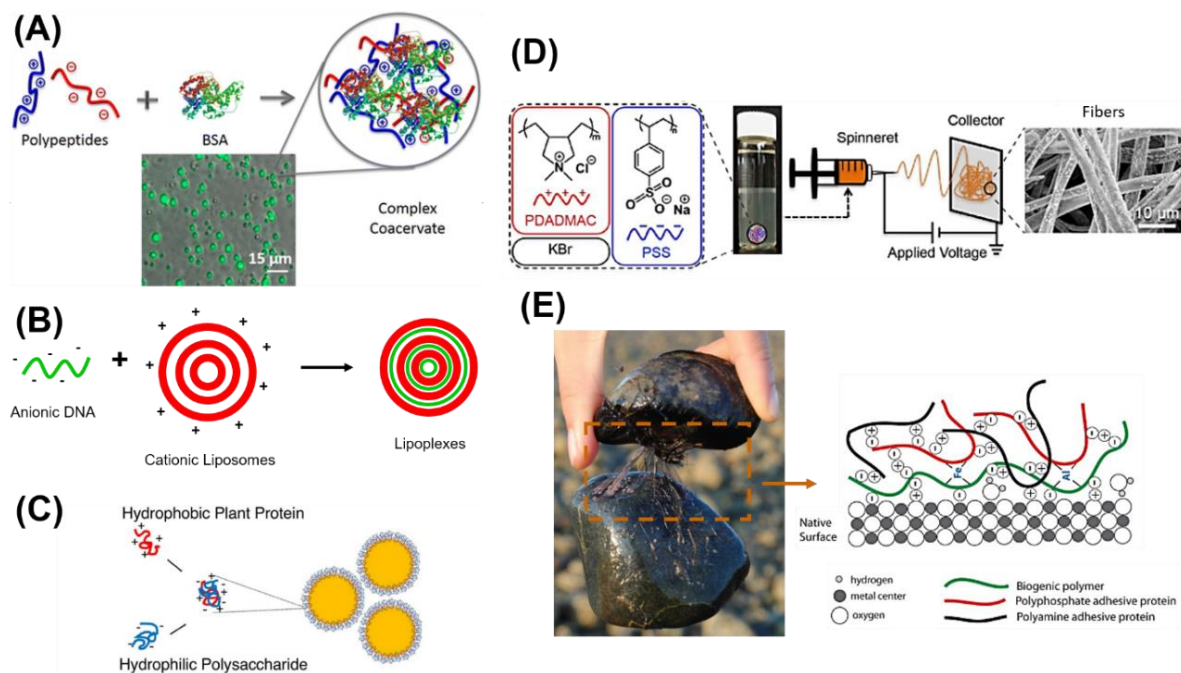
Figure 1. Electrostatic driven complex formation between oppositely charged (macro)species. **(A)**. Polypeptides complex formation with proteins and optical micrograph showing the fluorescence of encapsulated protein. **(B)**. Multilamellar lipoplexes formed by liposome-DNA complexation. **(C)**. Scheme of oil droplets of an emulsion stabilized by protein-polysaccharide complex. **(D)**. Scanning electron microscopy image of electrospun fibers from complex formation between poly(4-styrenesulfonic acid), PSS, and poly(diallyldimethylammonium chloride), $PDADMAC$, in aqueous solution containing potassium bromide (KBr). **(E)**. Mechanism of mussel adhesion onto rocks through underwater adhesive formation based on electrostatic complexation between biopolymers. Adapted from references 1, 4, 5, 7, and 8, respectively.

In this thesis, the electrostatic complexation between oppositely charged polyelectrolytes and surfactants is investigated. By a selective complexation of cationic surfactant ions to an anionic block of neutral-charged block copolymers, complexes, free of counterions, were prepared and studied from dilute particle dispersions to macroscopically homogeneous concentrated phases. Structural, colloidal and kinetic and thermodynamic features of these complexes were studied based on a variety of experimental techniques and comparison with similar systems in the literature.

The current thesis is basically divided in three chapters. The first chapter brings important information about surfactants, polyelectrolytes and their complexation in aqueous solution. Additionally, a conceptual background about the main experimental techniques used in this work is also given in chapter 1.

In chapter 2, a summary of the results is present, divided in different publications or manuscripts. In ***Paper I***, a review about the occurrence of liquid crystalline structures in complex dispersed particles is presented. ***Papers II*** is a systematic study about the effect of added long chain-alcohols to the aqueous phase behavior of block copolymer-surfactant dispersed complex particles. In ***Paper III***, it is shown how the preparation procedure impacts on the physicochemical properties of block copolymer-surfactant dispersed particles. ***Paper IV*** discuss information on dissociated species coexisting with the particle in the dispersions.

Paper V brings a potential application in interfacial catalysis for the block copolymer-surfactant particles surface-decorated with gold and silver nanoparticles. Finally, in **Paper VI**, structures at both surfactant and block copolymer length scales are investigated in concentrated hydrated samples. The conclusions and references are then displayed in chapter 3, followed by the papers and manuscripts in full version appended at the end of the thesis.

Chapter 1: Fundamentals

1. Surfactants

Surfactants are amphiphilic molecules, which means that they are formed by two distinct portions, one solvophilic and one solvophobic part. In water, these two parts are called hydrophilic and hydrophobic, respectively. Usually, the former is refereed as the headgroup of the surfactant and the later as the tail, as represented in Figure 2. The hydrophobic part is often an aliphatic hydrocarbon chain, while the hydrophilic part can be a nonionic or an ionic group, such as in the two cationic surfactants investigated in this work: *dodecyl-* and *hexadecyltrimethylammonium bromide* ($C_{12}TABr$ and $C_{16}TABr$), whose structures are displayed in Figure 2.[9,10]
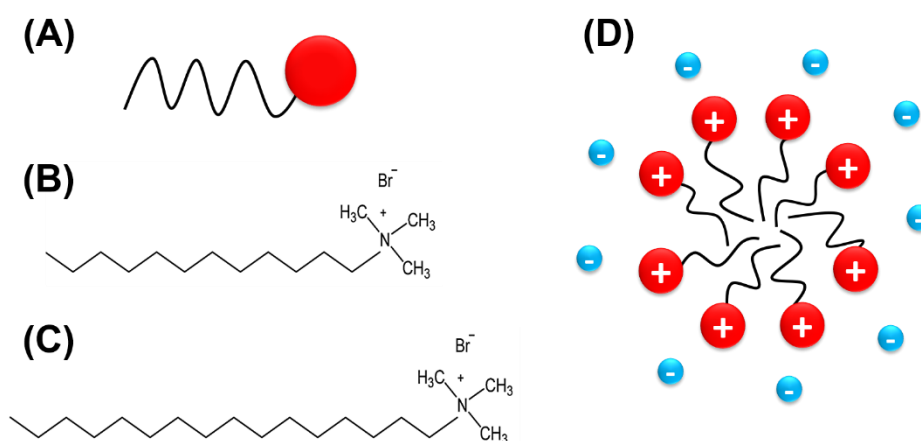
Figure 2. **(A)** Schematic view of a surfactant molecule, with the hydrophilic part represented in red and the hydrophobic part in black. Chemical structures of **(B)** dodecyl- and **(C)** hexadecyltrimethylammonium bromide cationic surfactants. **(D)** Schematic representation of a cationic surfactant micelle, where the hydrophilic headgroups face towards the aqueous solution and the hydrophobic tails are hidden from the solvent.

1.1. Surfactants in dilute aqueous solutions

When dissolved in water, the hydrophobic portion of the surfactant experiences unfavorable interactions with the solvent. In order to minimize such disadvantageous interactions, the surfactant molecules self-assemble into aggregates in which the hydrophobic part is hidden from the aqueous surrounding medium. The simplest aggregates formed by surfactant self-assembly in water are called micelles, displayed in Figure 2D. The formation of these aggregates takes place at a specific concentration, called critical micellar concentration (cmc). The surfactant self-assembly into micelles is a highly cooperative process and is governed by the hydrophobic effect, that is, it is entropically driven.[9,10]

Some surfactants self-assemble into spherical micelles, while others may form different types of aggregates, depending on their chemical structure and the way they pack during the association, which influence the curvature of the aggregate. One convenient way of predicting the aggregate shape is looking at the critical packing parameter, CPP, defined as:

$$CPP = v/la_o \qquad (1)$$

where v is the volume of the hydrophobic portion, l the length of the hydrocarbon tail and a_o the effective area per headgroup.[11] The volume v (in nm^3) and the length l (in nm), for a fully stretched hydrocarbon tail, can be calculated according to:

$$v = 0.0274 + 0.0269n \qquad (2)$$

$$l = 0.154 + 0.127n \qquad (3)$$

where n is the number of carbon atoms in the hydrocarbon tail.[12] Typical CPP values for aggregates with different shapes are displayed in Figure 3.
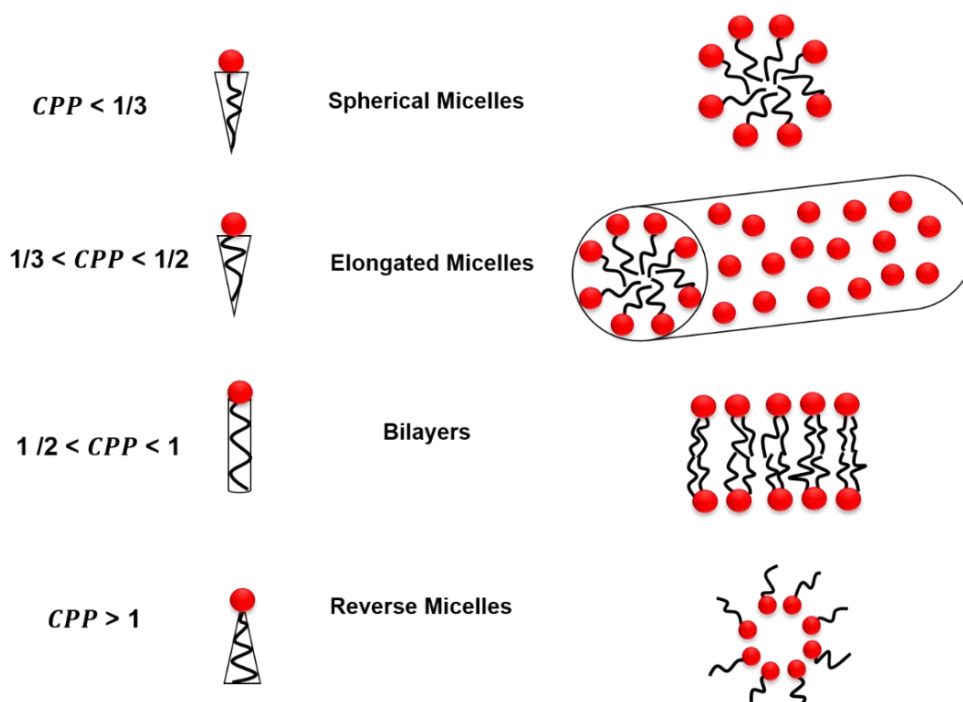
Figure 3. Values for critical packing parameter (CPP) and their respective molecular geometry and aggregate shape. Adapted from refs. 11 and 12.

Another way used to describe the shape of surfactant aggregates is based on the concept of curvature. Usually, a positive curvature is ascribed for spherical micelles, while bilayers have curvature close to zero and reverse structures, a negative curvature.[10]

1.2 Surfactants in concentrated aqueous solutions

As the surfactant concentration in water is increased, they form lyotropic liquid crystalline phases. The term liquid crystalline denotes the nature of such phases. They display a long-range order in one, two or three dimensions, due to the packing of the surfactant aggregates, like a crystal, but are disordered on the molecular length scale, like a liquid.[9,10] The type of liquid crystalline phase that is formed depends on the CPP of the surfactant and on its concentration. A commonly encountered sequence of liquid crystalline phases appears in a typical order where the decrease in the surfactant aggregate curvature is observed as the surfactant concentration is increased (or water concentration is decreased)[13], as illustrated in Figure 4.

Surfactant Concentration

Micellar Cubic Phase   **Hexagonal Phase**   **Lamellar Phase**
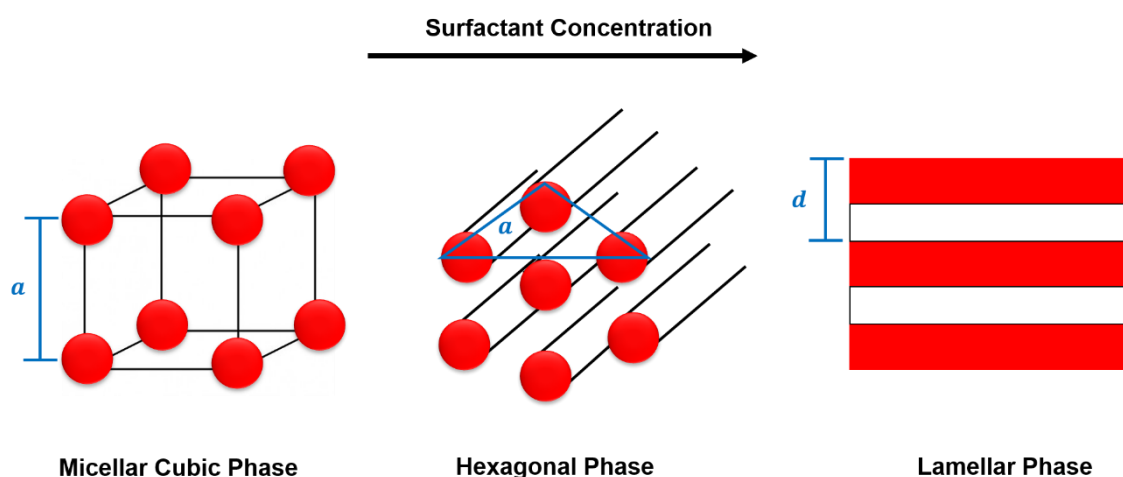
Figure 4. Liquid crystalline phases sequence as a function of surfactant concentration in aqueous solution. The cell parameter of each phase is also shown. Adapted from ref. 10.

The addition of a *cosurfactant* to a surfactant solution also influences its phase behavior. Due to its amphiphilic character, the cosurfactant situates at the interface of the aggregate in water, changing the effective area per headgroup and then favoring the formation of additional phases beyond those usually formed at a specific surfactant concentration. Examples of cosurfactants are middle- and *long-chain alcohols*.[9]

Phases with order in one or two dimensions are optically anisotropic and display birefringence under polarized light, since they can rotate the light. Three-dimensional phases are isotropic instead.[14] The liquid crystalline phases studied in this work are the micellar cubic, hexagonal, lamellar and the hexagonal and micellar reverse phases.

Micellar Cubic Phase

The micellar cubic phase is a three-dimensional structure formed at sufficiently high concentrations of spherical micelles that pack together in a cubic unit cell. It belongs to the *Pm3n* space group and its cell parameter a is defined as the mean distance between the center of two neighbor micelles arranged in the cubic cell (Figure 4).[9,10,13,14]

Hexagonal Phase

The hexagonal phase has a *p6mm* space group and is formed by elongated micelles arranged in a hexagonal pattern in such a way that each micelle is surrounded by other 6, forming a two-dimensional structure. Its characteristic cell parameter a is displayed in Figure 4.[9,10,13,14]

Lamellar Phase

The lamellar phase is formed by surfactant bilayers alternated with water layers, in which the surfactant headgroups face the aqueous domain, forming a one-dimensional structure. The cell parameter d is the distance between the lamellar mid-planes and is also represented in Figure 4. The lamellar phase can be subdivided in two different phases depending on the arrangements of the alkyl chains of the surfactant: L_α, where the chains are in a fluid state, and L_β, where they are in a gel-like state. [9,10,13,14]

Reverse Phases

The micellar and hexagonal reverse phases investigated in this work are similar to the normal aggregates described before but present a negative curvature and usually are formed at very low water contents. It is also favored at low surfactant concentrations by the addition of oils, such as hydrocarbons and long-chain alcohols. [9,10,13,14]

2. Polyelectrolytes

Polyelectrolytes are polymers in which the monomers are either negatively or positively charged in solution, at certain conditions. Due to the entropy gain of releasing the counterions into the solution, polyelectrolytes are usually more soluble in water than neutral polymers with similar molecular weights. Moreover, in aqueous solution, the polyelectrolyte is surrounded by its counterions because of the electrostatic attraction between them.[10,15,16]

A variety of polyelectrolytes possess charge that can be tuned by changes in the solution pH. This is the case of weak polyelectrolytes, like *poly(acrylic acid)*, *PAA* (Figure 5A). At low pH (below the pKa of the acid group) the polymer chains are protonated and adopt a coil conformation. As the pH is increased, the acid groups are deprotonated and at pH higher than pKa, they are fully deprotonated, and the polymer assumes an extended conformation.[10] Polyelectrolytes that are fully deprotonated in solution will be refereed here as a *polyion* (Figure 5B).
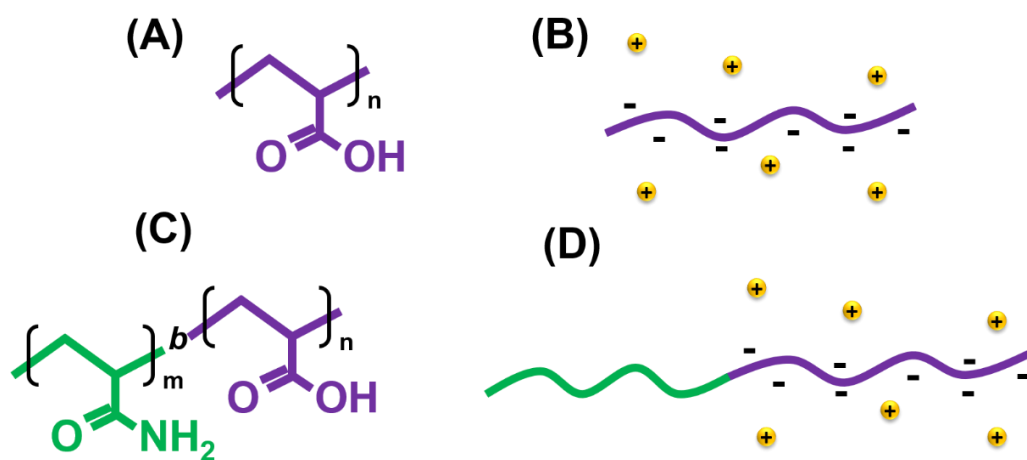
Figure 5. **(A)** Chemical structure of poly(acrylic acid). **(B)** Schematic representation of this polyelectrolyte in solution (polyion and its counterions). **(C)**. Chemical structure of poly(acrylic acid)-*block*-poly(acrylamide) copolymer. **(D)** Schematic representation of this neutral-charged block copolymer in solution.

In the present work, the polyelectrolyte is connected through a covalent bond to another polymer, forming a *block copolymer*, here abbreviated as BCP (Figure 4C). In this case, the other polymer consists in a neutral and water-soluble block, like *poly(acrylamide)*, $PAAm$, giving rise to poly(acrylamide)-*block*-poly(acrylic acid) $(PAAm - b - PAA)$. The resulting specie can be then classified as a *neutral-charged BCP* (Figure 5D).

Polyions display strong electrostatic attraction with oppositely charged species in solution, such as ionic surfactants and other polyions, leading to the formation of a variety of aggregates.[17-21] The different types of aggregates formed by electrostatic complexation between polyion and polyion or polyion and ionic surfactant have been widely studied in the last years and will be shortly explored in the next section, where a special focus on the polyion-surfactant ion complexes will be given.

3. Polyion-Surfactant Ion Complexes

A general picture of the polyion-surfactant ion interaction and the resulting aggregates is given in *Paper I*. Basically, the electrostatic interaction between polyions and oppositely charged surfactant ions, in solution, leads to an associative phase separation, most pronounced at the charge equivalence, and it is mainly driven by the entropic gain due to release of the small counterions and water molecules from the interacting species.[9,17-19]

The aggregates formed by the electrostatic complexation form a concentrated phase, while the counterions will be randomly distributed in solution, forming a dilute phase (Figure 6). It has been shown that the concentrated phase often displays liquid crystalline phases formed by the surfactant[20] and at sufficiently high salt concentrations, the charges are screened, and the complexes disassembled.[22,23]
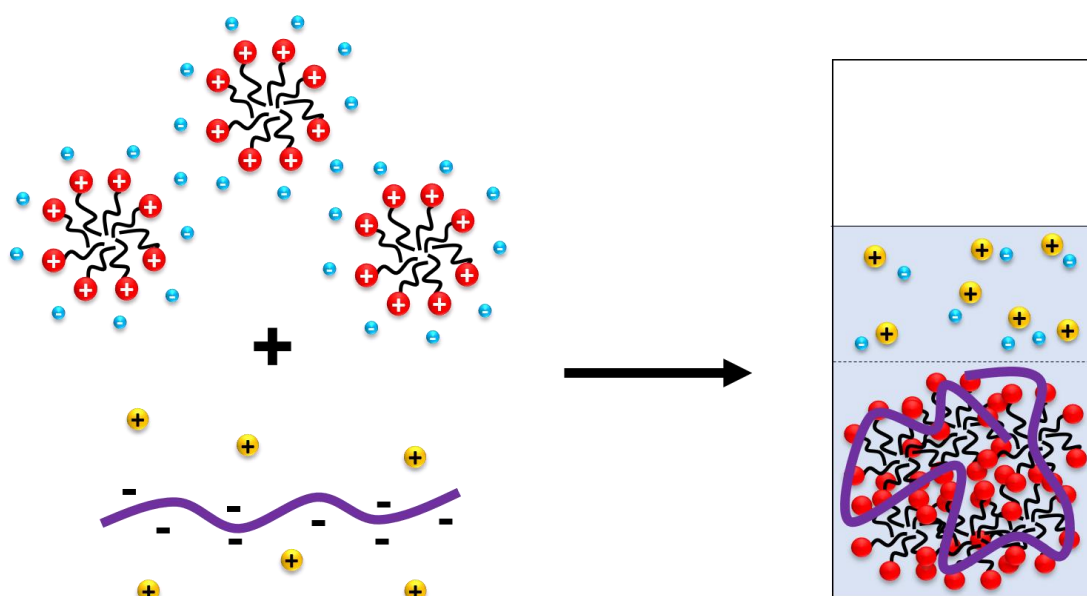
Figure 6. Representation of an associative phase separation by mixing ionic surfactant with oppositely charged polyelectrolyte in solution at charge equimolarity. Adapted from ref. 17.

One procedure that can be employed to avoid the phase separation is to use a neutral-charged BCP, instead of a normal (homo)polyelectrolyte. The interaction of neutral-charged BCP with oppositely charged surfactant ions at charge equivalence leads to the formation of water-dispersible compacted particles. The core of a dispersed particle contains several densely packed surfactant micelles interspersed with the anionic blocks of the copolymer, while the neutral hydrophilic blocks are enriched at the particle surface, giving rise to core-shell aggregates (Figure 7).[24-26]

The literature contains several terms for such structures, such as polyion complex micelles, PIC micelles,[27] complex coacervate core micelles, $C3Ms$,[26] and (inter)polyelectrolyte complexes, PEC,[28,29] the last one used when both oppositely charged species are polyelectrolytes. For convenience, we will here use the term $C3Ms$ or simply core-shell particles for the structures, formed in aqueous solutions, featuring a stabilizer shell consisting of neutral water-soluble units surrounding a water-insoluble (but hydrated) core consisting of complexed oppositely charged units.
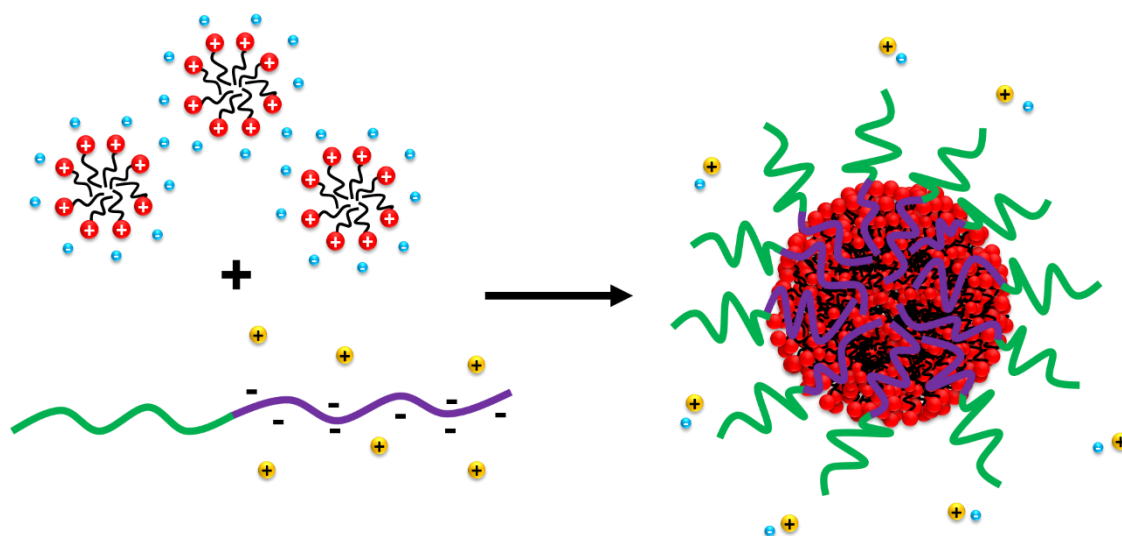
Figure 7. Representation of a core-shell particle formation through ionic surfactant micelles and oppositely charged ionic-neutral block copolymer at charge equimolarity. Adapted from ref. 26.

Regardless of the chemical nature of the components, $C3Ms$, i.e. the core-shell particles, are *conventionally prepared* by mixing individual aqueous solutions of the neutral-charged BCP and the oppositely charged surfactant, with their respective counterions, that is, the particles are formed in the presence of small amounts of simple salt.[26] In this work, we have expanded our studies in $C3Ms$ formed by $PAAm - b - PAA\ BCP$ and *dodecyl-* or *hexadecyltrimethylammonium bromide* surfactants by using a different approach, named *complex salt (CS)*.

3.1 The Complex Salt (CS) Approach

The phase behavior of a mixture composed of, for example, water, $C_{16}TABr$ surfactant and the sodium salt of PAA could be, at a first view, described in a ternary phase diagram, where each of the three components would be in one corner of the diagram.[30]

However, such a representation is insufficient because the system is comprised of water and four ionic species: the polyion, the surfactant ion and their accompanying simple counterions (Na^+ and Br^-), respectively. If a phase separation occurs in the mixture, each of the four ions can partition differently between the separating phases, subject to the condition that each phase must be macroscopically electroneutral. Hence, each phase generally requires four components (water and three of the four possible combinations of the ions into electroneutral salts) for its full description.

Such a system can be represented as a tetragonal pyramid, as illustrated in Figure 8. However, the construction of such three-dimensional diagrams is laborious and may lead to erroneous interpretation due to the presence of different mixing planes. To reduce the complexity of the systems, the group of Lennart Piculell, at Lund University, Sweden, proposed the elimination of one of the components, the $NaBr$ simple salt (formed by the simple counterions from both polyion and surfactant ion), by preparing a polyion-surfactant ion *complex salt (CS)*, at a 1:1 charge ratio between the polyion and surfactant ion. By using a simple acid-base titration between the polyelectrolyte in the acid form, that is with H^+ as the counterion, and the surfactant in the basic form, with OH^- as the counterion, the polyion neutralize the surfactant aggregates and no simple salt is formed.[31-33]

The CS approach made possible the study of truly binary systems formed by the complex and water and true ternary systems with a third component, such as long-chain alcohols.[34,35] Based on this methodology, our group has recently reported studies using $PAAm - b - CS\ BCP$ containing the acrylate block of $PAAm - b - PAA\ BCP$ neutralized by dodecyltrimethylammonium counterions, to produce core–shell particles dispersed in an aqueous medium.[36] In some of the works of this thesis, the $PAAm - b - CS\ BCP$ are also refereed as $BCPCS$, an acronym for *Block Copolymer Complex Salt*.

Notably, the obtained $C3Ms$ particles behave very differently from those *conventionally prepared,* that is prepared by mixing individual aqueous solutions of the neutral-charged BCP and the oppositely charged surfactant, with their respective counterions. This observation inspired us to expand the studies of dispersions containing $BCPCS$ based on $PAAm - b - PAA\ BCP$ and $C_{12}TABr$ and $C_{16}TABr$ surfactants with the aim to achieve additional information regarding the structure, (thermodynamic and kinetic) stability and potential uses for these systems.
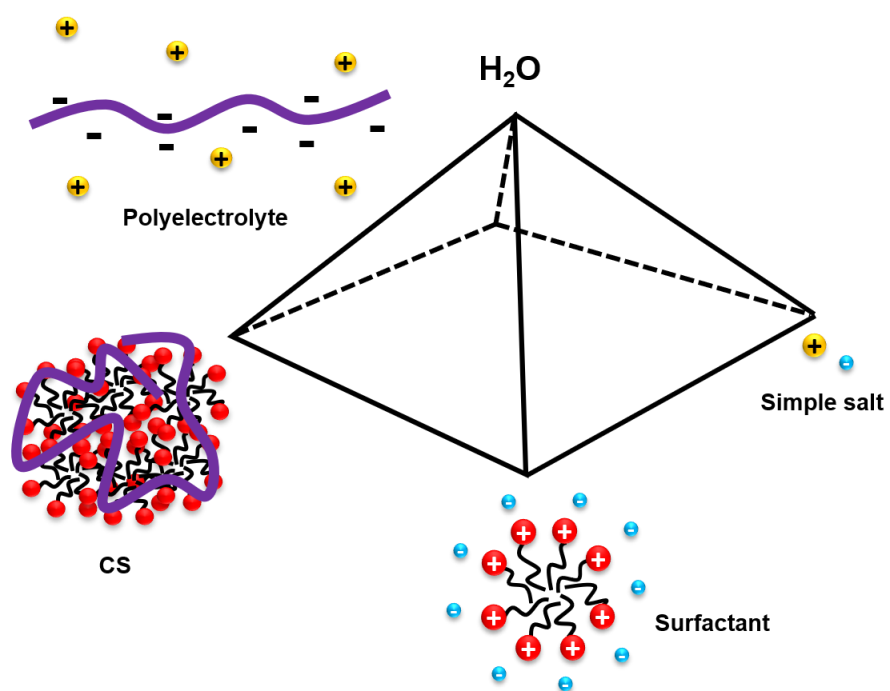
Figure 8. Representation of a three-dimensional phase diagram used to describe the phase behavior of polyelectrolyte and oppositely charged surfactant in aqueous solution. Adapted from ref. 31.

4. Experimental Techniques

4.1. Scattering techniques

Scattering techniques have been widely used to investigate surfactant, polymer and surfactant-polymer systems. These techniques provide useful information about important features of micelles, particles, and complexes, such as the size, shape, organization, interaction and stability in dilute and concentrated samples.

All scattering techniques have, basically, the same principle. The sample is illuminated with an incident beam of radiation (light, X-rays, neutrons) and interacts with it. This radiation is absorbed, transmitted and scattered. The scattered radiation is the most important in this case. In this thesis, a special focus will be given in the techniques based on the elastic scattering, where the frequencies of the incident and scattering radiations are the same and then it is assumed that no energy loss takes place.[37]

In a scattering experiment, a detector measures the intensity of scattered radiation at a specific angle θ, i.e. the angle between the wavevector of the incident beam $\vec{k_i}$ and the scattered beam $\vec{k_s}$. By subtracting $\vec{k_s}$ from $\vec{k_i}$, the scattering vector $\vec{q}$ is then obtained. Its absolute value is calculated as: [37]

$$q = \frac{4\pi\sin(\frac{\theta}{2})}{\lambda} \qquad (4)$$

where λ is the wavelength of the incident beam. Figure 9 shows a schematic representation of a scattering experiment and the origin of the scattering vector $\vec{q}$.
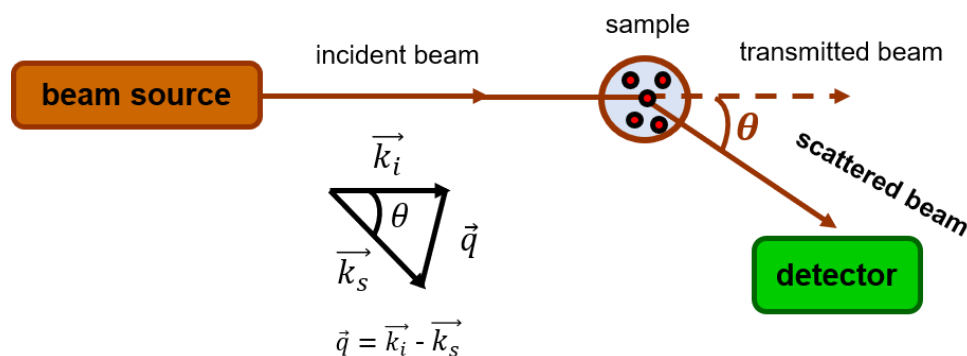
Figure 9. Schematic representation of a scattering experiment. Adapted from ref. 37.

4.1.1 Light Scattering

In light scattering, the radiation source is a laser beam, with $\lambda = 632.8$ nm in this thesis. The electric field of the light interacts with the electron cloud of the particles and induces oscillating dipoles, that scatter the light. To have a good scattering signal, there must be a contrast variation between the particles and the surrounding medium, that is, the solvent. This contrast variation usually comes from differences in the refractive index and electronic density of the sample. The intensity of scattered light is proportional to the contrast variation of the particles and the solvent. Basically, the light scattering is divided in Dynamic and Static Light Scattering.

Dynamic Light Scattering (DLS)

In solution, particles display a constant motion, called Brownian movement, and because of this, their local concentration fluctuates with time, which also promotes a fluctuation of scattered light as a function of time. In DLS, the intensity fluctuation of scattered light is used to obtain a normalized intensity correlation function $g^2(t)$, which is converted to an electric field correlation function $g^1(t)$ according to:[37,38]

$$g^2(t) = 1 + \beta |g^1(t)|^2 \qquad (5)$$

where β is a parameter that considers deviations from ideal correlation of the detector and t is the lag-time. This kind of analysis enables one to know the translation diffusion of the particle, that can be converted to particle size.

For systems comprised of monodisperse particles, $g^1(t)$ can be fitted to a single-exponential functional with a characteristic relaxation time, τ. For polydisperse particles, $g^1(t)$ is expressed in terms of a Laplace transformation of a distribution of relaxation times, $A(\tau)$:

$$g^1(t) = \int_{-\infty}^{+\infty} \tau A(\tau) \exp(-t/\tau) dln\tau \qquad (6)$$

All the correlation functions obtained during the light scattering experiments were analyzed with the help of a Regularized Positive Exponential Sum (REPES)[39], based on equation 6 and because it was obtained a monomodal distribution of particle sizes, a cumulant analysis was employed, where the $g^1(t)$ function is described as:[40]

$$\ln|g^1(t)| = -\Gamma\tau + \frac{1}{2!}\mu_2(\Gamma t)^2 - \cdots \qquad (7)$$

where Γ is the relaxation rate ($\Gamma = \tau^{-1}$) and μ_2 is the second cumulant.

The collective translational diffusion coefficient D of a particle is then defined as:

$$D = \frac{\Gamma}{q^2} \qquad (8)$$

D_o is the particle diffusion coefficient at infinite dilution and can be obtained by studying the concentration dependence of D values. It can be used to calculate the effective hydrodynamic radius $< R_H >_0$ of a particle by employing the Stokes-Einstein equation:[41]

$$< R_H >_0 = \frac{kT}{6\pi \eta_o D_o} \qquad (9)$$

where k is the Boltzmann constant, η_o the solvent viscosity and T, the temperature. Using D instead of D_o, equation 9 gives the apparent R_H. The DLS measurements were performed at IQ-UNICAMP and at Lund University, Sweden.

Static Light Scattering (SLS)

In a SLS experiment, the scattering intensity of a sample is collected at different angles. The measurements can provide information about the radius of gyration R_g of a particle. For this purpose, the raw data has to be converted to absolute intensities $I(q)$, that can be obtained by:

$$I(q) = \frac{I_{sample}(q) - I_{solvent}(q)}{I_{toluene}(q)} R_{toluene}(q) \left(\frac{n_{sample}}{n_{toluene}}\right)^2 \qquad (10)$$

which normalizes the measured sample intensities with the Rayleigh ratio $R_{toluene\ (q)}$ of a reference that is toluene, corrects for the background (the scattering of the cuvette filled with water $I_{solvent}(q)$ and with toluene $I_{toluene}(q)$) and considers the refractive indexes of the sample n_{sample} and of the toluene $n_{toluene}$.[37,38]

The R_g of a particle can be obtained by the Guinier approximation:[42]

$$I(q) = I(0)\exp\left(-\frac{R_g^2 q^2}{3}\right) \qquad (11)$$

The SLS measurements were performed at IQ-UNICAMP and at Lund University, Sweden.

4.1.2. Small Angle X-rays Scattering (SAXS)

A SAXS experiment is similar to a light scattering experiment. However, in this case the wavelength of the beam is different, 0.154 nm in this thesis, and, usually, the intensity of the scattered beam is expressed as:

$$I(q) = P(q)S(q) \qquad (12)$$

where $P(q)$ is the form factor, related to the size and shape of the particle, and $S(q)$ is the structure factor, related to interparticle interactions.[42,43] When particles are distributed without

any interparticle interactions, for example, in dilute solutions, then the observed scattering is entirely the form factor.

Models from the literature can be used to fit experimental data regarding the form factor and give important information about the particles, such as dimensions, scattering length density and polydispersity.

For concentrated systems forming liquid crystalline structures, that display long-range order, the SAXS scattering is basically a diffraction pattern, that follows the Bragg's Law: [42,43]

$$n\lambda = 2d\sin\theta \qquad (13)$$

where n is an integer, d is the distance between the lattice planes and θ is the Bragg angle, as illustrated in Figure 10.
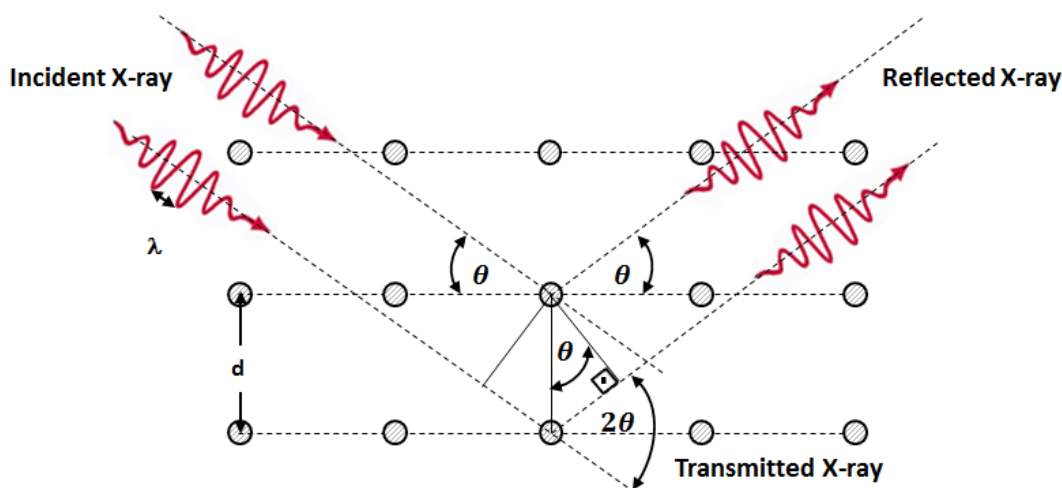
Figure 10. Schematic representation of a X-ray diffraction experiment. λ is the beam wavelength, d is the distance between the lattice planes and θ is the Bragg angle. Adapted from ref. 42.

Every crystalline structure is described by its unit cell, the smallest repeating unit in a crystal, and by its Miller Indices, denoted as h, k and l. They indicate the number of planes intersecting each unit axis of the cell. The symmetry planes in the different liquid crystalline phases originate different patterns depending on the phase.

A micellar cubic phase will have interferences in $I(q)$ at the relative peak ratios of $1^{1/2}$, $2^{1/2}$, $4^{1/2}$, $5^{1/2}$, $6^{1/2}$, etc., corresponding to the Miller Indices of (110), (200), (210), (211), (220), etc.; while for a hexagonal phase the peak ratios will be $1^{1/2}$, $3^{1/2}$, $4^{1/2}$, etc., corresponding to the Miller Indices of (100), (110), (200), etc. A lamellar phase will display peaks ratios at relative positions of $1^{1/2}$, $4^{1/2}$, $9^{1/2}$, etc., with Miller Indices of (100), (200), (300), etc.[43]

Because a lamellar phase consists in a set of infinite stacked planes (bilayers), the unit cell is the distance d between these planes:[43]

$$d = \frac{2\pi}{q_1} \qquad (14)$$

where q_1 is the position of the first scattering peak. The d-spacing can be calculated for any liquid crystalline phase and is used to estimate their unit cell parameter. For a hexagonal phase, this parameter is called a and represent the distance between the centers of the elongated micelles and is calculated as:[43]

$$a = \frac{2d}{\sqrt{3}} \qquad (15)$$

For a cubic phase, the cell parameter a is estimated based on the relations between q and the Miller Indices, as:[43]

$$\left(\frac{q}{2\pi}\right)^2 = \left(\frac{1}{a}\right)^2 (h^2 + k^2 + l^2) \qquad (16)$$

SAXS measurements were performed at the Brazilian Synchrotron Light Laboratory (LNLS, Brazil).

4.2 Laser Doppler Electrophoresis

When an electric field is applied to a solution, charged particles are attracted towards the electrode of opposite charge. The velocity at which the particle moves is called electrophoretic mobility U_E and depends on the particle charge and the surrounding medium. U_E is then measured by observing the Doppler shift in the scattered light.[44]

The surface charge of a particle is usually expressed in terms of its zeta potential ζ, i.e. the electric potential at the slipping plane. The zeta potential and electrophoretic mobility are related by the Henry equation:[44]

$$U_E = \frac{2\varepsilon\zeta f(ka)}{3\eta} \qquad (17)$$

where ε is the dielectric constant of the solvent, η is the viscosity of the medium and $f(ka)$ is the Henry's function. The laser doppler electrophoresis measurements were performed at IQ-UNICAMP.

4.3 Optical Microscopy

Optical microscopy is a technique that uses visible light and a system of lens to enhance the magnification of an object. The lenses are placed between the sample and the eye of the viewer to magnify the image so that it can be examined in great detail. The modern microscopes are connected to a camera in such a way that the image can be captured to generate

a micrograph. The resolution of the optical microscopy is limited by its use of light at wavelength in the visible domain. It is useful for the visualization of emulsion droplets, particles, and related aggregates in the micrometer size.[45] Currently, new techniques bring optical microscopy into the nanometric range of dimension. The optical microscopy measurements were performed at IQ-UNICAMP.

4.4 Cryogenic Transmission Electron Microscopy (Cryo-TEM)

Transmission electron microscopy (TEM) is a technique used to produce images by illuminating the sample with an electron beam and detecting the electrons that are transmitted through the sample. An image is formed from the interaction of the electrons with the sample as the beam is transmitted through the specimen. The image contrast is due to differential absorption of electrons by the material due to differences in composition, arrangement or thickness of the sample.

TEM is a powerful technique to study nanomaterials, but it is limited to dry samples. Because the particles investigated in this thesis are soft materials, i.e. formed by surfactant and polymer self-assembly in aqueous solution, drying would cause changes in the sample features. However, TEM can be equipped with additional devices that allow its use under cryogenic conditions, i.e. temperatures below -150°C. Such technique is called cryogenic Transmission Electron Microscopy, Cryo-TEM.[46]

In a Cryo-TEM experiment, a droplet of the sample is placed onto a carbon-coated copper grid under controlled environmental conditions, usually 25°C and 100% of humidity, to avoid solvent evaporation, using a vitrification system. The grid is then blotted with filter paper to remove excess of sample and to allow a thin film formation over the grid, which is rapidly plunged into liquid ethane at -180°C to ensure rapid vitrification of the water and avoid its crystallization. The sample can be stored in liquid nitrogen before being analyzed in a TEM microscope that possess a temperature-controlled sample holder.

Alternatively, soft colloids can be visualized in TEM by staining the samples with a heavy metal salt solution, such as uranyl acetate or lead citrate, in a procedure usually called negative staining. The heavy metal, whose solution can be spread over a liquid film containing the particles or mixed with the particle solution, bind to the aggregates, improving their contrast. The sample can be normally dried, and the particles remain stick over the grid, preserving your shape and average size. However, this technique is not substituted by Cryo-TEM in studies

where high-resolution images are needed. The Cryo-TEM measurements were performed at Lund University, Sweden.

4.5 Differential Scanning Calorimetry (DSC)

DSC is a technique used to study thermal events, such as phase and conformational transitions, in polymer and surfactant systems. The instrument possesses two identical cells that are filled with the sample and a reference solution and are heated at a same temperature range. The difference in heat capacity C_P between the two cells is measured and then reported as a function of temperature in a thermogram. A thermal transition is represented by a peak in the thermogram and the peak area can be used to estimate the change of enthalpy ΔH of the transition:[47]

$$\Delta H = \int_{T_i}^{T_f} C_P \, dT \qquad (18)$$

where T_i and T_f are the initial and final temperatures where the thermal event takes place, respectively. The temperature corresponding to the peak maximum is usually called as T_m. The DSC measurements were performed at IQ-UNICAMP.

4.6 Pulse-Field Gradient Nuclear Magnetic Resonance (PFG NMR)

PFG NMR methods are widely employed to measure translational diffusion of surfactants and polyions and their molecular assemblies and thus provide easily accessible ways to estimate their size via the Stokes–Einstein equation, in which the hydrodynamic radius is obtained. Moreover, information of bound and dissociated surfactant and polyion species can be quantified via their diffusion coefficients with respect to the diffusion of the particles.

A PFG NMR experiment is based on a sequence of pulses that is applied to the sample and in analyzing how the peak intensities in the ^{1}H NMR spectra vary as the gradient strength is increased. The attenuation of the signal intensity I is thus given by:[48]

$$I = I_o \exp\left(-D\gamma^2\delta^2 g^2\left(\Delta - \frac{1}{3}\delta\right)\right) \qquad (19)$$

where I_o is the signal intensity in the absence of gradients, D is the translational diffusion coefficient, γ is the magnetogyric ratio, δ is the time of gradient pulse and g is the gradient strength. In this thesis, the sequence of pulses that was employed is the stimulated echo (STE) with a pulse sequence of 90°-τ_1–90°-τ_2–90°-τ_1–echo.

In principle, any nonoverlapping peak between the surfactant and polyion can be used to analyze their diffusion. Based on a two-state model, which assumes that the molecule

is either bound to the particle or free in solution and chemical exchange between those two states is fast, the dissociated molecule population, α, is given by:[48]

$$D_{obs} = \alpha D_{free} + (1 - \alpha)D_{particle} \qquad (20)$$

where D_{obs} is the observed diffusion coefficient of the molecule (surfactant or polyion) in the presence of the particle, $D_{particle}$ is the particle diffusion coefficient, and D_{free} is the diffusion coefficient of free surfactant or polyion molecule, i.e. in the absence of particles. PFG NMR measurements were performed Lund University, Sweden.

4.7 UV-VIS Spectroscopy

When light passes through a transparent sample, a portion of the radiation can be absorbed. If this occurs, the residual radiation yields a spectrum with gaps, called absorption spectrum. Due to energy absorption, the electrons of the atoms that compose a molecule go from a state of low energy to a state of higher energy. The energy required to promote an electron from one state to the next lies in the ultraviolet (UV) and visible (VIS) range of electromagnetic spectrum, that is, the regions where the wavelengths range from 190 to 800 nm.[49]

Because molecules display several excited modes, the absorption occurs in a wide range of wavelengths and their UV-VIS spectrum consists in a band centered near the wavelength or the major transition. UV-VIS bands are characterized by their absorbance, which is a measure of the amount of radiation that is absorbed. The absorbance is proportional to the concentration of the substance and can be used to measure the concentration of a sample, according to the Beer-Lambert Law:

$$A = \varepsilon bc \qquad (21)$$

where A is the absorbance, ε is the molar extinction coefficient, b is the optical path length and c is the concentration.[49]

UV-VIS spectroscopy is also useful to study the Surface Plasmon Resonance (SPR) band of metal nanoparticles. SPR is the resonant oscillation of conduction electrons at the interface between negative and positive poles in the metal stimulated by the incident light. The position of the SPR band in an UV-VIS spectrum depends on the particle size and state of aggregation among other factors, such as dielectric constant of the solvent and refractive index. The UV-VIS spectroscopy measurements were performed at IQ-UNICAMP.

Chapter 2: Summary of Results

Because ***Paper I*** is a review and not a manuscript based on experimental data, it is not discussed in this chapter, but it is appended at the end of the thesis. In this chapter, the experimental results are presented as a summary of the papers or manuscripts to which they belong. However, they are not displayed in a chronological order, but in an order that makes some sense for experimental physical chemists: from dilute to concentrated systems. ***Paper II*** shows the effect of added long-chain alcohols to dilute particle dispersions.

Paper III compares particles prepared by the CS approach with those prepared by the *conventional method*, that is, by mixing individual aqueous solutions of surfactant and BCP with their respective counterions and give insights about the kinetic stability of the resulting dispersions. By studying the self-diffusion coefficients of surfactant ion, polyion and particles based on a NMR technique, information on dissociated species are discussed in ***Paper IV***.

In **Paper *V*** particles prepared by the CS approach are surface-decorated with gold and silver nanoparticles and the resulting conjugates are used as emulsion stabilizers and as catalysts for aerobic alcohol oxidation. Finally, in ***Paper VI***, concentrated samples are investigated and their phase behavior as a function of water concentration is studied.

2.1. *Paper II*

Early studies involving the CS approach comprised homopolymer poly(acrylate) mixed with surfactant ions. These works have shown that hydrated samples, which can swell up to ~ 50 wt% of water, display, basically, micellar cubic or hexagonal liquid crystalline structures, which depends on the surfactant ion alkyl chain length and on the water content. Later, additional mesophases were achieved by addition of long-chain alcohols in truly ternary mixtures (homopolymer CS/water/long-chain alcohols). These systems based on homopolymer, and *not* block copolymer, CS form macroscopically homogeneous phases, and, sometimes, are refereed as bulk systems.

Based on the previous experience with homopolymer CS, ***Paper II*** describes $BCPCS$ made from $PAAm_{42} - b - PAA_{42}$ BCP, where the acrylate charges are neutralized by dodecyl- or hexadecyltrimethylammonium surfactant counterions. The final products were named $PAAm_{42} - b - C_{12}TAPA_{42}$ and $PAAm_{42} - b - C_{16}TAPA_{42}$, according to the alkyl chain length of the surfactants used in their preparation. The dispersion of these complexes in water led to the formation of dilute aqueous dispersions of aggregates with a micellar cubic or a hexagonal liquid crystalline core and a diffuse hydrated shell.

Interestingly, the core structures agreed with those phases observed for maximum-swollen parent homopolymer CS, named here as $C_{12}TAPA_{30}$ and $C_{16}TAPA_{30}$. These particles possessed a negative surface charge, an average size around 200 nm and remained kinetically stable for several weeks. A striking difference between these and the previously reported $PAA - b - PAAm$/cationic surfactant particle dispersions is that particles *conventionally prepared* were reported as possessing disordered cores, smaller size and surface charge close to zero.

By the addition of suitable amounts of long-chain alcohols (octanol or decanol) the core structures varied, producing micellar cubic, hexagonal, lamellar, or reverse hexagonal liquid crystalline phases, as revealed by SAXS (Figure 11A). In addition, a disordered reverse micellar phase forms at the highest content of octanol. Again, these core structures are the same as those previously obtained for macroscopically homogeneous homopolymer poly(acrylate) CS/water/long-chain alcohol systems at the same long-chain alcohol/CS mass ratio (R). By employing dialysis, it was possible to achieve the initial liquid crystalline structure of the particles by removing the alcohol incorporated in their cores (Figure 11A). Interestingly, the average size of the particles was roughly the same, independently of the core structure (Figure 11B).
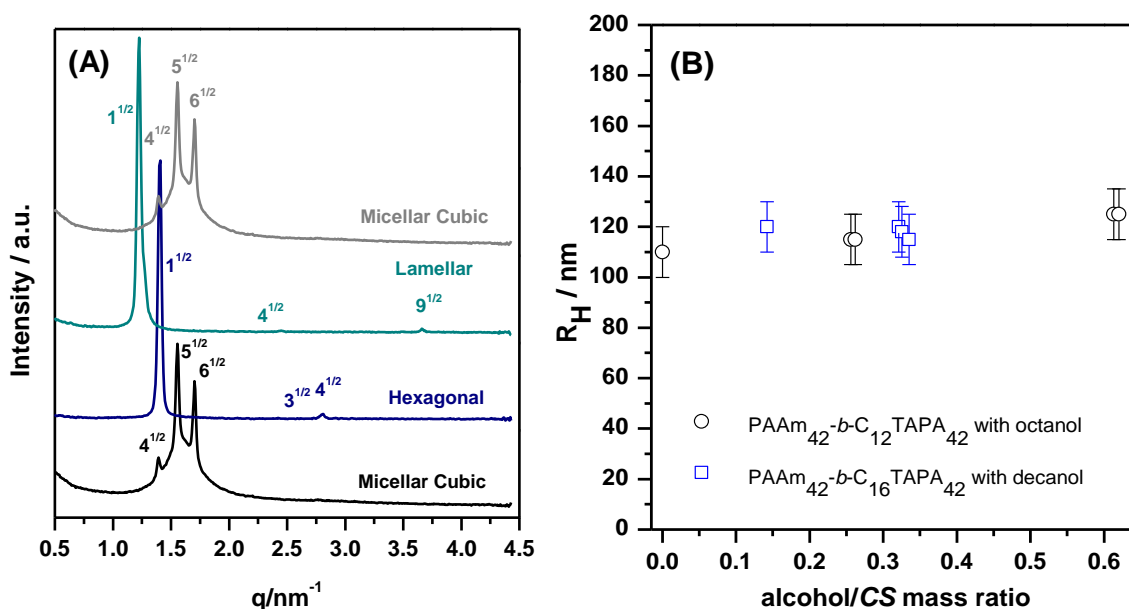
Figure 11. (**A**) SAXS patterns, shifted along the y-axis, for $PAAm_{42} - b - C_{12}TAPA_{42}$ particles loaded with different amounts of decanol at different alcohol/CS mass ratios (R): micellar cubic ($R = 0$), hexagonal ($R = 0.256$), lamellar ($R = 0.614$), and micellar cubic (dialyzed sample with $R = 0.614$). (**B**). Apparent hydrodynamic radius (R_H) of $PAAm_{42} - b - C_{12}TAPA_{42}$ and $PAAm_{42} - b - C_{16}TAPA_{42}$ particles loaded with different amounts of octanol or decanol. The values of R_H are presented as avg ± SD, triplicate of independent preparations.

This study was the first work in this thesis and has shown that: the core of dispersed $BCPCS$ reproduce the structures seen in the correspondent homopolymer CS; the possibility to switch the internal structure of the particles by simply adding or removing the alcohol; great difference from particles *conventionally prepared* that indicated strong evidences that the size of the particles is process-dependent. Specially the later finding, that is the striking differences between CS-based particles and particles *conventionally prepared,* inspired an expanded study, that composes the ***Paper III*** of this thesis and will be discussed in the next topic.

2.2 *Paper III*

The results of ***Paper II*** showed that the particles prepared by the CS approach displayed distinct properties when compared with the previously reported particles *conventionally prepared* by mixing the individual aqueous solutions containing the BCP and surfactant, with their respective counterions. It was questioned whether the small differences in composition, that is the presence or absence of low concentrations of inorganic ions, resulting from the two methods of preparation, could be the cause of the remarkable differences in the properties of the particles.

In ***Paper III***, $PAAm_{133} - b - C_{12}TAPA_{49}$ and $PAAm_{432} - b - C_{12}TAPA_{70}$ $BCPCS$ were prepared employing the CS approach and were dispersed in water to form particles named as $CS\_C_{12}S$ and $CS\_C_{12}L$, respectively. Particles *conventionally prepared* were also obtained employing the same surfactant and BCP and are referred as $CP\_C_{12}S$ and $CP\_C_{12}L$. In all cases, the first two letters of the acronyms denote for the approach used to prepare the particles (CS: complex salt, CP: conventionally prepared), C_{12} denotes the alkyl chain length of the surfactant and the terms S and L denote the length of the neutral BCP block (S: short, L: long). Additionally, $CS\_C_{12}S$ and $CS\_C_{12}L$ particles dispersed in 1 mM $NaBr$ aqueous solution were also prepared and are called $CS\_C_{12}S\#NaBr$ and $CS\_C_{12}L\#NaBr$.

A combination of SLS, DLS and SAXS revealed that particles prepared by the two methodologies display striking differences (Figure 12A). Because $CP\_C_{12}S$ and $CP\_C_{12}L$ particles are smaller, their cores are not large enough to contain a liquid crystalline arrangement. In addition, these particles display a spherical shape and the presence of small amounts of counterions shields the surface charge, originating particles with zeta potential close to zero, which implied a very poor colloidal stability of the dispersions (phase separation within days).

Regarding the $CS\_C_{12}S$ and $CS\_C_{12}L$ particles, this study showed that they have a non-spherical shape, which was confirmed by Cryo-TEM images. In addition, it also confirmed their nature previously observed in ***Paper II***: liquid crystalline cores with average size in the range of 200-300 nm and a negative surface charge. The dispersion of these particles in salt solution ($CS\_C_{12}S\#NaBr$ and $CS\_C_{12}L\#NaBr$) led to destabilization and a macroscopic phase separation within hours.
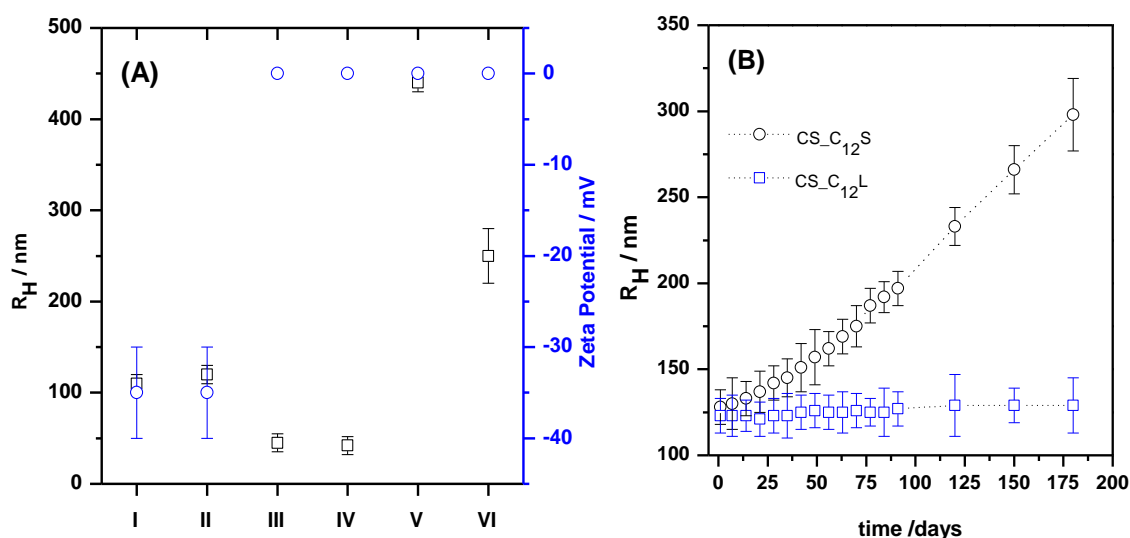
Figure 12. (**A**) Apparent hydrodynamic radius (R_H) and zeta potentials for I. $CS\_C_{12}S$. II. $CS\_C_{12}L$. III. $CP\_C_{12}S$. IV. $CP\_C_{12}L$. V. $CS\_C_{12}S\#NaBr$. VI. $CS\_C_{12}L\#NaBr$. (**B**) Time evolution of the apparent hydrodynamic radius (R_H) for $CS\_C_{12}S$ and $CS\_C_{12}L$ particles. The values of R_H and zeta potential are presented as avg $\pm$ SD, triplicate of independent preparations.

The colloidal stability of $CS\_C_{12}S$ and $CS\_C_{12}L$ particles was investigated as a function of time and the results revealed that, in addition to the electrostatic repulsion created by the negatively charged particles, the steric stabilization has a major contribution in the stabilization of the particles; the longer the neutral blocks of the BCP forming the corona (or shell), the higher the colloidal stability of the samples. Particles with shorter corona ($CS\_C_{12}S$) aggregate and separate out of the solution after around 6 months. $CS\_C_{12}L$ particles displayed colloidal stability superior to 6 months, with no signs of macroscopic phase separation (Figure 12B).

The results in this study have shown that particles, obtained by both methods, are metastable structures and display features that are process-dependent. Because particles prepared by the CS approach possess internal order and colloidal stability that can be tuned, they were selected for the next studies comprising this thesis.

2.3 *Paper IV*

By using the CS approach, surfactant ions and oppositely charged BCP electrostatically associate into particles, leading to a dense, surfactant-rich core stabilized by a neutral block corona. The resulting particles display a liquid crystalline inner structure and can be reproducible prepared with controlled average sizes. Yet, little is understood on dissociation of the constituent ionic species and their exchange between particles.

PFG NMR has been employed to study the complexed and free states of surfactant ions and BCP in the $C_{12}S$, $C_{16}S$ and $C_{12}L$ CS particles dispersions, at different concentrations, by means of their self-diffusion coefficients (D). It is possible to prepare, by centrifugation, systems that contained one phase concentrated in particles separated from a clear dilute phase. D values for both species in the two phases indicated that the dilute phase contained a fraction of small aggregates of surfactant ions and BCP, diffusing together at least an order of magnitude more rapidly than the large particles collected in the concentrated phase (Figure 13A).

The small aggregates in the dilute phase seems to be chemically similar to the large particles in the concentrated phase. Apart from these aggregates, a small amount of surfactant ions is dissociated from the small aggregates (Figure 13B) and the fraction of uncomplexed polyion is essentially zero, indicating that the polyion diffusion measured by PFG NMR mainly reports on the particle diffusion in both dilute and concentrated phases.
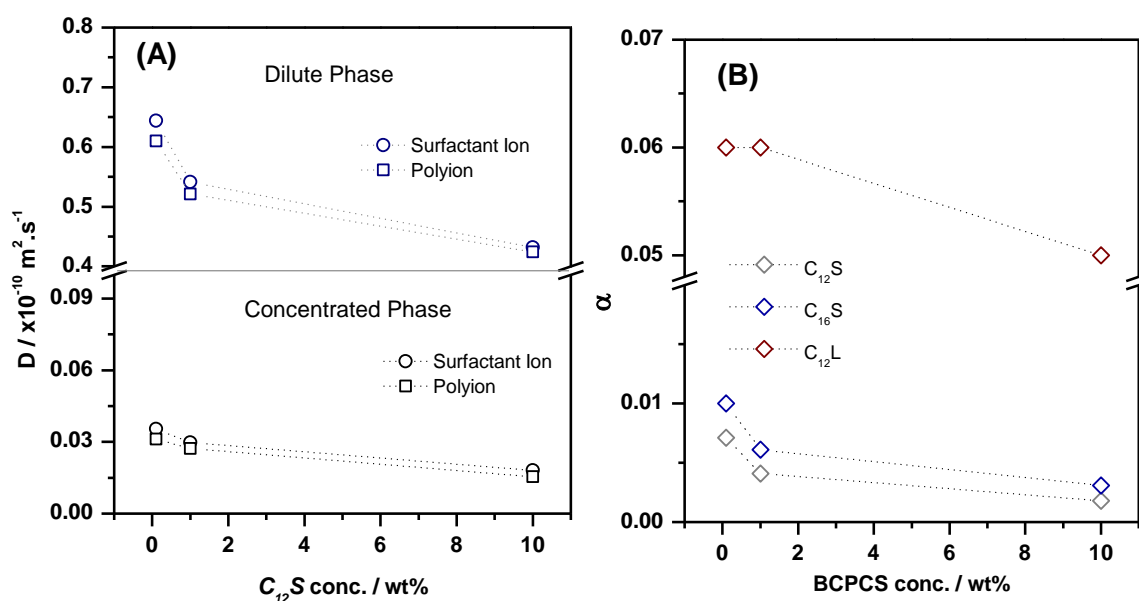
Figure 13. **(A)** Self-diffusion coefficients (D) for surfactant ion and polyion in the concentrated and dilute phases obtained for *centrifuged samples* at different concentrations for $C_{12}S$. **(B)** Fraction of dissociated surfactant ions (α) as a function of $BCPCS$ concentration in the dilute phases obtained by centrifuging $BCPCS$ samples at different overall (initial) concentrations. In all cases, the lines are guide to the eyes.

2.4 *Paper V*

Because $CS\_C_{12}L$ particles displayed enhanced colloidal stability (*Paper III*) and a tunable liquid crystalline core, they were surface-decorated with silver (Ag) or gold (Au) nanoparticles (NPs) in order to obtain planet-satellite nanostructures, in which the CS particles constitute the "planet" and the surrounding silver or gold NPs are the "satellites" (Figure 14A). The obtained conjugates were named as $CS-Ag$ and $CS-Au$.
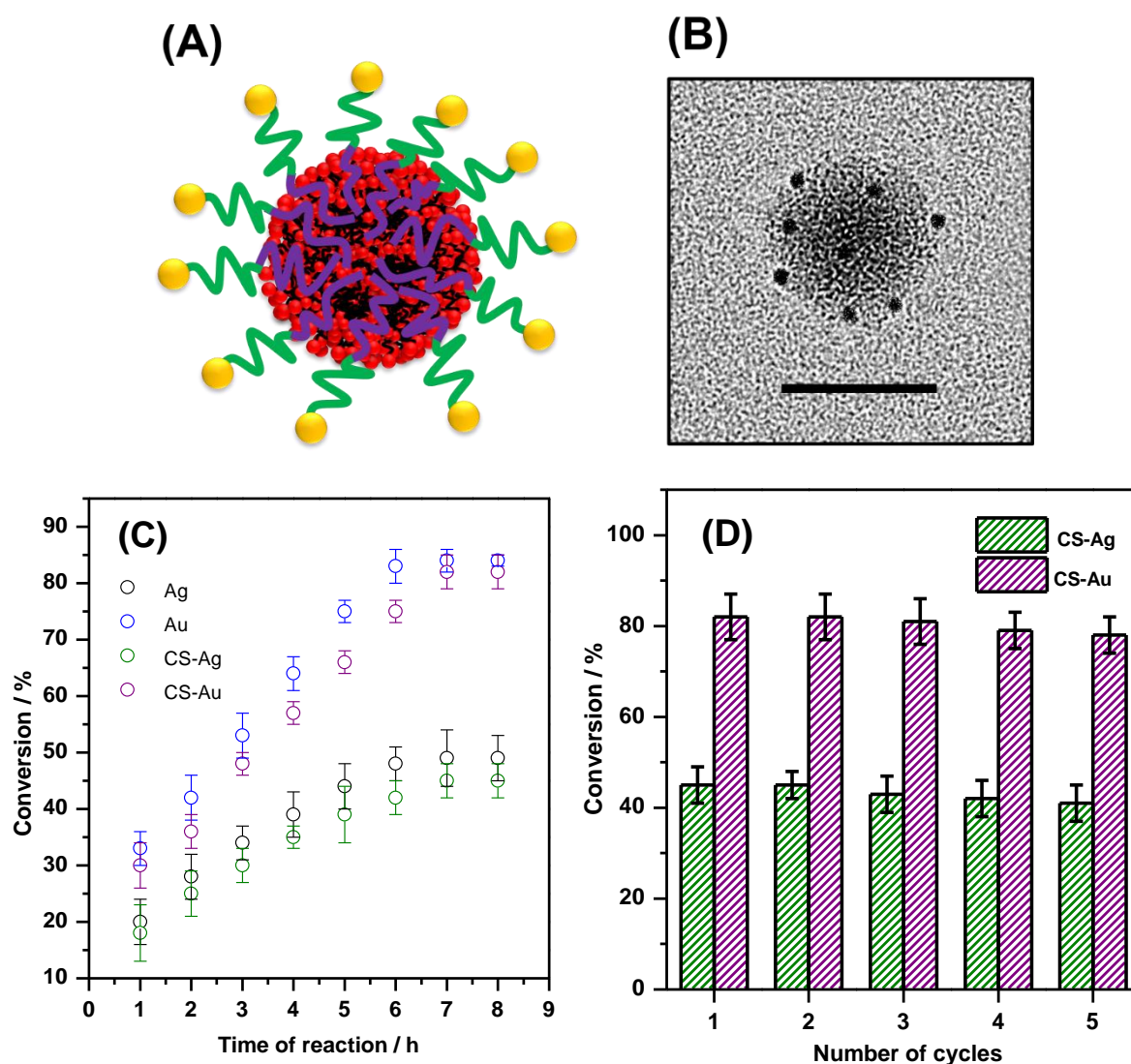
Figure 14. **(A)** Schematic representation of planet-satellite nanostructures. **(B)** Negative-stained TEM image of $CS-Ag$. Scale bar is 200 nm. **(C)** Conversion of benzyl alcohol to benzoic acid as a function of reaction time for the different catalysts. **(D)** Catalytic efficiency of $CS-Ag$ and $CS-Au$ conjugates for 5 recycle tests. The results are presented as avg ± SD, triplicate of independent preparations.

A combination of DLS, zeta potentials, SAXS, TEM measurements (Figure 14B) and UV-Vis spectroscopy results confirmed the formation of the nanostructures. They

presented excellent colloidal stability upon changes in solution pH or ionic strength, if compared with the bare metal NPs or with conjugates in which the "planet" is formed by *conventionally prepared* particles. In addition, $CS - Ag$ and $CS - Au$ displayed enhanced emulsification properties, stabilizing oil-in-water emulsions with long-term colloidal stability.

The resulting emulsions were used as medium for interfacially catalyzed aerobic oxidation of benzyl alcohol to benzoic acid, and the nanoconjugates displayed catalytic activity comparable to the bare metal NPs in aqueous medium (Figure 14C). The main advantages of using the obtained systems is the easier separation of the product, which concentrates in the water phase, from unreacted benzyl alcohol, which concentrates in the oil phase. Moreover, because the conjugates display enhanced colloidal stability, they can be easily recovered and reused with little loss of catalytic activity (Figure 14D).

2.5 *Paper VI*

There is a striking absence of studies of *concentrated* mixtures of $C3Ms$. This is surprising since it is well known that solvent-free melts of analogous BCP, that is, block copolymers where one block has surfactant molecules associated to the repeat units, typically form hierarchically ordered structures on both surfactant and BCP length scales. In addition, the finding that the *conventionally prepared* or CS-based particles possess properties that depend on the method of preparation (***Paper III***) raises questions about the equilibrium state of the dilute mixtures: are they true solutions or, in fact, non-equilibrium dispersions of an insoluble phase?

The last part of this thesis aimed to fill these gaps of knowledge. Therefore, we have here performed structural studies of $PAAm_{133} - b - PAA_{49}$ and $PAAm_{432} - b - PAA_{70}$ BCP neutralized by dodecyl- or hexadecyltrimethylammonium cationic surfactants (giving rise to samples named $C_{12}S, C_{12}L, C_{16}S$ and $C_{16}L$), prepared by the CS approach, over a broad range of concentrations (20-99 wt%) in water. One should note that this study would be best conducted for samples prepared by this approach because they are, as stated before, *free of counterions*, which would avoid effects of the high salt concentration as the concentration of the $BCPCS$ is increased.

The results, obtained by SAXS at different q-ranges, DLS and visual inspection, revealed for the first time, for hydrated samples, the formation of ordered hierarchical structures on both block copolymer and surfactant length scales (Figure 15), analogous to structures that have previously been reported for solvent-free block copolymer-surfactant complexes in the

solid or melt state. The structure on the BCP length scale (lamellar or hexagonal) depends on the block proportions of the copolymers used to obtain the complexes and resulted from the incompatibility, in water, between the $PAAm$ and CS blocks.
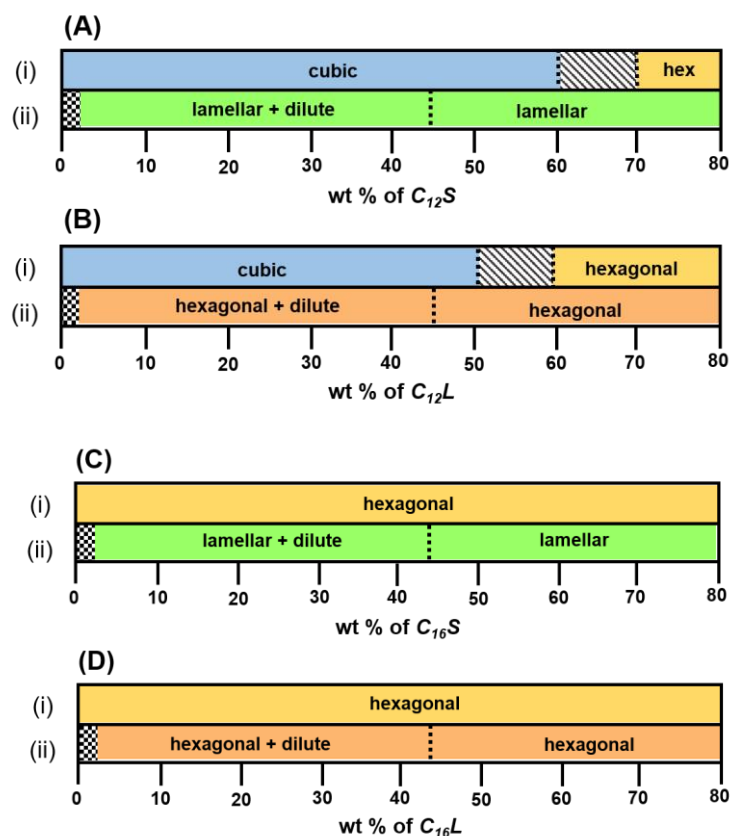
Figure 15. Diagrams of structures observed on CS (i) and BCP (ii) length scales in $BCPCS$/water mixtures: (A) $C_{12}S$. (B) $C_{12}L$ (C) $C_{16}S$. (D) $C_{16}L$. The hatched areas in A and B represent phase coexistences. In all cases, the squared areas represent dispersions in H_2O were no structure was observed at the BCP length scale.

The structure on the CS length scale (hexagonal or micellar cubic) depended not only on the surfactant alkyl chain length but also on the water concentration in CS domain. The latter water concentration could be tuned not only by the overall water content, but also by the appropriate choice of the block proportions, since the neutral block absorbs more or less water depending on its length, thereby concentrating the surfactant in the CS domain and so affecting the phase changes.

Although the formation of small aggregates in the dilute regime has been reported both for *conventionally prepared* and CS-based complexes, the detailed analysis of the structures on the BCP level strongly suggests that the hierarchical structures are in fact the equilibrium states for at least the salt-free complexes studied in this work, where the structures only take up water to a finite swelling limit.

Chapter 3: Conclusions

In this thesis, block copolymer-surfactant complexes ($BCPCS$) have been prepared, employing the *complex salt* (CS) approach, by an electrostatic association of poly(acrylamide)-*block*-poly(acrylic acid) block copolymers, with different block proportions, and dodecyl- and hexadecyltrimethylammonium cationic surfactant ions. The resulting complexes, free of any simple salt, were investigated in a wide range of concentration, from dilute dispersions to macroscopically homogeneous concentrated phases.

The dispersion of $BCPCS$ in aqueous solution originated particles whose cores display liquid crystalline structures, which can be tuned by the surfactant alkyl chain length and by adding or removing appropriate amounts of long-chain alcohols, indicating their potential use as an alternative to lipid-based liquid crystalline particles that have been widely studied over the last years because of their varied applications.

The CS approach constitutes a new path to produce internally ordered particles, with the advantage of possessing a robust switchable protocol to control the internal phases. Additionally, the core structures agree with the phases previously reported for hydrated homopolymer complex salts, indicating that, apparently, the confinement of the phases into small cores does not affect their structural properties.

The $BCPCS$ dispersions are metastable structures, similar to the parent *conventionally prepared* particles, and display kinetically stability due to steric and electrostatic repulsion arising from neutral polymeric block surface chains and negative surface charge, respectively. The colloidal and structural properties of the dispersions are dependent on the mixing pathways, but by using the CS procedure, it is possible to obtain particles with reproducible colloidal and structural features.

Apart from the internally-structured particles, the dispersion of $BCPCS$ also originates a fraction of small aggregates that are molecularly similar to the large particles, and a small amount of dissociated surfactant ions. The surface decoration of $BCPCS$ particles with gold and silver NPs originated sophisticated structures with tunable multifunctionalities thanks to the combination of the advantageous properties of the individual components. These nanostructures displayed excellent interfacial and catalytic properties and, additionally, they possess great potential in related areas where metal NPs are highly decided, such as sensors.

The hydration-dependent results obtained for concentrated samples have shown, for the first time, that selective attachment of amphiphile aggregates to one of the blocks

transformed the starting double-hydrophilic copolymer in a block copolymer consisting of incompatible blocks that aggregate into hierarchical structures when mixed with a selective solvent, water, in the present case. Such block incompatibility generated complexes displaying ordered structures in different lengths scales, i.e. structure-within-structures.

We have also demonstrated how these structures can be tuned independently by choosing the appropriate amphiphilic surfactant counterions, water content and by choosing the correct block proportions of the copolymers. The obtained results and comparison with the appropriate literature strongly suggests that the hierarchical structures are in fact the equilibrium states for the salt-free $BCPCS$ mixed with water.

Block copolymer self-assembly has attracted considerable attention for many decades because it can yield ordered hierarchical nanostructures that have been widely envisaged for multiple usages. From the above, the obtained results open an original and simple methodology to produce controlled hierarchical nanostructures that can be transferred to either copolymers and surfactants with different chemical properties.

References

1. Black, K. A.; Priftis, D.; Perry, S. L.; Yip, J.; Byun, W. Y.; Tirrell, M. Protein Encapsulation via Polypeptide Complex Coacervation. *ACS Macro Lett*. **2014**, *3*, 1088–1091.

2. da Silva, F. L. B.; Derreumaux, P.; Pasquali, S. Protein-RNA complexation driven by the charge regulation mechanism. *Biochem. Biophys. Res. Commun*. **2018**, *498*, 264-273.

3. Croguennec, T.; Tavares, G. M.; Bouhallab, S. Heteroprotein complex coacervation: A generic process. *Adv. Colloid Interface Sci*. **2017**, *239*, 115-126.

4. Wasungu, L.; Hoekstra, D. Cationic lipids, lipoplexes and intracellular delivery of genes. *J. Control. Release* **2006**, *116*, 255-264.

5. de Kruif, C. G.; Weinbreck, F.; de Vries, R. Complex coacervation of proteins and anionic polysaccharides. *Curr. Opin. Colloid Interface Sci*. **2004**, *9*, 340-349.

6. Schmitt, C.; Turgeon, S. L. Protein/polysaccharide complexes and coacervates in food systems. *Adv. Colloid Interface Sci*. **2011**, *167*, 63-70.

7. Meng, X.; Perry, S. L.; Schiffman, J. D. Complex Coacervation: Chemically Stable Fibers Electrospun from Aqueous Polyelectrolyte Solutions. *ACS Macro Lett*. **2017**, *6*, 505–511.

8. Stewart, R. J.; Wang, C.S.; Song, I. T.; Jones, J. P. The role of coacervation and phase transitions in the sandcastle worm adhesive system. *Adv. Colloid Interface Sci*. **2017**, *239*, 88-96.

9. Evans, D. F.; Wennerström, H. The Colloidal Domain, Where Physics, Chemistry, Biology and Technology Meet, 2nd ed., *Wiley*, **1999**.

10. Holmberg, K.; Jönsson, B.; Kronberg, B. Lindman, B. Surfactants and Polymers in Aqueous Solution, 2nd ed., *John Wiley & Sons*, **2007**.

11. Israelachvili, J. N. Intermolecular and Surface Forces, 1st ed., *Academic Press*, **1985**.

12. Tanford, C. The Hydrophobic Effect, *Wiley-Interscience*, **1973**.

13. Fontell, K. Cubic phases in surfactant and surfactant-like lipid systems. *Colloid Polym. Sci.* **1990**, *268*, 264-285.

14. Tiddy, G. J. T. Surfactant-water liquid crystal phases. *Phys. Rep*. **1980**, *57*, 1-46.

15. Young, R. J.; Lovell, P. A. Introduction to Polymers, 3rd ed., *CRC Press*, **2011**.

16. Fujita, H. Polymer Solutions, 1st ed., *Elsevier*, **1990**.

17. Hansson, P.; Lindman, B. Surfactant-polymer interactions. *Curr. Opin. Colloid Interface Sci*. **1996**, *1*, 604-613.

18. Langevin, D. Complexation of oppositely charged polyelectrolytes and surfactants in aqueous solutions. A review. *Adv. Colloid Interface Sci*. **2009**, *147-148*, 170-77.

19. Kogej, K. Association and structure formation in oppositely charged polyelectrolyte–surfactant mixtures. *Adv. Colloid Interface Sci*. **2010**, *158*, 68-83.

20. Piculell, L. Understanding and Exploiting the Phase Behavior of Mixtures of Oppositely Charged Polymers and Surfactants in Water. *Langmuir* **2013**, *29*, 10313–29.

21. Kabanov, A. V.; Kabanov, V. A. Interpolyelectrolyte and block ionomer complexes for gene delivery: physico-chemical aspects. *Adv. Drug Deliv. Rev.* **1998**, *30*, 49-60.

22. Skepö, M. Linse, P. Dissolution of a polyelectrolyte-macroion complex by addition of salt. *Phys. Rev. E* **2002**, *66*, 051807-1- 051807-7.

23. Hansson, P. Self-Assembly of Ionic Surfactants in Polyelectrolyte Solutions: A Model for Mixtures of Opposite Charge. *Langmuir* **2001**, *17*, 4167-180.

24. Kizilay, E.; Basak Kayitmazer, A.; Dubin, P. L. Complexation and coacervation of polyelectrolytes with oppositely charged colloids. *Adv. Colloid Interface Sci*. **2011**, *167*, 24-37.

25. Berret, J-F. Controlling electrostatic co-assembly using ion-containing copolymers: From surfactants to nanoparticles. *Adv. Colloid Interface Sci*. **2011**, *167*, 38-48.

26. Voets, I. K.; de Keizer, A.; Cohen Stuart, M. A. Complex coacervate core micelles. *Adv. Colloid Interface Sci*. **2009**, *147-148*, 300-318.

27. Harada, H.; Kataoka, K. Formation of Polyion Complex Micelles in an Aqueous Milieu from a Pair of Oppositely Charged Block Copolymers with Poly(ethylene glycol) Segments. *Macromolecules* **1995**, *28*, 5294-5299.

28. Wang, Q.; Schlenoff, J. B. The polyelectrolyte complex/coacervate continuum. *Macromolecules* **2014**, *47*, 3108–3116.

29. Marciel, A. B.; Srivastava, S.; Tirrell, M. V. Structure and rheology of polyelectrolyte complex coacervates. *Soft Matter* **2018**, *14*, 2454– 2464.

30. Thalberg, K.; Lindman, B.; Bergfeldt, K. Phase behavior of systems of polyacrylate and cationic surfactants. *Langmuir* **1991**, *7*, 2893–2898.

31. Svensson, A.; Piculell, L.; Cabane, B.; Ilekti, P. A New Approach to the Phase Behavior of Oppositely Charged Polymers and Surfactants. *J. Phys. Chem. B* **2002**, *106*, 1013– 1018.

32. Svensson, A.; Norrman, J.; Piculell, L. Phase Behavior of Polyion–Surfactant Ion Complex Salts: Effects of Surfactant Chain Length and Polyion Length. *J. Phys. Chem. B* **2006**, *110*, 10332– 10340.

33. Piculell, L.; Norrman, J.; Svensson, A. N.; Lynch, I.; Bernardes, J. S. Loh, W. Ionic surfactants with polymeric counterions. *Adv. Colloid Interface Sci*. **2009**, *147-148*, 228-236.

34. Bernardes, J. S.; Norrman, J.; Piculell, L.; Loh, W. Complex Polyion-Surfactant Ions Salts in Equilibrium in Water: Changing Aggregate Shape and Size by Adding Oil. *J. Phys. Chem. B* **2006**, *110*, 23433-442.

35. Bernardes, J. S.; Piculell, L.; Loh, W. Self-assembly of Polyion-Surfactant Ion Complex Salts in Mixtures with Water and n-Alcohols. *J. Phys. Chem. B* **2011**, *115*, 9050-058.

36. Vitorazi, L.; Berret, J-F.; Loh, W. Self-Assembly of Complex Salts of Cationic Surfactants and Anionic–Neutral Block Copolymers. Dispersions with Liquid-Crystalline Internal Structure. *Langmuir* **2013**, *29*, 14024–033.

37. Lindner, P.; Zemb, T. eds., Neutron, X-rays and Light. Scattering Methods Applied to Soft Condensed Matter. 1st ed., *Elsevier*, **2002**.

38. Brown, W. ed. Dynamic light scattering: the method and some applications. *Oxford University Press*, **1993**.

39. Jakeš, J. Regularized Positive Exponential Sum (REPES) Program - A Way of Inverting Laplace Transform Data Obtained by Dynamic Light Scattering. *Collect. Czech. Chem. Commun*. **1995**, *60*, 1781-1797.

40. Koppel, D. E. Analysis of macromolecular polydispersity in intensity correlation spectroscopy: the method of cumulants. *J. Chem. Phys*. **1972**, *57*, 4814 – 4820.

41. Kholodenko, A. L.; Douglas, J. F. Generalized Stokes-Einstein equation for spherical particle suspensions. *Phys. Rev. E* **1995**, *51*, 1081-1091.

42. Guiner, A.; Fournet, G. Small Angle Scattering of X-rays. *John Wiley & Sons*, **1955**.

43. Glatter, O.; Kratky, O. Small Angle X-ray Scattering. *Academic Press*, **1982**.

44. Hunter, R. J. Zeta Potential in Colloid Science. 1st ed., *Elsevier*, **1981**.

45. Clarke, A.; Eberhardt, C. Microscopy Techniques for Materials Science. 1st ed., *Woodhead Publishing*, **2002**.

46. Danino, D. Cryo-TEM of soft molecular assemblies. *Curr. Opin. Colloid Interface Sci*. **2012**, *17*, 316-329.

47. Olofsson, G.; Wang, G. Isothermal Titration and Temperature Scanning Calorimetric Studies of Polymer-Surfactant Systems. In Polymer-Surfactant Systems, Kwak J. C. T. ed., *Marcell Derek*, **1998**.

48. Söderman, O.; Stilbs, P. NMR Studies of Complex Surfactant Systems. *Prog. Nucl. Magn. Reson. Spectrosc*. **1994**, *26*, 445-482.

49. Pavia, D. L.; Lampman, G. M.; Kriz, G. S.; Vyvyan, G. A. Introduction to Spectroscopy. 5th ed., *Cengage Learning*, **2015**.

Appendices

Papers Included in This Thesis

Paper I. Ferreira, G. A.; Loh, W. Liquid crystalline nanoparticles formed by surfactant-polyelectrolyte complexes. *Curr. Opin. Colloid Int. Sci.* **2017**, *32*, 11-22.

My contributions to this paper: The author wrote the first version of the manuscript and contributed to the final editing of it.

Paper II: Ferreira, G. A.; Loh, W. Addition of n-Alcohols Induces a Variety of Liquid-Crystalline Structures in Surfactant-Rich Cores of Dispersed Block Copolymer/Surfactant Nanoparticles. *ACS Omega* **2016**, *1*, 1104–113.

My contributions to this paper: The author performed all the experiments and data treatment. The data analysis was performed together with the co-authors. The author wrote the first version of the manuscript and contributed to the final editing of it.

Paper III: Ferreira, G. A.; Piculell, L.; Loh, W. Impact of preparation procedure on the physicochemical properties of block copolymer nanoparticles containing surfactant-rich cores. *Manuscript*.

My contributions to this paper: The author performed all the experiments, data treatment and preliminary data analysis. The author wrote the first version of the manuscript.

Paper IV: Ferreira, G. A.; Piculell, L.; Loh, W. Molecular assembly in block copolymer-surfactant nanoparticle dispersions: Information on dissociated species from PFG NMR. *Manuscript*.

My contributions to this paper: The author performed all the experiments, data treatment and preliminary data analysis. The author wrote the first version of the manuscript.

Paper V: Ferreira, G. A.; Loh, W. Planet-Satellite Nanostructures Based on Block Copolymer-Surfactant Nanoparticles Surface-Decorated with Gold and Silver: A New Strategy for Interfacial Catalysis.

My contributions to this paper: The author performed all the experiments and data treatment. The data analysis was performed together with the co-authors. The author wrote the first version of the manuscript and contributed to the final editing of it.

Paper VI: Ferreira, G. A.; Piculell, L.; Loh, W. Hydration-Dependent Hierarchical Structures in Block Copolymer-Surfactant Complex Salts. *Macromolecules* **2018**, *51*, 9915–9924.

My contributions to this paper: The author performed all the experiments and data treatment. The data analysis was performed together with the co-authors. The author wrote the first version of the manuscript and contributed to the final editing of it.

Papers Not Included in This Thesis

Paper I: Percebom, A. M.; Ferreira, G. A.; Catini, D. R.; Bernardes, J. S.; Loh, W. Phase Behavior Controlled by the Addition of Long-Chain n-Alcohols in Systems of Cationic Surfactant/Anionic Polyion Complex Salts and Water. *J. Phys. Chem. B* **2018**, *122*, 4861–4869. **My contributions to this paper**: The author performed some of the DSC and WAXS experiments, treatment and analysis of all DSC data and wrote the introduction and discussion regarding the DSC results. The author contributed to the final editing of the manuscript.

Paper I

Liquid crystalline nanoparticles formed by oppositely charged surfactant-polyelectrolyte complexes

Guilherme A. Ferreira, Watson Loh *

Institute of Chemistry, University of Campinas (UNICAMP), P.O. Box 6154, 13083-970 Campinas, SP, Brazil

A B S T R A C T

Polyelectrolyte-surfactant (PE-S) complexes holding liquid crystalline (LC) structures have been widely studied over the last twenty years due to potential application in different fields. Several variables influence on important features of these PE-S complexes, such as surfactant and polyelectrolyte chemical structure (molecular architectures), charge molar ratio, environmental (pH, temperature, ionic strength) and mixing conditions (since non-equilibrium structures can be obtained), among many others that are discussed in this review. Depending on such variables, the PE-S complexes may display a variety of sizes, shapes, arrangements and LC phases. The short-range molecular arrangement is driven by the surfactant self-assembly though strongly influenced by the polyeletrolyte and also dependent on the presence of co-solutes (typically co-surfactants). In general, these structures reproduce features observed in the phase diagrams of surfactants for similar systems, which could then be used to tailor the formation of specific liquid crystalline structures. These correspondences are highlighted in this review along with some remarkable features reported for PE-S complexes and their consequences for potential applications.

© 2017 Elsevier Ltd. All rights reserved.

1. Introduction

Colloidal complexes formed by polyelectrolytes and oppositely charged surfactants (polyelectrolyte–surfactant complexes, PE–S) in aqueous solutions have been widely studied over years as a result of the great interest in nanostructured self-assembled systems, due to their important applications in different fields. These mixtures are frequently used in many industrial areas such as food, pharmaceutical, home care, detergents, paints, etc. Surfactants and polymers in aqueous solutions display a broad range of applications. Polymers are, for example, used to control the rheology of the formulations and surfactants are used to control their interfacial properties, such as surface tension, wettability, promote emulsification, etc. [1–3••,4–11]. Applications for PE-S complexes include coatings and encapsulation, such as, respectively, the polyion-surfactant ion complex salts [12•,13,14] and the now classic lipoplexes, lipid–DNA complexes that are widely studied aiming at gene therapy carriers [15–18]. Another related example is their application in personal care formulations such as shampoos, among others [19].

The binding of ionic surfactants to oppositely charged polyelectrolytes in solution can be cooperative, non-cooperative (random) or anti-cooperative, depending on the nature of the interaction between the mentioned species and quantitative information about the polymer–surfactant interaction can be obtained through binding isotherms (Fig. 1A) [1,19,20]. The cooperative association between oppositely charged polymers and surfactants in water is based on electrostatic and hydrophobic interactions and it is mainly driven by the entropic gain due to release of the small counterions and water molecules from the interacting species [19–22•]. It has been shown that such a process also involves a delicate balance of additional forces. Therefore, important aspects have to be considered, which can lead to a significant reinforcement in the interacting species once they have been brought together due to electrostatic attraction, such as: possibility of additional attractive interactions operating at short distances, as in the case of specific intermolecular interactions, i.e. hydrogen bonding, van der Waals forces, etc.; differences in chain configurations/conformations and differences in chain flexibility/stiffness [1,4,6,19,20].

The binding behavior of ionic surfactants to polyelectrolyte in solution may become substantially more complex as their concentrations increase. A cooperative binding of surfactant unimers to polyelectrolytes usually occurs above a critical surfactant concentration (cac), which is lower than the critical micelle concentration (cmc) of the pure surfactant in solution. As the surfactant concentration is increased, the first micelles, bound to the polyelectrolyte chains, are formed. Further increase of surfactant concentration leads to the formation of excess free "unbound" micelles (Fig. 1B) [1,6,20,21]. The pearl-necklace model is a simplistic description a polymer-surfactant association and is widely used as a general view of the binding processes at different

* Corresponding author.
  E-mail address: wloh@iqm.unicamp.br (W. Loh).
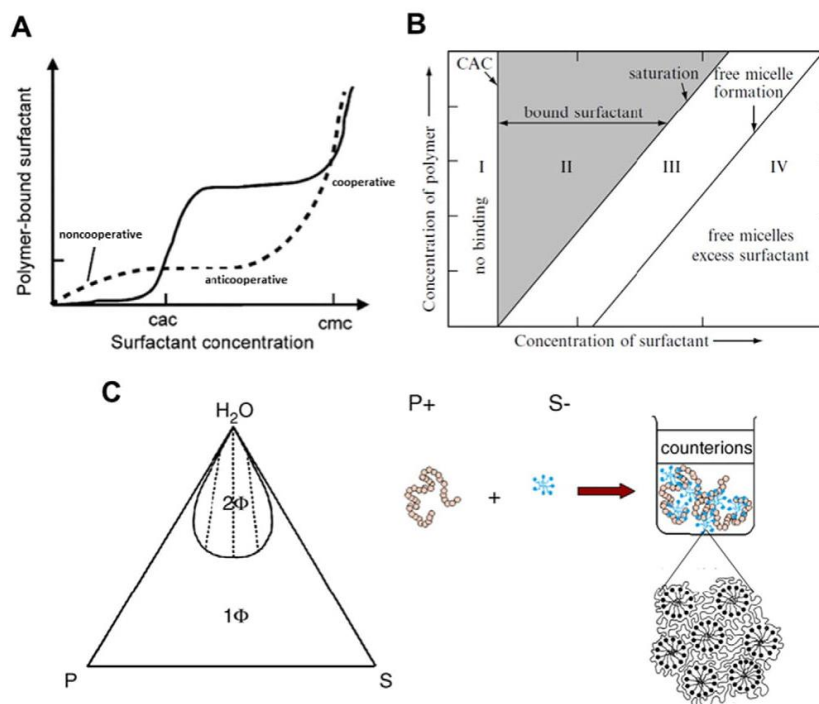
Fig. 1. A: Schematic binding isotherms for an ionic surfactant and oppositely charged polyelectrolyte, where the concentration of polymer-bound surfactant is plotted against the free surfactant concentration. Dotted line represents binding to hydrophobically modified polymer, where noncooperative, anticooperative and cooperative regions are seen. Solid line represents cooperative binding for unmodified polymer. B: Schematic diagram showing the typical association of a polymer with a surfactant at different concentration ranges. C: Schematic ternary phase diagram showing an associative phase separation, with the pearl-necklace model for polymer-surfactant assembly represented in the bottom right. The one-phase region and the two-phase region are denoted as 1Φ and 2Φ, respectively. Figs. A and C reprinted from ref. [20], with permission from Elsevier. Figs. B reprinted from ref. [19], with permission from John Wiley & Sons, Inc.

stages (Fig. 1C) [19]. The strong electrostatic interaction between oppositely charged polymer and surfactant leads to an associative phase separation of the PE-S complex (Fig. 1C) [3••,19,20].

Due to the great interest in investigating PE-S complexes for the last decades [22•,23•,24–29•,30•,31–34•,35–39•,40•,41–52•,53–70•,71••, 72–81•,82••,83–85••,86••,87••,88,89••,90–94•,95,96••,97,98••,99,100••,101••, 102,103••,104••,105–107], it is well-established that the binding of ionic surfactants to oppositely charged polyelectrolytes renders a broad rich diversity of complexes, regarding their shape, size, colloidal stability, absence or presence of long-range ordered structures, physicochemical aspects and applications. Typically, around charge equimolarity, insoluble complexes are formed, displaying various ordered crystalline-like phases. The interaction of double hydrophilic charged-neutral block copolymers, i.e. diblock copolymers in which both blocks are water-soluble, with surfactants leads to the formation of water-dispersible compacted particles, as will be discussed below. The above-described behavior has been commonly observed in a broad range of investigated dilute aqueous PE-S complexes.

It is important to emphasize that there are several examples in the literature on the *co*-assembly of polyelectrolytes with oppositely charged species in aqueous solution. Oppositely charged species include, in addition to the surfactants, synthetic polymers or biopolymers, such as proteins and DNA, nanoparticles, and polyelectrolyte block copolymer micelles [2,108–110]. In this review, we will focus our discussions on the formation, structure, dynamics, properties, and functions of complexes formed by polyelectrolytes of different architectures, such as synthetic homopolymers and charged-neutral block copolymers and biopolymers, with oppositely charged ionic surfactants, forming liquid crystalline structures in the dispersed state, excluding the investigations of the complexes in the solid or bulk state [111–114].

The formation of liquid-crystalline (LC) phases in complexes between oppositely charged surfactant and polyelectrolytes has been known for a long time [22•,23•,24,25] and, since then, these mesophases have been widely studied. Although their occurrence in such systems is known for more than three decades, there is an increasing interest in these particular materials, as they offer great versatility in structure control over a wide range of variables, These complex LC nanostructures have potential applications in different areas, covering issues from pharmacy, food, paintings, cosmetics, agriculture, among many others. In particular, an enormous effort has been made in the last years envisaging the development of such systems to biomedical applications. These complex LC colloids are excellent candidates as drug carriers due their ability to solubilize and carry specific compounds possessing biological activity and a large number of reports have focused their investigation aiming at this specific issue [57,70•,85••,86••,87••,89••,92,95,97,99,100••].

Such a strong interest has produced interesting systems and improved the knowledge about colloidal complexes displaying different LC phases. The formation of the refereed complexes involves the interplay of both electrostatic and hydrophobic interactions and the control over the obtained LC structure may be achieved by introducing variables that can modulate the interactions between the oppositely charged species, such as variations in the molecular structure of surfactant and polyelectrolyte, surfactant-to-polymer molar charge ratio, environmental conditions, i.e., pH, temperature, ionic strength, etc. Insights from the surfactants phase diagrams, in which the polelectrolyte may be replaced by multivalent counter-ions, and co-solutes may be considered too, are a valuable tool for the understanding and control over the structures formed.

In this paper, we will review the recent advances and describe some of the most important aspects regarding colloidal complexes based on

oppositely charged surfactants and polyelectrolytes holding liquid crystalline nanostructures. Examples of variables that usually alter some of the above-mentioned features will be described and the discussion will be illustrated by results described in different reports with important contributions to the field in the last few years.

1.1. The impact of polyelectrolyte architecture on the shape and internal organization of PE-S complexes

Several studies have reported the different morphologies of complexes formed by the complexation of surfactants and lipids and oppositely charged polyelectrolytes, depending on the solution conditions and also the structure of the polymer. More recently, it has been observed that although the basic nanostructures of some of these complexes are the same, the morphology of the complexes is affected by the polyelectrolyte rigidity and dissociation degree, controlled by the solution pH. Colloidal complexes formed by cationic lipid dioleoyl trimethylammonium propane, DOTAP, and the oppositely charged polyelectrolytes, sodium poly(acrylate), NaPA, and sodium poly(styrenesulfonate), NaPSS, have been thoroughly investigated over a broad range of surfactant-to-polyelectrolyte molar charge ratios, Z. The influence of the molecular weight of NaPSS has been also investigated, where 70 and 1000 kDa polymers were studied. The PAA and PSS polyelectrolytes are both negatively charged however, they differ in rigidity: PAA is a very flexible polymer, whereas PSS is much stiffer due to sulfontate groups limiting the polyelectrolyte conformation.

It has been demonstrated by cryogenic transmission electron microscopy (cryo-TEM) and small angle X-ray scattering (SAXS) measurements that the solution complexation of polyelectrolyte NaPA and NaPSS to DOTAP led to the formation of multilamellar complexes The

mixtures prepared with the lipid and NaPA (15 kDa) at different charge ratios of 0.5, 1, and 2, led to the formation of onion-like multilamellar complexes with tight layers (Fig. 2A). The size of the lamellar particles varied from hundreds of nanometers to about 1 μm. Aggregates of these large particles were also seen above charge equimolarity, due to local charge caused by the irregular coverage of polyelectrolyte molecules on the surface of the complexes. The addition of NaPSS also led to the formation of multilamellar complexes. However, the complexes were not round and globular as they were with the NaPA, forming non-spherical aggregates, with no defined concentric round shapes (Fig. 2B). As previously mentioned, the difference in flexibility and, consequently, persistence length of the two polyelectrolytes is seen to influence the organization of the polymer chains in round defined spherical structures, as can be seen for DOTAP and NaPA. It has been also shown that the molecular weight of the polyelectrolyte had no influence on the morphology nor interlamellar spacing of the complexes.

The effect of pH on the self-assembly of didodecyldimethylammonium bromide (DDAB), a double-tailed cationic surfactant with the above-mentioned polyelectrolytes, at Z = 1, has been also studied. The pH upon mixing of DDAB and NaPA solutions was 7.4. Cryo-TEM images (Fig. 2C) show again multilamellar complexes, with surfactant layers sandwiched by polymer layers, because the polyelectrolyte carboxyl groups are deprotonated, so the electrostatic attraction with the positively charged surfactants is strong. The increase in the solution pH to 11.4 did not affect the nanostructure. In contrast, lowering the pH to 2.4 promoted the formation of unilamellar vesicles (Fig. 2D), because as the pH is lowered, the carboxylic groups on the NaPAA backbone become neutral, and the attraction between the surfactant and polyelectrolyte molecules is weakened. The mixing of DDAB and NaPSS solutions at Z = 1 gives a pH = 4.7, and, again, multilamellar structures are formed (Fig. 2E).
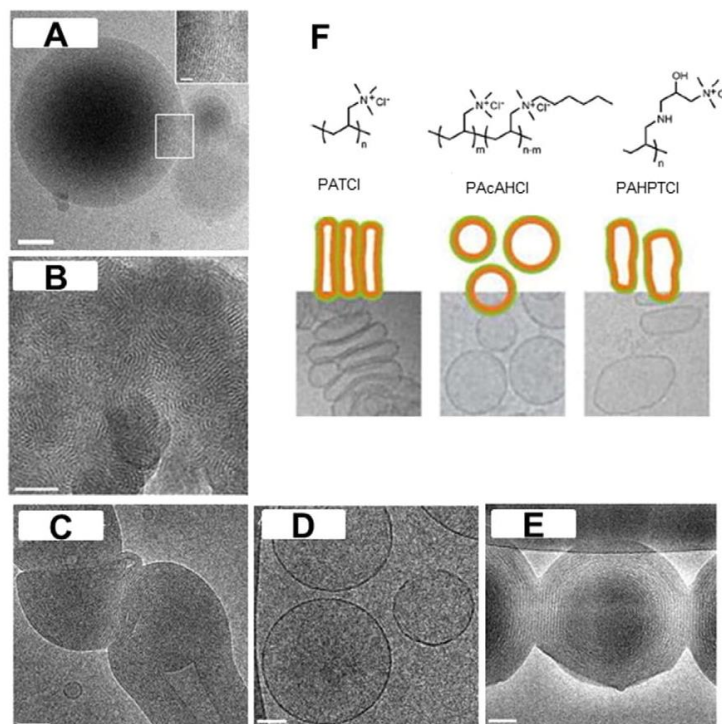
Fig. 2. Cryo-TEM images for: A. DOTAP/NaPA complexes at Z = 2; B. DOTAP/NaPSS 1000 kDa at Z = 1; C. DDAB/NaPA complexes at pH = 7.4 and Z = 1; D. DDAB/NaPA complexes at pH = 2.4 and Z = 1; E. DDAB/NaPSS at pH = 4.7 and Z = 1; F. anionic unilamellar vesicles surface covered with different polycations. Figs. A–E: inset shows higher magnifications of the white rectangle. Bars correspond to 50 nm in the main pictures and 10 nm in the inset. Figs. A–E reprinted with permission from ref. [103**].
Copyright (2016) American Chemical Society. Fig. F reprinted from ref. [89**], with permission from Elsevier.

However, pH variation to higher (11.5) and lower (2.5) values did not affect the observed nanostructure. The sulfonate groups acts as strong acids, and the protons are disassociated over the entire pH range. This leads to charged side groups that preserve electrostatic attraction with DDAB molecules over all examined pH values. At Z = 1 and pH = 4.7 (Fig. 2E), the stiffness of the NaPSS chains and its great affinity towards the bilayers led to the formation of faceted particles with highly-sandwiched layers of surfactant and polyelectrolyte, forming hexagonal-like nanoparticles, even though the SAXS data indicated that the initial lamellar phase remained unchanged.

Lipid and surfactant vesicles are widely used for in vitro or in vivo delivery of agents with biological important. However, these aggregates typically display low stability in contact with biological media, where a numerous factors, such as high ionic strength, variations in pH and the presence of (macro)molecules that can adsorb on their surfaces, such as proteins, cause their aggregation and, in some, cases, the disruption of their bilayers and, consequently, breaking down the vesicles. More recently, several studies have reported that the decoration with one or multiple layers of polyelectrolytes consists in a method for stabilization of lipid vesicles and the resulting polyelectrolyte-coated liposomes were considerably more stable than the conventional ones [115].

It has been also shown that the polycations differing in their chemical structures can deeply impact in the type, shape and colloidal stability of anionic lipid unilamellar vesicles in serum medium [89••]. The addition of polycations, at very small amounts, can induce the formation of vesicle aggregates. Further increase of polymer concentration, induces dissociation of the aggregates and formation of isolated vesicles coated with the polycations. It has been demonstrated that the coverage of the anionic vesicles with poly(allyltrimethylammonium chloride), PATCl, in serum medium caused the transition from spherical unilamellar aggregates to flattened cylinders (Fig. 2F), that tend to break into smaller vesicles. Addition of poly(allyltrimethylammonium chloride–co–allyl-N,N-dimethyl-N-hexylammonium chloride), PAcAHCl, had little effect in the vesicles shape, that remained rather spherical (Fig. 2F). Poly[(3-allylamino-2-hydroxypropyl)trimethylammonium chloride], PAHPTCl, caused the formation of well-separated unilamellar "amoeba-like" vesicles (Fig. 2F), that became more rounded and finally disintegrate into smaller lipid vesicles displaying a nearly globular shape.

These results clearly demonstrate the effect of polycation architecture (the presence of hydrophobic alkyl side groups and the localization of the cationic groups with regard to the main chain) on stabilization of lipid vesicles. The hydrophobically modified PAcAHCl polycation, can readily enter into the lipid bilayers without changing the lamellar structure, preserving the vesicular shape and improving its stability in serum medium. These results show that it is possible to cover the surface of lipid vesicles without changing the shape and size of the aggregates, while the colloidal stability in complex aqueous medium is improved and open new possibilities to the development of specific drug delivery systems more resistant to the environment conditions, keeping its initial physicochemical properties intact.

The interaction of double hydrophilic charged-neutral block copolymers with oppositely charged surfactants has been also studied in the last years, aiming at production of dispersed complexes with improved colloidal stability due to the presence of the extra hydrophilic neutral blocks in the polyelectrolyte architecture. Such co-assembly leads to the formation of water-dispersible compacted particles. The core of a dispersed particle contains densely packed surfactant aggregates interspersed with the anionic blocks of the copolymer, while the neutral hydrophilic blocks are enriched at the particle surface, giving rise to core-shell-like particles. The first reports of such systems were focused on complexes formed by the poly(ethylene oxide)-block-poly(methacrylic acid), PEO-b-PMAA, block copolymer and N-dodecylpyridinium chloride, DPCl, surfactant [22•]. Core-shell particles formed by the poly(acrylamide)-block-poly(acrylic acid) copolymer, PAAm-b-PAA, and dodecyltrimethylammonium bromide

surfactant, DTAB, were also extensively investigated in the last two decades [30•,31,32,35,81•,104••].

More recently, the PEO-b-PMAA/DPCl colloidal complexes were revisited aiming at the full characterization of the first system reported as a dispersion of core-shell PE-S particles, for the understanding of the thermodynamic and kinetic aspects involved in the co-assembly of these species [71••,82••]. It was shown that different types of aggregates are produced by mixing solutions of the individual components at varying surfactant-to-methacrylate block charge ratios (Z). By using static and dynamic light scattering measurements, it was observed that, at very small Z values, there is the coexistence of loose aggregates of electrostatically bound surfactants to PMAA blocks with free copolymer chains. Up to Z = 0.6, the number and the size of these aggregates increase with the surfactant concentration. Around Z = 0.5, the authors have also observed the formation of aggregates containing well defined cores formed by DPCl micelles attached to coiled PMAA chains (Fig. 3A).

As the surfactant concentration is further increased, formation of compact core-shell nanoparticles with a core formed by densely packed DPCl micelles and PEO shell starting slightly before charge equimolarity (Z = 1) was observed. At this point, the hydrodynamic radius (R_H) and radius of gyration (R_g) of the particles, at around 100 nm, achieves a minimum value in the investigated Z-range, indicating the formation of highly compacted block copolymer-surfactant nanoparticles. Above charge equivalence (Z > 1), coexistence of the core-shell nanoparticles with free DPCl micelles is observed. The dependence on Z of the self-diffusion coefficients of both surfactant and block copolymer measured by spin echo NMR (nuclear magnetic resonance spectroscopy) also suggested a four-step process in the behavior of the aqueous PEO–b-PMAA/DPCl systems. 2D ^{1}H NMR NOESY experiments have confirmed the formation of mixed cores containing the DPCl surfactant complexed with the PMAA anionic blocks. The signals of the PEO blocks, forming the outer part of the particles, showed weak correlation with DPCl, indicating that surfactant molecules do not interact significantly with the PEO blocks, which was confirmed by isothermal titration calorimetry (ITC) experiments. Additional small angle neutron scattering (SANS) studies also confirmed the above-mentioned compactness of the larger aggregates upon increasing Z.

SAXS measurements were employed to investigate the packing of surfactant micelles in the nanoparticles cores, indicating that the formation of highly ordered LC core structures is dependent on both block copolymer concentration and Z values. At low block copolymer concentration (c = 1 g L^{-1}), the surfactant micelles are disordered up to Z ca. 2, as evidenced by the lack of Bragg peaks. For higher Z ratios, SAXS data suggested a fcc cubic packing of the DPCl micelles in the core. The increase of block copolymer concentration (c = 5 g L^{-1}) revealed that the formation of ordered cores occurs at Z around 1, giving rise to nanoparticles displaying Pm3n micellar cubic LC core structures (Fig. 3B). The cubic structure remained unchanged when the sample was diluted down to the copolymer concentration of 0.3 g L^{-1}. This may be an indication that the liquid crystalline structures in the cores are kinetically frozen, because they remain preserved after sample dilution. In addition, cryo-TEM studies confirmed the presence of internally structured nanoparticles, depending on the block copolymer concentration and Z range (Fig. 3A), besides the other structures formed at different Z values. The kinetics of LC core formation was also investigated using time-resolved SAXS, revealing that the formation of ordered LC cores is very fast as the first Bragg peaks were observable from the very beginning of the measurement, i.e., ca. 50 ms after mixing of components.

In addition to the complexes formed by charged-neutral block copolymers and oppositely charged surfactants, that form the above-mentioned core-shell particles, there is also an increasing interest in studying the association between surfactants with amphiphilic block copolymers. In solution, such copolymers segregate their blocks into micelles, containing a collapsed core and extended neutral (lio)hydrophilic chains. Most part of the studies on interactions of amphiphilic block copolymer micelles with ionic surfactants focused
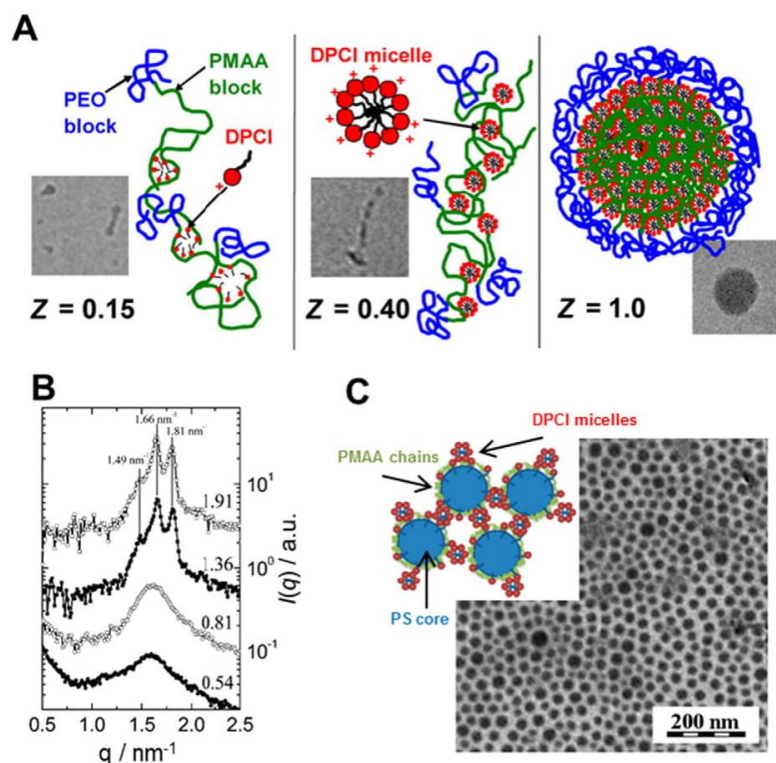
Fig. 3. A. Representation of the self-assembled PEO-b-PMAA/DPCl structures in solution as a function of the surfactant/polymer molar charge ratio (Z) and their respective cryo-TEM images. B. SAXS patterns for aqueous PEO-b-PMAA/DPCl complexes at copolymer concentration of 5 g L^{-1}. Z values are indicated above the corresponding curves. C. cryo-TEM image of PS-b-PMAA/DPCl complexes at Z = 1.1 and copolymer concentration of 1 g L^{-1}. Inset shows a representation of PS-b-PMAA/DPCl micellar complexes. Figs. A and B reprinted with permission from ref. [71**].
Copyright (2012) American Chemical Society. Fig. C adapted with permission from ref. [101**]. Copyright (2016) American Chemical Society.

mostly on polymeric micelles with neutral coronas. However, the studies involving hydrophilic charged-hydrophobic block copolymer micelles with surfactants have received more attention recently [116–118].

Morphological changes in polystyrene-*block*-poly(methacrylic acid) (PS-b-PMAA) micelles upon addition of DPCl surfactant have been recently investigated [101**] and it was observed that, depending on the amount of surfactant, i.e., the mixture Z values, there are three different stages of interaction. At low Z (<0.4), DPCl is bound to the hydrophobic inner moiety of the PMAA chains as nonmicellized unimers; as the surfactant concentration is increased, DPCl micelles are formed and bind in the ionized outer part of the corona, leading to charge neutralization of the chains; further increase of DPCl concentration (Z > 0.8) promotes the aggregation of the large block copolymer micelles decorated with small surfactant micelles (Fig. 3C). These results indicate that the surfactant bound in the interior part of the PMAA chains is disordered and, unlike polyelectrolyte–surfactant complexes formed by free polyelectrolyte chains, does not self-assemble into packed surfactant micelles. The high density of the corona forming PE chains and insufficient space for the accommodation of micelles may impose spatial restrictions to the packing of DPCl micelles and the following formation of densely packed aggregates at the outer surface of the block copolymer micelles. The hydrophobic PS core of the block copolymer micelles remains unchanged upon addition of surfactant, confirming the previously reported nature of amphiphilic block copolymer micelles with kinetically frozen cores [118]. The above-mentioned results clearly demonstrate the impact of polyelectrolyte chemistry on the size, shape, colloidal stability and liquid crystalline structure in PE-S complexes.

1.2. Surfactant molecular structure also influences the PE-S complexes

Depending on the applications of PE-S complexes, the use of specific species is desired to achieve biocompatibility. This can be achieved by employing combinations where both components, polyelectrolyte and surfactant, are derived from biological resources. In the last years new studies has been performed on complexes formed by ionic surfactants and oppositely charged polysaccharides, such as cationic modified cellulose [33,42,43,46,56] hyaluronic acid [95,119] and chitosan [50,61,85**,86**,87**]. Chitosan is a deacetylated form of chitin and consists of a linear polymer of α (1 → 4)-linked 2-amino-2-deoxy-β-D-glucopyranose. Due the presence of amino groups on its chemical structure, chitosan is easily ionized with a positive charge when dissolved in acidic solutions, typically at pH < 6 [120].

Aiming at the formation of water-dispersible biocompatible chitosan/surfactant complexes, some recent reports [86**,87**] have focused on the structural investigation of colloidal complexes based on chitosan and oppositely charged alkyl ethylene oxide carboxylate surfactants. Beside their biocompatibility, this class of surfactants is interesting because the headgroup area can be tuned by changes in both temperature (ethylene oxide groups) and pH (carboxylate groups). In addition, alkyl and oligoethylene chain lengths can be easily changed, opening further possibilities on combinations between polyelectrolyte and surfactant. Complexes of nonaoxyethylene oleylether carboxylic acid (C$_{18:1}$EO$_9$CH$_2$COOH or simply C$_{18:1}$E$_9$Ac) and chitosan were prepared at pH values between 3.5 and 5.0 in a manner to control the degree of ionization of the surfactant from 0.15 at pH 3.5 to 0.62 at pH 5.0, by varying the pH around its pKa, whereas the ionization of

chitosan is only slightly affected. The studies also investigated structural features of the complexes as a function of the surfactant to chitosan charge mole ratio (Z), ranging from 0 to 0.3 [86**].

From results obtained by means of dynamic and static light scattering measurements it was reported that, below a certain Z value that depends on pH, no structural rearrangement of the chitosan chains occurs with the addition of nonmicellized surfactant. At sufficiently high surfactant content (higher Z), i.e., above the *cmc* of the surfactant, an aggregation of chitosan chains as the consequence of the presence of bridging micelles is observed, giving rise to a network formed by polyelectrolyte chains decorated with some surfactant micelles. Additional micelles become incorporated into the already-existing complexes, resulting in a compaction of the complex aggregates, forming a one-dimensional ordered aggregate in the form of cylinders, with a total length from 20 to 50 nm, formed by an average of two to five micelles per aggregate. The tendency of forming elongated objects has been found in several mixtures of polyelectrolytes and oppositely charged micelles and, usually, is governed by the surfactant molecular and micellar architecture [34*,36,41,50,52*,66,77,78,98**]. In this case, it has been also demonstrated that $C_{18:1}E_9Ac$ surfactant forms ellipsoidal micelles, confirming the above mentioned tendency.

At sufficiently high Z values, the network is fully disrupted and aggregates with a core-shell structure are formed, with a volume fraction of densely packed micelles of 0.5 to 0.7 per core. The formation of such core-shell particles has been widely reported in mixtures of block copolymers and surfactants as a result of the formation of a hydrophobic, water-insoluble complex stabilized by a hydrophilic nonionic shell, as previously discussed above. The authors rationalized the formation of a stabilizing chitosan corona at Z < 1 in terms of the stiffness and length of the polyelectrolyte chains. The formation of a stoichiometric complex would require a tight bending of the PE around the surfactant micelles. A more favorable situation is reached if some of the chitosan chains are involved in complex formation, and the excess charge in the remaining chains has the tendency to be solubilized, therefore forming a stabilizing charged corona in the outer part of the chitosan/surfactant particles. A corresponding structural phase diagram as a function of pH, i.e. the degree of ionization of the surfactant, and Z for this particular system has been reported and is displayed in Fig. 4A.

By varying the molecular structure of the surfactant [87**], it was found that both alkyl and ethylene oxide chain lengths influence the final structure and shape of the micelles and of the chitosan/surfactant complexes (Fig. 4C). C_8E_5Ac and $C_{12}E_{10}Ac$, possessing a large headgroup compared to the hydrophobic part of the surfactant, aggregate into spherical micelles, in the form of core-shell spheres. $C_{12}E_{4.5}Ac$ tends to aggregate, in water, forming a mixture of large unilamellar vesicles and long cylinders. At pH 4, chitosan/$C_{12}E_{10}Ac$ complexes follow the same trend as observed in chitosan/$C_{18:1}E_9Ac$ mixtures discussed above. As Z is increased, the complexes evolve from one-dimensional
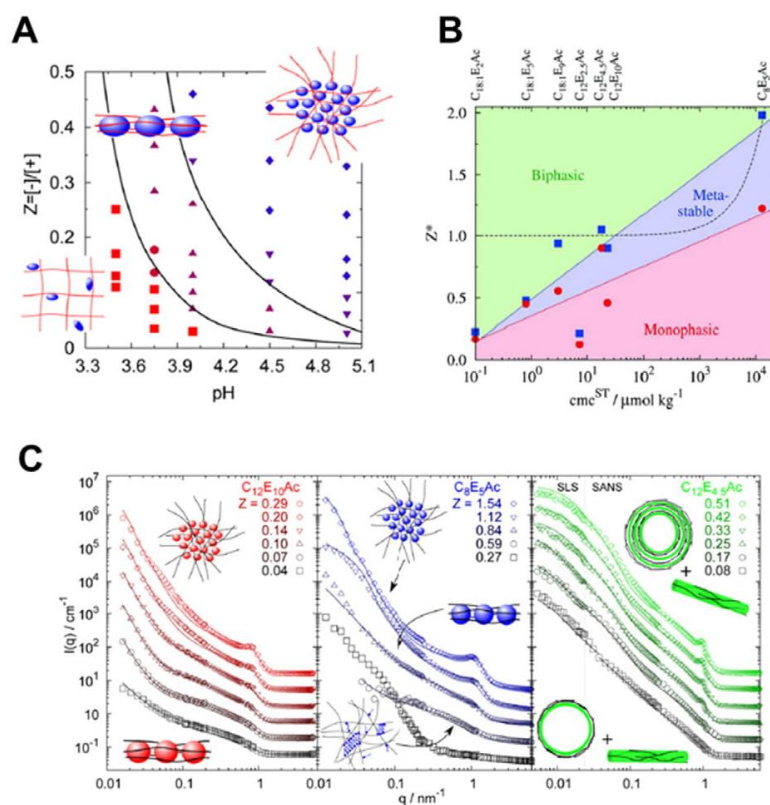
Fig. 4. A. Phase diagram for chitosan/$C_{18:1}E_9Ac$ complexes at different pH and surfactant-to-polyelectrolyte molar charge ratios, Z. The symbols ■, ▲ and ◆ represent decorated network, 1D–ordered complex, and densely packed core — shell particles complexes, respectively. ● and ▼ represent mixtures with intermediate structures between the above-mentioned models. B. Critical mixing ratio Z*, i.e., Z value at which phase separation is observed, reported as a function of the *cmc* of the different surfactants obtained at pH 4.0. Full squares are Z* values for phase separation observed immediately after mixing solutions containing the individual components and full circles for phase separation observed 10 days after sample preparation. Full lines are only a guide for the eyes. Dotted line indicates equimolarity taking into account the *cmc* of the free surfactant. C. SANS patterns for complexes of the indicated alkyl ether carboxylate surfactants and chitosan at different Z values and pH = 4. Insets show representation of the complexes arrangement obtained by the fitting of the points, represented by the solid lines. Fig. A reprinted with permission from ref. [86**].

ordered structures composed of aligned micelles embedded in a chitosan network to core-shell particles containing densely packed micelles within the core and a stabilizing chitosan corona. Interestingly, the number of micelles per cylinder and the length of the cylinders are very similar in complexes formed by chitosan with $C_{18:1}E_9Ac$ and $C_{12}E_{10}Ac$, despite the different alkyl chains of the surfactants. The same trend was also observed for C_8E_5Ac, with a dense packing of micelles at high Z and formation of linearly ordered complexes at intermediate Z.

The complexation of chitosan with $C_{12}E_{4.5}Ac$ formed vesicles with ordered multilayered structures, with alternating layers of surfactant and chitosan. It has been shown that the number of layers depends on the charge molar ratio Z, while the interlamellar spacing remains constant. The bending rigidity of the bilayers increased with Z, indicating that the presence of a semi-rigid polymer in the bilayer interstices, such as chitosan, produces an increasingly stiff vesicle wall. Increasing the number of layers, a decrease in the core size is observed. However, the overall size of the vesicles is retained at around 100 nm. This is a rather unexpected result, as it indicates that instead of a classical layer-by-layer growth widely observed, for example, in lipid bilayers, the additional layers are internalized in the vesicle.

In all investigated systems, it was observed that further increase in surfactant concentration leads to phase separation of the dispersions (Fig. 4B), with formation of a liquid transparent solution and a second phase rich in polymer and surfactant (solid complex). Results from SAXS revealed that the structures formed upon complexation between chitosan and the different alkyl ethylene oxide carboxylate surfactants in solution are retained in the solid state. It was also observed that no particular long-range ordering was seen in the solid complexes formed with $C_{18:1}E_2Ac$ and $C_{12}E_{2.5}Ac$, the most hydrophobic surfactants.

1.3. The role of a third component on the PE-S complex formation and properties

In contrast to the variety of the structures in complexes formed by polyelectrolyte and oppositely charged surfactants, solely, much less information is known about the structural features of water-dispersible polyelectrolyte/surfactant complexes in the presence of a third component. Usually, polymer-surfactant mixtures are used in complex formulations, where the presence of cosurfactants, salts, nonionic additives, thickeners, etc., is remarkable and the influence of such components on the phase behavior of PE-S complexes may be well understood in order to improve or preserve the desired applications for such systems. Due to this, an effort has been made in the last years aiming at the characterization of PE-S complexes in the presence of a third component. The most studied systems are comprised of nonionic additives, such as the sugar- and ethylene oxide-based surfactants, long chain n-alcohols and PEO-based block copolymers [40*,53,63,65,69,80,84,90,91,96**,98**, 104**].

The impact of dodecyl maltoside ($C_{12}G_2$), a sugar-derived nonionic surfactant, on the interaction between poly(diallyldimethylammonium chloride) (PDADMAC) and SDS was extensively studied in the recent years [90,96**,98**]. The choice was made based on the fact that previous reports in the literature have shown different impacts of uncharged amphiphiles on the liquid crystalline structures formed in PE/S dispersed complexes: in some cases, the addition of the additive induced the complete disappearance of long range order in the complexes, while in others, it leaded to the transition to other types of structures [91]. It has been observed that the nonionic surfactant influences the formation of the complexes between PDADMAC and SDS [96**,98**], since in the absence or presence of different concentrations of $C_{12}G_2$, abrupt variations of electrophoretic mobility and the turbidity of the mixtures, prepared by the simple mixing of individual solutions, occurred at different SDS concentration, for a constant PDADMAC content (Fig. 5A and B).

In the absence of the nonionic surfactant, PE/S complexes are formed at low SDS concentrations. Increasing the SDS-to-PDADMAC ratio, the net charge of the nanoparticles is reduced, whereas the turbidity of the mixture increases until charge neutralization where phase separation is observed. Further increase of SDS concentration leads to a charge reversal and redispersion of the complexes (Fig. 5B). It has been shown that the addition of $C_{12}G_2$ increases the binding of SDS to the polycation and that it shifts the concentration range of phase separation to lower SDS-to-PDADMAC ratios (Fig. 5A and B). At high Z, PDADMAC/mixed surfactant aggregates are formed presenting a decreased colloidal stability if compared with complexes formed by solely the polyelectrolyte and SDS. The complexation of PDAMAC with mixed micelles led to the formation of particles with reduced surface charge, as evidenced by their electrophoretic mobility measurements.

SAXS analyzes revealed that the complexes formed at excess of PDAMAC are cylindrical-like structures and that the addition of $C_{12}G_2$ did not change the dimensions of the complex aggregates, formed by short cylinders (length at around 20 nm) with aggregation numbers between 200 and 250. Again, the shape of the aggregates is related to the form of the surfactant micelles, since it has been demonstrated that both SDS and $C_{12}G_2$ surfactant self-assembles into elliptical micelles. At SDS excess, a suspension of large aggregates and precipitates are observed to coexist in solution. In both states, scattering data indicated cylinders organized in a hexagonal LC structure with spacing at around 3.8 nm. The average spacing among cylinders arranged in a hexagonal structure remained unchanged at low $C_{12}G_2$ concentration (1 mM) and reached 4.6 nm when the sugar-based surfactant concentration is 10 mM.

SAXS analyses in the solid complex precipitates formed at SDS excess show Bragg peaks at 1 and $3^{1/2}$ positions (Fig. 5C), revealing the hexagonal structure retained from the dispersed state at low $C_{12}G_2$ concentration. When SDS concentration is increased (10 mM), however, the solid complex exhibits superimposed peaks in the SAXS patterns, indicating the presence of two or more coexisting phases, which have not been properly identified. The supernatant solution was also analyzed and data revealed globular micelles, similar to the ones formed without the polyelectrolyte. The results indicated that addition of small amounts of dodecyl maltoside does not lead to significant changes in the structure of PDADMAC/SDS complexes in the solution and solid states. The only exception is for samples at SDS-to-PDADMAC ratios close to charge neutralization or SDS excess and high concentration of $C_{12}G_2$ where the precipitate forms a multiphasic structure and the aggregates in solution are not cylindrical-like, as in polyelectrolyte excess.

More recently, the effect of added long chain n-alcohols on the internal structure of dispersed complex salts were investigated, featuring new insights about the role of a third component on the PE-S complexes [104**]. Poly(acrylamide)-b-complex salts made from poly(acrylate-b-acrylamide) block copolymer containing the acrylate blocks neutralized by dodecyl- or hexadecyltrimethylammonium surfactant counterions, form kinetically stable aqueous dispersions of hierarchical aggregates with a liquid crystalline micellar cubic or hexagonal structures, respectively, complex salt core and a diffuse hydrated shell. By the addition of suitable amounts of octanol or decanol, the liquid crystalline interior can be tuned, producing additional lamellar, reverse hexagonal phases and reverse micellar phases, depending on the alkyl chain length and amount of the n-alcohol. These core structures are the same as those previously obtained for bulk, i.e., non-dispersed homopolymer poly(acrylate) complex salt/water/n-alcohol systems at the corresponding compositions, as seen in Fig. 5D [40*,63].

The exact structure correspondence between dispersed and macroscopic bulk phases is not, a priori, expected, since one would expect some influence of the poly(acrylamide) chains of the block copolymer in the surfactant aggregate arrangement. The presence of a core-shell interface and the consequent confinement of the LC structures are also expected to affect the mesophase geometry. However, such effects were not seen, indicating an important characteristic on the phase behavior of PE-S complexes: the dispersed colloidal complexes are able to reproduce and retain some remarkable features from the bulk structures. Such fact expands the possibilities to achieve a more accurate
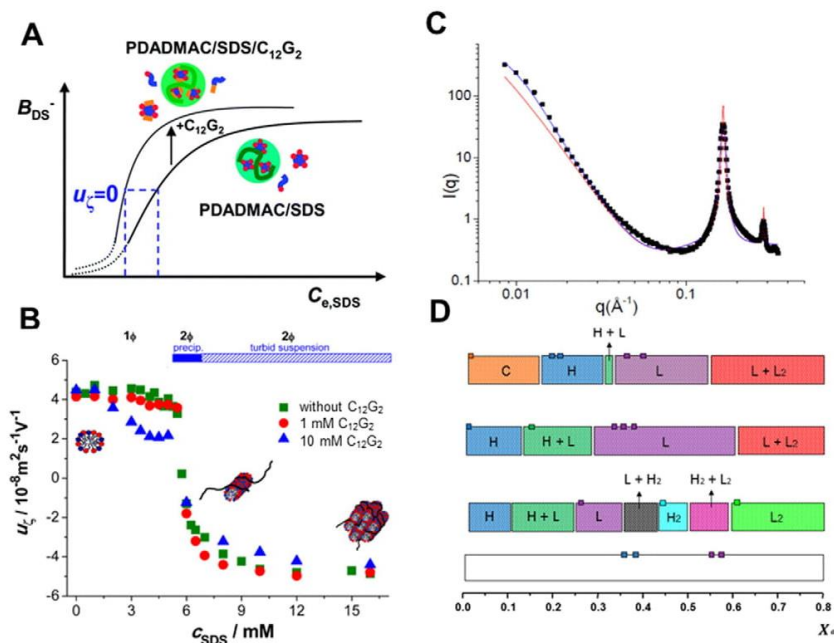
Fig. 5. A. Schematic illustration of the variation of the bound amount of dodecyl sulfate ions (B_{DS-}) on the PDADMAC as a function of the free SDS concentration ($c_{e,SDS}$) in the absence and presence of $C_{12}G_2$. The graph also illustrates by dashed blue lines those free SDS concentrations where the charges of the PDADMAC molecules are neutralized in the absence and presence of $C_{12}G_2$ (i.e. at $u_\zeta = 0$). B. Mean electrophoretic mobility (u_ζ) of the PDADMAC/SDS/DDM complexes as a function of SDS concentration at polymer concentration of 1000 mg L^{-1} in the presence of different amounts of $C_{12}G_2$. C. SAXS data and fitting curves for the hexagonal solid complex obtained at excess SDS in the presence of $C_{12}G_2$. D. Phase evolution as a function of n-alcohol content for the homopolymer complex salt systems from top to bottom: $C_{12}TAPA_{30}$/water/decanol; $C_{16}TAPA_{30}$/water/decanol; $C_{16}TAPA_{30}$/water/octanol; $C_{12}TAPA_{30}$/water/octanol. Since the $C_{12}TAPA_{30}$/octanol system was not included in the previous studies, the reference phase diagram for these mixtures is lacking. The points indicate the calculated compositions and determined structures of the cores of our copolymer nanoparticles The color correspondence between the points and phase regions indicates the agreement between poly(acrylamide)-b-CS core structure and bulk phases, depending on the true n-alcohols compositions (X_a). Legends: C = cubic, H = hexagonal, L = lamellar, H_2 = reverse hexagonal, L_2 = reverse micelles. CS/water mass ratio along the phase sequence = 0.45. Fig. A reproduced from Ref. [90] with permission of The Royal Society of Chemistry. Figs. B and C reprinted with permission from ref. [98].
Copyright (2015) American Chemical Society. Fig. D reprinted with permission from ref. [104]. Copyright (2016) American Chemical Society.

control over the LC formed structures, giving grounds to the design of new materials with improved physicochemical properties for envisaged applications. It is important to highlight that such results were observed for stoichiometric polyion-surfactant ion "complex salts", free of counterions, where a more accurate control over the phase behavior is achieved, since the number of components is kept at a minimum, making it possible to study effects of adding or replacing a single component to the system. Therefore, the methodology of dispersing the components in the form of previously prepared complex salts is advantageous over the simple mixture of stoichiometric mixtures of polyelectrolyte and surfactant.

1.4. PE-S complex formation at solution interfaces

In contrast to the more commonly studied polyelectrolyte/surfactant complexes in bulk or in solution, the formation of such complexes at solution interfaces has been sparsely investigated and, until a short time ago, was far from being well understood. Aiming at the use of the full potential of such systems, new investigations in the fields of liquid crystals formed at polymer and surfactant solution interfaces due to electrostatic complexation became the focus of new investigations in the last years [85,94,100].

It is well known that LC structures have the ability to solubilize a diversity of agents with different physicochemical properties and interests because they are composed of hydrophilic and hydrophobic regions that can solubilize specific molecules, such as drugs, depending on the intermolecular interactions. Furthermore, it is also known that the type of LC structure controls the rate of drug release from these

aggregates [121]. Therefore, the highly ordered structures formed in oppositely charged surfactant and polymer systems can be exploited for application in drug delivery and release. Based on that, recent reports focused on the liquid crystalline phases formed at the interface between surfactant and polymer solutions, studying how the nanostructures are influenced by changes in the environment, such as temperature, concentration and pH, and the release of incorporated model drug from the LC structures [85,94,100].

It has been recently demonstrated [100] that complexes at solution interfaces can be formed by two different agents with important biological applications: colistin and heparin. Colistin is an amphiphilic polypeptide widely used as an antibiotic in infectious diseases. The protonation of the primary amine groups on colistin molecular structure at physiological pH establishes an overall positive charge [100]. Heparin is a highly sulfated anionic polysaccharide, composed of repeating glucosamine and uronic acid residues and plays a crucial role in various processes in the body such as blood coagulation, cell adhesion, cell growth, and inflammatory responses [122]. Concentrated solutions of colistin and heparin at charge equivalence can be brought into contact so that molecules are able to interact at a well-defined interface.

Birefringence at the liquid–liquid interface of the solutions containing the two species can be observed and is a qualitative indication of the formation of an anisotropic mesophase (Fig. 6A). SAXS confirmed the presence of a lamellar phase (L_α) at the colistin–heparin interface, with an interlamellar spacing (d) of 4.0 nm (Fig. 6A). Because such complexes formed by biocompatible species are envisaged towards biological applications, the pellet consisting of the colistin–heparin complex has been tested either for activity measurements against a strain of
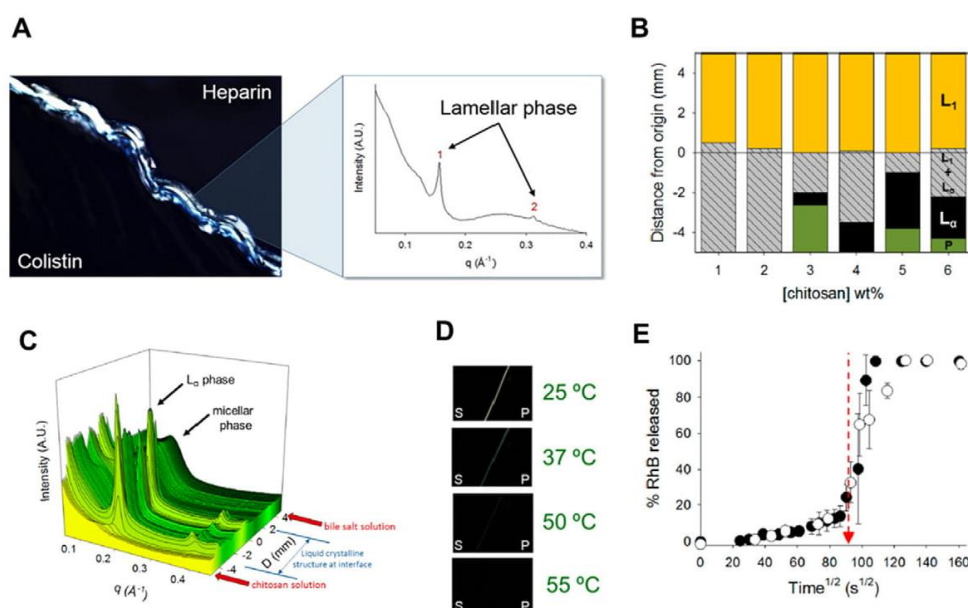
Fig. 6. A. Birefringence of the lamellar phase formed at the interface of 50 wt% colistin and 5 wt% heparin solutions observed under polarized light and the corresponding SAXS patterns with a 1:2 peak ratio reflections. B. Effect of polymer concentration on the liquid-crystalline phases evolution across the bile salt–chitosan interface. Bar charts illustrate regions of bulk polymer (P, green), micellar phase (L_1, yellow), coexisting micellar and lamellar phases ($L_1 + L_\alpha$, patterned gray), and pure lamellar phase (L_α, black). C. SAXS patterns as a function of distance solutions interface, D, in a system comprised of 4 wt% chitosan (bottom) and 30 wt% bile salt solution. D. Images taken of the sample under polarized light at different temperatures, illustrating the disappearance of birefringence at the surfactant–polymer interface above 50 °C. E. Cumulative release profile of Rhodamine B (RhB) from bile salt–chitosan capsules, where the environmental temperature was increased from 37 to 50 °C (●) or when the bile salt solution was replaced by 4% NaCl solution at 37 °C (○), as indicated by the dashed arrow. Fig. A reprinted with permission from ref. [100**].
Copyright (2016) American Chemical Society. Figs. B, C, D and E reprinted with permission from ref. [85**]. Copyright (2014) American Chemical Society.

bacteria and for its release behavior in aqueous media or NaCl solution. The role of added salt is also important since electrostatic interactions are partially screened when electrolytes are present. It is known that the complexation depends not only on salt concentration, but also on the nature of the ions [51,68,88,89**].

Interestingly, the authors have observed that the colistin/heparin complexes possess antimicrobial activity, suggesting that colistin is able to escape from the liquid crystalline structure into the surrounding medium keeping its native bactericidal activity. In addition, it has been also observed that saline solution is not a significant contributing factor to the release of colistin, indicating strong electrostatic interactions between the oppositely charged species in the complex. The relatively slow release of colistin from the lamellar phase gel complexes could provide means of delivering sustained release of an antibiotic and related antimicrobial activity. The viscosity of the lamellar gel phase would be important during the application process, where it is usually envisaged a more freely flowing formulation.

The complexation and formation of liquid crystalline structures at solution interfaces and surroundings have also been investigated for chitosan/bile salts systems [85**]. Bile salts are molecules with a steroidal skeleton, possessing hydrophobic groups on their convex surface, whereas the hydroxyl groups are located on the concave face. This arrangement renders bile salt molecules amphiphilicity, which is crucial for spontaneous aggregation in aqueous solution [123]. When approximately equal volumes of bile salt solution (30 wt% of sodium taurodeoxycholate) are mixed with the 4% chitosan solution within a flat cell, an interface is created, again, exhibiting birefringence, which was later confirmed to be lamellar (L_α) phase by SAXS, with an interlamellar spacing of 3.2 nm. In addition, a micellar isotropic phase has been reported to exist within bile salt solution, at around 4 mm away from the point of origin, which was indicated by the broad peak at low q values in the SAXS patterns (Fig. 6B and C). It has been demonstrated

that the polymer concentration plays an important role on the development of LC phase across the bile salt–chitosan interface, leading to considerable changes in the spatial distribution of the different formed phases within the solution (Fig. 6B). The authors have observed that the increase in polymer concentration have not influenced the type of phase formed at the interface or the interlamellar distance of the lamellar phase formed, but rather the extent to which L_α phase existed across the surfactant–polymer interface (Fig. 6B).

The structural integrity of the lamellar phase has been also examined in response to temperature and it was observed that this phase persists up until 45 °C, above which the highly ordered lamellar structure disappeared (Fig. 6D). The amount of lamellar phase formed in the bile salt–chitosan system was found to decrease upon exposure to salt solution, due to the weakening of binding between positively charged chitosan and negative bile salt in solution, probing the electrostatic interactions between such species. This demonstrates that changes in environmental conditions can modulate the lamellar phase and has potential for triggering release of specific agents from within the complexes. Aiming at the development of a responsive LC drug delivery system, the rate of diffusion of a model hydrophilic drug, Rhodamine B (RhB), from within capsules formed by the lamellar complex has been studied due to temperature and salt stimuli. Both triggers were shown to increase the rate of RhB release (Fig. 6E), confirming the potential application of these complexes in stimuli-responsive or sustained-release drug delivery.

1.5. Concluding remarks

Due to the numerous fields of potential applications for PE-S LC complexes, such systems have been widely investigated over the last twenty years. Such efforts have shown that a variety of nanoassemblies can be obtained, displaying different structural and physicochemical properties. Taking into account the different studied systems, general features

can be observed regarding the PE-S complexes. Although the LC structure is driven by surfactant self-assembly, the formation, shape and kinetic stability of such dispersed PE-S complexes are influenced by both polyelectrolyte and surfactant molecular architectures. It has been shown that depending on the nature of the polymer, being charged homopolymer or charged-neutral double hydrophilic block copolymer, either water-insoluble compact or water-dispersible core-shell particles are formed, respectively. The polyelectrolyte stiffness also plays an important role in the shape, arrangement of the complexes and solubility of the complexes in aqueous solution. The type of liquid crystalline resulting phases is highly dependent on the surfactant molecular geometry, since the surfactant assembled structure is retained in the complex formation. In this way, the knowledge on the phase behavior of surfactants in solution is highly demanded in order to improve the design of PE-S complexes holding LC structures.

It has been also observed that the formation and the presence or absence of LC phases depend on the environmental conditions, such as pH, temperature, and ionic strength, because they can alter the electrostatic and hydrophobic interactions that that govern this complexation. Their structural and colloidal features have been also demonstrated to be process-dependent, i.e., the mixing conditions influence the size, shape, stability, etc., in the obtained PE-S complexes, indicating the non-equilibrium nature of some of these aggregates. Another important feature is that although these dispersed complexes are comprised of kinetically-stabilized nanoparticles, they are able to reproduce some properties from bulk equilibrium phases.

Despite the fact that the systems have been widely studied in the last years, specific applications are still lacking. Significant effort has been made in order to study the release properties of PE-S-based drug delivery systems. However, no pharmaceutical product based on such complex mixtures is available elsewhere at the moment. Examples of LC particles already available in commercial formulations include cubosomes, which are dispersions of bicontinuous cubic lipid phases [121] and the PE-S LC particles present a large potential for similar uses. The hierarchical arrangement of PE-S particles is also an interesting field to be accurately studied, because previous reports have indicated the formation of colloidal crystals, i.e., highly ordered array of particles, formed by polymer-based assembles, which are now applied in different fields, such as photonics, optics and templating of nanostructured materials [124].

Acknowledgments

References and recommended reading^{*,**}

[1] Langevin D. Complexation of oppositely charged polyelectrolytes and surfactants in aqueous solutions. A review. Adv Colloid Interface Sci 2009;147–148:170–7. http://dx.doi.org/10.1016/j.cis.2008.08.013.

[2] Berret J-F. Controlling electrostatic co-assembly using ion-containing copolymers: from surfactants to nanoparticles. Adv Colloid Interface Sci 2011;167:38–48. http://dx.doi.org/10.1016/j.cis.2011.01.008.

[3] Piculell L. Understanding and exploiting the phase behavior of mixtures of oppositely charged polymers and surfactants in water. Langmuir 2013;29:10313–29. http://dx.doi.org/10.1021/la401026j.

[4] Kogej K. Association and structure formation in oppositely charged polyelectrolyte–surfactant mixtures. Adv Colloid Interface Sci 2010;158:68–83. http://dx.doi.org/10.1016/j.cis.2009.04.003.

[5] Chiappisi L, Hoffmann I, Gradzielski M. Complexes of oppositely charged polyelectrolytes and surfactants – recent developments in the field of biologically derived polyelectrolytes. Soft Matter 2013;9:3896–909. http://dx.doi.org/10.1039/C3SM27698H.

[6] Hansson P. Self-assembly of ionic surfactants in polyelectrolyte solutions: a model for mixtures of opposite charge. Langmuir 2001;17:4167–80. http://dx.doi.org/10.1021/la010390i.

[7] Zhao W, Wang Y. Coacervation with surfactants: from single-chain surfactants to gemini surfactants. Adv Colloid Interface Sci 2017;239:199–212. http://dx.doi.org/10.1016/j.cis.2016.04.005.

[8] Zhou S, Chu B. Assembled materials: polyelectrolyte–surfactant complexes. Adv Mater 2000;12:545–66.

[9] Piculell L, Norrman J, Svensson A, Lynch I, Bernardes JS, Loh W. Ionic surfactants with polymeric counterions. Adv Colloid Interface Sci 2009;147–148:228–36. http://dx.doi.org/10.1016/j.cis.2008.09.009.

[10] Thünemann AF. Polyelectrolyte–surfactant complexes (synthesis, structure and materials aspects). Prog Polym Sci 2002;27:1473–572. http://dx.doi.org/10.1016/S0079-6700(02)00017-5.

[11] Kizilay E, Basak Kayitmazer A, Dubin PL. Complexation and coacervation of polyelectrolytes with oppositely charged colloids. Adv Colloid Interface Sci 2011;167:24–37. http://dx.doi.org/10.1016/j.cis.2011.06.006.

[12] Gustavsson C, Li J, Edler KJ, Piculell L. Water-responsive internally structured polymer–surfactant films on solid surfaces. Langmuir 2014;30:12525–31. http://dx.doi.org/10.1021/la503210g.

[13] Gustavsson C, Obiols-Rabosa M, Piculell L. Water-insoluble surface coatings of polyion–surfactant ion complex salts respond to additives in a surrounding aqueous solution. Langmuir 2015;31:6487–96. http://dx.doi.org/10.1021/acs.langmuir.5b00831.

[14] Li J, Gustavsson C, Piculell L. Time- and space-resolved SAXS experiments inform on phase transition kinetics in hydrated, liquid-crystalline films of polyion–surfactant ion "complex salts". Langmuir 2016;32:5102–10. http://dx.doi.org/10.1021/acs.langmuir.6b00935.

[15] Koltover I, Salditt T, Rädler JO, Safinya CR. An inverted hexagonal phase of cationic liposome-DNA complexes related to DNA release and delivery. Science 1998;281:78–81. http://dx.doi.org/10.1126/science.281.5373.78.

[16] Rädler JO, Koltover I, Jamieson A, Salditt T, Safinya CR. Structure and interfacial aspects of self-assembled cationic lipid–DNA gene carrier complexes. Langmuir 1998;14:4272–83. http://dx.doi.org/10.1021/la980360o.

[17] Wasungu L, Hoekstra D. Cationic lipids, lipoplexes and intracellular delivery of genes. J Control Release 2006;116:255–64. http://dx.doi.org/10.1016/j.jconrel.2006.06.024.

[18] de Ilarduya CT, Sun Y, Düzgüneş N. Gene delivery by lipoplexes and polyplexes. Eur J Pharm Sci 2010;40:159–70. http://dx.doi.org/10.1016/j.ejps.2010.03.019.

[19] Holmberg K, Jönsson B, Kronberg B, Lindman B. Surfactants and polymers in aqueous solution. 2nd ed. Wiley; 2002.

[20] Nylander T, Samoshina Y, Lindman B. Formation of polyelectrolyte–surfactant complexes on surfaces. Adv Colloid Interface Sci 2006;123–126:105–23. http://dx.doi.org/10.1016/j.cis.2006.07.005.

[21] Chiappisi L, Gradzielski M. Co-assembly in chitosan–surfactant mixtures: thermodynamics, structures, interfacial properties and applications. Adv Colloid Interface Sci 2015;220:92–107. http://dx.doi.org/10.1016/j.cis.2015.03.003.

[22] Bronich TK, Kabanov AV, Kabanov VA, Yu K, Eisenberg A. Soluble complexes from poly(ethylene oxide)-block-polymethacrylate anions and N-alkylpyridinium Cations. Macromolecules 1997;30:3519–25. http://dx.doi.org/10.1021/ma9701970.

[23] Ilekti P, Piculell L, Tournilhac F, Cabane B. How to concentrate an aqueous polyelectrolyte/surfactant mixture by adding water. J Phys Chem B 1998;102:344–51. http://dx.doi.org/10.1021/jp972575x.

[24] Kabanov AV, Bronich TK, Kabanov VA, Yu K, Eisenberg A. Spontaneous formation of vesicles from complexes of block Ionomers and surfactants. J Am Chem Soc 1998;120:9941–2. http://dx.doi.org/10.1021/ja981922t.

[25] Zhou S, Yeh F, Burger C, Chu B. Formation and transition of highly ordered structures of polyelectrolyte–surfactant complexes. J Phys Chem B 1999;103:2107–12. http://dx.doi.org/10.1021/jp984331y.

[26] Wang Y, Kimura K, Dubin PL, Jaeger W. Polyelectrolyte–micelle coacervation: effects of micelle surface charge density, polymer molecular weight, and polymer/surfactant ratio. Macromolecules 2000;33:3324–31. http://dx.doi.org/10.1021/ma991886y.

[27] Kogej K, Evmenenko G, Theunissen E, Berghmans H, Reynaers H. Investigation of structures in polyelectrolyte/surfactant complexes by X-ray scattering. Langmuir 2001;17:3175–84. http://dx.doi.org/10.1021/la001249x.

[28] Merta J, Tokkeli M, Ikonen T, Serimaa R, Stenius P. Structure of cationic starch (CS)/anionic surfactant complexes studied by small-angle X-ray scattering (SAXS). Macromolecules 2001;34:2937–46. http://dx.doi.org/10.1021/ma001793c.

[29] Svensson A, Piculell L, Cabane B, Ilekti P. A new approach to the phase behavior of oppositely charged polymers and surfactants. J Phys Chem B 2002;106:1013–8. http://dx.doi.org/10.1021/jp0120458.

[30] Berret J-F, Cristobal G, Hervé P, Grillo I. Structure of colloidal complexes obtained from neutral/poly-electrolyte copolymers and oppositely charged surfactants. Eur Phys J E 2002;9:301–11.

[31] Hervé P, Destarac M, Berret J-F, Lal J, Oberdisse J, Grillo I. Novel core-shell structure for colloids made of neutral/polyelectrolyte diblock copolymers and oppositely charged surfactants. Europhys Lett 2002;58:912–8.

[32] Berret J-F, Hervé P, Aguerre-Chariol O, Oberdisse J. Colloidal complexes obtained from charged block copolymers and surfactants: a comparison between small-angle neutron scattering, Cryo-TEM, and simulations. J Phys Chem B 2003;107:8111–8. http://dx.doi.org/10.1021/jp027740+.

[33] Guillot S, Delsanti M, Désert S, Langevin D. Surfactant-induced collapse of polymer chains and monodisperse growth of aggregates near the precipitation boundary in carboxymethylcellulose–DTAB aqueous solutions. Langmuir 2003;19:230–7. http://dx.doi.org/10.1021/la0206561.

---

[*] Of special interest.
^{**} Of outstanding interest.

[34] Nizri G, Magdassi S, Schimdt J, Cohen Y, Talmon Y. Microstructural characterization of micro- and nanoparticles formed by polymer-surfactant interactions. Langmuir 2004;20:4380–5. http://dx.doi.org/10.1021/la0364441.

[35] Berret J-F, Vigolo B, Eng R, Hervé P, Grillo I, Yang L. Electrostatic self-assembly of oppositely charged copolymers and surfactants: a light, neutron, and X-ray scattering study. Macromolecules 2004;37:4922–30. http://dx.doi.org/10.1021/ma0498722.

[36] Zhou S, Liang D, Burger C, Yeh F, Chu B. Nanostructures of complexes formed by calf thymus DNA interacting with cationic surfactants. Biomacromolecules 2004;5: 1256–61. http://dx.doi.org/10.1021/bm034524d.

[37] Wang C, Tam KC. Interaction between polyelectrolyte and oppositely charged surfactant: effect of charge density. J Phys Chem B 2004;108:8976–82. http://dx.doi.org/10.1021/jp049647m.

[38] Wang X, Li Y, Li J, Wang J, Wang Y, Guo Z, et al. Salt effect on the complex formation between polyelectrolyte and oppositely charged surfactant in aqueous solution. J Phys Chem B 2005;109:10807–12. http://dx.doi.org/10.1021/jp0450585.

[39] Svensson A, Norrman J, Piculell L. Phase behavior of polyion-surfactant ion complex salts: effects of surfactant chain length and polyion length. J Phys Chem B 2006; 110:10332–40. http://dx.doi.org/10.1021/jp057402j.

[40] Bernardes JS, Norrman J, Piculell L, Loh W. Complex polyion-surfactant ions salts in equilibrium in water: changing aggregate shape and size by adding oil. J Phys Chem B 2006;110:23433–42. http://dx.doi.org/10.1021/jp0636165.

[41] Norrman J, Lynch I, Piculell L. Phase behavior of aqueous polyion-surfactant ion complex salts: effects of polyion charge density. J Phys Chem B 2007;111: 8402–10. http://dx.doi.org/10.1021/jp067303l.

[42] Trabelsi S, Albouy P-A, Impéror-Clerc M, Guillot S, Langevin D. X-ray diffraction study of the structure of carboxymethylcellulose–cationic surfactant complexes. ChemPhysChem 2007;8:2379–85. http://dx.doi.org/10.1002/cphc.200700378.

[43] Trabelsi S, Guillot S, Ritacco H, Boué F, Langevin D. Nanostructures of colloidal complexes formed in oppositely charged polyelectrolyte/surfactant dilute aqueous solutions. Eur Phys J E 2007;23:305–11. http://dx.doi.org/10.1140/epje/i2006-10192-y.

[44] Mezei A, Mészáros R, Varga I, Gilányi T. Effect of mixing on the formation of complexes of hyperbranched cationic polyelectrolytes and anionic surfactants. Langmuir 2007;23:4237–47. http://dx.doi.org/10.1021/la0635294.

[45] Pispas S. Complexes of polyelectrolyte-neutral hydrophilic block copolymers with oppositely charged surfactant and polyelectrolyte. J Phys Chem B 2007;111: 8351–9. http://dx.doi.org/10.1021/jp067437z.

[46] Pacios IE, Lindman B, Thuresson K. Polyelectrolyte–surfactant complexes with long range order. J Colloid Interface Sci 2008;319:330–7. http://dx.doi.org/10.1016/j.jcis.2007.11.029.

[47] Dubin PL, Li Y, Jaeger W. Mesophase separation in polyelectrolyte-mixed micelles coacervates. Langmuir 2008;24:4544–9. http://dx.doi.org/10.1021/la702405d.

[48] Nizri G, Lagerge S, Kamyshny A, Major DT, Magdassi S. Polymer–surfactant interactions: Binding mechanism of sodium dodecyl sulfate to poly(diallyldimethylammonium chloride). J Colloid Interface Sci 2008;320:74–81. http://dx.doi.org/10.1016/j.jcis.2008.01.016.

[49] Kelarakis A, Castelletto V, Krysmann MJ, Havredaki V, Viras K, Hamley IW. Polymer−surfactant vesicular complexes in aqueous medium. Langmuir 2008; 24:3767–72. http://dx.doi.org/10.1021/la703745z.

[50] Onesippe C, Lagerge S. Study of the complex formation between sodium dodecyl sulfate and chitosan. Colloids Surf A 2008;317:100–8. http://dx.doi.org/10.1016/j.colsurfa.2007.10.002.

[51] Hammond MR, Li C, Tsitsilianis C, Mezzenga R. Hierarchical self-organization in polyelectrolyte-surfactant complexes based on heteroarm star block copolyampholytes. Soft Matter 2009;5:2371–7. http://dx.doi.org/10.1039/b817219f.

[52] Nizri G, Makarasky A, Magdassi S, Talmon Y. Nanostructures formed by self-assembly of negatively charged polymer and cationic surfactants. Langmuir 2009;24:1980–5. http://dx.doi.org/10.1021/la8031013.

[53] Pojják K, Mészáros R. Novel self-assemblies of oppositely charged polyelectrolytes and surfactants in the presence of neutral polymer. Langmuir 2009;25:13336–9. http://dx.doi.org/10.1021/la903761r.

[54] Liberatore MW, Wyatt NB, Henry M, Dubin PL, Foun E. Shear-induced phase separation in polyelectrolyte/mixed micelle coacervates. Langmuir 2009;25:13376–83. http://dx.doi.org/10.1021/la903260r.

[55] Ábrahám Á, Mezei A, Mészáros R. The effect of salt on the association between linear cationic polyelectrolytes and sodium dodecyl sulfate. Soft Matter 2009;5: 3718–26. http://dx.doi.org/10.1039/B903158H.

[56] Svensson AV, Huang L, Johnson ES, Nylander T, Piculell L. Surface deposition and phase behavior of oppositely charged polyion/surfactant ion complexes. 1. Cationic guar versus cationic hydroxyethylcellulose in mixtures with anionic surfactants. ACS Appl Mater Interfaces 2009;1:2431–42. http://dx.doi.org/10.1021/am900378b.

[57] Bilalov A, Olsson U, Lindman B. A cubic DNA-lipid complex. Soft Matter 2009;5: 3827–30. http://dx.doi.org/10.1039/B908939J.

[58] Knaapila M, Evans RC, Garamus VM, Almásy L, Székely NK, Gutacker A, et al. Structure and "Surfactochromic" properties of conjugated polyelectrolyte (CPE): surfactant complexes between a cationic polythiophene and SDS in water. Langmuir 2010;26:15634–43. http://dx.doi.org/10.1021/la102591b.

[59] Kristen N, von Klitzing R. Effect of polyelectrolyte/surfactant combinations on the stability of foam films. Soft Matter 2010;6:849–61. http://dx.doi.org/10.1039/B917297A.

[60] Bykova AG, Lina S-Y, Logliob G, Lyadinskayac VV, Millerd R, Noskov BA. Impact of surfactant chain length on dynamic surface properties of alkyltrimethylammonium bromide/polyacrylic acid solutions. Colloids Surf A 2010;354:382–9. http://dx.doi.org/10.1016/j.colsurfa.2009.09.015.

[61] Bonnaud M, Weiss J, McClements DJ. Interaction of a food-grade cationic surfactant (Lauric Arginate) with food-grade biopolymers (pectin, carrageenan, xanthan, alginate, dextran, and chitosan). J Agric Food Chem 2010;58:9770–7. http://dx.doi.org/10.1021/jf101309h.

[62] Wang H, Wang Y. Studies on interaction of poly(sodium acrylate) and poly(sodium styrenesulfonate) with cationic surfactants: effects of polyelectrolyte molar mass, chain flexibility, and surfactant architecture. J Phys Chem B 2010;114:10409–16. http://dx.doi.org/10.1021/jp9102405.

[63] Bernardes JS, Piculell L, Loh W. Self-assembly of polyion-surfactant ion complex salts in mixtures with water and n-alcohols. J Phys Chem B 2011;115:9050–8. http://dx.doi.org/10.1021/jp202413q.

[64] Kizilay E, Maccarrone S, Foun E, Dinsmore AD, Dubin PL. Cluster formation in polyelectrolyte−micelle complex coacervation. J Phys Chem B 2011;115: 7256–63. http://dx.doi.org/10.1021/jp109788r.

[65] Pojják K, Mészáros R. Preparation of stable electroneutral nanoparticles of sodium dodecyl sulfate and branched poly(ethylenimine) in the presence of pluronic F108 copolymer. Langmuir 2011;27:14797–806. http://dx.doi.org/10.1021/la203759r.

[66] Štěpánek M, Matějíček P, Procházka K, Filippov SG, Angelov B, Šlouf M, et al. Polyelectrolyte−surfactant complexes formed by poly[3,5-bis(trimethylammoniummethyl)4-hydroxystyrene iodide]-block-poly(ethylene oxide) and sodium dodecyl sulfate in aqueous solutions. Langmuir 2011; 27:5275–81. http://dx.doi.org/10.1021/la200442s.

[67] Hoffmann I, Heunemann P, Prévost S, Schweins R, Wagner NJ, Gradzielski M. Self-aggregation of mixtures of oppositely charged polyelectrolytes and surfactants studied by rheology, dynamic light scattering and small-angle neutron scattering. Langmuir 2011;27:4386–96. http://dx.doi.org/10.1021/la104588b.

[68] Pojják K, Bertalanits E, Mészáros R. Effect of salt on the equilibrium and nonequilibrium features of polyelectrolyte/surfactant association. Langmuir 2011;27: 9139–47. http://dx.doi.org/10.1021/la2021353.

[69] Percebom AM, Piculell L, Loh W. Polyion–surfactant ion complex salts formed by a random anionic copolyacid at different molar ratios of cationic surfactant: phase behavior with water and n-alcohols. J Phys Chem B 2012;116:2376–84. http://dx.doi.org/10.1021/jp2103403.

[70] Golan S, Talmon Y. Nanostructure of complexes between cationic lipids and an oppositely charged polyelectrolyte. Langmuir 2012;28:1668–72. http://dx.doi.org/10.1021/la204095s.

[71] Uchman M, Stepanek M, Prevost S, Angelov B, Bednar J, Appavou MS, et al. Coassembly of poly(ethylene oxide)-block-poly(methacrylic acid) and N-Dodecylpyridinium chloride in aqueous solutions leading to ordered micellar assemblies within copolymer aggregates. Macromolecules 2012;45:6471–80. http://dx.doi.org/10.1021/ma301510j.

[72] Li D, Kelkar MS, Wagner NJ. Phase behavior and molecular thermodynamics of coacervation in oppositely charged polyelectrolyte/surfactant systems: a cationic polymer JR 400 and anionic surfactant SDS mixture. Langmuir 2012;28: 10348–62. http://dx.doi.org/10.1021/la301475s.

[73] Sitar S, Goderis B, Hansson P, Kogej K. Phase diagram and structures in mixtures of poly(styrenesulfonate anion) and alkyltrimethylammonium cations in water: significance of specific hydrophobic interaction. J Phys Chem B 2012;116:4634–45. http://dx.doi.org/10.1021/jp212263b.

[74] Li L, Rosenthal M, Zhang H, Hernandez JJ, Drechsler M, Phan KH, et al. Light-switchable vesicles from liquid-crystalline homopolymer−surfactant complexes. Angew Chem Int Ed 2012;51:11616–9. http://dx.doi.org/10.1002/anie.201205660.

[75] Carlstedt J, Bilalovab A, Olsson U. Aqueous phase behavior of polyelectrolytes with amphiphilic counterions modulated by cyclodextrin: the role of polyion flexibility. Phys Chem Chem Phys 2012;14:9574–7. http://dx.doi.org/10.1039/C2CP41353A.

[76] Bilalov A, Carlstedt J, Krivstova E, Lindman B, Olsson U. DNA with amphiphilic counterions: tuning colloidal DNA with cyclodextrin. Soft Matter 2012;8: 4988–94. http://dx.doi.org/10.1039/C2SM25058F.

[77] Štěpánek M, Škvarla J, Uchman M, Procházka K, Angelov B, Kováčik L, et al. Worm-like core–shell nanoparticles formed by co-assembly of double hydrophilic block polyelectrolyte with oppositely charged fluorosurfactant. Soft Matter 2012;8: 9412–7. http://dx.doi.org/10.1039/C2SM25588J.

[78] Hajduová J, Procházka K, Šlouf M, Angelov B, Mountrichas G, Pispas S, et al. Polyelectrolyte–surfactant complexes of poly[3,5-bis(dimethylaminomethyl)-4-hydroxystyrene]-block-poly(ethylene oxide) and sodium dodecyl sulfate: anomalous self-assembly behavior. Langmuir 2013;29:5443–9. http://dx.doi.org/10.1021/la400583z.

[79] Kizilay E, Dinsmore AD, Hoagland DA, Sund L, Dubin PL. Evolution of hierarchical structures in polyelectrolyte−micelle coacervate. Soft Matter 2013;9:7320–32. http://dx.doi.org/10.1039/C3SM50591J.

[80] Pojják K, Fegyver E, Mészáros R. Effect of linear nonionic polymer additives on the kinetic stability of dispersions of poly(diallyldimethylammonium chloride)/sodium dodecylsulfate nanoparticles. Langmuir 2013;29:10077–86. http://dx.doi.org/10.1021/la4021542.

[81] Vitorazi L, Berret J-F, Loh W. Self-assembly of complex salts of cationic surfactants and anionic–neutral block copolymers. Dispersions with liquid-crystalline internal structure. Langmuir 2013;29:14024–33. http://dx.doi.org/10.1021/la402624u.

[82] Uchman M, Gradzielski M, Angelov B, Tosner Z, Oh J, Chang T, et al. Thermodynamic and kinetic aspects of coassembly of PEO–PMAA block copolymer and DPCl surfactants into ordered nanoparticles in aqueous solutions studied by ITC, NMR, and time-resolved SAXS techniques. Macromolecules 2013;46:2172–81. http://dx.doi.org/10.1021/ma302503w.

[83] Percebom AM, Barbosa LRS, Itri R, Loh W. How does the ethoxylated grafting of polyelectrolytes affect the self-assembly of polyanion–cationic surfactant complex salts? Langmuir 2014;30:11493–503. http://dx.doi.org/10.1021/la5019604.

[84] Fegyver E, Mészáros R. Fine-tuning the nonequilibrium behavior of oppositely charged macromolecule/surfactant mixtures via the addition of nonionic amphiphiles. Langmuir 2014;30:15114–26. http://dx.doi.org/10.1021/la503928x.

[85] Tangso KJ, Lindberg S, Hartley PG, Knott R, Spicer P, Boyd BJ. Formation of liquid-crystalline structures in the bile salt–chitosan system and triggered release from lamellar phase bile salt–chitosan capsules. ACS Appl Mater Interfaces 2014;6: 12363–71. http://dx.doi.org/10.1021/am502192t.

[86] Chiappisi L, Prévost S, Grillo I, Gradzielski M. Chitosan/alkylethoxy carboxylates: a surprising variety of structures. Langmuir 2014;30:1778–87. http://dx.doi.org/10.1021/la404718e.

[87] Chiappisi L, Prévost S, Grillo I, Gradzielski M. From crab shells to smart systems: chitosan–alkylethoxy carboxylate complexes. Langmuir 2014;30:10608–16. http://dx.doi.org/10.1021/la502569p.

[88] Lin J-H, Hou S-S. Effects of organic salts on polymer–surfactant interactions: roles of Bu₄NBr and Pr₄NBr in PVP–SDS complexation. Macromolecules 2014;47:6418–29. http://dx.doi.org/10.1021/ma5012232.

[89] Wytrwal M, Bednar J, Nowakowska M, Wydro P, Kepczynska M. Interactions of serum with polyelectrolyte-stabilized liposomes: Cryo-TEM studies. Colloids Surf B 2014;120:152–9. http://dx.doi.org/10.1016/j.colsurfb.2014.02.040.

[90] Fegyver E, Mészáros R. The impact of nonionic surfactant additives on the nonequilibrium association between oppositely charged polyelectrolytes and ionic surfactants. Soft Matter 2014;10:1953–62. http://dx.doi.org/10.1039/C3SM52889H.

[91] Janiak J, Tomšič M, Lundberg D, Olofsson G, Piculell L, Schillén K. Soluble aggregates in aqueous solutions of polyion–surfactant ion complex salts and a nonionic surfactant. J Phys Chem B 2014;118:9745–56. http://dx.doi.org/10.1021/jp411701g.

[92] Ábrahám Á, Kardos A, Mezei A, Campbell RA, Varga I. Effects of ionic strength on the surface tension and nonequilibrium interfacial characteristics of poly(sodium styrenesulfonate)/dodecyltrimethylammonium bromide mixtures. Langmuir 2014;30:4970–9. http://dx.doi.org/10.1021/la500637v.

[93] Zakrevskyy Y, Cywinski P, Cywinska M, Paasche J, Lomadze N, Reich O, et al. Interaction of photosensitive surfactant with DNA and poly acrylic acid. J Chem Phys 2014. http://dx.doi.org/10.1063/1.4862679.

[94] Tangso JK, Patel H, Lindberg S, Hartley PG, Knott R, Spicer PT, et al. Controlling the mesostructure formation within the Shell of novel cubic/hexagonal phase cetyltrimethylammonium bromide–poly(acrylamide-acrylic acid) capsules for pH stimulated release. ACS Appl Mater Interfaces 2015;7:24501–9. http://dx.doi.org/10.1021/acsami.5b05821.

[95] Bračič M, Hansson P, Pérez L, Zemljič LF, Kogej K. Interaction of sodium hyaluronate with a biocompatible cationic surfactant from lysine: a binding study. Langmuir 2015;31:12043–53. http://dx.doi.org/10.1021/acs.langmuir.5b03548.

[96] Fegyver E, Mészáros R. Complexation between sodium poly(styrenesulfonate) and alkyltrimethylammonium bromides in the presence of dodecyl maltoside. J Phys Chem B 2015;119:5336–46. http://dx.doi.org/10.1021/acs.jpcb.5b01206.

[97] Covisa R, Vivesa T, Gaillardc C, Benoitd M, Benvegnua T. Interactions and hybrid complex formation of anionic algal polysaccharides with a cationic glycine betaine-derived surfactant. Carbohydr Polym 2015;121:436–48. http://dx.doi.org/10.1016/j.carbpol.2015.01.001.

[98] Plazzotta B, Fegyver E, Mészáros R, Pedersen JS. Anisometric polyelectrolyte/mixed surfactant nanoassemblies formed by the association of poly(diallyldimethylammonium chloride) with sodium dodecyl sulfate and dodecyl maltoside. Langmuir 2015;31:7242–50. http://dx.doi.org/10.1021/acs.langmuir.5b01280.

[99] Sharipova AA, Aidarova SB, Grigoriev D, Mutalieva B, Madibekova G, Tleuova A, et al. Polymer–surfactant complexes for microencapsulation of vitamin E and its release. Colloids Surf B Biointerfaces 2016;137:152–7. http://dx.doi.org/10.1016/j.colsurfb.2015.03.063.

[100] Tangso KJ, da Cunha PHCD, Spicer P, Li J, Boyd BJ. Antimicrobial activity from colistin–heparin lamellar-phase complexes for the coating of biomedical devices. ACS Appl Mater Interfaces 2016;8:31321–9. http://dx.doi.org/10.1021/acsami.6b10027.

[101] Delisavva F, Uchman M, Škvarla J, Woźniak E, Pavlova E, Šlouf M, et al. Influence of corona structure on binding of an ionic surfactant in oppositely charged amphiphilic polyelectrolyte micelles. Langmuir 2016;32:4059–65. http://dx.doi.org/10.1021/acs.langmuir.6b00700.

[102] Bodnár K, Fegyver E, Nagy M, Mészáros R. Impact of polyelectrolyte chemistry on the thermodynamic stability of oppositely charged macromolecule/surfactant mixtures. Langmuir 2016;32:1259–68. http://dx.doi.org/10.1021/acs.langmuir.5b04431.

[103] Ram-On M, Cohen Y, Talmon Y. Effect of polyelectrolyte stiffness and solution pH on the nanostructure of complexes formed by cationic amphiphiles and negatively charged polyelectrolytes. J Phys Chem B 2016;120:5907–15. http://dx.doi.org/10.1021/acs.jpcb.6b01138.

[104] Ferreira GA, Loh W. Addition of n-alcohols induces a variety of liquid-crystalline structures in surfactant-rich cores of dispersed block copolymer/surfactant nanoparticles. ACS Omega 2016;1:1104–13. http://dx.doi.org/10.1021/acsomega.6b00267.

[105] Szczepanowicz K, Para G, Wilk KA, Warszyński P. Co-adsorption of polyanions and esterquat surfactants; effect on formation and stability of micellar core nanocapsules. Colloids Surf A 2017;519:117–24. http://dx.doi.org/10.1016/j.colsurfa.2016.07.069.

[106] di Gregorio MC, Gubitosi M, Travaglini L, Pavel NV, Jover A, Meijide F, et al. Supramolecular assembly of a thermoresponsive steroidal surfactant with an oppositely charged thermoresponsive block copolymer. Phys Chem Chem Phys 2017;19: 1504–15. http://dx.doi.org/10.1039/C6CP05665B.

[107] Kaczmarek D, Diget JS, Nyström B, Gyulaia G, Mészáros R, Gilányi T, Varga I. Response of block copolyelectrolyte complexes to addition of ionic surfactants. Colloids Surf A 2017. http://dx.doi.org/10.1016/j.colsurfa.2017.04.078 in press.

[108] Gerola AP, Wanderlind EH, Gomes YS, Giusti LA, García-Río L, Nome RA, et al. Supramolecular polymer/surfactant complexes as catalysts for phosphate transfer reactions. ACS Catal 2017;7:2230–9. http://dx.doi.org/10.1021/acscatal.7b00097.

[109] Voets IK, de Keizer E, Stuart MAC. Complex coacervate core micelles. Adv Colloid Interface Sci 2009;147–148:300–18. http://dx.doi.org/10.1016/j.cis.2008.09.012.

[110] Pergushov DV, Müller AH, Schacher FH. Micellar interpolyelectrolyte complexes. Chem Soc Rev 2012;41:6888–901. http://dx.doi.org/10.1039/c2cs35135h.

[111] Cooper CL, Dubin PL, Kayitmazer AB, Turksen S. Polyelectrolyte–protein complexes. Curr Opin Colloid Interface Sci 2005;10:52–78. http://dx.doi.org/10.1016/j.cocis.2005.05.007.

[112] Antonietti M, Conrad J, Thünemann AF. Polyelectrolyte-surfactant complexes: a new type of solid, mesomorphous material. Macromolecules 1994;27:6007–11. http://dx.doi.org/10.1021/ma00099a011.

[113] Antonietti M, Burger C, Thünemann AF. Polyelectrolyte-surfactant complexes: a new class of highly ordered polymer materials. Trends Polym Sci 1997;5:262–7.

[114] Ober CK, Wegner G. Polyelectrolyte–surfactant complexes in the solid state: facile building blocks for self-organizing materials. Adv Mater 1997;9:17–31. http://dx.doi.org/10.1002/adma.19970090104.

[115] Antunes FE, Marques EF, Miguel MG, Lindman B. Polymer–vesicle association. Adv Colloid Interface Sci 2009;147–148:18–35. http://dx.doi.org/10.1016/j.cis.2008.10.001.

[116] Sastry NV, Hoffmann H. Interaction of amphiphilic block copolymer micelles with surfactants. Colloids Surf A 2004;250:247–61. http://dx.doi.org/10.1016/j.colsurfa.2004.07.025.

[117] Pispas S. Soluble complexes of sodium poly(isoprene-*b*-methacrylate) micelles with cationic surfactants in aqueous media. J Phys Chem B 2006;110:2649–55. http://dx.doi.org/10.1021/jp056008i.

[118] Jacquin M, Muller P, Cottet H, Crooks R, Théodoly O. Controlling the melting of kinetically frozen poly(butyl acrylate-*b*-acrylic acid) micelles via addition of surfactant. Langmuir 2007;23:9939–48. http://dx.doi.org/10.1021/la700370f.

[119] Thalberg K, Lindman B. Interaction between hyaluronan and cationic surfactants. J Phys Chem 1989;93:1478–83. http://dx.doi.org/10.1021/j100341a058.

[120] Rinaudo M. Chitin and chitosan: Properties and applications. Prog Polym Sci 2006; 31:603–32. http://dx.doi.org/10.1016/j.progpolymsci.2006.06.001.

[121] Guo C, Wang J, Cao F, Lee RJ, Zhai G. Lyotropic liquid crystal systems in drug delivery. Drug Discov Today 2010;15:1032–40. http://dx.doi.org/10.1016/j.drudis.2010.09.006.

[122] Rabenstein DL. Heparin and heparan sulfate: structure and function. Nat Prod Rep 2002;19:312–33. http://dx.doi.org/10.1039/B100916H.

[123] Ju C, Bohne C. Dynamics of probe complexation to bile salt aggregates. J Phys Chem 1996;100:3847–54. http://dx.doi.org/10.1021/jp952657q.

[124] Xia Y, Gates B, Yin Y, Lu Y. Monodispersed colloidal spheres: old materials with new applications. Adv Mater 2000;12:693–713. http://dx.doi.org/10.1002/(SICI)1521-4095(200005)12:10<693::AID-ADMA693>3.0.CO;2-J.

Copyright Clearance Center

RightsLink®

Home | Account Info | Help | ✉

Title:	Liquid crystalline nanoparticles formed by oppositely charged surfactant-polyelectrolyte complexes
Author:	Guilherme A. Ferreira, Watson Loh
Publication:	Current Opinion in Colloid & Interface Science
Publisher:	Elsevier
Date:	November 2017

© 2017 Elsevier Ltd. All rights reserved.

Logged in as:
Guilherme Ferreira
Account #:
3001166781

LOGOUT

BACK | CLOSE WINDOW

Paper II

Addition of *n*-Alcohols Induces a Variety of Liquid-Crystalline Structures in Surfactant-Rich Cores of Dispersed Block Copolymer/Surfactant Nanoparticles

Guilherme A. Ferreira,[†] Lennart Piculell,[‡] and Watson Loh*,[†]

[†]Institute of Chemistry, University of Campinas (UNICAMP), P.O. Box 6154, 13083-970 Campinas, São Paulo, Brazil
[‡]Division of Physical Chemistry, Lund University, P.O. Box 124, S-221 00 Lund, Sweden

 Supporting Information

ABSTRACT: Poly(acrylamide)-*b*-complex salts made from a symmetric poly(acrylate-*b*-acrylamide) block copolymer, where the acrylate charges are neutralized by cationic surfactant counterions, form kinetically stable aqueous dispersions of hierarchical aggregates with a liquid-crystalline complex salt core and a diffuse hydrated shell. By the addition of suitable amounts of long-chain alcohols, such as octanol or decanol, the structure of the internal phase can be varied, producing micellar cubic, hexagonal, lamellar, or reverse hexagonal liquid-crystalline phases. In addition, a disordered reverse micellar phase forms at the highest content of octanol. These core structures are the same as those previously obtained for macroscopic homopolymer poly(acrylate) complex salt/water/*n*-alcohol systems at the corresponding compositions. The poly-(acrylamide)-*b*-complex salt dispersions are kinetically stable for several weeks, with their colloidal properties and internal structures remaining unchanged. The methodology described here establishes an easy and robust protocol for the preparation of colloidal nanoparticles with variable but controlled internal structures.
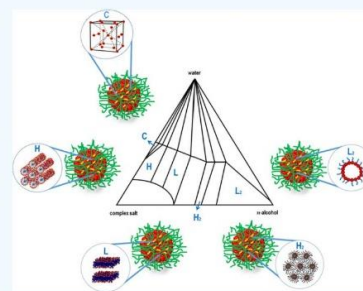
■ INTRODUCTION

Several studies of water-dispersible core–shell nanoparticles made from charged–neutral block copolymers and oppositely charged surfactants have been reported in the last years.[1−6] The most studied systems involve alkyltrimethylammonium cationic surfactants and the block copolymer poly(acrylic acid-*b*-acrylamide) [P(AA-*b*-AAm)].[1−3,5,6] When such complexes are prepared by mixing individual aqueous solutions of the charged–neutral block copolymer and the charged surfactant, the species associates into colloidal complexes in the form of core–shell nanoparticles. In addition, these solutions contain the original simple counterions of the charged polymer and the surfactant. The core of the nanoparticle contains densely packed surfactant micelles surrounded by polyion blocks. The outer part of the colloidal complex is a corona composed of neutral poly(acrylamide) blocks. Further studies revealed that the micelles in the core of the particles, prepared as described, were arranged in a disordered state, showing no long-range order.[1,2,5,6]

The use of stoichiometric polyion–surfactant ion "complex salts" (CSs), free of other ions, was proposed a few years ago as an alternative strategy to study the phase behavior of polymer/surfactant complexes. The principal advantage of this strategy is that the number of components is kept at a minimum, making it possible to study the effects of adding a single component to the system or replacing one by another, in isolation. This allowed the determination of truly binary phase diagrams for CS mixtures with water[7−9] and the assessment of the effect of added *n*-alcohols or other organic solvents on their ternary phase behavior.[10−13] On the basis of this methodology, our group has recently reported studies using poly(acrylamide)-*b*-CS block copolymers containing the hydrophilic block copolymer poly(acrylate-*b*-acrylamide), neutralized by dodecyl-trimethylammonium counterions, to produce core–shell nanoparticles dispersed in an aqueous medium.[3] Notably, the dispersions produced from the block copolymers containing stoichiometric CSs invariably gave nanoparticle cores displaying a micellar cubic liquid-crystalline structure, agreeing with that previously observed for maximally water-swollen homopolymer dodecyltrimethylammonium–polyacrylate CS.[8−10] Nanoparticles prepared by mixing individual aqueous solutions of the anionic–neutral block copolymer and the cationic surfactant, referred here as "conventionally prepared", behave different from that obtained by dispersing poly(acrylamide)-*b*-CS in water, as will be described in the present report.

Nanoparticles with liquid-crystalline cores are known to be formed by different chemical systems. Examples include the cubosomes,[14] which are dispersions of bicontinuous cubic phases studied for their potential for drug delivery. Other more recent examples are from studies reported by Lindman and co-

workers,[15] and in the last few years, reports by Uchman[16] have described internally structured particles using the complexation between surfactants and polyions. During the past years, a series of studies have reported the formation of colloidal complexes made from oppositely charged surfactants and charged–neutral block copolymers.[1,2,4–6,17,18] These liquid-crystalline nanoparticles have also been studied aiming at the control and change of their internal structures by specific triggers such as enzymes[19] and near infrared light,[20] to make them suitable for important practical applications such as drug delivery. It has previously been shown that, for example, differences in the liquid-crystalline structure can change the drug diffusion and hence the release, with research progressing toward the use of in situ changes to control the drug release by these liquid-crystalline matrices.[21]

In this work, we have expanded our studies of dispersions containing stoichiometric CSs of the symmetric block copolymer P(AA$_{42}$-b-AAm$_{42}$) and dodecyl- or hexadecyltrimethylammonium cationic surfactants (C$_{12}$TA$^+$ and C$_{16}$TA$^+$) with the aim to achieve additional internal structures by adding long-chain alcohols. This strategy is based on the previous experience of systems formed by the corresponding homopolymer CS, water, and various n-alcohols.[10–13] Small angle X-ray scattering (SAXS) has been used to identify and characterize the liquid-crystalline interior of the aggregates. In addition, the average radius and the zeta potential of the colloidal nanoparticles have been investigated.

■ RESULTS

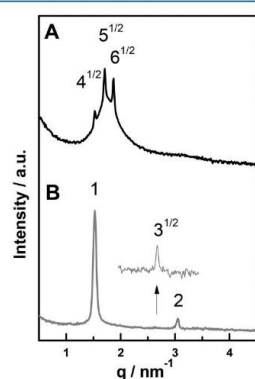**Internal Structure.** *Poly(acrylamide)-b-CS Nanoparticles Dispersed in Water.* Figure 1 shows the SAXS patterns

Figure 1. SAXS patterns obtained for (A) PAAm$_{42}$-b-C$_{12}$TAPA$_{42}$ nanoparticles displaying a cubic internal structure and (B) PAAm$_{42}$-b-C$_{16}$TAPA$_{42}$ nanoparticles with a hexagonal interior. Samples containing 1.0 wt % of poly(acrylamide)-b-CS, analyzed at 25 °C.

obtained for dispersions of PAAm$_{42}$-b-C$_{12}$TAPA$_{42}$ or PAAm$_{42}$-b-C$_{16}$TAPA$_{42}$ in water. The scattering peaks (Figure 1A) for the former system had a spacing ratio of $4^{1/2}$:$5^{1/2}$:$6^{1/2}$, indicating a $Pm\bar{3}n$ cubic structure. For the PAAm$_{42}$-b-C$_{16}$TAPA$_{42}$ dispersion (Figure 1B), the peak positions at 1:$3^{1/2}$:2 reveal a hexagonal $P6mm$ structure. The lattice parameter for the cubic structure in PAAm$_{42}$-b-C$_{12}$TAPA$_{42}$ is 8.40 nm, which is very similar to that previously obtained in the dodecyltrimethylammonium–poly-(acrylate) CS/water bulk cubic phase.[9,10] A similar close

correspondence has been recently observed between the cubic structures of the homopolymer CS and the cubic cores of CS nanoparticles from asymmetric poly(acrylamide)-b-CS block copolymers.[3] For the hexagonal phase in the PAAm$_{42}$-b-C$_{16}$TAPA$_{42}$ core, we now find a = 4.84 nm, also in very close agreement with the bulk phase formed in the corresponding hexadecyltrimethylammonium–poly(acrylate) CS/water system.[9,10]

n-Alcohol-Loaded Nanoparticles. Previous studies have shown that long-chain n-alcohols added to aqueous homopolymer CSs induce a series of phase changes as the ratio of alcohol/CS increases in the mixed aggregates.[10,12] To prepare nanoparticles with different internal liquid-crystalline structures, different amounts of octanol and decanol were added to the poly(acrylamide)-b-CS block copolymer dispersions, exploiting the cosurfactant behavior of the n-alcohols. Table 1 summarizes the results obtained at different n-alcohol/CS mass ratios (R), including $R = 0$. It is important to note that the R values were calculated taking into account only the CS block of the poly(acrylamide)-b-CSs. Now, the findings for each of the four combinations of CS and n-alcohol will be described in detail.

PAAm$_{42}$-b-C$_{12}$TAPA$_{42}$ Nanoparticles + Octanol or Decanol. For increasing *decanol* contents in the aqueous dispersions of PAAm$_{42}$-b-C$_{12}$TAPA$_{42}$, the internal structure of the aggregates changed in the following sequence: cubic, normal hexagonal, and lamellar. At a low decanol content ($R = 0.256$), the CS core displays a normal hexagonal phase with Bragg peak positions of 1:$3^{1/2}$:2 in the SAXS patterns (Figure 2A). When the decanol fraction is increased further ($R = 0.613$), SAXS peaks with a spacing ratio of 1:2:3 indicate the formation of a lamellar structure (Figure 2B). The same sequence of structures, as with decanol, was observed with added *octanol* (Figure 2C,D). SAXS patterns for additional decanol and octanol concentrations in PAAm$_{42}$-b-C$_{12}$TAPA$_{42}$ dispersions (see Table 1), indicating hexagonal and lamellar structures, are presented in Figure S1. The repeat distances (d) between the bilayers in the lamellar structures in the core of PAAm$_{42}$-b-C$_{12}$TAPA$_{42}$ nanoparticles was 4.72 nm when using decanol and d = 4.68 nm for octanol.

PAAm$_{42}$-b-C$_{16}$TAPA$_{42}$ Nanoparticles + Octanol or Decanol. Figure 3 shows the SAXS patterns obtained for PAAm$_{42}$-b-C$_{16}$TAPA$_{42}$ nanoparticles with different amounts of *decanol*. At a low decanol content ($R = 0.142$), the SAXS pattern (Figure 3A) from the complex showed scattering peaks with a spacing ratio of 1:$3^{1/2}$:$4^{1/2}$:$7^{1/2}$, indicating a structure with hexagonal packing of cylindrical micelles, as for the alcohol-free sample (Figure 1B). However, some other peaks also appear. These peaks show a regular spacing ratio of 1:2:3, indicating a Pm space group for a lamellar structure being formed inside of the nanoparticles. Therefore, this SAXS pattern could be attributed to a mixture of two different structures of Pm lamellar and $P6mm$ hexagonal. Further addition of decanol ($R = 0.321$) leads to the formation of a pure lamellar phase, with d = 4.34 nm (Figure 3B). SAXS patterns for other decanol compositions (see Table 1) indicating a lamellar structure, with d = 4.34 nm, are presented in Figure S2.

With increasing contents of *octanol*, the CS core of PAAm$_{42}$-b-C$_{16}$TAPA$_{42}$ nanoparticles changed from normal to inverted structures. At low octanol contents ($R = 0.818$), the SAXS pattern revealed 1:2 Bragg reflections, indicating a lamellar structure, with d = 4.31 nm (Figure 4A). As more octanol was added ($R = 4.067$), the peak positions at 1:$3^{1/2}$:2 (Figure 4B) revealed that another hexagonal structure was achieved. There are two possible 2D hexagonal structures. One is the normal

Table 1. Liquid-Crystalline Structures and Their Lattice Parameters for Poly(acrylamide)-*b*-CS Nanoparticles at Varying *n*-Alcohol/CS Mass Ratios (*R*)

poly(acrylamide)-*b*-CS	*R* (octanol)	*R* (decanol)	core structure	lattice parameter
PAAm$_{42}$-*b*-C$_{12}$TAPA$_{42}$	0	0	cubic	a = 8.40 nm
	0.256		hexagonal	a = 4.53 nm
	0.262		hexagonal	a = 4.56 nm
	0.613		lamellar	d = 4.68 nm
	0.620		lamellar	d = 4.68 nm
		0.256	hexagonal	a = 4.42 nm
		0.262	hexagonal	a = 4.52 nm
		0.613	lamellar	d = 4.72 nm
		0.620	lamellar	d = 4.72 nm
PAAm$_{42}$-*b*-C$_{16}$TAPA$_{42}$	0	0	hexagonal	a = 4.84 nm
	0.818		lamellar	d = 4.31 nm
	4.067		reverse hexagonal	a = 3.86 nm
	8.540		reverse micellar	d = 4.10 nm^a
		0.142	hexagonal + lamellar	a = 5.28 nm, d = 4.34 nm
		0.321	lamellar	d = 4.34 nm
		0.325	lamellar	d = 4.34 nm
		0.335	lamellar	d = 4.34 nm

^{a}Micelle−micelle correlation distance.

phase (also referred as H$_I$ phase), already discussed above, in which the hydrophobic alkyl chains of the surfactants are located inside of the cylinders with the hydrophilic polar headgroups facing the surface of the cylinder, surrounded by a continuous water domain containing the negatively charged poly(acrylate) chains. Another is the reverse phase (H$_{II}$ phase), where the water phase is located inside of the cylinders, with the hydrophobic surfactant chains facing toward a continuous alcohol domain surrounding the cylinders.[22]

From a symmetry point of view, both structures (normal and reverse) are 2D hexagonal and possess peak position ratios of 1:3$^{1/2}$:2. In Figure 4B, the structure could be identified as reverse hexagonal, once the nanoparticles are rich in octanol. Still further addition of octanol (R = 8.540) leads to the formation of a reverse micellar phase, referred to as the L$_2$ phase. This phase consists of an isotropic and disordered solution of reverse micelles. A SAXS pattern for the L$_2$ phase, shown in Figure 4C, presents only a broad peak corresponding to the micelle−micelle correlation distance of around 4.1 nm.

Reversibility of n-Alcohol-Induced Structural Transitions. To confirm the reversibility of the structural transitions by the incorporation of *n*-alcohols to the nanoparticle cores, an aqueous dispersion of 1.0 wt % PAAm$_{42}$-*b*-C$_{12}$TAPA$_{42}$, prepared by using decanol to promote the formation of a lamellar phase, was dialyzed against deionized water for 3 days. The reference sample containing no *n*-alcohol presented a cubic interior (Figure 5A), as already discussed above and the decanol-loaded nanoparticles at R = 0.613, a lamellar liquid-crystalline structure (Figure 5B). After 3 days of dialysis, the latter sample presented a SAXS pattern (Figure 5C) that was virtually identical to that from the initially *n*-alcohol-free reference sample (cubic $Pm\bar{3}n$ with the same lattice parameter), confirming the full reversibility of this process.

Thermal Phase Behavior. It is well known that lamellar phases formed by lipid/surfactant liquid crystals present a characteristic thermotropic phase behavior. They undergo the gel-to-liquid-crystalline phase transition (L$_\beta$−L$_\alpha$) upon increasing the temperature. Below the transition temperature, T_m, the surfactant alkyl chains are in a solidlike state. Above T_m, the surfactant molecules are in the fluid liquid-crystalline state, in

which the conformational disorder of alkyl chains predominates.[23] Differential scanning calorimetry (DSC) was used to determine the thermal phase behavior in lamellar PAAm$_{42}$-*b*-C$_{16}$TAPA$_{42}$ nanoparticles. In a similar manner, a lamellar sample prepared using the homopolymer CS C$_{16}$TAPA$_{30}$, prepared in the same way as in the earlier work,[10] was also analyzed. Figure 6 compares the DSC thermograms obtained for the two samples that possess the same decanol/CS mass ratio.

By integrating the peaks in the thermograms, one can determine the enthalpy change (ΔH) associated with the phase transition. Table 2 shows the measured ΔH values of the gel-to-liquid crystalline transition as well as the transition temperature (T_m) and peak width ($\Delta T_{1/2}$) obtained from the DSC measurements. Again, the thermotropic data for the poly-(acrylamide)-*b*-CS nanoparticles clearly agree with those found for the corresponding homopolymer CS, with the same *n*-alcohol content.

Colloidal Properties of the Nanoparticles. To complete the physicochemical characterization of the liquid-crystalline nanoparticles, particles in freshly prepared dispersions were also characterized by their hydrodynamic radii (R_H) and zeta potentials (ζ). Table 3 summarizes the results for nanoparticles featuring all of the different internal structures. The average radius was around 120 nm for all nanoparticles. The polydispersity index (PDI) of the nanoparticles was consistently 0.1.

Comparing the nanoparticles prepared using pure PAAm$_{42}$-*b*-C$_{12}$TAPA$_{42}$ or PAAm$_{42}$-*b*-C$_{16}$TAPA$_{42}$ in water (no added *n*-alcohol), the former displayed zeta potential values that were slightly more negative (around −35 mV) than the latter (around −25 mV). For all combinations of block copolymer and alcohol, the absolute value of the nanoparticle zeta potential decreased with an increase in *n*-alcohol content (Table 3).

■ DISCUSSION

Nature of the Colloidal Nanoparticles. A striking difference between ours and the previously reported poly-(acrylate-*b*-acrylamide)/cationic surfactant nanoparticle disper-
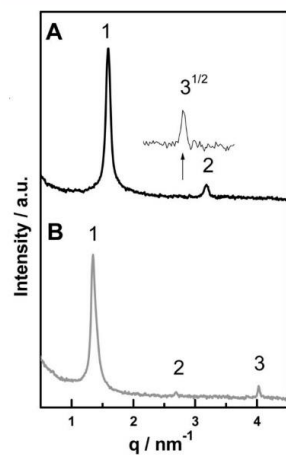
Figure 2. SAXS patterns for $PAAm_{42}$-b-$C_{12}TAPA_{42}$ nanoparticles with varying amounts of added decanol (A) $R = 0.256$; (B) $R = 0.613$; or octanol (C) $R = 0.256$; (D) $R = 0.613$ displaying hexagonal or lamellar structures. All samples containing 1.0 wt % of poly(acrylamide)-b-CS, analyzed at 25 °C.

Figure 3. SAXS patterns for decanol-loaded $PAAm_{42}$-b-$C_{16}TAPA_{42}$ nanoparticles displaying (A) coexistence of hexagonal (labeled with asterisks) and lamellar structures for $R = 0.142$ and (B) lamellar core structures for $R = 0.321$. Samples containing 1.0 wt % of poly(acrylamide)-b-CS, analyzed at 25 °C.
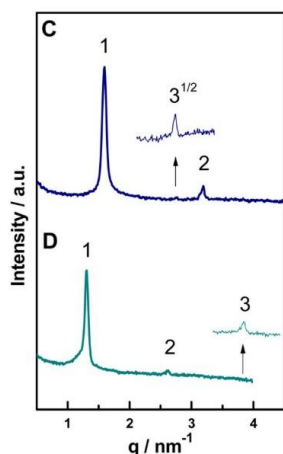
Figure 4. SAXS patterns for octanol-loaded $PAAm_{42}$-b-$C_{16}TAPA_{42}$ displaying (A) lamellar for $R = 0.818$, (B) reverse hexagonal for $R = 4.067$, and (C) reverse micellar core structures for $R = 8.540$. Samples containing 1.0 wt % of poly(acrylamide)-b-CS, analyzed at 25 °C.

sions is the occurrence or not of liquid-crystalline structures in the nanoparticle cores. Nanoparticles conventionally prepared were reported as possessing disordered cores.[1,2,5,6] The strategy for preparing nanoparticles containing CS cores reported in the present work was chosen to allow a more accurate control of the phase behavior of the species and ensured the formation of nanoparticles with a liquid-crystalline interior and the evaluation of the effect of added n-alcohols on the structured nanoparticle cores.

It is questionable whether the small differences in composition (the presence or absence of low concentrations of inorganic ions), resulting from the two methods of preparation, could by itself be the cause of the difference in the nanoparticle core structure. The particle size could be more important: available data on particle size show that the nanoparticles prepared by dispersing poly(acrylamide)-b-CS display larger cores. By using our procedure, nanoparticles with an average radius slightly larger than 100 nm are produced.

The size ratio core/lattice parameter (n) of the nanoparticles studied in this report was estimated by simply dividing the average particle diameter by the lattice parameter for each phase, as detailed in the Supporting Information. This ratio varied in the range 27 ± 5 for all internal structures (see Table S1). For conventionally prepared nanoparticles, the cores are much smaller and may be too small to accommodate a number of units sufficient to form a crystalline structure with long-range order. Taking into account the average size of conventionally prepared nanoparticles (~30 nm)[1] and the lattice parameter of a cubic phase (8.4 nm), for example, n is around 3, which is
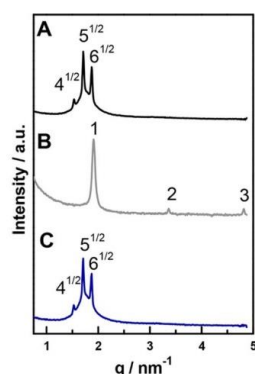
Figure 5. SAXS patterns for a 1.0 wt % dispersion of $PAAm_{42}$-b-$C_{12}TAPA_{42}$ showing the reversibility of alcohol-induced structural changes: (A) cubic structure in the n-alcohol-free reference dispersion; (B) lamellar structure with added decanol at $R = 0.613$; (C) return to cubic structure after 3 days of dialysis of the latter sample against deionized water. All measurements were performed at 25 °C.
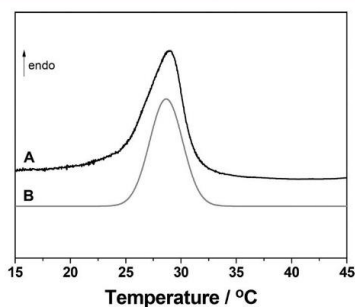
Figure 6. DSC thermograms for (A) 46.7 wt % $C_{16}TAPA_{30}$, 19.1 wt % water, 15.2 wt % decanol system and (B) an aqueous dispersion containing 1.0 wt % $PAAm_{42}$-b-$C_{16}TAPA_{42}$ and 0.8 wt % decanol. $R = 0.325$ for both samples.

Table 2. Transition Temperatures (T_m), Peak Width ($\Delta T_{1/2}$), and Transition Enthalpies (ΔH), with Standard Deviation, for the Gel-to-Liquid-Crystalline Phase Transition for 1.0 wt % $PAAm_{42}$-b-$C_{16}TAPA_{42}$ Dispersion and $C_{16}TAPA_{30}$/Water/Decanol System[a]

complex salt	T_m (°C)	$\Delta T_{1/2}$ (°C)	ΔH (kJ·mol^{-1})[b]
$PAAm_{42}$-b-$C_{16}TAPA_{42}$	28.7	3.7	36 ± 1
$C_{16}TAPA_{30}$	28.9	3.6	35 ± 1

[a]$R = 0.325$ for both samples. [b]ΔH expressed as kJ per mole of alkyl chains (surfactant + n-alcohol).

around 10-fold lower than what is described in this paper and most likely not enough to constitute a liquid-crystalline domain. Similar arguments were used, for example, by Guillot et al.,[24] to explain the absence of a liquid-crystalline order in hexosomes (dispersions of reverse hexagonal lipid-based phases) below 30 nm (the lattice parameter being $a = 5.82$ nm).

Colloidal complexes similar to those studied here are known to display properties that depend on the sample preparation procedures. Cationic lipid–polyelectrolyte (DOTAP/PAA)

complexes were reported as systems out of equilibrium.[17] Polyelectrolyte complex dispersions formed by oppositely charged polymers in aqueous media were also described to vary in size, structure, and stability depending on the mixing conditions.[25] Tarahovsky et al.[26] described lipoplexes (DNA–lipid complexes) with phase preferences depending on the sample preparation. Nizri et al.[27] reported the study [by means of cryo-transmission electron microscopy (TEM) and dynamic light scattering (DLS)] of liquid-crystalline nanoparticles formed by the direct mixing of C_xTAB ($x = 10$–16) and sodium poly(acrylate) solutions, leading to different surfactant/polymer molar charge ratios (Z). They described a wide range of particle sizes depending on the Z values, the surfactant alkyl chain length, and the way the experiments were conducted. These findings are also valid in complex dispersions composed of positively charged polymers and negatively charged surfactants.[28,29] The commonly encountered history dependence suggests that the nanoparticles studied in the present work are not equilibrium structures and that their size is process-dependent, which is consistent with the properties of colloidal dispersions. Nevertheless, we have established a method to produce, in a reproducible fashion, nanoparticles with colloidal properties that remain unchanged for several weeks. It is known that the shape of the internally structured nanoparticles may display changes depending on the core structure, giving rise to anisotropic geometries.[30] However, such an investigation has not been conducted thoroughly yet and discussions about the shape of the produced nanoparticles are out of the scope of the present report.

Although the CSs were prepared at a charge molar ratio (polymer/surfactant) equal to 1, the produced nanoparticles possess a net negative charge, as indicated by their zeta potential values. This indicates that there is a dissociation of surfactant ions from the surface of the CS core of the nanoparticles, producing an excess of anionic acrylate charges at the core surface. The nanoparticles containing the dodecyltrimethylammonium surfactant ion had a slightly more negative zeta potential than those with the hexadecyltrimethylammonium surfactant. This can be related to the difference in hydrophobicity and, hence, in aqueous solubility of the two surfactant ions, as reflected in their different critical micelle concentration (cmc) values,[31] with the dodecyltrimethylammonium surfactant ion displaying more dissociation in the aqueous phase. The addition of n-alcohols promoted a decrease in the zeta potential of the liquid-crystalline nanoparticles. The incorporation of nonionic cosolutes into amphiphilic aggregates may induce a charge dilution, yielding nanoparticles with a lower surface charge. The higher the proportion of n-alcohol located in the surfactant aggregates, the higher the decrease in the zeta potential value.

Colloidal nanoparticles have a tendency to agglomerate as a result of van der Waals attractive forces. Two modes of preventing the agglomeration and stabilizing the nanoparticle dispersions kinetically are via electrostatic and steric stabilization, and the resultant dispersion stability is a balance between repulsive and attractive forces between the particles. The electrostatic stabilization results from the repulsion between the nanoparticles caused by the dissociated counterions in the electrostatic double layer. The steric repulsion between nanoparticles surface-covered with polymer chains may also contribute to the kinetic stabilization of the nanoparticles.[32] It is believed that the poly(acrylamide) neutral chains composing the shell may contribute to the stabilization of the colloidal

Table 3. Hydrodynamic Radii (R_H), Polydispersity Index (PDI), and Zeta Potential (ζ) for Poly(acrylamide)-b-CS Nanoparticles at Varying n-Alcohol/CS Mass Ratios (R) (av ± SD, Triplicate of Independent Preparations)

poly(acrylamide)-b-CS	R (octanol)	R (decanol)	R_H ± SD (nm)	PDI	ζ ± SD (mV)
PAAm$_{42}$-b-C$_{12}$TAPA$_{42}$	0	0	110 ± 10	0.12	−35 ± 5
	0.256		115 ± 10	0.14	−30 ± 5
	0.262		115 ± 10	0.13	−28 ± 4
	0.613		125 ± 10	0.15	−25 ± 5
	0.620		125 ± 10	0.13	−22 ± 5
		0.256	120 ± 10	0.11	−32 ± 3
		0.262	120 ± 10	0.12	−30 ± 5
		0.613	115 ± 10	0.14	−25 ± 5
		0.620	115 ± 10	0.10	−23 ± 5
PAAm$_{42}$-b-C$_{16}$TAPA$_{42}$	0	0	115 ± 10	0.11	−25 ± 5
	0.818		120 ± 10	0.13	−22 ± 5
	4.067		120 ± 10	0.12	−20 ± 2
	8.540		130 ± 10	0.10	−14 ± 5
		0.142	120 ± 10	0.13	−25 ± 5
		0.321	120 ± 10	0.12	−20 ± 5
		0.325	118 ± 10	0.15	−20 ± 5
		0.335	115 ± 10	0.12	−18 ± 5

nanoparticles, together with the surface charge, through both steric and electrostatic stabilization mechanisms. It has been observed that the colloidal dispersions are kinetically stable with no sign of macroscopic phase separation for several weeks. The observed variations in the zeta potential values could have consequences for the long-term colloidal stability of the nanoparticle dispersions; however, the latter topic is beyond the scope of the present study.

Internal Structure of the Nanoparticles. Previously reported ternary phase diagrams[10,12] have shown that CS/n-alcohol mixtures, such as pure CSs, display a finite maximum water uptake when equilibrated against excess water. With added decanol or octanol, the maximum water uptake of the CS/n-alcohol mixtures varied in the range 35−55 wt %, depending on the specific choices of CSs and n-alcohol and their mixing ratio. An obvious question is then whether the maximally water-swollen cores of poly(acrylamide)-b-CS nanoparticles obey the same phase diagrams, that is, if the same structure is obtained, at a given n-alcohol/surfactant ion ratio, in the nanoparticle core as for the corresponding homopolymer CS/alcohol mixture. This direct comparison was made and is presented in Figure 7 below.

Because of a non-negligible fraction of the alcohol residing in the water phase of the very dilute dispersions of poly-(acrylamide)-b-CS studied here, previously reported[31] partition coefficients of the n-alcohols between dodecyl- and hexadecyl-trimethylammonium bromide micelles and water were used to calculate the true mole fractions of alcohol, X_a, of the mixed surfactant aggregates in the cores, based on overall sample compositions. The points in Figure 7 indicate the thus calculated compositions and the determined structures of the cores of the copolymer nanoparticles. As a background in Figure 7, reference phase boundaries shown have been calculated from data for maximally swollen C$_x$TAPA$_{30}$/n-alcohol mixtures, taken from refs 10 and 12. Clearly, there is an exact correspondence, within the resolution of the two studies, between the two types of maximally swollen CS/n-alcohol mixtures. Because the C$_{12}$TAPA$_{30}$/octanol system was not included in the previous studies, the reference phase diagram for these mixtures is lacking in Figure 7D.
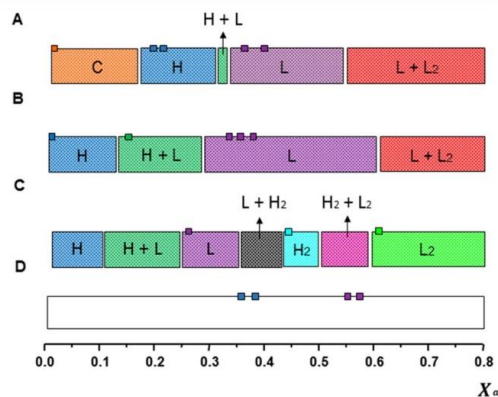
Figure 7. Phase evolution as a function of n-alcohol content for the systems: (A) C$_{12}$TAPA$_{30}$/water/decanol; (B) C$_{16}$TAPA$_{30}$/water/decanol; (C) C$_{16}$TAPA$_{30}$/water/octanol; (D) C$_{12}$TAPA$_{30}$/water/octanol. Legend: C = cubic, H = hexagonal, L = lamellar, H$_2$ = reverse hexagonal, and L$_2$ = reverse micelles. These phase diagrams, based on the data from refs 10 and 12, refer to maximally water-swollen CS samples with an overall CS/water mass ratio of 0.45. The inserted points show structures for the corresponding poly-(acrylamide)-b-CS/n-alcohol systems, using the same color codes as in the reference phase diagrams, obtained in the present study. The core compositions shown are based on the true n-alcohol contents (see text).

As shown above, it was possible to reproduce the structures found in homopolymer CS/water/n-alcohol ternary mixtures in the cores of the corresponding poly(acrylamide)-b-CS nanoparticles dispersed in an aqueous medium. In addition, the lattice parameters were also very similar, based on the data of refs 10 and 12. The close correspondence found is not self-evident because one would expect some influence of the poly(acrylamide) chains of the block copolymer on the surfactant aggregate arrangement. A comparison of the effective radii of the nanoparticles, approximately 100 nm, with the 11 nm length of a fully stretched block of 42 acrylamide units

implies that a fraction of the poly(acrylamide) blocks must necessarily reside among the surfactant aggregates in the cores. However, apparently, they affect neither the mesophase structure nor the aggregate-to-aggregate distance represented by the lattice parameters, for any of the structures investigated.

Moreover, it was a priori expected that the core–shell interface and the consequent confinement of these structures could impose restrictions on the lattice parameters of 2D or 3D internal structures, but such effects were not seen. Confinement effects on the arrangement of the liquid-crystalline structures in the inner part have previously been reported. Golan and Talmon[17] described lamellar structures in the form of onion-like aggregates formed in complexes between cationic lipids and oppositely charged polyions. The same arrangement of bilayered structures was found in colloidal complexes formed by the electrostatic association between ionic lipids and an oligonucleotide.[33] Cubosomes[34] and hexosomes[35] with distorted structures were also reported elsewhere.

In some samples, two different internal structures were found to coexist in the liquid-crystalline nanoparticle dispersions. The systems must then feature either particles with two phases coresiding in the same core or a mixture of two kinds of particles featuring single-phase cores of two very different structures that also differ substantially in composition. The average n-alcohol mole fractions in the particle cores are in the same range as for the corresponding bulk systems belonging to a three-phase region (hexagonal, lamellar, and excess isotropic solution). Hence, again, the structural data agree with those for the homopolymer CSs. From the corresponding homopolymer CS phase diagrams (see Figure 7), it can be inferred that there is a large difference in the alcohol content between the two coexisting phases in the hexagonal/lamellar two-phase area, for example. Guillot et al.[24] have also reported oil-loaded liquid-crystalline nanoparticles, in which the SAXS data indicated phase coexistence, depending on the oil content. In their interpretation, the possibility to have a mixture of nanoparticles having different internal liquid-crystalline structures was rejected because the oil would be transferred from oil-rich nanoparticles to the oil-poor ones. On similar grounds, we favor the interpretation that mixed-phase dispersions of the systems studied here contain nanoparticles with the two phases coresiding in the same core. However, the present results do not allow us to distinguish these two cases.

The n-alcohols, when incorporated in surfactant aggregates, can give two different effects commonly known as cosurfactant and cosolvent effects, leading to changes in the structure of the aggregate.[10,12] Decanol acts as a cosurfactant, being incorporated with the surfactant ions in the mixed aggregates, where the hydroxyl groups are located at the interface.[36] This effect results in an increase in the critical packing parameter, favoring the formation of structures with low and even inverted curvatures.[12] Reverse structures, such as the reverse hexagonal and micellar phases, are seen to form only for octanol and at high octanol mole fractions. From this, one can conclude that octanol functions as a cosolvent better than decanol forming an octanol-continuous domain that can dissolve the reverse CS aggregates, leading to the formation of an isotropic L_2 phase at the highest octanol contents. This is in accordance with previous findings, for homopolymer CSs, that the efficiency as a cosolvent increases for shorter alcohols.[10,12,13] The estimated solubility of the homopolymer CS $C_{16}TAPA_{30}$ is 10 and 40% in decanol and octanol, respectively.[10]

In contrast to the nanoparticles containing normal ordered phases, there are few reports on liquid-crystalline nanoparticles with reverse structures; the latter reports concern essentially lipid–water dispersions.[37−39] In the present study, two different reverse phases were found: a disordered micellar and a hexagonal phase. The reverse hexagonal phase is composed of cylindrical micelles, in which the polymer/aqueous phase is located inside of the cylinders with the surfactant alkyl chains facing the outside of the oil phase. Bernardes et al.[13] studied reverse micelles in bulk systems formed by poly(acrylate)–hexadecyltrimethylammonium CSs, water, and different alcohols (octanol, hexanol, and butanol). Their results indicated the formation of alcohol-soluble aggregates, where each aggregate had a core of one polyion chain in water, surrounded by neutralizing surfactant ions. Such an aggregate was described as a reverse micelle with a spine.

A few findings of nanoparticles with reverse internal structures have been reported in the literature, such as the aqueous tetradecane-loaded monolinolein particles, which can display cubic, hexagonal, discontinuous cubic, and micellar reverse structures, depending on the oil content.[38] Nakano et al.[37] and Tran et al.[39] have also reported reverse particles occurring in monoolein-based aqueous dispersions, when a fatty acid (oleic or decanoic) is added to the system. More recently, citrem (citric acid ester of glycerides) nanoparticles dispersed in an aqueous medium were also shown to comprise the internal reverse micellar (L_2) structure when mixed with lipids.[40] However, our study is the first report on nonlipid nanoparticles displaying reverse liquid-crystalline structures at room temperature.

Depending on the n-alcohol fraction incorporated into the core, the nanoparticles may display a lamellar interior structure. Bilayers in the gel phase are highly ordered and packed structures.[23] In some cases, the cooling of confined bilayers below the T_m does not result in gel phase formation, which is attributed to the presence of an effective area constraint. It was also shown that the curvature of the bilayers affects its properties compared to the planar lamellar state. For vesicles of both lipids and surfactants, the transition temperature is found to decrease gradually with decreasing vesicle size for aggregates smaller than ±70 nm in diameter.[41,42] In the limit of high curvature, for very small vesicles, the formation of gel domains is strongly suppressed, which is directly related to the increase in the bending modulus of gel bilayers with respect to bilayers in the fluid state.[43]

In view of these previous findings, the quantitative agreement between dispersed poly(acrylamide)-b-CSs and nondispersed homopolymer CSs regarding both T_m and ΔH for the thermally induced L_β–L_α phase transition is quite remarkable. It indicates that, apparently, there is no significant curvature or confinement effect on the lamellar structures composing the core of n-alcohol-loaded dispersed nanoparticles. This result thus follows the general pattern found here and in one previous[3] study that the dispersed poly(acrylamide)-b-CS systems reproduce the phase behavior of bulk homopolymer CSs.

By dialysis, it was possible to achieve the initial liquid-crystalline structure of the nanoparticles by removing the n-alcohol incorporated in the core of the nanoparticles. This highlights the possibility to switch the internal structure of the poly(acrylamide)-b-CS nanoparticles from water-continuous to oil-continuous, or vice versa, by simply adding or removing the alcohol.

■ CONCLUSIONS AND OUTLOOK

In this work, we were able to reproduce the liquid-crystalline phases of the bulk systems in the cores of poly(acrylamide)-b-CS nanoparticles. The various phases were achieved by the incorporation of n-alcohols in the ordered cores, acting as cosurfactants, inducing variation in the packing parameter of the surfactant aggregates, and for n-octanol, as a cosolvent in reverse structures. The SAXS data revealed the following liquid-crystalline phases, depending on the nature and concentration of n-alcohol: cubic, hexagonal, lamellar, reverse hexagonal, and reverse micellar phase. Apparently, the confinement of the phases into nanometric cores does not change their structural properties. DLS measurements revealed nanoparticles with ∼100 nm average radius. These dispersions are kinetically stable, most likely due to steric and electrostatic repulsion arising from PAAm surface chains and negative zeta potentials, respectively. The colloidal and structural properties of the dispersions are dependent on the mixing pathways, but by using our procedure to prepare poly(acrylamide)-b-CS nanoparticles, we were able to obtain liquid-crystalline core nanoparticles with reproducible colloidal and structural features.

In summary, the investigated poly(acrylamide)-b-CS dispersed systems present a rich structural variety in the cores of the nanoparticles, which can be controlled in a systematic way by the addition or removal of n-alcohols. This is interesting as a versatile system for the purposes of delivering active agents and stimuli-responsive systems, for example. The present study also contributes to a better understanding of the nature of polyion/oppositely charged surfactant interactions and the mapping of ordered liquid-crystalline structures confined in colloidal domains. Over the years, lipid-based liquid-crystalline nanoparticles have become the subject of many scientific studies pointing out their applications as drug-delivery systems, surface coatings, and environmentally responsive colloids and their use as versatile model particles for soft matter studies, for example. We present here a chemically different way to produce these internally structured nanoparticles, with the advantage of possessing a potential switchable mechanism that allows a precise control of the internal phase. The knowledge of liquid-crystalline structures is fundamental in the design of colloidal materials with desired properties and functions, as evidenced by the huge research effort on various applications of polymer/surfactant dispersions. Thus, the information reported in the present study is encouraging for future work involving cryo-TEM, aiming at the determination of the aggregates shape and arrangement of the confined liquid-crystalline structures and to elucidate the possible phase coexistence in the nanoparticle core and how the coexisting phases are arranged.

■ EXPERIMENTAL SECTION

Chemicals. The acid form of the symmetric block copolymer P(AA$_{42}$-b-AAm$_{42}$) was synthesized using controlled radical polymerization as described in a previous work of our group.[3] Dodecyltrimethylammonium bromide and hexadecyltrimethylammonium bromide, (C$_{12}$TABr and C$_{16}$TABr, respectively) of 99% purity were purchased from Sigma-Aldrich (USA). The alcohols used were n-octanol (Sigma, USA) and n-decanol (Fluka, USA); both were of the highest purity available (99%) and used as received. Deionized water with a resistivity above 18.2 MΩ·cm^{-1} as obtained by a Milli-Q system was used in all experiments.

Preparation of Poly(acrylamide)-b-CS Block Copolymers. All poly(acrylamide)-b-CS block copolymers were prepared by titrating the hydroxide form of the surfactants (C$_{12}$TA$^+$ and C$_{16}$TA$^+$) obtained by an ion-exchange step, with aqueous solutions of the acid P(AA$_{42}$-b-AAm$_{42}$) until the equivalence point, following the general procedure described earlier for CSs prepared in our laboratories.[6,8,9,12] The equivalence point at pH 8.6−8.9 was found to be the same as that determined using the homopolymers.[6−9] The mixture was left overnight at 4 °C and its pH was adjusted to the equivalence point when necessary, with P(AA$_{42}$-b-AAm$_{42}$) solution. The poly(acrylamide)-b-CS block copolymers were freeze-dried to obtain their powders, which were kept in a desiccator. The final products were named PAAm$_{42}$-b-C$_{12}$TAPA$_{42}$ and PAAm$_{42}$-b-C$_{16}$TAPA$_{42}$ according to the alkyl chain length of the surfactants used in their preparation.

Sample Preparation. The dispersions were prepared by vortexing the appropriate amounts of CSs and water for approximately 1 min to achieve the final poly(acrylamide)-b-CS concentration of 1.0 wt %. The samples containing n-alcohols were prepared in the same way, with the addition of desired amounts of octanol or decanol to the solids before adding water and vortexing.

Techniques. *SAXS.* SAXS measurements were taken to identify the liquid-crystalline structures formed in the nanoparticle cores. The measurements were taken at the SAXS1 beamline of the Brazilian Synchrotron Light Laboratory, LNLS, in Campinas, Brazil. The samples were positioned in a cell with two flat mica windows, and a thermal bath connected to the sample holder was used for temperature control. The X-ray wavelength was 1.608 Å, and the sample-to-detector distance was around 0.6 m, as calibrated using silver behenate. The obtained charge-coupled device (CCD) images were integrated and treated with Fit2D software[44] to obtain the scattering function I(q), where $q = (4\pi/\lambda) \sin(\theta/2)$, with λ being the wavelength and θ being the scattering angle. The relative diffraction peak positions were used to identify the mesophase structures of the liquid-crystalline nanoparticles. The interplanar distance (d) between two reflecting planes is given by $d = 2\pi/q$, which enables us to calculate the corresponding mean lattice parameter (a). The scattering pattern of the so-called L$_2$ (micellar reverse) phase shows only one broad correlation peak, corresponding to the micelle−micelle correlation distance. All measurements were recorded at 25 °C.

DSC. DSC measurements of the poly(acrylamide)-b-CS block copolymer dispersions were taken using a Microcal VP high sensitivity differential scanning calorimeter (Microcal Inc. Northampton, MA, USA) equipped with 0.542 mL twin total-fill cells. Scanning was performed at a heating rate of 60 °C h^{-1} from 10 to 80 °C. For the concentrated homopolymer CS samples, the DSC measurements were taken using a Q1000 differential scanning calorimeter, TA Instruments. Around 5 mg of sample was hermetically sealed into an aluminum pan. Measurements were taken at a heating rate of 90 °C·h^{-1} from 10 to 80 °C. In all cases, the analyses were made with null prescan, producing fully reproducible results when comparing consecutive runs. Transition enthalpies were obtained by integrating the area under the thermograms along the temperature range. The calorimetric analyses were made in triplicate.

DLS. The dispersions were evaluated using DLS at 25 °C, using a Malvern Nano Zetasizer instrument with a 632.8 nm laser and a detector positioned at 173°. From the apparent

diffusion coefficients, the hydrodynamic radii (R_H) of the nanoparticles were determined using the Stokes–Einstein relationship for translational diffusion. The zeta potential (ζ) was estimated based on the electrophoretic mobility measurements using the Smoluchowski model.

■ ASSOCIATED CONTENT

Ⓢ Supporting Information

The Supporting Information is available free of charge on the ACS Publications website at DOI: 10.1021/acsomega.6b00267.

SAXS patterns for n-alcohol-loaded poly(acrylamide)-b-CS nanoparticles with different values of R and size ratio, core/parameter for all investigated samples (PDF)

■ AUTHOR INFORMATION

Corresponding Author
*E-mail: wloh@iqm.unicamp.br. Phone: +55 19 35213148. Fax: +55 19 35213023.

ORCID ⊙
Guilherme A. Ferreira: 0000-0002-4932-3666

Author Contributions
All the experimental work was designed by the three authors, conducted by G.A.F. and the results analyzed and discussed by the three authors. All authors have contributed and given approval to the final version of the manuscript.

Notes
The authors declare no competing financial interest.

■ ACKNOWLEDGMENTS

■ REFERENCES

(1) Berret, J.-F.; Cristobal, G.; Hervé, P.; Oberdisse, J.; Grillo, I. Structure of colloidal complexes obtained from neutral/poly-electrolyte copolymers and oppositely charged surfactants. Eur. Phys. J. E: Soft Matter Biol. Phys. 2002, 9, 301–311.

(2) Berret, J.-F.; Hervé, P.; Aguerre-Chariol, O.; Oberdisse, J. Colloidal complexes obtained from charged block copolymers and surfactants: A comparison between small-angle neutron scattering, cryo-TEM, and simulations. J. Phys. Chem. B 2003, 107, 8111–8118.

(3) Vitorazi, L.; Berret, J.-F.; Loh, W. Self-Assembly of Complex Salts of Cationic Surfactants and Anionic–Neutral Block Copolymers. Dispersions with Liquid-Crystalline Internal Structure. Langmuir 2013, 29, 14024–14033.

(4) Uchman, M.; Štěpánek, M.; Prévost, S.; Angelov, B.; Bednár, J.; Appavou, M.-S.; Gradzielski, M.; Procházka, K. Coassembly of Poly(ethylene oxide)-block-poly(methacrylic acid) and N-Dodecylpyridinium Chloride in Aqueous Solutions Leading to Ordered Micellar Assemblies within Copolymer Aggregates. Macromolecules 2012, 45, 6471–6480.

(5) Hervé, P.; Destarac, M.; Berret, J.-F.; Lal, J.; Oberdisse, J.; Grillo, I. Novel Core–Shell Structure for Colloids Made of Neutral/Polyelectrolyte Diblock Copolymers and Oppositely Charged Surfactants. Europhys. Lett. 2002, 58, 912–918.

(6) Berret, J.-F.; Vigolo, B.; Eng, R.; Hervé, P.; Grillo, I.; Yang, L. Electrostatic Self-Assembly of Oppositely Charged Copolymers and Surfactants: A Light, Neutron, and X-Ray Scattering Study. Macromolecules 2004, 37, 4922–4930.

(7) Piculell, L. Understanding and Exploiting the Phase Behavior of Mixtures of Oppositely Charged Polymers and Surfactants in Water. Langmuir 2013, 29, 10313–10329.

(8) Svensson, A.; Piculell, L.; Cabane, B.; Ilekti, P. A New Approach to the Phase Behavior of Oppositely Charged Polymers and Surfactants. J. Phys. Chem. B 2002, 106, 1013–1018.

(9) Svensson, A.; Norrman, J.; Piculell, L. Phase Behavior of Polyion–Surfactant Ion Complex Salts: Effects of Surfactant Chain Length and Polyion Length. J. Phys. Chem. B 2006, 110, 10332–10340.

(10) Bernardes, J. S.; Norrman, J.; Piculell, L.; Loh, W. Complex Polyion–Surfactant Ion Salts in Equilibrium with Water: Changing Aggregate Shape and Size by Adding Oil. J. Phys. Chem. B 2006, 110, 23433–23442.

(11) Bernardes, J. S.; Loh, W. Structure and phase equilibria of mixtures of the complex salt hexadecyltrimethylammonium polymethacrylate, water and different oils. J. Colloid Interface Sci. 2008, 318, 411–420.

(12) Bernardes, J. S.; Piculell, L.; Loh, W. Self-Assembly of Polyion–Surfactant Ion Complex Salts in Mixtures with Water and n-Alcohols. J. Phys. Chem. B 2011, 115, 9050–9058.

(13) Bernardes, J. S.; da Silva, M. A.; Piculell, L.; Loh, W. Reverse micelles with spines: L_2 phases of surfactant ion–polyion complex salts, n-alcohols and water investigated by rheology, NMR diffusion and SAXS measurements. Soft Matter 2010, 6, 144–153.

(14) Spicer, P. T.; Hayden, K. L.; Lynch, M. L.; Ofori-Boateng, A.; Burns, J. L. Novel Process for Producing Cubic Liquid Crystalline Nanoparticles (Cubosomes). Langmuir 2001, 17, 5748–5756.

(15) Rosa, M.; Infante, M. R.; Miguel, M. d. G.; Lindman, B. Spontaneous formation of vesicles and dispersed cubic and hexagonal particles in amino acid-based catanionic surfactant systems. Langmuir 2006, 22, 5588–5596.

(16) Uchman, M.; Gradzielski, M.; Angelov, B.; Tošner, Z.; Oh, J.; Chang, T.; Štěpánek, M.; Procházka, K. Thermodynamic and Kinetic Aspects of Coassembly of PEO–PMAA Block Copolymer and DPCl Surfactants into Ordered Nanoparticles in Aqueous Solutions Studied by ITC, NMR, and Time-Resolved SAXS Techniques. Macromolecules 2013, 46, 2172–2181.

(17) Golan, S.; Talmon, Y. Nanostructure of Complexes between Cationic Lipids and an Oppositely Charged Polyelectrolyte. Langmuir 2012, 28, 1668–1672.

(18) Tangso, K. J.; Patel, H.; Lindberg, S.; Hartley, P. G.; Knott, R.; Spicer, P. T.; Boyd, B. J. Controlling the Mesostructure Formation within the Shell of Novel Cubic/Hexagonal Phase Cetyltrimethylammonium Bromide–Poly(acrylamide-acrylic acid) Capsules for pH Stimulated Release. ACS Appl. Mater. Interfaces 2015, 7, 24501–24509.

(19) Wadsäter, M.; Barauskas, J.; Nylander, T.; Tiberg, F. Formation of Highly Structured Cubic Micellar Lipid Nanoparticles of Soy Phosphatidylcholine and Glycerol Dioleate and Their Degradation by Triacylglycerol Lipase. ACS Appl. Mater. Interfaces 2014, 6, 7063–7069.

(20) Fong, W.-K.; Hanley, T. L.; Thierry, B.; Kirby, N.; Waddingtin, L. J.; Boyd, B. J. Controlling the Nanostructure of Gold Nanorod–Lyotropic Liquid-Crystalline Hybrid Materials Using Near-Infrared Laser Irradiation. Langmuir 2012, 28, 14450–14460.

(21) Lee, K. W. Y.; Nguyen, T.-H.; Hanley, T.; Boyd, B. J. Nanostructure of liquid crystalline matrix determines in vitro sustained release and in vivo oral absorption kinetics for hydrophilic model drugs. Int. J. Pharm. 2009, 365, 190–199.

(22) Zhou, S.; Liang, D.; Burger, C.; Yeh, F.; Chu, B. Nanostructures of Complexes Formed by Calf Thymus DNA Interacting with Cationic Surfactants. Biomacromolecules 2004, 5, 1256–1261.

(23) Ferreira, G. A.; Loh, W. Structural parameters of lamellar phases formed by the self-assembly of dialkyldimethylammonium bromides in aqueous solution. J. Braz. Chem. Soc. 2016, 27, 392–401.

(24) Guillot, S.; Salentinig, S.; Chemelli, A.; Sagalowicz, L.; Leser, M. E.; Glatter, O. Influence of stabilizer concentration on the internal

liquid crystalline order and the size of oil-loaded monolinolein-based dispersions. *Langmuir* **2010**, *26*, 6222−6229.

(25) Buchhammer, H.-M.; Mende, M.; Oelmann, M. Formation of mono-sized polyelectrolyte complex dispersions: Effects of polymer structure, concentration and mixing conditions. *Colloids Surf., A* **2003**, *218*, 151−159.

(26) Tarahovsky, Y. S.; Koynova, R.; MacDonald, R. C. DNA Release from Lipoplexes by Anionic Lipids: Correlation with Lipid Meso-morphism, Interfacial Curvature, and Membrane Fusion. *Biophys. J.* **2004**, *87*, 1054−1064.

(27) Nizri, G.; Makarsky, A.; Magdassi, S.; Talmon, Y. Nanostruc-tures formed by self-assembly of negatively charged polymer and cationic surfactants. *Langmuir* **2009**, *25*, 1980−1985.

(28) Nizri, G.; Magdassi, S.; Schimdt, J.; Cohen, Y.; Talmon, Y. Microstructural Characterization of Micro- and Nanoparticles Formed by Polymer−Surfactant Interactions. *Langmuir* **2004**, *20*, 4380−4385.

(29) Pojják, K.; Fegyver, E.; Mészáros, R. Effect of Linear Nonionic Polymer Additives on the Kinetic Stability of Dispersions of Poly(diallyldimethylammonium chloride)/Sodium Dodecylsulfate Nanoparticles. *Langmuir* **2013**, *29*, 10077−10086.

(30) Kulkarni, C. V. Lipid crystallization: From self-assembly to hierarchical and biological ordering. *Nanoscale* **2012**, *4*, 5779−5791.

(31) Abu-Hamdiyyah, M.; Kumari, K. Partitioning of amphiphilic additives between the micelles of *n*-alkyltrimethylammonium bromides and the surrounding aqueous solution as a function of surfactant chain length. *J. Phys. Chem.* **1990**, *94*, 2518−2523.

(32) Wiese, G. R.; Healy, T. W. Effect of particle size on colloid stability. *Trans. Faraday Soc.* **1970**, *66*, 490−499.

(33) Weisman, S.; Hirsch-Lerner, D.; Barenholz, Y.; Talmon, Y. Nanostructure of cationic lipid−oligonucleotide complexes. *Biophys. J.* **2004**, *87*, 609−614.

(34) Angelov, B.; Angelova, A.; Drechsler, M.; Garamus, V. M.; Mutafchieva, R.; Lesieur, S. Identification of large channels in cationic PEGylated cubosome nanoparticles by synchrotron radiation SAXS and cryo-TEM imaging. *Soft Matter* **2015**, *11*, 3686−3692.

(35) Sagalowicz, L.; Michel, M.; Adrian, M.; Frossard, P.; Rouvet, M.; Watzke, H. J.; Yaghmur, A.; De Campo, L.; Glatter, O.; Leser, M. E. Crystallography of dispersed liquid crystalline phases studied by cryo-transmission electron microscopy. *J. Microsc.* **2006**, *221*, 110−121.

(36) Teixeira, C. V.; Itri, R.; do Amaral, L. Q. Decanol Effect on Micellar Structure and Phase Transitions. *Langmuir* **1999**, *15*, 936−939.

(37) Nakano, M.; Teshigawara, T.; Sugita, A.; Leesajakul, W.; Taniguchi, A.; Kamo, T.; Matsuoka, H.; Handa, T. Dispersions of Liquid Crystalline Phases of the Monoolein/Oleic Acid/Pluronic F127 System. *Langmuir* **2002**, *18*, 9283−9288.

(38) Yaghmur, A.; de Campo, L.; Salentinig, S.; Sagalowicz, L.; Leser, M. E.; Glatter, O. Oil-loaded monolinolein-based particles with confined inverse discontinuous cubic structure (*Fd3m*). *Langmuir* **2006**, *22*, 517−521.

(39) Tran, N.; Mulet, X.; Hawley, A. M.; Hinton, T. M.; Mudie, S. T.; Muir, B. W.; Giakoumatos, E. C.; Waddington, L. J.; Kirby, N. M.; Drummond, C. J. Nanostructure and cytotoxicity of self-assembled monoolein−capric acid lyotropic liquid crystalline nanoparticles. *RSC Adv.* **2015**, *5*, 26785−26795.

(40) Hedegaard, S. F.; Nilsson, C.; Laurinmäki, P.; Butcher, S.; Urtti, A.; Yaghmur, A. Nanostructured aqueous dispersions of citrem interacting with lipids and PEGylated lipids. *RSC Adv.* **2013**, *3*, 24576−24585.

(41) Biltonen, R. L.; Lichtenberg, D. The use of differential scanning calorimetry as a tool to characterize liposome preparations. *Chem. Phys. Lipids* **1993**, *64*, 129−142.

(42) Koynova, R.; Caffrey, M. Phases and phase transitions of the phosphatidylcholines. *Biochim. Biophys. Acta, Rev. Biomembr.* **1998**, *1376*, 91−145.

(43) Risselada, H. J.; Marrink, S. J. The freezing process of small lipid vesicles at molecular resolution. *Soft Matter* **2009**, *5*, 4531−4541.

(44) Hammersley, A. P. FIT2D: An Introduction and Overview. *European Synchrotron Radiation Facility Internal Report*, 1997.

Addition of *n*-Alcohols Induces a Variety of Liquid-Crystalline Structures in Surfactant-Rich Cores of Dispersed Block Copolymer/Surfactant Nanoparticles

Guilherme A. Ferreira[1], Lennart Piculell[2], Watson Loh[1]*

1. Institute of Chemistry, University of Campinas (UNICAMP), P.O. Box 6154, 13083-970, Campinas – SP, Brazil.

2. Division of Physical Chemistry, Lund University, P.O. Box 124, S-221 00, Lund, Sweden.

Corresponding Author

* (W. L.) e-mail: wloh@iqm.unicamp.br; Tel.: +55 19 35213148; Fax: +55 19 35213023

Supporting Information
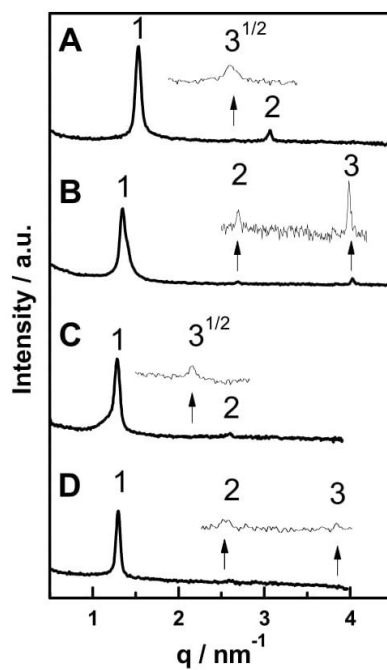
Figure S1. SAXS patterns for PAAm$_{42}$-b-C$_{12}$TAPA$_{42}$ nanoparticles with varying amounts of added decanol A) $R = 0.262$; B) $R = 0.620$; or octanol C) $R = 0.262$; D) $R = 0.620$ displaying hexagonal or lamellar structures. All samples contained 1.0 wt % of poly(acrylamide)-b-CS, analyzed at 25°C.
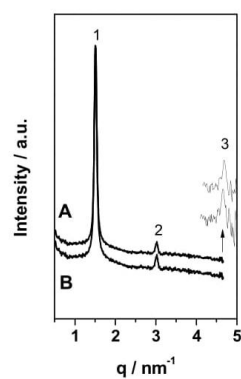
Figure S2. SAXS profiles for PAAm$_{42}$-b-C$_{16}$TAPA$_{42}$ nanoparticles with interior displaying lamellar structures by the addition of different amounts of decanol A) R = 0.325; B) R = 0.335; Samples containing 1.0 wt. % of poly(acrylamide)-b-CS. Analyses performed at 25°C.

Table S1. Size ratio core/lattice parameter (n) for the different poly(acrylamide)-b-CS nanoparticles employed in this work.

Poly(acrylamide)-b-CS	R (octanol)	R (decanol)	n
PAAm$_{42}$-b-C$_{12}$TAPA$_{42}$	0	0	13
	0.256	-	26
	0.262	-	25
	0.613	-	27
	0.620	-	27
	-	0.256	27
	-	0.262	27
	-	0.613	25
	-	0.620	25
PAAm$_{42}$-b-C$_{16}$TAPA$_{42}$	0	0	24
	0.818	-	28
	4.067	-	32
	8.540	-	32
	-	0.142	28
	-	0.321	28
	-	0.325	27
	-	0.335	27

"n" represents size ratio core/lattice parameter and is calculates based on the equation $n = (D_H / a)$, where D_H is the hydrodynamic diameter ($D_H = 2R_H$) and a is the lattice parameter for each

structure. The length of the PAAm chains is neglected as we assume that it is much smaller than the core size.

Regarding Incident 2312863 Permission to reproduce paper from ACS Publication

support@services.acs.org <support@services.acs.org>   22 de outubro de 2018 22:40
Para: guilhermeferreyra@gmail.com

ACS
Chemistry for Life®

Dear Dr. Guilherme A. Ferreira,

Thank you for contacting ACS Publications Support.

Your permission request is granted and there is no fee for this reuse. In your planned reuse, you must cite the ACS article as the source, add this direct link <https://pubs.acs.org/doi/abs/10.1021/acsomega.6b00267>, and include a notice to readers that further permissions related to the material excerpted should be directed to the ACS.

Should you need further assistance, please let us know.

Sincerely,

Noemi D. Cabalza

ACS Customer Services & Information

Website: https://help.acs.org/

Incident Information:

Incident #:   2312863

Date Created: 2018-10-23T09:14:26

Priority: 3

Customer: Guilherme A. Ferreira

Title: Permission to reproduce paper from ACS Publication

Paper III

Impact of preparation procedure on the physicochemical properties of block copolymer nanoparticles containing surfactant-rich cores.

Guilherme A. Ferreira[1], Lennart Piculell[2], Watson Loh[1,]*

[1]Institute of Chemistry, University of Campinas (UNICAMP), P.O Box 6154, Campinas-SP, Brazil.

[2]Division of Physical Chemistry, Lund University, Box 124, SE-221 00 Lund, Sweden

* e-mail: wloh@iqm.unicamp.br

ABSTRACT

Complex coacervate core micelles (C3Ms) formed by a stabilizing corona consisting of poly(acrylamide) water-soluble blocks surrounding a core consisting of poly(acrylate)-dodecyltrimethylammonium hydrated complex have been prepared by different approaches: the conventional mixing (CP approach) of solutions containing the block copolymer and surfactant, with their respective simple counterions, and dispersion of a freeze-dried complex prepared in the absence of simple counterions (CS approach). The complexes were then investigated under different conditions: dispersion of a salt-free CS in salt-free water, and dispersion of a salt-free CS in a dilute salt solution, the latter condition yielding dispersions with the same composition as the conventional mixing (CP) process. Additionally, a dispersion of a salt-containing freeze-dried CP in pure water has also been studied. The obtained particles have been characterized by light and X-ray scattering techniques, zeta potential and cryogenic transmission electron microscopy. Particles prepared by the CP approach display spherical shape, disordered cores, low surface charge that resulted in poor colloidal stability and are smaller than those prepared by the CS method, that display a micellar cubic core and colloidal stability that can be tuned by the length of the neutral block composing the corona. In addition, particles prepared by the CS approach are oblate rather than spherical. Our results demonstrate that these C3Ms are metastable structures, with physicochemical properties strongly dependent on the preparation procedure.

1. INTRODUCTION

Complex coacervate core micelles (C3Ms) are particles formed by water-soluble neutral-charged block copolymers and oppositely charged macroions in solution. The oppositely charged species can be ionic surfactants, charged homopolymers or other neutral-cahrged block copolymers. C3Ms usually display a stabilizing corona consisting of neutral water-soluble blocks of the copolymer surrounding a core consisting of complexed oppositely charged units. Their cores, which are water-insoluble but hydrated, can display a liquid- or solid-like arrangement.[1] Several reports have shown that the physicochemical properties of C3Ms are process-dependent, indicating that they are not equilibrium structures but metastable aggregates.[2-8]

Among the several examples of C3Ms presented in the literature, water-dispersible core-shell nanoparticles made from charged−neutral block copolymers (BCP) and oppositely charged surfactants have also been reported, where the most studied systems were comprised of alkyltrimethylammonium cationic surfactants and the block copolymer poly(acrylamide-*b*-acrylic acid), here abbreviated as PAAm-*b*-PAA.[9-14] These nanoparticles were described as possessing a core that contains several densely packed-surfactant micelles surrounded by the anionic block of the copolymer, due to the electrostatic association between the oppositely charged species. The outer part consists in a corona composed by the neutral PAAm chains.[9-12]

It has been described, basically, two methodologies to prepare the core-shell particles. The conventional procedure is based on the mixing of individual aqueous solutions containing the neutral-charged block copolymer and the charged surfactant, with their respective counterions, in a charge ratio of 1.[9-12] Such approach will be refereed here as *CP*, referring to *conventional procedure*. Extensive studies have shown that the particles, with average size of 50 nm, prepared by the CP approach display cores arranged in a disordered state, showing no long-range order. In addition, these nanoparticles were shown to display a spherical shape and, because of the low surface charge, a poor colloidal stability.[9-12]

Our group has recently expanded the studies on PAAm-*b*-PAA-cationic surfactant particles by employing a new methodology based on the *complex salt* (*CS*) approach.[13,14] In this case, the acrylate units of the BCP are neutralized by alkyltrimethylammonium cationic surfactant ions, giving rise to block copolymer complex salts, here abbreviated as BCPCS, free of counterions. Interestingly, the dispersions produced from BCPCS gave particle cores displaying a *Pm3n* micellar cubic or hexagonal liquid crystalline structure, depending on the surfactant ion alkyl chain length.[13,14]

In addition, particles prepared by the CS approach displayed larger average sizes, in the 200-300 nm range, besides a negative surface which implicated in an enhanced colloidal stability, producing particles that remained essentially unchanged for several weeks.[14] Similar results were found for BCPCS dispersed particles, featuring other neutral blocks, poly(ethylene oxide), PEO, and poly(N-isopropylacrylamide), PNIPAm.[15]

It is questionable whether the small differences in composition, that is the presence (CP approach) or absence (CS approach) of low concentrations of inorganic ions, resulting from the two methods of preparation, could be the cause of the remarkable differences in the properties of the particles. It is known that important properties of the nanoparticles, such as their shape, may display changes depending on the preparation procedure and the fact that the particles prepared by the two methods display striking differences in the surface charge may implicate in differences in the colloidal stability of the dispersions as the time evolve. Additionally, the length of the neutral blocks, i.e. the corona thickness, may also influence on the particle's stability. However, such an investigation has not been conducted thoroughly yet and discussions about the size, shape and long-range order in core-shell particles prepared by the SM and CS approaches of the produced nanoparticles are lacking in the reports to date.

Then, in this context we are interested in investigating the colloidal and structural characteristics of particles composed of PAAm-b-PAA BCP and dodecyltrimethylammonium cationic surfactant prepared by two different methodologies. The impact of copolymer block proportions, absence and presence of simple counterions and mixing conditions are also investigated. Static and Dynamic Light Scattering (SLS and DLS) coupled with SAXS (Small Angle X-ray Scattering) have been employed to characterize the variety of particles obtained in terms of size, shape and colloidal stability. In addition, samples were also investigated by means zeta potential, besides cryogenic transmission electron microscopy (Cryo-TEM) for selected samples.

2. EXPERIMENTAL

Chemicals. The block copolymer PAAm$_{133}$-b-PAA$_{49}$ in which the subscript characters refer to the weight average number of repeating units of each block, was synthesized and characterized as described earlier[13]. PAAm$_{422}$-b-PAA$_{69}$ was a gift from Rhodia (Cranbury, USA). The properties of the block copolymers are presented in Table 1. Dodecylltrimethylammonium bromide, (C$_{12}$TABr) and Sodium Bromide (NaBr), of 99% purity, were purchased from Sigma-Aldrich (USA) and used as received. Deionized water with

a resistivity above 18.2 MΩ.cm^{-1}, as obtained by a Milli-Q$^{®}$ system, was used in all experiments.

Table 1 – Weight average molar mass of the blocks and dispersity (*D*) of the PAAm-*b*-PAA block copolymers employed in this work.

Block copolymer	PAAm / g.mol^{-1}	PAA / g.mol^{-1}	D^1
PAAm$_{133}$-*b*-PAA$_{49}$	9415	3500	2.1[2]
PAAm$_{432}$-*b*-PAA$_{70}$	30680	5000	1.6[3]

1 – D = M_w/M_n, as determined by gel permeation chromatography

2 – According to ref. 16

3 – According to ref. 10

Preparation of salt-free particles by the CS approach. The two BCPCS were prepared following the general procedure described earlier.[13-15] Briefly, the hydroxide form of the C$_{12}$TABr surfactant, obtained by an ion-exchange step, was titrated with aqueous solutions of the BCP in the acid form until the equivalence point (pH 8.6-8.9). The resulting mixtures were left overnight at 4°C and their pH were adjusted to the equivalence point when necessary, with the corresponding BCP solution. The BCPCS in the solid form were isolated from the solution by freeze-drying the mixture and were kept in a desiccator. The particle dispersions were prepared by vortexing (Vortex-Genie 2 mixer - Scientific Industries, operating at 3200 rpm) for ca. 1 minute, the appropriate amounts of BCPCS in water to achieve the final solid concentration of 1.0 wt %. The particles obtained by employing this methodology will be refereed as CS_C$_{12}$S and CS_C$_{12}$L, where the term CS denotes for the approach used to prepare them (CS, in this case), C$_{12}$ for the surfactant alkyl chain length and S and L referrer to the length of the PAAm block in the BCP employed in the synthesis, *S* for the BCP with a short PAAm block (PAAm$_{133}$-*b*-PAA$_{49}$) and *L* for the BCP with a long PAAm block (PAAm$_{432}$-*b*-PAA$_{70}$).

Preparation of salt-containing particles by the CS approach. The same procedure was employed to prepare the salt-containing dispersions, where the BCP were dispersed in 1 mM NaBr aqueous solution. The samples were named as CS_C$_{12}$S#NaBr and CS_C$_{12}$L#NaBr.

Preparation of particles by the CP approach. Individual dilute aqueous solutions containing the sodium salt of the BCP and C$_{12}$TABr were mixed in a vortex vibrator for ca. 1 minute. The concentrations of the initial solutions were adjusted in a such a manner to achieve

a final molar charge ratio of 1 in the mixture. Following the same trend, the samples obtained in this step were named as CP_C_{12}S and CP_C_{12}L.

Techniques. *Dynamic and Static Light Scattering (DLS and SLS).* Light scattering measurements were performed on a CGS-3-based compact goniometer system (ALV-GmbH, Langen, Germany), equipped with a detection system in a pseudo−cross-geometry, with a 22 mW He−Ne laser (λ= 632.8 nm) and an ALV 7004 multi-tau correlator. cis-Decalin was used as the refractive index-matching liquid. DLS was performed at the detection angle (θ) of 90° for 0.001-0.01 wt% dilute samples. SLS measurements were performed at 20°≤θ≤140° in intervals of 5° for samples at the same concentration range. The refractive index increment for the particle dispersions was taken from Vitorazi et al.[13] The effective hydrodynamic radii $< R_H >_0$ from DLS (cumulant analysis and Stokes-Einstein approximation) and the effective radius of gyration $< R_g >_0$ from SLS (Guinier analysis) were calculated according to conventional methods.[17,18] A Malvern Nano Zetasizer instrument with a 632.8 nm laser and detector positioned at 173° was employed to measure the apparent R_H of the dispersed particles in the colloidal stability studies. The zeta potential (ζ) was estimated based on the electrophoretic mobility measurements using the Smoluchowski model.

Small angle X-ray scattering (SAXS). SAXS measurements were performed at the SAXS1 beamline of the Brazilian Synchrotron Light Laboratory, LNLS, in Campinas, Brazil. The samples were positioned in a cell with two flat mica windows and a thermal bath connected to the sample holder was used for temperature control. The X-ray wavelength was 1.608 Å and the sample-to-detector distance was calibrated employing silver behenate. The obtained CCD images were integrated and treated with the software Fit2D[19] to obtain the scattering function $I(q)$, where $q = \left({4\pi}/{\lambda} \right) sin\left(\theta/2 \right)$, with λ being the wavelength and θ the scattering angle. Some measurements were also performed using a Ganesha 300XL SAXSLab instrument, housed at Physical Chemistry – Lund University, equipped with a sealed micro-focus X-ray tube with λ = 1.54 Å and a pin-hole collimated beam with an asymmetrically positioned 2D 300K Pilatus detector. In this case, samples were analyzed in 1.3 mm diameter quartz glass capillaries (Hilgenberg). SASView software[20] was used to fit experimental data of dilute 0.01 wt% samples to the "Core-Shell Ellipsoid" and "Core-Shell Sphere" models, which are described in details in references 21 and 22. The relative diffraction peak positions observed in the 1.0 wt% samples were used to identify the structures formed. The interplanar spacing (d) between two reflecting planes is given by $d = {2\pi}/{q}$, which enables us to calculate the corresponding mean lattice parameter (a).[23] All measurements were performed at 25°C.

Cryogenic Transmission Electron Microscopy (Cryo-TEM). Specimens were prepared in a controlled environment vitrification system (CEVS) at 25°C at 100% relative humidity, to prevent evaporation from the specimen, as described elsewhere.[24] 5 μl of 1 wt% CS_C$_{12}$S and CS_C$_{12}$L freshly prepared and 6 months-aged dispersions were placed on a carbon film supported by a cupper grid and blotted from the front and from the back with filter paper to reduce film thickness, after different relaxation times: 0 and 10 s. The grid was quenched in liquid ethane at − 196 °C, stored under liquid nitrogen (–196 °C) and transferred to a Cryo-TEM (Philips CM120 BioTWIN Cryo) equipped with a post-column energy filter (Gatan GIF 100), using an Oxford CT3500 cryo-holder and its workstation. The acceleration voltage was 120 kV and the working temperature was below − 180 °C. The images were digitally recorded with a CCD camera (Gatan MSC 791) under low-dose conditions.

3. RESULTS

3.1 Light and X-ray scattering study of dilute particle dispersions

DLS experiments were performed at θ=90° for 0.001-0.01 wt% dilute samples. By extrapolating the diffusion coefficients values (D) to concentration c = 0 (Fig. 1A), the effective D values, i.e. the D values at infinite dilution, were obtained for the investigated particles and converted to effective hydrodynamic radius, $< R_H >_0$, presented in Table 2. SLS measurements were performed at 20°≤θ≤140° in intervals of 5° for samples in the same concentration range, that is 0.001-0.01 wt%. By employing the Guinier analysis of the SLS data (Fig. 1B, for samples at 0.01 wt%), the effective radius of gyration $< R_g >_0$ were also obtained by extrapolating the R_g values to c = 0 (Fig. 1C) and are displayed in Table 2.

For the particles prepared by the CP approach (CP_C$_{12}$S and CP_C$_{12}$L), the $< R_g >_0/< R_H >_0$ shape factor values between 0.756 and 0.763 are in good agreement with the value for a sphere (0.775).[25] However, for all investigated particles prepared employing the CS approach, the shape factor values were far from what is expected for a homogeneous sphere (Table 2), indicating the shape of elongated objects.[26] This was confirmed by SAXS analysis coupled with SLS data, to cover a large q-range.
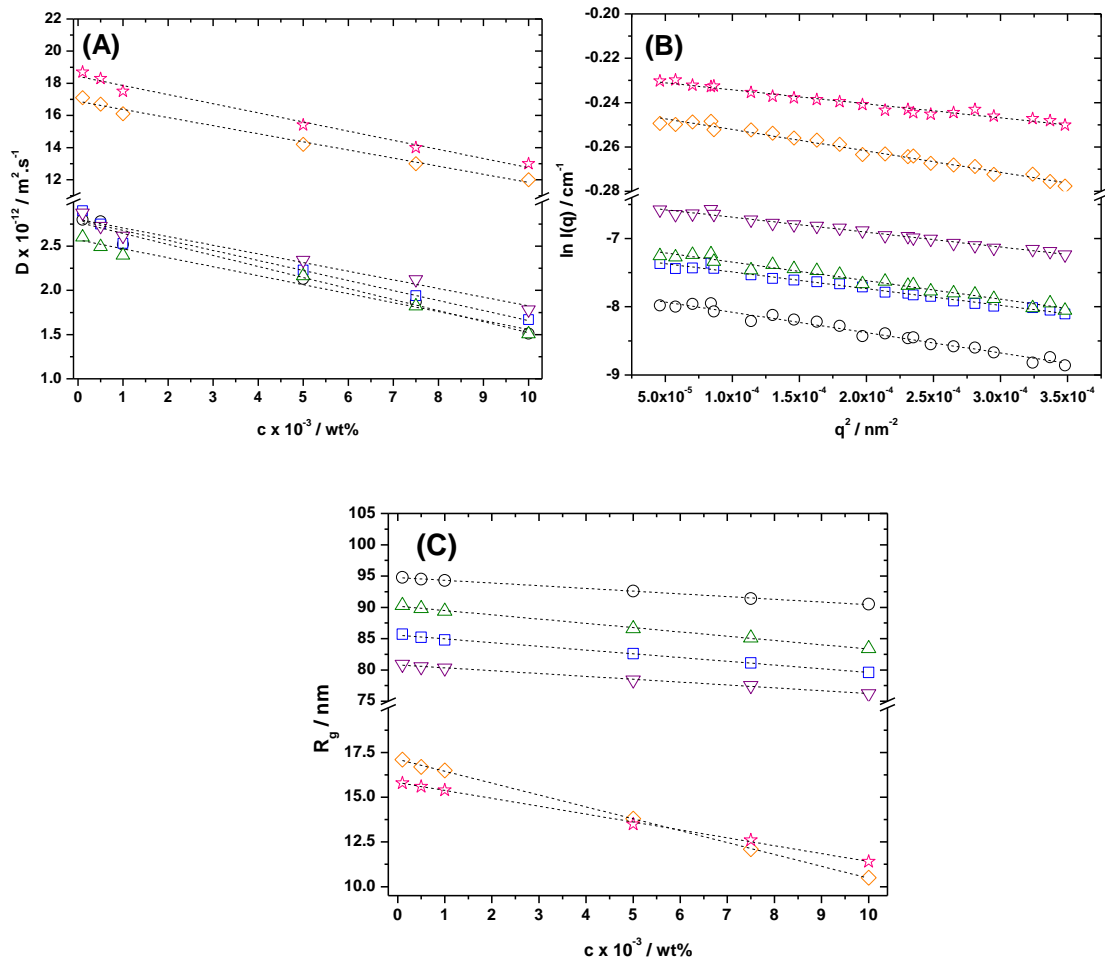
Fig. 1. (A) Diffusion coefficients (*D*) as a function of sample concentration (c) calculated based on DLS data at θ=90°. Dashed lines are linear fits employed to extrapolate data to c = 0. **(B)** Guinier plots based on SLS data for samples at 0.01 wt% concentration. Dashed lines are linear fits. **(C)** Radius of gyration (R_g) as a function of sample concentration measured by SLS. Dashed lines are linear fits employed to extrapolate data to c = 0. ○ CS_C$_{12}$S, □ CS_C$_{12}$L, △ CS_C$_{12}$S#NaBr, ▽ CS_C$_{12}$L#NaBr, ◇ CP_C$_{12}$S, ✳ CP_C$_{12}$L.

Table 2. Effective hydrodynamic radius $< R_H >_0$, effective radius of gyration $< R_g >_0$ and $< R_g >_0/< R_H >_0$ shape factor for all the investigated samples.

Sample	$< R_H >_0$ / nm[1]	$< R_g >_0$ / nm[2]	$< R_g >_0/< R_H >_0$
CS_C$_{12}$S	97.4	94.8	0.973
CS_C$_{12}$L	87.5	85.7	0.979
CS_C$_{12}$S#NaBr	91.9	90.3	0.982
CS_C$_{12}$L#NaBr	82.2	80.9	0.984
CP_C$_{12}$S	22.6	17.1	0.756
CP_C$_{12}$L	20.7	15.8	0.763

1. Obtained from DLS data at θ=90° based on data displayed in Fig. 1A.

2. Obtained from SLS data and Guinier analysis (Fig. 1B and 1C).

Fig. 2 shows SLS + SAXS plots for all investigated samples. The experimental data for the particles prepared by the CS approach were best fitted with a core-shell oblate ellipsoid model, which dimensions are displayed in Table 3, confirming the existence of flattened objects, as suggested by light scattering results presented above. Also, in agreements with the previously displayed results, CP_C$_{12}$S and CP_C$_{12}$L scattering data were fitted with a core-shell sphere, with dimensions also presented in Table 3. Hence, the light and X-ray scattering results for dilute particle dispersions indicated great similarities between salt-free and salt-containing particles prepared employing the CS methodology (Fig, 2A) and notable differences when compared with the samples prepared by the simple mixing of the individual solutions of the components with their respective counterions, that is CP_C$_{12}$S and CP_C$_{12}$L (Fig. 2B).
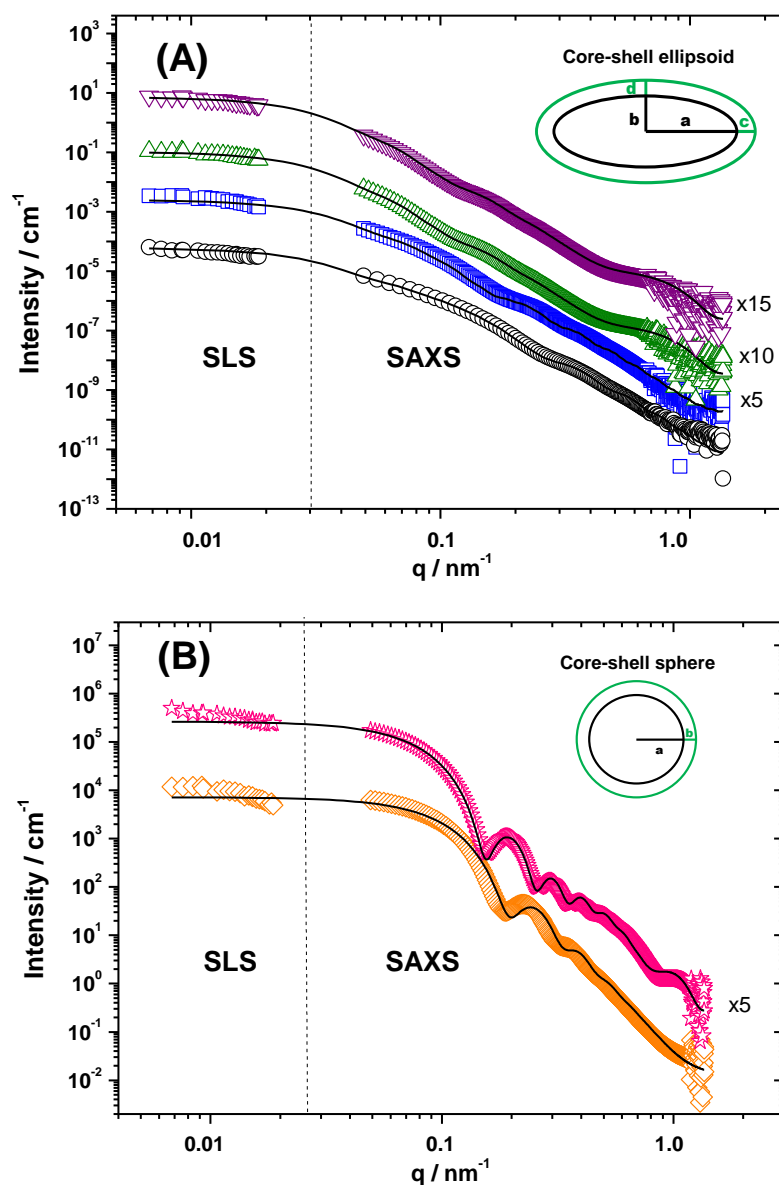
Fig. 2. SLS and SAXS data for 0.01 wt% samples. **(A)** ○ CS_C_{12}S, □ CS_C_{12}L, △ CS_C_{12}S#NaBr, ∇ CS_C_{12}L#NaBr. Black lines represent the best fit for core-shell oblate ellipsoid according to the model described in ref. 21. The inset shows a representation of the core-shell ellipsoid in which a, b, c and d represent the equatorial radius of the core, the polar radius of the core, the thickness of the shell at equator and the thickness of the shell at polar, respectively. **(B)** ◇ CP_C_{12}S, ✳ CP_C_{12}L. Black lines represent the best fit for core-shell sphere according to the model described in ref. 22. The inset shows a representation of the core-shell sphere in which a and b represent the radius core and the thickness of the shell, respectively.

Table 3. Dimensions obtained for the different investigated particles derived from the best fits obtained for the experimental light and X-ray scattering data according to the core-shell ellipsoid and sphere models.

Sample	Fitted model	Dimensions / nm[1,2]
CS_C_{12}S	Core-shell ellipsoid	a = 84.0, b = 22.0, c = d = 3.5
CS_C_{12}L		a = 85.0, b = 26.0, c = 9.0, d = 12.0
CS_C_{12}S#NaBr		a = 90.0, b = 16.0, c = d = 3.0
CS_C_{12}L#NaBr		a = 88.0, b = 20.0, c = 9.0, d = 13.0
CP_C_{12}S	Core-shell sphere	a = 20.0, b = 3.0
CP_C_{12}L		a = 18.0, b = 12.0

1. In the core-shell ellipsoid model, a, b, c and d represent the equatorial radius of the core, the polar radius of the core, the thickness of the shell at equator and the thickness of the shell at polar, respectively. In the core-shell sphere model, a and b represent the radius core and the thickness of the shell, respectively.

2. All the obtained parameters were obtained assuming a polydispersity index of 0.12 and 0.13 for the radius of the core in in the ellipsoid and sphere models, respectively.

3.2 SAXS on particle dispersions at 1.0 w%

Particles prepared by the CS and CP approach at 1.0 wt% concentration were characterized by SAXS at wide q-range to check the presence of long-range order in their cores. Fig. 3A shows SAXS patterns obtained for CS_C_{12}S and CS_C_{12}L dispersions. The scattering peaks displaying a spacing ratio of $4^{1/2}:5^{1/2}:6^{1/2}$ indicated a *Pm3n* micellar cubic structure in the particle cores.[23] The lattice parameters (a) for the cubic phases were 8.40 nm, in agreement with previous results on similar systems.[13-15,27] For the salt-containing particles (CS_C_{12}S#NaBr and CS_C_{12}L#NaBr) the core structures were also micellar cubic (Fig. 3B). However, in the presence of NaBr, the lattice parameters of the liquid-crystalline structures have increased to $a = 9.0$ nm.
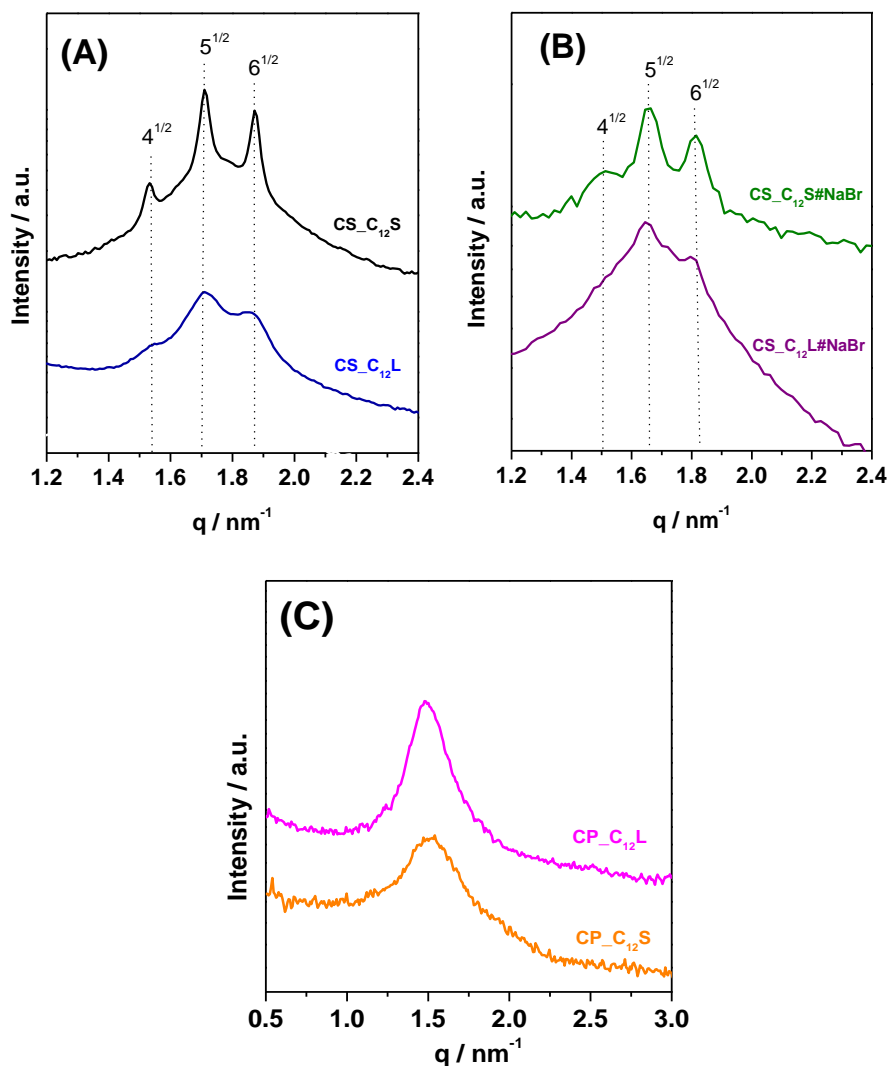
Fig. 3. SAXS patterns obtained for samples at 1.0 wt%. (A) CS_C_{12}S and CS_C_{12}L. (B) CS_C_{12}S#NaBr and CS_C_{12}L#NaBr. (C) CP_C_{12}S and CP_C_{12}L.

The particles prepared by the CP approach, that is CP_C_{12}S and CP_C_{12}L, displayed only one scattering peak in the SAXS patterns (Fig.3C), indicating the formation of cores in which the surfactant micelles are arranged in a disordered state, i.e. they are amorphous. These results are consistent with what has been previously reported for core-shell particles formed by the surfactant and block copolymer with their respective counterions.[9-12] The observed correlation peak at $q \sim 1.5$ nm^{-1} corresponds to the 4 nm inter-micellar average distance, as described elsewhere. [9-12]

The average crystalline core size (ξ) for particles displaying a liquid crystalline cubic core was estimated based on Scherrer equation[23], considering the full width at half maximum of the highest intensity diffraction peak in the SAXS patterns (Fig.3A and B). The results are summarized in Table 4. CS_C_{12}L particles displayed larger crystalline core size if

compared with the parent CS_C$_{12}$S. All particles dispersed in NaBr aqueous solutions present core sizes smaller than those prepared in pure water.

Table 4 – Average crystalline core size (ξ) for particles displaying a liquid crystalline core dispersed in water and in NaBr aqueous solution.

Sample	Core structure	ξ / nm
CS_C$_{12}$S	micellar cubic	140
CS_C$_{12}$L	micellar cubic	78
CS_C$_{12}$S#NaBr	micellar cubic	51
CS_C$_{12}$L#NaBr	micellar cubic	45

3.3 Colloidal stability study

Freshly prepared 0.01 wt% dilute dispersions were characterized regarding their apparent hydrodynamic radii (R_H) and zeta potentials (ζ). Table 5 summarizes the results for all the different investigated particles. The average R_H values for the salt-free particles prepared by the CS approach, CS_C$_{12}$S and CS_C$_{12}$L, was around 110-120 nm. The polydispersity index (PDI) was consistently ca. 0.1. All particles displayed a negative surface charge, as evidenced by their zeta potentials values.

Table 5. Apparent hydrodynamic radius (R_H), polydispersity index (PDI) and zeta potential (ζ) for all investigated samples (avg. $\pm$ SD, triplicate of independent preparations).

Sample	R_H / nm[1]	PDI	ζ / mV
CS_C$_{12}$S	110$\pm$10	0.12	-35$\pm$5
CS_C$_{12}$L	120$\pm$10	0.13	-35$\pm$5
CS_C$_{12}$S#NaBr	440$\pm$20; 110$\pm$20	0.40	0
CS_C$_{12}$L#NaBr	250$\pm$30	0.31	0
CP_C$_{12}$S	45$\pm$10	0.20	0
CP_C$_{12}$L	42$\pm$10	0.20	0

1. Measured in a Malvern instrument at θ=90°

According to Table 5, particles prepared employing the CS methodology but dispersed in 1 mM aqueous NaBr solution displayed average R_H values larger, as well as the PDI. Surprisingly, the zeta potentials values decreased to ca. 0 in the presence of small amounts

of salt. Particles prepared by the CP approach, displayed a distribution of size around 40 nm and zeta potential values close to charge neutrality.

The colloidal stability of the different particle dispersions as a function of time of sample preparation was also studied by means of their hydrodynamic radii (R_H) from time zero (the time of sample preparation) up to 6 months. This study was conducted only in CS_C$_{12}$S and CS_C$_{12}$L samples, in which an enhanced stability was visually observed (Fig.4A and B). CS_C$_{12}$S#NaBr and CS_C$_{12}$L#NaBr particles displayed very poor colloidal stability (Fig.4C and D), presenting a macroscopic phase separation within few hours of sample preparation. CP_C$_{12}$S and CP_C$_{12}$L also presented the same behavior and phase-separated after few days (Fig.4E and F).
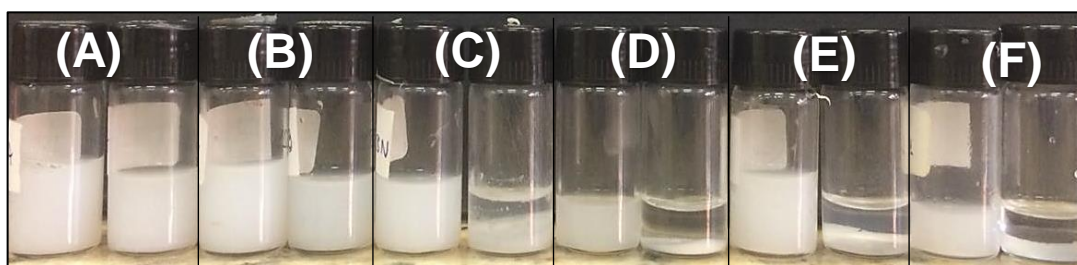

Fig. 4. Photographs of freshly prepared (left side) and 7 days-aged (right side) particle dispersions prepared by different methodologies. (A) CS_C$_{12}$S. (B) CS_C$_{12}$L. (C) CS_C$_{12}$S#NaBr. (D) CS_C$_{12}$L#NaBr. (E) CP_C$_{12}$S. (F) CP_C$_{12}$L.

CS_C$_{12}$S and CS_C$_{12}$L dispersions are stable for several months, without any signs of macroscopic phase separation. The CS_C$_{12}$S particles displayed two distinct phases after around 6 months. At the same time, CS_C$_{12}$L dispersions visual aspect remained unchanged, displaying a homogeneous opaque appearance, as in the freshly-prepared samples. Quantitative analysis of the data displayed in Fig. 5A corroborates the information obtained by visual inspection. It is possible to observe that the average size of the CS_C$_{12}$S particles presented a continuous increase over the investigated period, reaching an average radius of around 300 nm, where the macroscopic phase separation takes place.

The aggregation and consequent phase separation observed for CS_C$_{12}$S particles after around 6 months were reversible. The redispersion by vortex mixing the solid phase at the bottom of the sample gave nanoparticles with a similar average size than the non-aged dispersions (Fig.5, red symbol). In an opposite manner, CS_C$_{12}$L remained stable, with no changes in their average size (Fig. 5A).
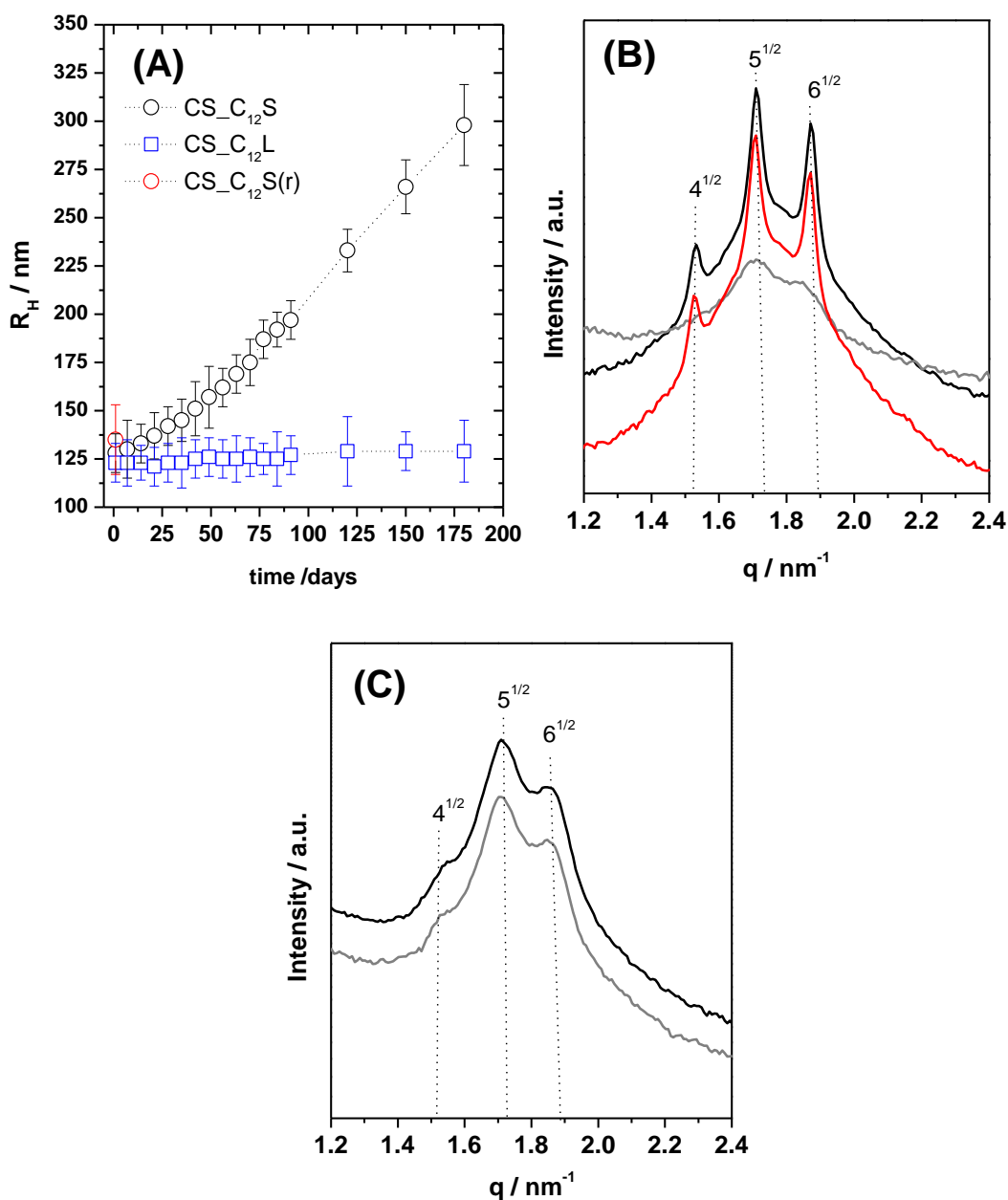
Fig. 5 (A) Evolution of the apparent hydrodynamic radius (R_H) as a function of time of sample preparation for CS_C_{12}S and CS_C_{12}L particles. CS_C_{12}S (r) denotes a 6 months-aged sample after redispersion by vortex mixing. Dashed lines are guide to the eyes. Results are displayed as avg $\pm$ SD (three independent preparations) **(B)** Evolution of SAXS patterns as a function of time of sample preparation for CS_C_{12}S: freshly prepared (black line), 6 months-aged (gray line) and 6 months-aged sample after redispersion by vortex mixing (red line). **(C)** Evolution of SAXS patterns as a function of time of sample preparation for CS_C_{12}L: freshly prepared (black line) and 6 months-aged (gray lines) sample.

SAXS patterns (Fig.5B) were recorded for freshly prepared and 6 months-aged CS_C_{12}S samples, in intact dispersions, to better understand the aging effects observed in the

above-mentioned results. The core structures, i.e. micellar cubic arrangement, remained unchanged over the investigated period. However, it is possible to note that the Bragg peaks became broader as the time of sample preparation increased. The SAXS patterns were recovered after redispersion by vortex mixing of the 6 months-aged sample (Fig.5B). In addition, SAXS results confirmed that CS_C_{12}L samples remained essentially unchanged over the investigated time (Fig.5C).

To better understand the striking differences in the colloidal stability of particles prepared by the CS and CP approach, the dispersions prepared by the CP approach were freeze-dried after sample preparation. The resulting particles in the powder form were mixed with water using a vortex vibrator for ca 1 minute. Large aggregates in solution were formed, instead of dispersed nanometric particles, as illustrated in Fig. 6. The freeze-drying and redispersion of particles by the CS approach have not altered their aspect when compared with the freshly prepared dispersions (Fig. 6).
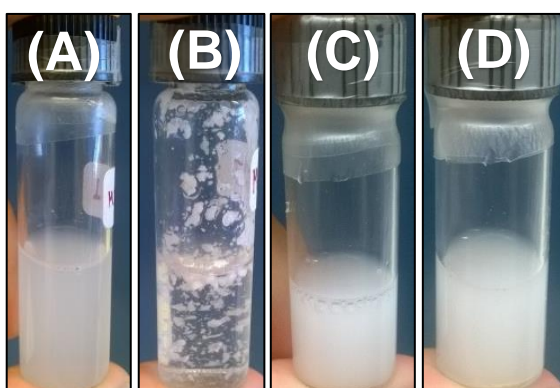

Fig. 6. Photographs of the particle dispersions. (A) CP_C_{12}S freshly prepared. (B) CP_C_{12}S after freeze-drying and redispersion. (C) CS_C_{12}S freshly prepared. (D) CS_C_{12}S after freeze-drying and redispersion.

3.4. Cryo-TEM study of selected samples

Cryo-TEM was employed, as a complementary technique, to investigate important features of the particle dispersions, such as their shape and colloidal stability. For this purpose, CS_C_{12}S and CS_C_{12}L freshly prepared and 6 months-aged samples at 1.0 wt% concentration were studied. Fig. 7A and B show an overall view of CS_C_{12}S freshly prepared dispersion, where is seen several semi-spherical and elongated particles (Fig. 7A). Magnification (Fig. 7B) clearly shows particles with long range order, with an average size in the range of 200-300 nm, which corroborates the light and X-ray scattering results. Similar results were found for CS_C_{12}L samples (Fig. 7C and D).

Freshly prepared $CS\_C_{12}S$ specimens have been tilted during data collection at different angles. At 0° tilting angle, the image displays a spherical-shaped particle (Fig. 7E). However, by tilting the specimen to 60° angle, the image shows that the particle has shrink along one dimension, assuming a flattened shape (Fig. 7F). Similar results were found for a set of visualized $CS\_C_{12}S$ particles, as well as for $CS\_C_{12}L$. Aged $CS\_C_{12}S$ sample displayed a pattern of light domains separated by dark boundaries of uniform thickness covering the surface (Fig. 7G), instead of the well dispersed particles seen in the non-aged samples. $CS\_C_{12}L$ aged sample remained essentially unchanged (Fig. 7H).
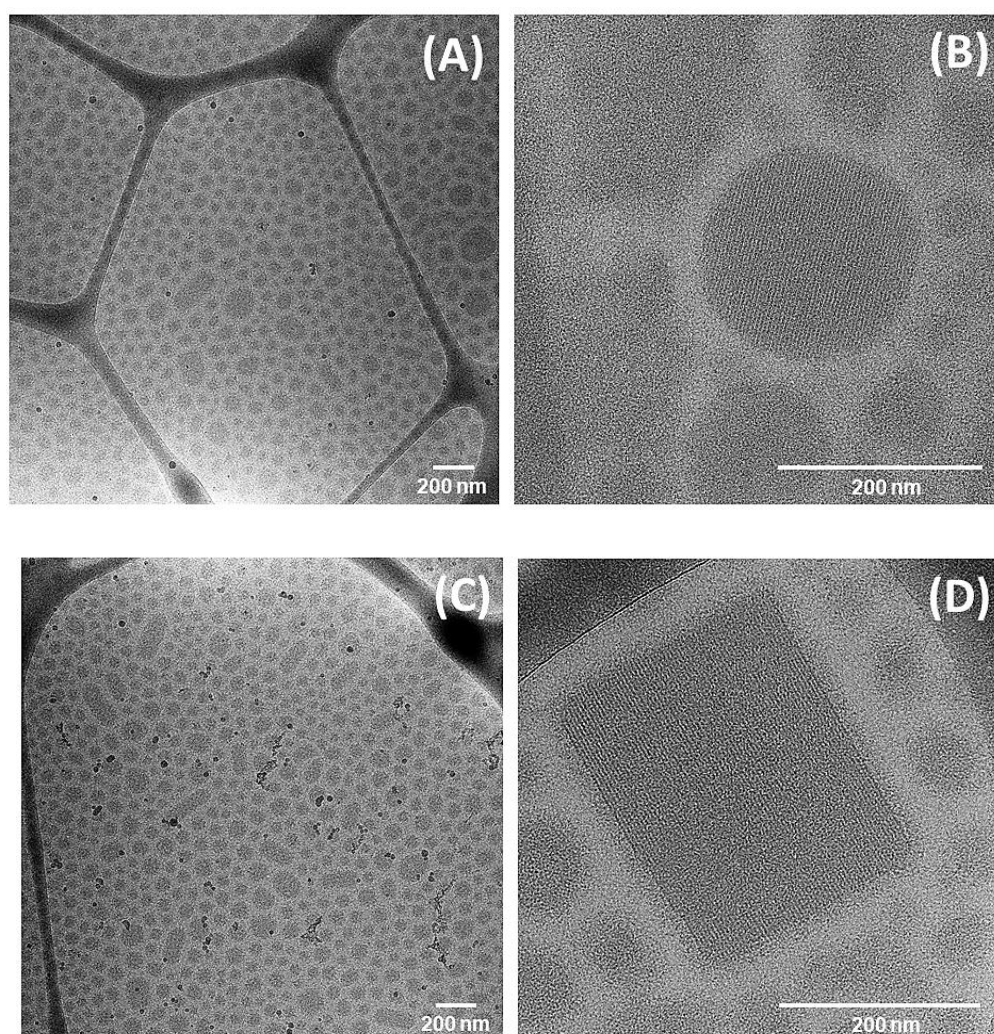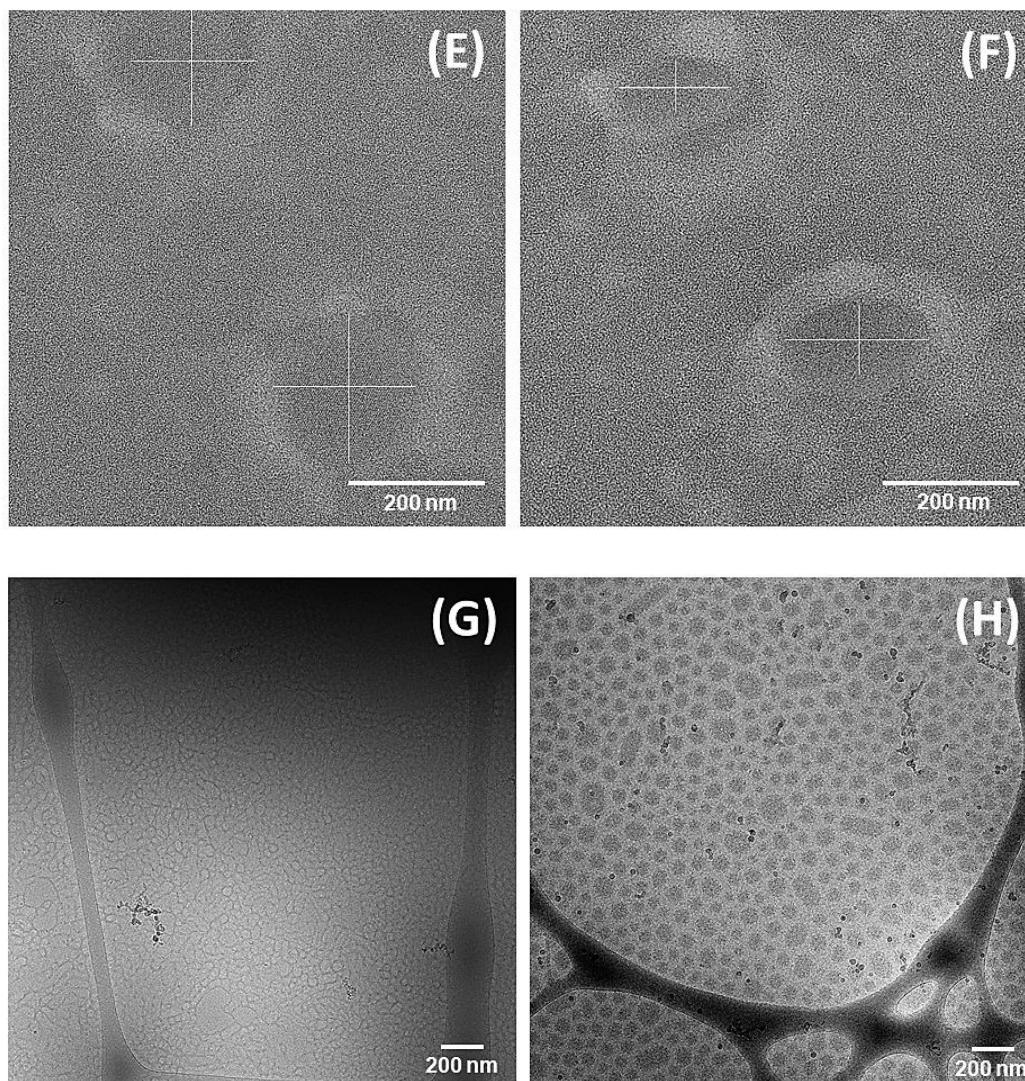
Fig.7 Cryo-TEM images obtained for 1 wt% samples. (A) and (B) CS_C_{12}S (freshly prepared). (C) and (D) CS_C_{12}L (freshly prepared). (E) CS_C_{12}S (freshly prepared) at 0° tilting angle. (F). CS_C_{12}S (freshly prepared) at 60° tilting angle. (G). CS_C_{12}S (6 months-aged). (H) CS_C_{12}L (6 months-aged).

4. DISCUSSION

Core-shell structures are formed as discrete particles at small concentration of all investigated dispersions in water. The aggregate inner structures are formed by several surfactant micelles organized in a micellar cubic or amorphous arrangement depending on the preparation procedure. It is questionable if the small differences in the composition of the samples could be the cause of the remarkable differences in the arrangement in the particle cores. In a previous report, it was assumed that the particle size could be more important on the formation of long-range order in the cores. Because the particles obtained by the CP approach

display smaller average size, their cores would not be large enough to constitute a liquid-crystalline domain.[14]

It has been also noticed that the PAAm block length also plays an important role on the long-range order of the internally-structured particles. SAXS data (Fig. 3A) for micellar cubic CS_C$_{12}$S and CS_C$_{12}$L particles, displaying a very similar average size as measured by DLS, show smaller domain size for CS_C$_{12}$L particles (Table 5). Similar behavior has been observed for salt containing CS samples (Fig. 3B and Table 5).

Hence, variations in the long-range ordered domain sizes may be related to the long PAAm block in CS_C$_{12}$L particles, in which the corona takes up a larger fraction of the particle with decreased core sizes. In fact, it has been demonstrated that, for block copolymers with very long PAAm blocks, the core size is so small that does not display long-range order.[13] Similar arguments were also used to explain the formation and stability of C3Ms. It has been shown that a corona block that is three times longer than the core block is a prerequisite for stable micelles and with very asymmetric block length ratios, no micelles are formed.[28] In addition, if the neutral block is too short, the C3Ms form a macroscopic precipitate.[28]

By comparing particles prepared by the same approach, the commonly encountered preparation dependence suggests that these particles are not equilibrium structures and that their size is process-dependent, which is consistent with the properties of colloidal, i.e. kinetically stable, dispersions. By using the CS approach, it is possible to achieve particles with the same average size, even though they display different block copolymer lengths[13], neutral blocks (such as PEO and PNIPAM)[15] and core structures.[14] Particles prepared by the CP approach also display reproducible size, regardless of the block copolymer length.

Apart from the average size, another striking difference by comparing CS- and CP-based particle dispersions is that the first display a negative surface charge, as evidenced by their zeta potential values, while the later ones possess surface charge close to zero (Table 5). The presence of negative surface charge in the particles is related to the surfactant dissociation from the complex core into the aqueous phase and has been discussed before in one of our previous report.[14] Similar behavior is expected in CP-based particles.

However, the presence of surfactant and block copolymer counterions (bromide and sodium, respectively), even at small concentrations, seems to shield the surface charge of these particles, leading to aggregates with zeta potentials close to charge neutrality. This is confirmed by comparing the results for CS_C$_{12}$S#NaBr and CS_C$_{12}$L#NaBr dispersions (Table 5). At 1 mM of salt, the surface charge of these particles is completely vanished, indicating the great role of the counterions on the zeta potential of the currently studied particles.

The observed variations in the zeta potential values could imply in the long-term colloidal stability of the particle dispersions depending on the preparation procedure, because the kinetic stability comes from both electrostatic and steric repulsive forces. In fact, particles prepared by the CS approach presented enhanced colloidal stability, with no signs of macroscopic phase separation for months, as illustrated in Fig. 4. Oppositely, salt-containing particles, either those prepared by the CP approach or CS_C_{12}S#NaBr and CS_C_{12}L#NaBr, displayed very poor colloidal stability. Such results indicate the importance of the surface charge on the stabilization of the particles.

However, by comparing the stability of CS_C_{12}S and CS_C_{12}L particle dispersions, which possess the same average zeta potentials, one could note that the corona thickness, i.e. the PAAm block length, also plays an important role in the particle stabilization (Fig. 5A), the thicker the corona, the higher the stability of the particle dispersions. Hence, one could conclude that the neutral block composing the corona contribute to the stabilization of the colloids, together with the surface charge, through electrostatic and steric stabilization mechanisms, with the latter being more important if a highly kinetically stable dispersion is desired for salt-free CS particles.

The Cryo-TEM images obtained for selected samples confirmed the formation of long-range ordered cores for CS_C_{12}S and CS_C_{12}L, as evidenced by the presence of several crystalline planes (Fig. 7A-D). The images obtained by tilting the specimens also indicated anisometric particles, which are thinner in one of the dimensions (Fig. 7 E and F), corroborating the results obtained by light and X-rays scattering, that indicated oblate-like particles in both cases.

This is consistent with previous reports on similar polyelectrolyte-surfactant dispersed particles, that also indicated internally-structured anisometric particles, instead of simple spherical arrangement.[29] A special case where long-rang ordered particles with spherical shape was seen is those holding a lamellar inner structure.[30] Berret *et al*.[10] have reported Cryo-TEM images of CP-based particles that corroborate the absence of internal structure and round-shape aggregates, as inferred in the present work.

Cryo-TEM images seem also to agree with the results obtained in the colloidal stability study. While aged CS_C_{12}S presented a striking difference if compared to the freshly prepared dispersions (Fig. 7G), aged CS_C_{12}L features remained essentially unchanged (Fig 7H). However, we have observed that the preparation procedure for the Cryo-TEM analysis originated a variety of structures with distinct features and these results have to be further investigated.

5. CONCLUSIONS

C3Ms based on PAAm-b-PAA block copolymer, with different block proportions, and cationic dodecyltrimethylammonium bromide surfactant have been prepared by two different approaches and studied. It has been shown that the particles prepared by mixing individual aqueous solutions containing the components (CP approach), with their respective counterions, are round-shaped and display a liquid-like core, while those prepared in the absence of simple counterions (CS approach) presented cores large enough to sustain a liquid-crystalline core, which structure is determined by the surfactant. In addition, these particles displayed flat-like shape, with one dimension significantly smaller than the other.

Small amounts of simple counterions, plays an important role on the surface charge and, consequently, on the colloidal stability of the particle dispersions. More importantly, the corona thickness also contributes to the stabilization of the aggregates. Both effects prevent irreversible particle aggregation. In the absence of surface charge and long neutral blocks composing the shell, the particles will reversible aggregate and a macroscopic phase separation takes place.

C3Ms have been widely studied in the last decade and their equilibrium nature have been highly discussed. Here we show that C3Ms prepared by the CS approach are metastable structures and display features that are process-dependent, agreeing with our recent report[16] that indicated that hierarchical structures formed in both block copolymer and surfactant length scales are the equilibrium structures for these entities.

ASSOCIATED CONTENT

Supporting information

SAXS, DLS and Cryo-TEM results for CS_C_{12}L particles prepared employing poly(ethylene oxide-*b*-acrylic acid) (PEO_{511}-*b*-PAA_{77}) as the neutral-ionic block copolymer.

REFERENCES

1. Voets, I. K.; de Keizer, A.; Cohen Stuart, M. A. Complex coacervate core micelles. *Adv. Colloid Interface Sci*. **2009**, *147-148*, 300-318.

2. Bronich, T. K.; Kabanov, A. V.; Kabanov, V. A.; Yu, K.; Eisenberg, A. Soluble Complexes from Poly(ethylene oxide)-block-polymethacrylate Anions and N-Alkylpyridinium Cations. *Macromolecules* **1997**, *30*, 3519–25.

3. Bronich, T. K.; Popov, A. M.; Eisenberg, A.; Kabanov, V. A.; Kabanov, A. V. Effects of Block Length and Structure of Surfactant on Self-Assembly and Solution Behavior of Block Ionomer Complexes. *Langmuir* **2000**, *16*, 481–489.

4. Voets, I. K.; de Keizer, A.; Cohen Stuart, M. A. Core and Corona Structure of Mixed Polymeric Micelles. *Macromolecules* **2006**, *39*, 5952–5955.

5. Uchman, M.; Štěpánek, M.; Prévost, S.; Angelov, B.; Bednár, J.; Appavou, M.-S.; Gradzielski, M.; Procházka, K. Coassembly of Poly(ethylene oxide)-*block*-poly(methacrylic acid) and N-Dodecylpyridinium Chloride in Aqueous Solutions Leading to Ordered Micellar Assemblies within Copolymer Aggregates. *Macromolecules* **2012**, *45*, 6471– 6480.

6. van der Kooij.; Spruijt, E.; Voets, I. K.; Fokkink, R.; Cohen Stuart, M. A.; van der Gucht, J. On the Stability and Morphology of Complex Coacervate Core Micelles: From Spherical to Wormlike Micelles. *Langmuir* **2012**, *28*, 14180–14191.

7. Uchman, M.; Gradzielski, M.; Angelov, B.; Tošner, Z.; Oh, J.; Chang, T.; Štěpánek, M.; Procházka, K. Thermodynamic and Kinetic Aspects of Coassembly of PEO–PMAA Block Copolymer and DPCl Surfactants into Ordered Nanoparticles in Aqueous Solutions Studied by ITC, NMR, and Time-Resolved SAXS Techniques *Macromolecules*. **2013**, *46*, 2172– 2181.

8. Krogstad, D. V.; Lynd, N. A.; Miyajima, D.; Gopez, J.; Hawker, C. J.; Kramer, E. J.; Tirrell, M. V. Structural Evolution of Polyelectrolyte Complex Core Micelles and Ordered-Phase Bulk Materials. *Macromolecules* **2014**, *47*, 8026–8032.

9. Berret, J. F.; Cristobal, G.; Hervé, P.; Grillo, I. Structure of colloidal complexes obtained from neutral/poly-electrolyte copolymers and oppositely charged surfactants. *Eur. Phys. J. E* **2002**, *9*, 301-311.

10. Berret, J. F.; Hervé, P.; Aguerre-Chariol, O.; Oberdisse, J. Colloidal complexes obtained from charged block copolymers and surfactants: A comparison between small-angle neutron scattering, Cryo-TEM, and simulations. *J. Phys. Chem. B* **2003**, *107*, 8111-8118.

11. Hervé, P.; Destarac, M.; Berret, J.-F.; Lal, J.; Oberdisse, J.; Grillo, I. Novel Core-shell Structure for Colloids Made of Neutral/ Polyelectrolyte Diblock Copolymers and Oppositely Charged Surfactants. *Europhys. Lett*. **2002**, *58*, 912−918.

12. Berret, J.-F.; Vigolo, B.; Eng, R.; Hervé, P.; Grillo, I.; Yang, L. Electrostatic Self-assembly of Oppositely Charged Copolymers and Surfactants: a Light, Neutron, and X-ray Scattering Study. *Macromolecules* **2004**, *37*, 4922−4930.

13. Vitorazi, L.; Berret, J-F.; Loh, W. Self-Assembly of Complex Salts of Cationic Surfactants and Anionic–Neutral Block Copolymers. Dispersions with Liquid-Crystalline Internal Structure. *Langmuir* **2013**, *29*, 14024–14033.

14. Ferreira, G. A.; Loh, W. Addition of n-Alcohols Induces a Variety of Liquid-Crystalline Structures in Surfactant-Rich Cores of Dispersed Block Copolymer/Surfactant Nanoparticles. *ACS Omega* **2016**, *1*, 1104–113.

15. Carneiro, N. M.; Percebom, A. M.; Loh, W. Quest for Thermoresponsive Block Copolymer Nanoparticles with Liquid–Crystalline Surfactant Cores. *ACS Omega* **2017**, *2*, 5518–5528.

16. Ferreira, G. A.; Piculell, L.; Loh, W. Hydration-dependent hierarchical structures in block copolymer-surfactant complex salts. *Macromolecules* **2018**, 51, 9915–9924.

17. Berne, B. J.; Pecora, R. Dynamic Light Scattering with Applications to Chemistry, Biology and Physics, 2nd ed., *Dover*, **2000**.

18. Lindner, P.; Zemb, T. eds., Neutron, X-rays and Light. Scattering Methods Applied to Soft Condensed Matter. 1st ed., *Elsevier*, **2002**.

19. Hammersley, A. P.; *Scientific Software FIT2D*, ESRF Synchrotron, France, **2009**

20. SasView Software, http://www.sasview.org.

21. Berr, S. S. Solvent isotope effects on alkytrimethylammonium bromide micelles as a function of alkyl chain length. *J. Phys. Chem.* **1987**, *91*, 4760–4765.

22. Guinier A.; Fournet, G. Small-Angle Scattering of X-Rays, *John Wiley and Sons*, **1955**.

23. Glatter, O.; Kratky, O. Small Angle X-ray Scattering. **1982**, Academic Press.

24. Wadsäter, M.; Barauskas, J.; Tiberg, F.; Nylander, T. The lipolytic degradation of highly structured cubic micellar nanoparticles of soy phosphatidylcholine and glycerol dioleate by phospholipase A2 and triacylglycerol lipase. *Chem. Phys. Lipids* **2018**, *211*, 86-92.

25. Chu, B.; Liu, T. Characterization of nanoparticles by scattering techniques. *J. Nanoparticle Res.* **2000**, *2*, 29-41.

26. Loscalzo, J.; Slayter, H.; Handin, R. I.; Farber, D. Subunit Structure and Assembly of Von Willebrand Factor Polymer. *Biophys J*. **1986**, *49*, 49–50.

27. Svensson, A.; Norrman, J.; Piculell, L. Phase Behavior of Polyion-Surfactant Ion Complex Salts: Effects of Surfactant Chain Length and Polyion Length. *J. Phys. Chem. B* **2006**, *110*, 10332-10340.

28. van der Burgh, S.; de Keizer, A.; Cohen Stuart, M. A. Complex Coacervation Core Micelles. Colloidal Stability and Aggregation Mechanism. *Langmuir* **2004**, *20*, 1073-1084.

29. Plazzotta, B.; Fegyver, E.; Mészáros, R.; Pedersen, J. S. Anisometric Polyelectrolyte/Mixed Surfactant Nanoassemblies Formed by the Association of Poly(diallyldimethylammonium chloride) with Sodium Dodecyl Sulfate and Dodecyl Maltoside. *Langmuir* **2015**, *31*, 7242–250.

30. Ram-On, M.; Cohen, Y.; Talmon, Y. Effect of Polyelectrolyte Stiffness and Solution pH on the Nanostructure of Complexes Formed by Cationic Amphiphiles and Negatively Charged Polyelectrolytes. *J. Phys. Chem. B* **2016**, *120*, 5907–915.

Supporting Information

Impact of preparation procedure on the physicochemical properties of block copolymer nanoparticles containing surfactant-rich cores.

Guilherme A. Ferreira[1], Lennart Piculell[2], Watson Loh[1,*]

[1]Institute of Chemistry, University of Campinas (UNICAMP), P.O Box 6154, Campinas-SP, Brazil.

[2]Division of Physical Chemistry, Lund University, Box 124, SE-221 00 Lund, Sweden

* e-mail: wloh@iqm.unicamp.br
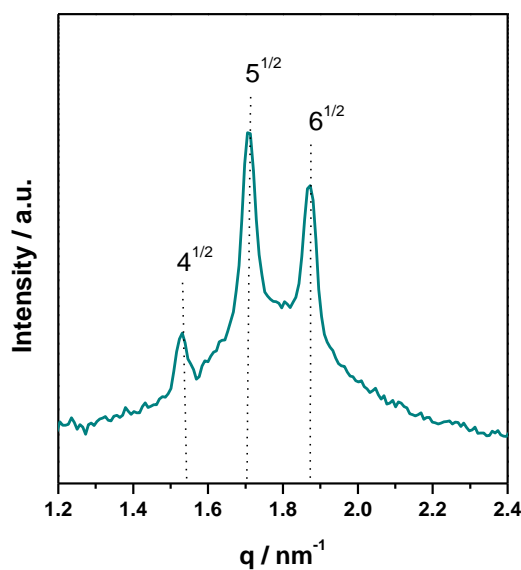
Fig. S1. SAXS patterns obtained for CS_C12L dispersion at 1.0 wt%, prepared employing PEO_{511}-*b*-PAA_{77} as the neutral-ionic block copolymer.

Table S1. Apparent hydrodynamic radius (R_H), polydispersity index (PDI) and zeta potential (ζ) for freshly prepared CS_C12L dispersion, prepared employing PEO_{511}-*b*-PAA_{77} as the neutral-ionic block copolymer (avg. $\pm$ SD, triplicate of independent preparations).

Sample	R_H / nm[1]	PDI	ζ / mV
CS_C_{12}S	120$\pm$10	0.14	-33$\pm$5

1. Measured in a Malvern instrument at θ=90°
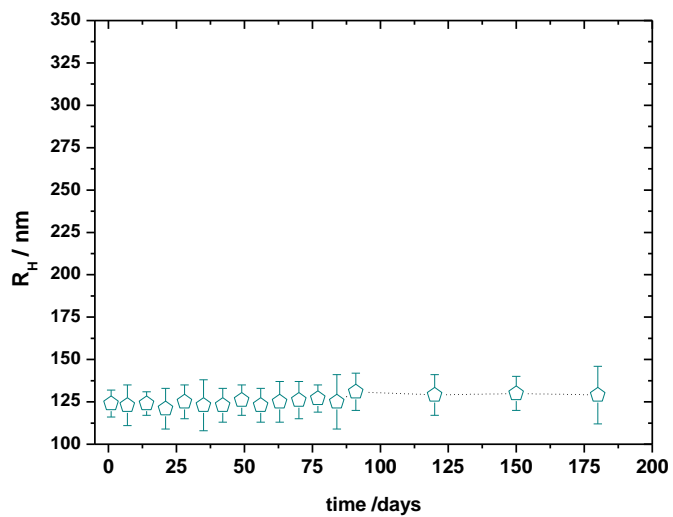
Fig. S2 Evolution of the apparent hydrodynamic radius (R_H) as a function of time of sample preparation for CS_C12L dispersion at 1.0 wt%, prepared employing PEO_{511}-b-PAA_{77} as the neutral-ionic block copolymer.
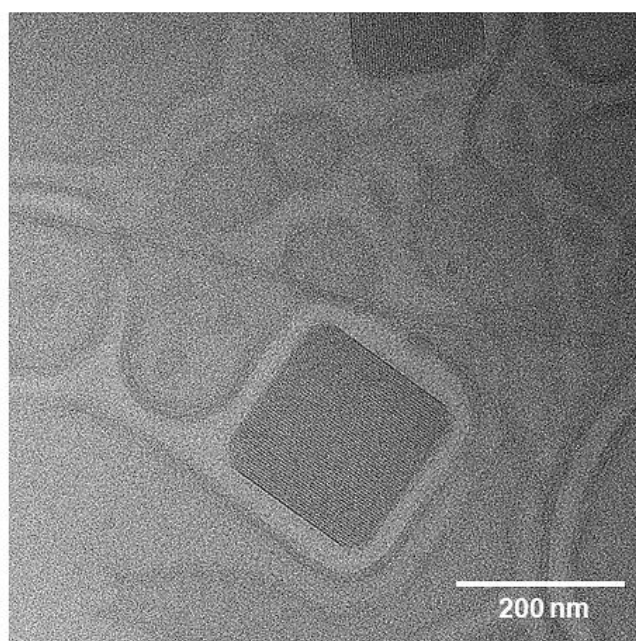
Fig. S3. Cryo-TEM image of 1 wt% freshly prepared CS_C_{12}L particle dispersion prepared employing PEO_{511}-b-PAA_{77} as the neutral-ionic block copolymer.

Paper IV

Molecular assembly in block copolymer-surfactant nanoparticle dispersions: Information on dissociated species from PFG NMR.

Guilherme A. Ferreira[1], Lennart Piculell[2*], Watson Loh[1*]

[1]*Institute of Chemistry, University of Campinas (UNICAMP), P.O. Box 6154, 13083-970, Campinas – SP, Brazil.*
[2]*Division of Physical Chemistry, Lund University, P.O. Box 124, S-221 00, Lund, Sweden*

* *wloh@iqm.unicamp.br*
* *lennart.piculell@fkem1.lu.se*

Abstract

Structured block copolymer-surfactant particles are formed when complexes of charged ionic-neutral block copolymers, neutralized by surfactant counterions, are dispersed in aqueous media. The charged species stay electrostatically associated in water, leading to a hydrated surfactant-rich core stabilized by a neutral block corona. The resulting core-shell particles have been previously studied in terms of their average size, core structures and colloidal stability. Yet, little is understood regarding the extent of dissociation of the constituent ionic species and their exchange between the particles. Here, we address these issues by measuring the self-diffusion coefficients (D) of the surfactant ions and polyions employing Pulse-Field Gradient Nuclear Magnetic Resonance (PFG NMR). Additional measurements based on Dynamic Light Scattering (DLS) and conductivity were also performed. It is possible to prepare, by centrifugation, systems that contained one phase concentrated in particles separated from a clear dilute phase. D values for surfactant and block copolymer in the two phases indicated that the dilute phase contained a fraction of small aggregates of surfactant ions and anionic-neutral block copolymers, diffusing together at least an order of magnitude more rapidly than the particles. The fraction of block copolymer found in the dilute phase was nearly constant, independently of the overall concentration of the dispersions.

Introduction

Several reports have studied the electrostatic complexation between water-soluble neutral-ionic block copolymers (BCP) and oppositely charged species in solution. The resulting structures are collectively known in the literature as complex coacervate core micelles, C3Ms, and feature a stabilizer corona of neutral water-soluble polymeric block surrounding a hydrated core consisting of complexed oppositely charged units.[1-6]

The most commonly studied oppositely charged species in C3Ms are block-copolymers and surfactants. In recent years, equimolar mixtures of poly(acrylamide)-*block*-poly(acrylic acid) (PAAm-*b*-PAA) and a cationic surfactant, with their respective counterions have been studied.[7-10] Extensive results have shown that the resulting aggregates displayed an average diameter of 50 nm and surfactant-rich cores with no long-range order.

Recently, however, studies involving the above-mentioned complex mixtures have been expanded by employing a new methodology based on the *complex salt* (CS) approach. In the latter approach, the water-insoluble complexes are prepared by neutralizing the acrylate units of the BCP are neutralized by alkyltrimethylammonium cationic surfactant ions in a simple acid-base titration reaction, resulting in block copolymer complex salts, here abbreviated as BCPCS, free of counterions.

Notably, by dispersing the freeze-dried BCPCS in water, particles with a diameter of ca. 300 nm with particle cores displaying long-range liquid crystalline structures were obtained. Such BCPCS dispersed particles have been studied by our group in the last years, regarding their colloidal and core-structure features, by varying the molecular composition of the complexed species and by adding extra components, such as cosurfactants.[11-13]

Very recently, the phase behavior as a function of the water content in concentrated BCPCS systems has also been investigated.[14] The latter study showed that the BCPCS did not truly dissolve in water; mixtures containing more than *ca.* 50 wt% water were actually phase-separated into a concentrated ordered phase and a dilute phase. Because of the similar densities of the BCPCS and water, a separation into two macroscopic phase separation of the concentrated systems was difficult to achieve in normal water; even after extensive centrifugation a uniformly turbid mixture was obtained. However, when D_2O was used as a solvent, the centrifugation of water-rich samples resulted in a macroscopic separation of a dilute bottom phase from a concentrated top phase.

Regardless of the composition of BCPCS or the regime concentration in hydrated samples, our knowledge on the molecular aggregation into C3Ms is incomplete. Methods such

as scattering techniques and electron microscopy are primarily sensitive to the large particles that are formed, but information on the possible existence of also smaller particles and dissociated individual molecules in the dispersions is still lacking.

Because of this, we investigate in this work, by means of Pulse-Field Gradient Nuclear Magnetic Resonance (PFG NMR), the molecular assembly in BCPCS dispersions. PFG NMR methods are widely employed to measure translational diffusion of surfactants and BCP and their molecular assemblies and thus provide easily accessible ways to estimate their size via the Stokes–Einstein equation, in which the hydrodynamic radius is obtained.[15-20] Moreover, information of bound and dissociated surfactant and BCP species can be obtained via their diffusion coefficients. Dynamic Light Scattering (DLS) and conductivity measurements have here also been employed as complementary techniques.

Here we study dispersions, in D_2O, of BCPCS with two different block proportions, neutralized by dodecyl- or hexadecyltrimethylammonium surfactant ions, at 0.1, 1 and 10 wt%. In addition, we study individually the top and bottom phases that separate on centrifugation of such dispersions at the same three initial concentrations.

Experimental

Chemicals. The synthesis of the block copolymer $PAAm_{133}$-b-PAA_{49} was described earlier[11]. $PAAm_{422}$-b-PAA_{69} was a gift from Rhodia (Cranbury, USA). Both polymers have been used in previous studies by in our group, and their characterization is described in references 12 and 14. In both cases, the subscript characters refer to the weight average number of repeating units of each block (Table 1). Dodecyl- and Hexadecylltrimethylammonium bromide, $C_{12}TABr$ and $C_{16}TABr$, of 99% purity, and D_2O (99.9% D atoms), were purchased from Sigma-Aldrich (USA) and used as received. Deionized water with a resistivity above 18.2 $M\Omega.cm^{-1}$, as obtained by a Milli-Q® system, was used in the preparation of the BCPCS as stated below.

Table 1 – Weight average molar mass of the blocks and dispersity (*D*) of the PAAm-*b*-PAA block copolymers employed in this work.

Block copolymer	PAAm / g.mol^{-1}	PAA / g.mol^{-1}	D [1]
PAAm$_{133}$-*b*-PAA$_{49}$	9415	3500	2.1 [2]
PAAm$_{432}$-*b*-PAA$_{70}$	30680	5000	1.6 [3]

1 – D = M_w/M_n , as determined by gel permeation chromatography

2 – According to ref. 14

3 – According to ref. 10

Preparation of the BCPCS. Three BCPCS were prepared following the general procedure described earlier.[11-13] Briefly, the hydroxide form of the surfactants, obtained by an ion-exchange step, was titrated with aqueous solutions of the BCP in the acid form until the equivalence point (pH 8.6-8.9). The resulting mixtures were left overnight at 4°C and their pH values were adjusted to the equivalence point, when necessary, with the corresponding BCP solution. The BCPCS in the solid form were isolated from the solution by freeze-drying the mixture and were kept in a desiccator. The BCPCS obtained by employing this methodology will be refereed as C$_{12}$S, C$_{16}$S and C$_{12}$L, where the terms C$_{12}$ and C$_{16}$ denote the surfactant alkyl chain length and S and L refer to the length of the PAAm block in the BCP employed in the synthesis; S for the BCP with a short PAAm block (PAAm$_{133}$-*b*-PAA$_{49}$) and L for the BCP with a long PAAm block (PAAm$_{432}$-*b*-PAA$_{70}$).

Preparation of the particle dispersions. The particle dispersions were prepared by vortexing (Vortex-Genie 2 mixer - Scientific Industries, operating at 3200 rpm) for ca. 1 minute, the appropriate amounts of BCPCS in D$_2$O to achieve the final solid concentration of 0.1, 1.0 and 10.0 wt %. These samples were studied as prepared and will be refereed as *intact samples*. In addition, dispersions at 0.1, 1.0 and 10.0 wt%, prepared following the same procedure, were centrifuged for 24 hours at 30000 rpm prior to the measurements. Both concentrated (upper) and dilute (bottom) phases formed by centrifugation were collected and studied. These samples will be refereed as *centrifuged samples*.

NMR measurements. The NMR experiments were performed on a Bruker DMX-200 operating at 200 MHz proton resonance frequency equipped with a Bruker diffusion probe having a maximum gradient strength of 9.6 Tm^{-1}. Pulsed field gradients (PFGs) where generated in a Bruker DIFF-25 gradient probe driven by a BAFPA-40unit. These measurements were performed using a maximum gradient strength of 4.52 Tm^{-1}, with a pulse gradient time of 1.0 ms and the time between the start of two gradient pulses was 20 ms. The method used in

this work was the stimulated echo (PFG-SE) with a pulse sequence of 90°-τ_1–90°-τ_2–90°-τ_1–echo.[15] In this experiment, the attenuation of the signal intensity I is given by[15] :

$$I = I_o \exp\left(-D\gamma^2\delta^2 g^2 \left(\Delta - \frac{1}{3}\delta\right)\right) \quad (1)$$

where I_o is the signal intensity in the absence of gradients, D is the translational diffusion coefficient, γ is the magnetogyric ratio, δ is the time of gradient pulse, Δ is the diffusion time, and g is the gradient strength. All measurements were carried out at 25.0$\pm$0.5°C. All data processing and fitting of the diffusion coefficients has been done using the spectrometer software (Topspin 2.1, Bruker). Each diffusion coefficient results from the fit of 12-14 data points (peak areas).

In principle, any non-overlapping peak from the surfactant or the polyion can be used to analyze the diffusion of the respective species. Based on a two-state model, assuming that the molecule is either bound to the particle or free in solution and that the chemical exchange between those two states is fast, the observed diffusion coefficient is given by[15]

$$D_{obs} = \alpha D_{free} + (1 - \alpha)D_{particle} \quad (2)$$

where D_{obs} is the observed diffusion coefficient of the molecule (surfactant or polyion) in the dispersion, $D_{particle}$ is the particle diffusion coefficient, D_{free} is the diffusion coefficient of free surfactant ion or polyion, and α is the fraction of free dissociated molecules. Molecular diffusion coefficients of surfactant ions and polyions, corresponding to D_{free} in eq. 2, were measured and are displayed in Table 2.

Table 2. Molecular self-diffusion coefficients of surfactant ions and polyions.

Molecule	D / x 10^{-10} m^2.s^{-1}
C$_{12}$TA^{+a}	4.86
C$_{16}$TA^{+b}	4.14
PAAm$_{133}$-b-PAA$_{49}{}^c$	0.66
PAAm$_{432}$-b-PAA$_{70}{}^d$	0.31

a. In 10 mM C$_{12}$TABr solution (cmc = 12 mM)

b. In 0.7 mM C$_{16}$TABr solution (cmc = 1 mM)

c. In 10 mM, based on AA monomer, PAAm$_{133}$-b-PAA$_{49}$ solution

d. In 10 mM, based on AA monomer, PAAm$_{432}$-b-PAA$_{70}$ solution

The self-diffusion coefficients for particles or molecules at infinite dilution, D_0, can be obtained by considering obstruction effects according to:[21]

$$D_{obs} = D_o\,(1 - k\varphi) \qquad (3)$$

where k is a constant related to particle shape and φ is the volume fraction of particles in the sample. In a previous report, it was found that the BCPCS particles were non-spherical, similar to an oblate,[22] which gives $k \sim 0.75$.[23] The φ values were calculated assuming that the density of the BCPCS is 1 g/cm^3 and assuming that the particle's cores contain 50 vol% of water. The D_0 can be converted to effective hydrodynamic radius, $< R_H >_0$, according to:[21]

$$< R_H >_0 = \frac{kT}{6\pi\eta_o D_o} \qquad (4)$$

where k is the Boltzmann constant, η_o the solvent viscosity and T, the temperature.

Dynamic Light Scattering (DLS). Light scattering measurements were performed on a CGS-3-based compact goniometer system (ALV-GmbH, Langen, Germany), equipped with a detection system in a pseudo−cross-geometry, with a 22 mW He−Ne laser (λ= 632.8 nm) and an ALV 7004 multi-tau correlator. cis-Decalin was used as the refractive index-matching liquid. DLS was performed at the detection angle (θ) of 90° for 0.001-0.01 wt% dilute samples. By extrapolating the diffusion coefficients (D) to concentration c = 0, the effective D values (D_0), i.e. the D values at infinite dilution, were obtained for the investigated particles and converted to effective hydrodynamic radius, $< R_H >_0$, according to eq. 4. The obtained results are displayed in Figure S1 and Table S1.

Results

Intact Samples. Samples containing $C_{12}S$, $C_{16}S$ and $C_{12}L$ at 1.0 wt% were studied as prepared. The surfactant ion self-diffusion was analyzed from the methyl proton signal of the trimethylammonium headgroup, located at 3.1 ppm in the ^{1}H NMR spectra. The BCP diffusion coefficient was obtained from the signal of the protons of methylene group at 1.8 ppm. Figure 1A shows the obtained self-diffusion coefficients for surfactant ions and polyions in all investigated *intact samples*.
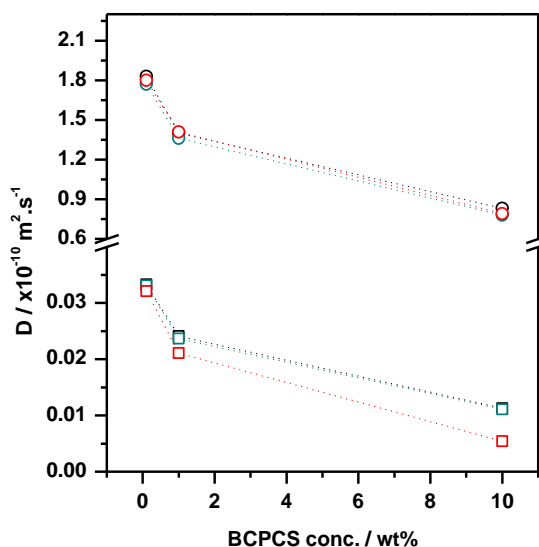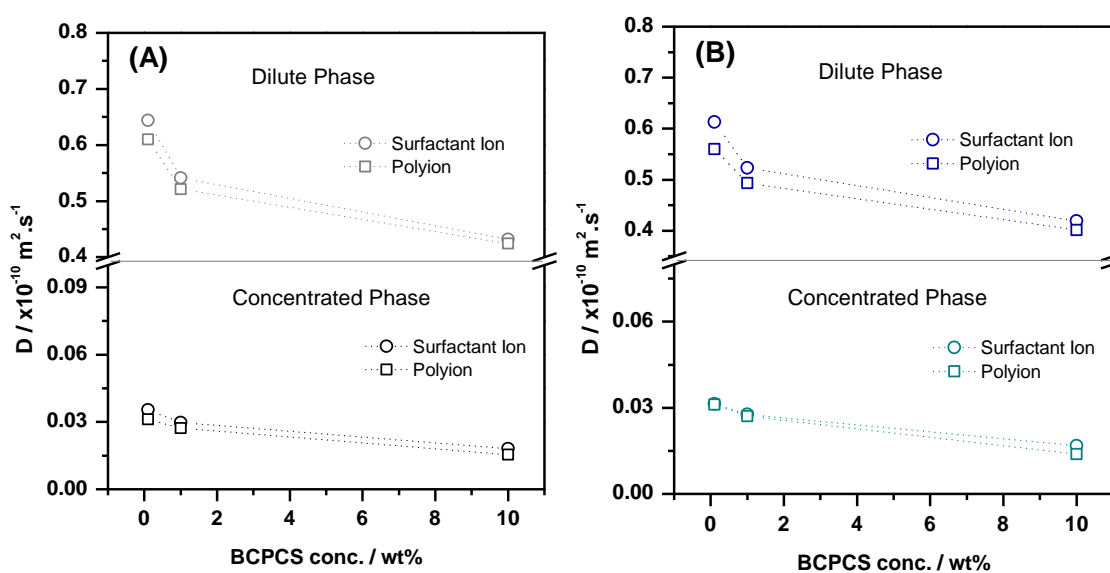
Figure 1. Self-diffusion coefficient values (D) as a function of concentration for: $C_{12}TA^+$ ions (○) polyion (□) in $C_{12}S$; $C_{16}TA^+$ ions (○) polyion (□) in $C_{16}S$; $C_{12}TA^+$ ions (○) polyion (□) in $C_{12}L$.

Centrifuged Samples. The self-diffusion coefficients of surfactant ions and polyions in the concentrated and dilute phases obtained by centrifuging the BCPCS dispersions at different overall concentrations were also measured and are displayed in Figure 2. Based on the methylene peak areas in the ^1H NMR spectra, the concentration of BCP in the dilute phase was estimated for each of the investigated samples. The results are displayed in Figure 3.
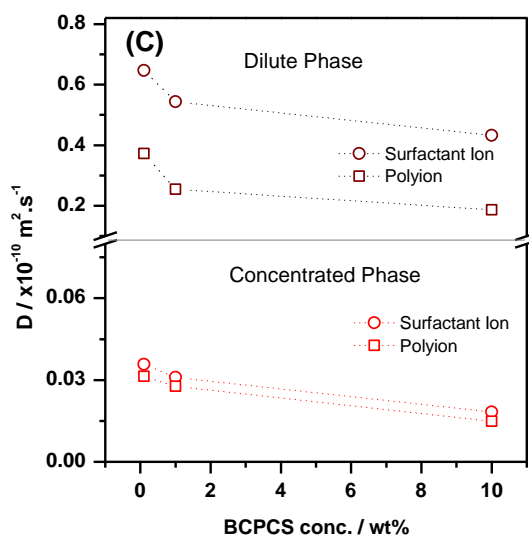
Figure 2. Self-diffusion coefficients (*D*) for surfactant ion and polyion in the concentrated and dilute phases obtained for *centrifuged samples* at different (overall) initial concentrations for **(A)**. $C_{12}S$. **(B)** $C_{16}S$. **(C)** $C_{12}L$. The lines are guide to the eyes.
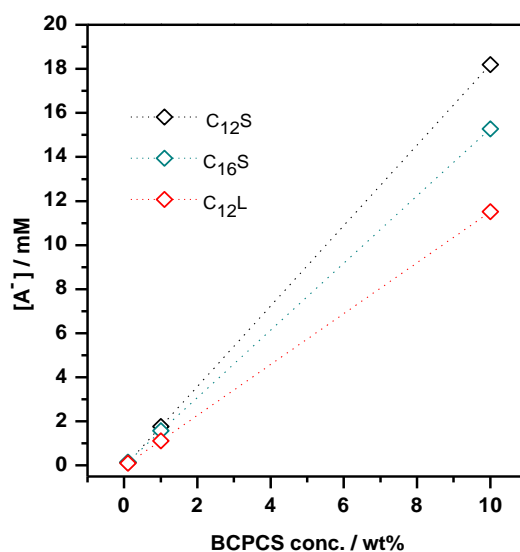

Figure 3. Concentration of BCP (expressed as acrylate (A^-) concentration) in the dilute phase obtained in the *centrifuged samples* as a function of overall initial BCPCS concentration. The lines are guide to the eyes.

Discussion

The self-diffusion coefficient values for polyions in *intact samples* (Figure 1A) and in the concentrated phase of the *centrifuged samples* (Figure 2A-C) were similar, indicating that they predominantly contained particles of similar size. By using eq. 3 and 4, the diffusion coefficients for *intact samples* were corrected with respect to obstruction factors and converted to effective hydrodynamic radius $< R_H >_0$, the results are shown in Figure 5. These sizes were also compared with the $< R_H >_0$ values obtained by DLS (Figure S1, Table S1) for *intact* 1

wt% dispersions of BCPCS. The results are also shown in Figure 5. The observation that the effective particle sizes obtained by PFG NMR and DLS are very similar for *intact samples* at 1 wt%, indicate that the self-diffusion coefficient values for polyion basically corresponds to the self-diffusion coefficients of the particles. This result consistently indicates that the polyions are essentially all incorporated into BCPCS aggregates. Since the particle concentration in each phase of *centrifuged samples* was not determined, we have not performed similar comparisons regarding $< R_H >_0$ values obtained by DLS and by PFG NMR.

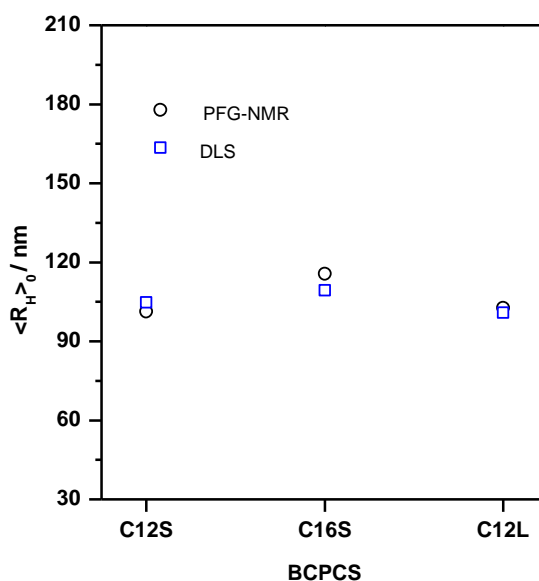**Figure 4**. Effective hydrodynamic radius, $< R_H >_0$, obtained for polyions by PFG NMR in *intact samples* at 1 wt%. As a comparison, $< R_H >_0$ for BCPCS particles obtained by DLS is also shown (blue squares).

The fraction of dissociated surfactant ions (α) was therefore tentatively calculated from the observed diffusion coefficients based on equation 2 and the molecular diffusion coefficients of surfactant ions displayed in Table 2. Since we found that essentially all polyions were incorporated in BCPCS aggregates, $D_{particle}$ was assumed to be given by the measured self-diffusion coefficient of polyions. Surprisingly, for *intact samples* (Figure 1B), equation 2 gave very high α values, indicating that up to 30 % of the surfactant ions were dissociated from the particles in all BCPCS. This value may *a priori* be considered unrealistic; such a large fraction of surfactant ions simply cannot be dissociated from the BCPCS complexes in a system where no other ions than surfactant ions are present to neutralize the polyion charges. Additional measurements of solution conductivity (Figure S2), confirmed that the calculated α values for *intact samples* from PFG NMR data were unrealistic.

At this stage we are unable to explain quantitatively the very high diffusion coefficient that we reproducibly observed (several additional measurements were made) for the surfactant ion in *intact samples*. We strongly suspect, however, that the assumption of rapid exchange may not hold for the surfactant ion, and that all surfactant ions may not be visible in the high-resolution NMR spectrum. The cores of the large BCPCS particles are known to contain surfactant ions arranged in ordered liquid crystalline structures, resulting[16] in slow surfactant diffusion coefficients and very broad spectra. Further analysis and experiments are required, however, for a verification of this hypothesis and a quantitative explanation of the obtained results.

By contrast, for *centrifuged samples* of all three BCPCS, the observed self-diffusion coefficients for polyion and surfactant ion were quite similar in the concentrated phase, with the surfactant ion diffusion being only slightly more rapid than the polyion ion diffusion. This result indicates that the surfactant ions are also essentially quantitatively incorporated in the large BCPCS particles and makes the surfactant diffusion coefficients obtained for the *intact samples* more remarkable. Nevertheless, our reasons to doubt that we are observing a true average diffusion coefficient for *all* surfactant ions must hold also for these concentrated dispersions of large BCPCS particles. Therefore, we refrain from calculations of α for these systems.

A rather unexpected result of our study concerns the finding of small particles in the dilute phases of centrifuged samples. Notably, the concentration of block copolymer found in the dilute phase (Figure 3) increased with the overall BCPCS concentration, but the *fraction* (corresponding to the percentage of BCP in the dilute phase in respect to the overall BCP concentration of the sample) of the total BCPCS found in the dilute phase was nearly constant, independently of the overall concentration of the dispersions, as shown in Figure 6. A weak but consistent dependence on the BCPCS was found, however, indicating a slightly larger fraction the dilute phase of the BCPCS with the longer neutral block.
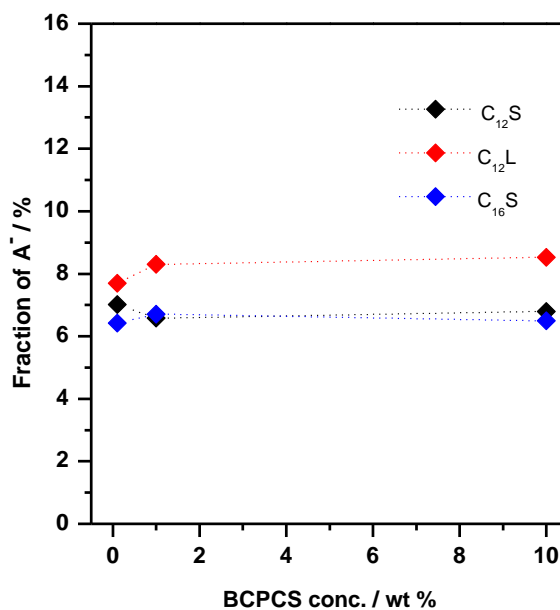
Figure 6. Fraction of block copolymer, expressed in terms of acrylate (A⁻) concentration, in the dilute phase for *centrifuged samples* as a function of overall concentration for the different BCPCS.

Clearly, for a truly binary mixture of BCPCS composed of strictly *monodisperse* polyions and surfactant counterions, the concentration of BCPCS in the dilute phase would be independent of the overall concentration of the system at thermodynamic equilibrium, since it would then simply correspond to the solubility of the BCPCS in water. One conceivable origin of a constant soluble polymer *fraction* in the dilute phase could thus be the existence of a molecularly distinct fraction of polymer, which is unable to form complexes with the surfactant owing to a low or vanishing content of charged units. However, this explanation is ruled out in our case by the finding from NMR that the dilute phase also contains surfactant ions, and that the diffusion coefficients of these surfactant ions show that they are, in fact, associated with the polyions. The surfactant ion diffusion coefficients are much lower than the respective molecular diffusion coefficients (Table 2), and their concentration dependence closely follows that of the polyions (Figure 2).

The polyion diffusion in the dilute phases, in turn, varies as expected from the molecular masses of the respective polyions, i.e. increases in the sequence $D(C_{12}L) < D(C_{16}S) \approx D(C_{12}S)$. The complex diffusion coefficients show a rather strong concentration dependence, but for the lowest initial concentration they in fact approach the diffusion coefficients of the respective single polyions (Figure 2 and Table 2). Collectively, the data thus indicate that the dilute system contains small BCPCS complexes, each containing surfactant and at most a few polyions, the latter being of a size comparable with the *average* size of the BCP used in the complex formation.

Owing to a lack of evidence suggesting that the properties of the polyions in the dilute phase complexes differ markedly from the average properties of the respective samples, we must think of a different explanation for their existence. One possibility is that the small aggregates in the dilute phase simply represent a fraction of very small aggregates from a wide distribution of aggregate sizes. We must then assume that the same size distribution is reproducibly created during the dispersion of the BCPCS in water, that it is only weakly dependent on the initial concentration of BCPCS used to produce the dispersion, and that the created particles are stable in time.

In any case, the complexes of the dilute phases are sufficiently small to justify the assumption of rapid exchange and narrow NMR linewidths, so that the use of eq. 2 should be legitimate for these systems. Hence, we have used eq. 2 to calculate the dissociated fraction of surfactant ions (α), and the results are shown in Figure 7.
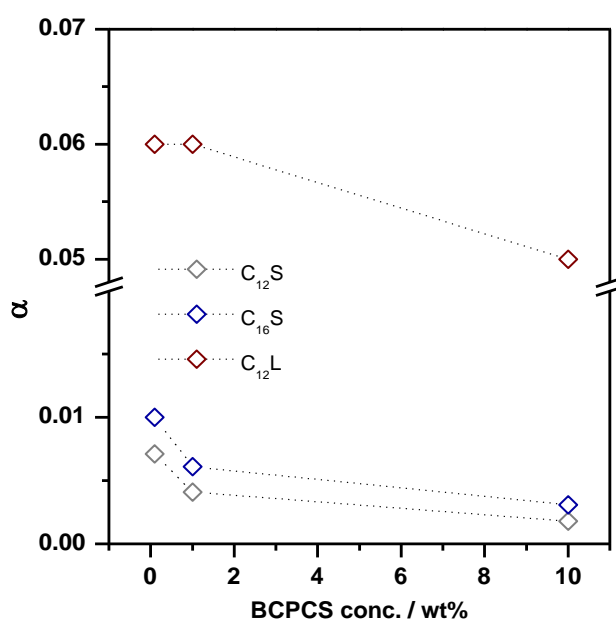

Figure 7. Fraction of dissociated surfactant ions (α) as a function of BCPCS concentration in the dilute phases obtained by centrifuging BCPCS samples at different overall (initial) concentrations. The lines are guide to the eyes.

In the calculations, we have assumed that $D_{particle}$ equals the measured diffusion coefficient of the polyion in each sample. For $C_{12}S$ and $C_{16}S$ the fractions of free surfactant ions are very small, indicating that the latter are in fact self-assembled into micelles complexed to the polyions, in agreement with experimental evidence on the nature of polyion-surfactant ion complexation in dilute solution.[5,6] Interestingly, α is significantly larger for $C_{12}L$, indicating

that the presence of a large neutral block on the polyion may hinder the micellization of the surfactant at the polyion to some extent.

Previous findings that the particles obtained by dispersing the BCPCS have properties, like size and core structure, that depend on the method of preparation strongly suggested that the mixtures are, in fact, non-equilibrium dispersions of an insoluble BCPCS phase.[22] The small aggregates observed in the dilute phase of *centrifuged samples* are interpreted as a fraction of small BCPCS aggregates that coexist with the large particles, besides a small fraction of dissociated surfactant ions. The small aggregates are formed by block copolymer chains in which the surfactant ions are connected to the anionic block.

Conclusions

The obtained results suggest that the dispersion of BCPCS generates a fraction of small aggregates, apart from the large particles. The molecular components in the dilute phase seem to be very similar those in the concentrated phase, that is block copolymer chains with attached surfactant ions, suggesting that BCPCS is truly a single component, i.e. it does not dissolve to form species that are molecularly different in the dilute phase. Apart from these aggregates, a small amount of surfactant ions is dissociated from the complexes and the fraction of uncomplexed polyion is essentially zero. Further control experiments will be performed to better understand the rapid diffusion of surfactant ions in intact samples.

ASSOCIATED CONTENT
Supporting information
DLS and conductivity results for investigated particle dispersions.

References

1. Harada, H.; Kataoka, K. Formation of Polyion Complex Micelles in an Aqueous Milieu from a Pair of Oppositely Charged Block Copolymers with Poly(ethylene glycol) Segments. *Macromolecules* **1995**, *28*, 5294—5299

2. van der Burgh, S.; de Keizer, A.; Cohen Stuart, M. A. Complex Coacervation Core Micelles. Colloidal Stability and Aggregation Mechanism. *Langmuir* **2004**, *20*, 1073-1084.

3. Cohen Stuart, M. A.; Hofs, B.; Voets, I. K.; de Keizer, A. Assembly of polyelectrolyte-containing block copolymers in aqueous media. *Curr Opin Colloid Interface Sci* **2005**, *10*, 30-36.

4. Voets, I. K.; de Keizer, A.; de Waard, P.; Frederik, P. M.; Bomans, P. H. H.; Schmalz, H.; Walther, A.; King, S. M.; Leermarkes, F. A. M.; Cohen Stuart, M. A. Double-Faced Micelles from Water-Soluble Polymers. *Angew. Chem. Int. Ed.* **2006**, *45*, 6673 –6676.

5. Voets, I. K.; de Keizer, A.; Cohen Stuart, M. A. Complex coacervate core micelles. *Adv. Colloid Interface Sci.* **2009**, *147-148*, 300-318.

6. Ferreira, G. A.; Loh, W. Liquid crystalline nanoparticles formed by surfactant-polyelectrolyte complexes. *Curr. Opin. Colloid Int. Sci* **2017**, 32, 11-22.

7. Berret, J. F.; Cristobal, G.; Hervé, P.; Grillo, I. Structure of colloidal complexes obtained from neutral/poly-electrolyte copolymers and oppositely charged surfactants. *Eur. Phys. J. E* **2002**, *9*, 301-311.

8. Berret, J. F.; Hervé, P.; Aguerre-Chariol, O.; Oberdisse, J. Colloidal complexes obtained from charged block copolymers and surfactants: A comparison between small-angle neutron scattering, Cryo-TEM, and simulations. *J. Phys. Chem. B* **2003**, *107*, 8111-8118.

9. Hervé, P.; Destarac, M.; Berret, J.-F.; Lal, J.; Oberdisse, J.; Grillo, I. Novel Core-shell Structure for Colloids Made of Neutral/ Polyelectrolyte Diblock Copolymers and Oppositely Charged Surfactants. *Europhys. Lett.* **2002**, *58*, 912−918.

10. Berret, J.-F.; Vigolo, B.; Eng, R.; Hervé, P.; Grillo, I.; Yang, L. Electrostatic Self-assembly of Oppositely Charged Copolymers and Surfactants: a Light, Neutron, and X-ray Scattering Study. *Macromolecules* **2004**, *37*, 4922−4930.

11. Vitorazi, L.; Berret, J-F.; Loh, W. Self-Assembly of Complex Salts of Cationic Surfactants and Anionic–Neutral Block Copolymers. Dispersions with Liquid-Crystalline Internal Structure. *Langmuir* **2013**, *29*, 14024–14033.

12. Ferreira, G. A.; Loh, W. Addition of n-Alcohols Induces a Variety of Liquid-Crystalline Structures in Surfactant-Rich Cores of Dispersed Block Copolymer/Surfactant Nanoparticles. *ACS Omega* **2016**, *1*, 1104–113.

13. Carneiro, N. M.; Percebom, A. M.; Loh, W. Quest for Thermoresponsive Block Copolymer Nanoparticles with Liquid–Crystalline Surfactant Cores. *ACS Omega* **2017**, *2*, 5518–5528.

14. Ferreira, G. A.; Piculell, L.; Loh, W. Hydration-dependent hierarchical structures in block copolymer-surfactant complex salts. *Macromolecules* **2018**, 51, 9915–9924.

15. Söderman, O.; Stilbs, S. NMR Studies of Complex Surfactant Systems. *Prog. Nucl. Magn. Reson. Spectrosc*. **1994**, *26*, 445-482.

16. Svensson, A.; Topgaard, D.; Piculell, L.; Söderman, O. Molecular Self-Diffusion in Micellar and Discrete Cubic Phases of an Ionic Surfactant with Mixed Monovalent/Polymeric Counterions. *J. Phys. Chem. B* **2003**, *107*, 13241–13250.

17. Cabaleiro-Lago, C.; Nilsson, M.; Söderman, O. Self-Diffusion NMR Studies of the Host−Guest Interaction between β-Cyclodextrin and Alkyltrimethylammonium Bromide Surfactants. *Langmuir* **2005**, *21*, 11637–11644.

18. Bernardes, J. S.; da Silva, M. A.; Piculell, L. Loh, W. Reverse micelles with spines: L2 phases of surfactant ion-polyion complex salts, n-alcohols and water investigated by rheology, NMR diffusion and SAXS measurements. *Soft Matter* **2010**, *6*, 144–153.

19. Percebom, A. M.; Janiak, J.; Schillén, K.; Picuell, L. Loh, W. Micellization of water-soluble complex salts of an ionic surfactant with hairy polymeric counterions. *Soft Matter* **2013**, *9*, 515-526.

20. Janiak, J.; Piculell, L.; Schillén, K.; Lundberg, D. Responsive release of polyanions from soluble aggregates formed with a hydrolyzable cationic surfactant and a nonionic surfactant. *Soft Matter* **2013**, *9,* 4103-4112.

21. Söderman, O.; Stilbs, P.; Price, W. S. NMR Studies of Surfactants. *Concepts Magn. Reson*., **2004**, 23A, 121-135.

22. Ferreira, G. A.; Piculell, L.; Loh, W. Impact of preparation procedure on the physicochemical properties of block copolymer nanoparticles containing surfactant-rich cores. *Manuscript*.

23. Jönsson, B.; Wennerström, H.; Nilsson, P. G.; Linse, P. Self-diffusion of small molecules in colloidal systems. *Colloid Polym. Sci* **1986**, *264*, 77-88.

Supplementary Information

Molecular assembly in block copolymer-surfactant nanoparticle dispersions: Information on dissociated species from PFG NMR.

Guilherme A. Ferreira[1], Lennart Piculell[2*], Watson Loh[1*]

[1]*Institute of Chemistry, University of Campinas (UNICAMP), P.O. Box 6154, 13083-970, Campinas – SP, Brazil.*

[2]*Division of Physical Chemistry, Lund University, P.O. Box 124, S-221 00, Lund, Sweden*

* *wloh@iqm.unicamp.br*

* *lennart.piculell@fkem1.lu.se*
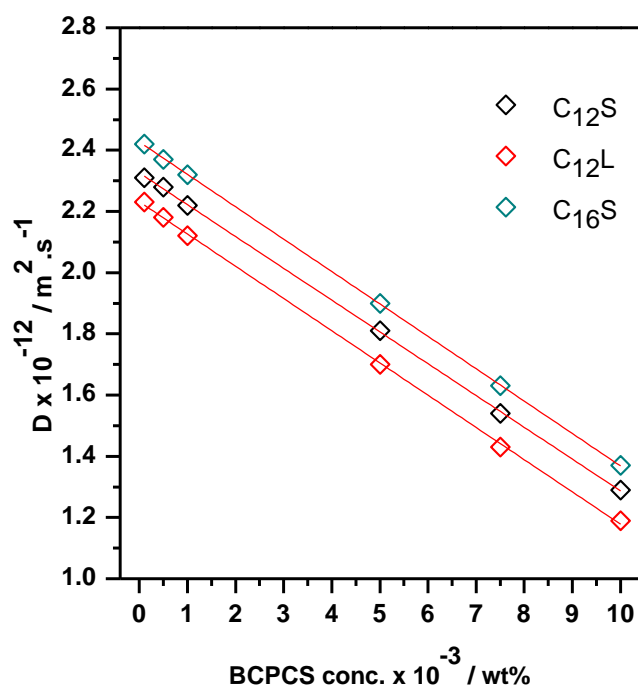
Dynamic Light Scattering (DLS)

Figure S1. Diffusion coefficients (*D*) as a function of BCPCS concentration obtained by DLS in D$_2$O. Red lines represent the linear fits used to extrapolate data to c = 0.

Table S1. Effective hydrodynamic radii ($< R_H >_0$) for BCPCS dispersed particles in D$_2$O obtained by DLS and data displayed in Figure S1.

BCPCS	$< R_H >_0$ / nm
C$_{12}$S	104.7
C$_{16}$S	100.9
C$_{12}$L	109.3

Conductivity

Aqueous solutions of C$_{12}$TABr and C$_{16}$TABr surfactant, as a function of surfactant ion concentration were prepared, and their conductivity was measured in a digital conductivity meter. The results are displayed in Figure S2. The conductivity of the C$_{12}$S, C$_{16}$S and C$_{12}$L *intact samples* at 1 wt% is also displayed in the same figure (horizontal lines). If one assumes $\alpha = 0.3$ (see text in the main article), the concentration of dissociated surfactant ions in the solution would be around 6 mM, 5.4 mM and 4 mM for C$_{12}$S, C$_{16}$S and C$_{12}$L, respectively (based on the molecular weight of a BCPCS unimer - diblock copolymer chain with its

associated surfactant counterions). Clearly, the results in Figure S2 show that the measured conductivities of *intact samples* at 1 wt% corresponds to much lower concentrations of free surfactant ions.

Figure S2. **(A).** Conductivity (κ) of C_{12}TABr solutions as a function of C_{12}TA$^+$ surfactant ion concentration (open symbols). The horizontal lines denote the conductivity of C_{12}S (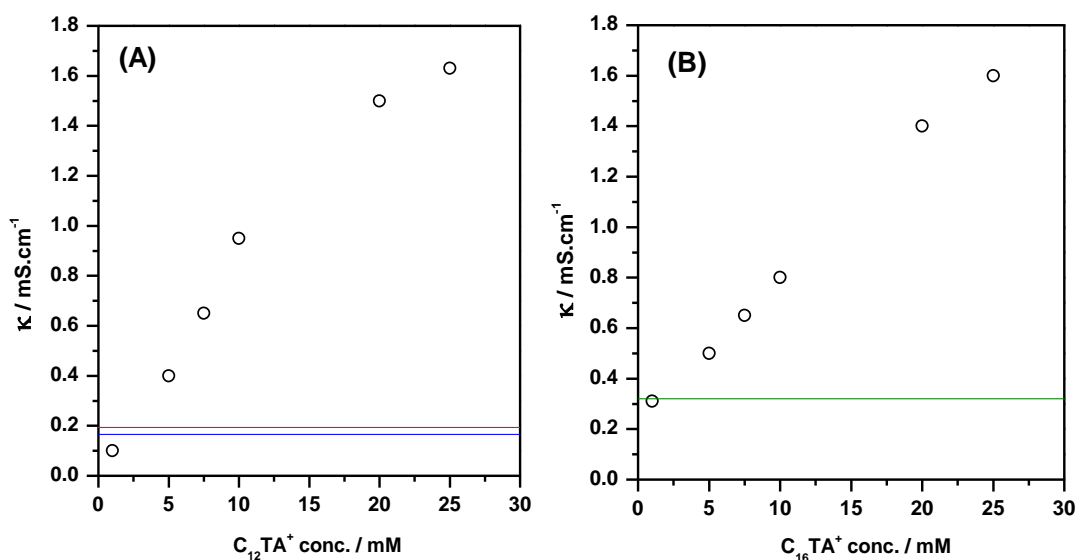red) and C_{12}L (blue) *intact samples* at 1 wt%. **(B).** Conductivity (κ) of C_{16}TABr solutions as a function of C_{16}TA$^+$ surfactant ion concentration (open symbols). The horizontal green line denotes the conductivity of C_{16}S *intact sample* at 1 wt%.

Paper V

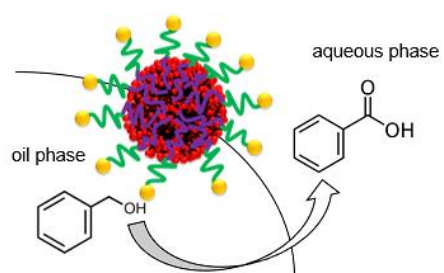# Planet-Satellite Nanostructures Based on Block Copolymer-Surfactant Nanoparticles Surface-Decorated with Gold and Silver: A New Strategy for Interfacial Catalysis

Guilherme A. Ferreira, Watson Loh*

Institute of Chemistry, University of Campinas (UNICAMP), P.O. Box 6154, 13083-970 Campinas, São Paulo, Brazil

*E-mail: wloh@iqm.unicamp.br

TABLE OF CONTENTS USE ONLY

ABSTRACT

Gold (Au) and silver (Ag) nanoparticles (NPs) were covalently conjugated onto the surface of thiol-functionalized block copolymer particles containing surfactant-rich liquid crystalline cores. The resulting planet-satellite nanoconjugates displayed enhanced colloidal stability upon changes in solution pH or ionic strength and interfacial properties that resulted in the stabilization of oil-in-water emulsions. These biphasic systems were used as medium for catalyzed aerobic oxidation of benzyl alcohol to benzoic acid and the nanoconjugates displayed catalytic activity comparable to the single Ag and Au NPs in aqueous medium, with the advantage of an easier and more efficient separation of unreacted alcohol and product from reaction medium, making this the first report on interfacial gold- and silver-catalyzed aerobic alcohol oxidation. These results, and the flexibility of the present approach, support the proposal of this methodology as a general platform for interfacial catalysis based on these novel nanomaterials.

INTRODUCTION

Gold (Au) and silver (Ag) nanoparticles (NPs) have been extensively studied in the last years due to their tunable properties, such as size, shape and surface, making them suitable for applications in a wide range of fields including catalysis, sensors and nanomedicine.[1] More recently, the conjugation of metal NPs to other nanomaterials, including polymer-based structures (micelles,[2-6] microgels,[7-8] particles[9-10]), carbon nanotubes,[11] dendrimers,[12] cellulose nanocrystals,[13] silica and other inorganic nanoparticles[14] were the subject of various studies resulting in the proposition of novel applications. Among the different types of conjugates investigated, hybrid nanostructures based on Ag and Au NPs and polymer-based nanomaterials have received great attention. In these conjugates, the metal NPs can be located into the core, along the whole structure, or at the outer surface of the polymer-based nanomaterials, in the last case generating planet-satellite nanostructures, in which the polymer-based nanomaterial comprises the planet and the metal NPs, the satellites.[6,15,16]

The fabrication of polymer-based planet-satellite nanostructures is particularly interesting because it was shown that the surface-exposed metal NPs can be easily accessed by species in the surrounding media, a step that is crucial for catalysis and sensing purposes. Such a strategy also allows the control of the inter-particle distance of surface-located metal NPs which is well known to impact on their optical, electronic and magnetic properties.[6] Using this approach, several nanoconjugate systems have been described in the recent years, aiming at different potential applications. Block copolymer micelles;[2-6] pH- and temperature-responsive microgels[7-8] and cross-linked polymer particles[9-10] are examples of polymeric nanomaterials assembled with Au and Ag NPs which have been used for catalytic, stimuli-responsive and drug delivery purposes.

The potential uses of the planet-satellite nanostructures in a variety of fields strongly depends on their colloidal stability, regarding both polymer and metal NPs, because in most of

the cases, the nanoconjugates are finely-tuned to display specific properties that must remain unchanged upon suitable variations in environment conditions, specially the pH and ionic strength. Hence, the fabrication of new polymer-based nanoconjugates with excellent colloidal stability is highly desired.

Core-shell particles, collectively known as complex coacervate core micelles (C3Ms), made from charged−neutral block copolymers and oppositely charged surfactant ions have been widely reported in the last years and the most studied systems are comprised of alkyltrimethylammonium cationic surfactants and the block copolymer poly(acrylamide)-*block*-poly(acrylic acid), PAAm-*b*-PAA.[17-24] The particles core contains several densely packed-surfactant micelles surrounded by the anionic block of the copolymer and the outer part consists in a corona composed by the neutral PAAm chains. By using the "complex salt" (CS) approach[21-24], the production of dispersed particles with a variety of surfactant-rich liquid crystalline cores were shown to be achieved. In addition, these particles, refereed here as CS, were shown to display enhanced colloidal stability.[22,23] It was noted that the CS particles display different properties, such as size, surface charge and core structure, if compared with those typically found for particles, refereed here as CP, prepared by the conventional procedure of mixing polyelectrolyte and surfactant in water, with their respective simple counterions.[17-20]

Because liquid crystalline particles have been widely studied for a variety of applications[25], specially the loading and release of substances, and have been reported to display long-term colloidal stability,[22,23] the selective attachment of Au and Ag NPs to the surface of CS particles was investigated in the present work aiming at the fabrication of functional nanoconjugates owing to the combination of the properties of both nanomaterials (Figure 1). The interfacial activity of the nanoconjugates was investigated and the catalytic efficiency of the nanoconjugates was tested towards the aerobic alcohol oxidation reaction at the interface of oil-in-water emulsions. Interfacial catalysis is an important topic because the interfacial contact

between two distinct phases can initiate or accelerate, due to the large contact area, the reaction between substances that are dissolved in or constitute different phases. Another advantage of interfacial catalysis is the ease in recovering the unreacted substance and the product when they display differences in their solubilities, causing each one to concentrate in a different phase.[26,27]
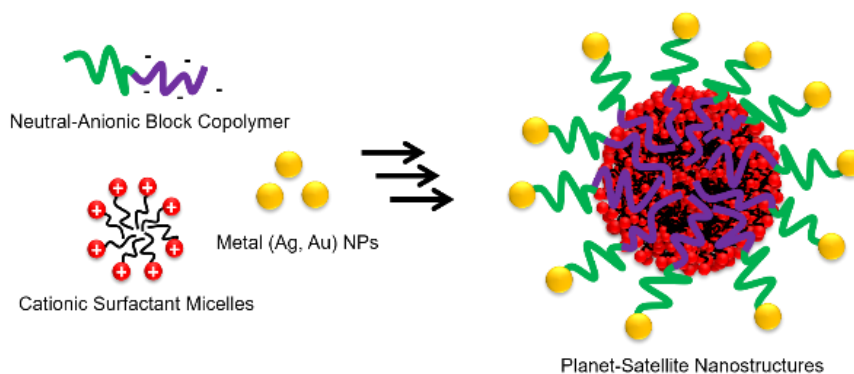

Figure 1. Schematic representation of planet-satellite nanostructures formed by block copolymer nanoparticles with surfactant-rich cores surface-decorated with Ag and Au NPs.

EXPERIMENTAL

Chemicals

The block copolymer PAAm$_{422}$-b-PAA$_{69}$, in which the subscript characters refer to the average number of repeating units of each block, was a gift from Rhodia (Cranbury, USA) and characterized by proton nuclear magnetic resonance (^{1}H-NMR) and gel permeation chromatography (GPC). Dodecyltrimethylammonium bromide, (C$_{12}$TABr), Silver Nitrate (AgNO$_3$), Tetrachloroauric Acid Trihydrate (HAuCl$_4$.3H$_2$O), Poly(N-vinyl-2-pyrrolidone) (PVP) 50 KDa, Sodium Borohydride (NaBH$_4$) and Sodium Chloride (NaCl) were purchased from Sigma-Aldrich (USA). Benzyl Alcohol (C$_7$H$_8$O), Benzoic Acid (C$_7$H$_6$O$_2$), Potassium Carbonate (K$_2$CO$_3$), Ethyl Acetate (C$_4$H$_8$O$_2$) and Hydrochloric Acid (HCl) were purchased from Synth (Brazil). Mineral Oil Nujol® was purchased from Mantecorp (Brazil) and consisted in a mixture of higher alkanes from C$_{15}$ to C$_{30}$. All the chemicals were purchased with the

highest available purity and used as received. The anion-exchange resin Dowex Monosphere 550A (OH) was purchased from Sigma-Aldrich (USA) and used after activation with 1 M Sodium Hydroxide (NaOH; Sigma-Aldrich, USA) solution. Deionized water with a resistivity greater than 18.2 MΩ.cm^{-1}, obtained from a Milli-Q$^{®}$ system, was used in all experiments.

Preparation and characterization of CS particles

The CS used in the present work was prepared following the general procedure described earlier in our laboratories.[21-23] Briefly, the hydroxide form of the dodecyltrimethylammonium surfactant, here abbreviated as $C_{12}TA^+$, obtained by a previous ion-exchange step, was titrated with 0.5 M, in acrylate monomer, aqueous solution of the block copolymer in the acid form until the equivalence point, usually at pH 8.6-8.9. The mixture was then left overnight at 4°C and its pH was adjusted to the equivalence point when necessary, with the block copolymer solution. The CS was freeze-dried to obtain a powder, which was kept in a desiccator. The CS dispersed particles were prepared by vortexing the appropriate amount of CS and water for approximately 1 min to achieve the final CS concentration of 1.0 wt %. As a reference, particles conventionally prepared by the simple mixing of the solutions containing the surfactant, with its respective counterion, and the block copolymer were also prepared in a charge molar ratio of 1:1.[17-20] These particles were named here as CP, referring to the conventional procedure used to produce them.

Small Angle X-ray Scattering (SAXS) was performed to characterize the liquid-crystalline core of the CS and CP particles. The measurements were taken at the SAXS1 beamline of the Brazilian Synchrotron Light Laboratory, LNLS, in Campinas, Brazil, as described previously.[21-23] The dispersions, diluted to 0.01 wt%, were also evaluated using Dynamic Light Scattering (DLS) using a Malvern Nano Zetasizer instrument with a 632.8 nm laser and a detector positioned at 173°. From the apparent diffusion coefficients, the

hydrodynamic diameter (D_H) of the particles were determined using the Stokes–Einstein relationship for translational diffusion. The zeta potential (ζ) was estimated based on the electrophoretic mobility measurements using the Smoluchowski model.

Transmission Electron Microscopy (TEM) images were recorded on a Zeiss CEM902 microscope using an operating voltage of 120 kV. Samples were prepared from about a drop (5 µL) of particle dispersion, diluted to 0.01 wt%, that was mixed with a drop of 1 wt % uranyl acetate solution. The resulting solution was then deposited on a 200 mesh formvar-coated copper grid and dried in air at room temperature. The dilution and negative staining were employed for CS and CP particles, as well as for their conjugates with metal NPs, due to their low contrast under electron beam and to avoid particle aggregation or disruption caused by sample drying.

Preparation of Ag and Au NPs

Ag and Au NPs with an average size of 5 nm were synthesized by an adapted method described elsewhere.[28] Briefly, aqueous solutions (10 mL) containing the silver or gold salts in the concentration of 1 mM were stirred with 0.2 mmol of PVP 50 KDa (based on pyrrolidone monomer). The pH was brought to 9 by adding 1 M NaOH aqueous solution. After that, 0.3 mL of $NaBH_4$ (100 mM) was added. The mixture was stirred for another 1 h and a yellow or pink aqueous dispersion containing the Ag or Au NPs, respectively, was obtained and kept at room temperature, after their pH was adjusted to 7 by adding 1 M HCl aqueous solution. The samples were characterized by DLS, zeta potential, TEM and UV-Vis spectroscopy, using an HP8453 spectrometer. The metal concentration in the NPs dispersions was obtained by Inductively Coupled Plasma Optical Emission Spectrometry (ICP-OES) in a Perkin Elmer Optima 3000 DV spectrometer. The particle sizes were measured using the TEM images manually with the help of ImageJ Software sizing tool.

Conjugation of Ag and Au NPs to CS and CP particles

To ensure that the metal NPs would be bound to the CS particles, the surface of the later were functionalized with thiol (SH) groups because of their strong interaction with Ag and Au NPs. The xanthate ($SCSOCH_2CH_3$) terminal groups bounded to the PAAm block were reduced to thiol groups by a reaction with excess sodium borohydride, as described elsewhere.[6,29] The amount of converted thiol groups was determined by the Ellman's method[30] from the corresponding calibration curve elaborated based on L-Glutathione Reduced (Sigma-Aldrich, USA) standard solutions (Figure S1). Later, the CS particles surface-functionalized with SH groups and the Ag or Au NPs were mixed, under magnetic stirring, at room temperature, in a 1:1 mass proportion. The pH of the final dispersions was then adjusted to 7. The obtained conjugates were named as CS-Ag and CS-Au, to describe the CS particles surface-decorated with Ag and Au NPs, respectively. These conjugates were characterized by DLS, zeta potentials, TEM and UV-Vis spectroscopy. Following the same procedure, CP conjugates with Ag and Au NPs, refereed here as CP-Ag and CP-Au, were prepared and characterized.

Colloidal stability tests

The stability of the dispersions containing the conjugates (CS-Ag, CS-Au, CP-Ag, CP-Au) was studied over a wide range of sodium chloride concentration and pH. The ionic strength was adjusted by adding salt, from 100 to 500 mM of NaCl, and the pH of the dispersions was varied from 2 to 10 using 1 M HCl or NaOH aqueous solutions. The resulting dispersions were then analyzed by UV-Vis spectroscopy and by visual inspection. The colloidal stability of the parent Ag and Au NPs as a function of salt concentration and pH were also studied as a control experiment.

Emulsification tests

The ability of the CS-Ag and CS-Au conjugates to stabilize oil-in-water emulsions was tested by vortexing the aqueous conjugate dispersions (1 wt%) with mineral oil, in a volume proportion of 8:2, for around 1 minute. The average size of the droplets, as well as the emulsions stability over the time, were analyzed by optical microscopy using a Nikon E800 microscope. As a reference, Ag and Au NPs and CS and CP particles were also tested as emulsifiers.

Interfacial catalytic tests

Because of the results obtained in the colloidal stability and emulsification tests, that will be presented below, the oil-in-water emulsions stabilized by CS-Ag and CS-Au conjugates were chosen for catalytic tests involving the aerobic oxidation of alcohols to carboxylic acids. This reaction was chosen as a proof-of-concept because it has already been reported to be catalyzed by Au NPs, at room temperature, in aqueous medium under mild basic pH.[31] The tests were performed as follows: in a tube containing 8 mL of the CS-Ag or CS-Au aqueous dispersions, with metal concentration of 0.5 mM (as determined by ICP-OES), 0.75 mmol of potassium carbonate and 0.25 mmol of benzyl alcohol, the later dissolved in 2 mL of mineral oil, were added and the resulting mixture was vortexed for 1 minute and kept under mild magnetic stirring at room temperature.

At each hour, 1 mL of the reaction mixture was collected and centrifuged at 5000 rpm to break the emulsion and separate the aqueous and oil phases. The aqueous phase, containing the product in the form of potassium benzoate, was quenched by adding HCl 1 M and washed with 3 portions of 4 mL ethyl acetate. The organic phase was then analyzed by UV-Vis spectroscopy ($\lambda = 230$ nm) and the amount of benzoic acid was quantified based on a previously obtained calibration curve (Figure. S2).

At the end of the reaction, i.e. the time in which the product concentration remained unchanged, the remaining emulsion was centrifuged at 5000 rpm for 1 hour and the conjugates, settled at the bottom of the vessel, were recovered, redispersed and used again in a new reaction, to check the catalyst recycling. This recycling test was performed 5 times for each of the catalysts (CS-Ag and CS-Au). At the end of each cycle, the metal concentration in the aqueous phase was determined by ICP-OES. As a control experiment, the Ag and Au NPs were also used as catalysts in the aerobic oxidation of benzyl alcohol to benzoic acid in aqueous medium.

RESULTS AND DISCUSSION

CS and CP particles

Figure 2 shows the SAXS pattern obtained for CS dispersed particles. The peaks with a spacing ratio of $4^{1/2}:5^{1/2}:6^{1/2}$, indicated a $Pm\overline{3}n$ micellar cubic liquid crystalline structure, with a lattice parameter of 8.4 nm. Interestingly, it shows that the dispersion of stoichiometric CS containing water-soluble neutral blocks produced particles with core structures that agree with the phases previously observed for maximally water-swollen corresponding homopolymer CS.[21-23] Additional results also showed that CS particles with a variety of liquid crystalline core structures can be prepared from CS containing other combinations between surfactant ions and neutral-charged block copolymers, as well as cosurfactants, such as long chain n-alcohols, indicating the versality of the system in terms of an accurate control over the core structures when compared with the traditional lipid-based liquid crystalline dispersions. [21-23]
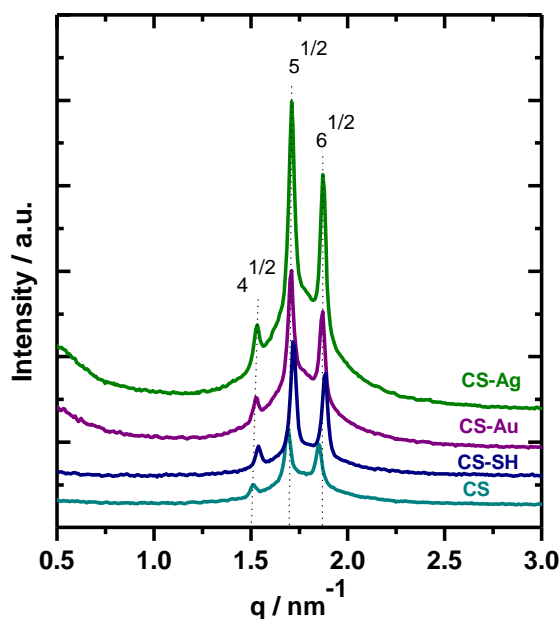
Figure 2. SAXS patterns (shifted along the y-axis) for the CS particles, CS particles surface-functionalized with thiol groups (CS-SH) and CS particles conjugated to Ag and Au NPs (CS-Ag and CS-Au). Arrows indicate the expected peak positions, according to the peak ratios of the correspondent phase considering the first peak.

The freshly prepared dispersions were also characterized regarding their hydrodynamic diameter (D_H) and zeta potential values and the results are displayed in Figure 3A and B, respectively. The average size of the CS particles was around 250 nm with a polydispersity index (PDI) consistently around 0.1. By using our procedure, particles with the above-mentioned average size are easily produced but the literature on similar systems [17-23] suggests that these particles are out of equilibrium and that their size is process-dependent, which is consistent with the properties of any colloidal dispersion. The zeta potential values (Figure 3B) suggest that the CS particles display a negative surface charge of around -35 mV due to, probably, the dissociation of surfactant ions from the CS core of the particles, producing an excess of anionic acrylate charges at the core surface.[22] These CS dispersions displayed

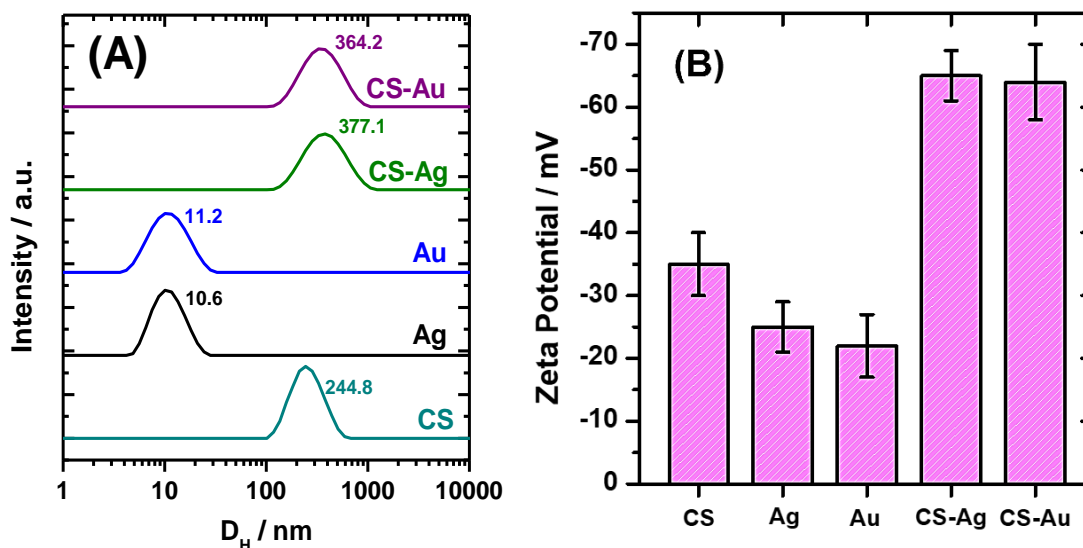particles with average size that remained unchanged over several months, with no signs of macroscopic phase separation.[22]

Figure 3. Size distribution obtained by DLS (A) and zeta potential values (B) for CS particles, Ag and Au NPs and CS particles conjugated to Ag (CS-Ag) and Au (CS-Au) NPs. In A, the average size is indicated for each of the investigated systems. In B, the mean zeta potential values are displayed as the avg $\pm$ SD, from triplicates of independent preparations.

The TEM images obtained for CS particles, shown in Figure S3, corroborate the DLS data, indicating spherical aggregates with diameter in the range of 100-200 nm. It is important to emphasize that these particles are self-assembled structures that only exist as dispersed aggregates in aqueous solution. By removing the solvent, the particles aggregate, forming large objects. To avoid such segregation, the samples used for TEM analysis were diluted to 0.01 wt% and negative-stained with uranyl acetate, that helps fixating the aggregates and both in increasing the contrast of the organic material under the beam of electrons and setting the particles at the solid substrate.

As a reference, CP particles were also prepared and characterized. It is already known that these particles, prepared by mixing individual aqueous solutions of the charged–neutral block copolymer and the charged surfactant, with their respective counterions, are also core-shell aggregates. Further studies revealed that the micelles in the core of the particles are arranged in a disordered state.[17-20] The SAXS data (Figure S4) displayed no scattering peak, confirming the amorphous nature of the CP particles. As discussed in detail in a previous report[22], the smaller core size could be the cause of absence of liquid crystalline structure in the CP particles. Available data on particle size (Figure 3A and S3) show that the CS particles display larger cores than the CP particles (Figure S3 and S5). Hence, the later would not be large enough to constitute a liquid crystalline domain. Another important difference from CS particles is that the CP ones display a surface charge close to zero, as evidenced by their zeta potential values (Figure S5).

Ag and Au NPs

A synthetic route described elsewhere[28] was adapted to prepare metal NPs with diameter around 5 nm. DLS (Figure 3A) and TEM data (Figure S6) present the average size of Ag and Au NPs and, additionally, show that they are spherical and well-dispersed. The size distribution histograms based on TEM images are also displayed in Figure S6. UV-Vis spectroscopy was also employed to characterize the metal NPs because of the sensitivity of their surface plasmon resonance (SPR) band to their size and state of aggregation.[32] Figure 4A and B show the UV-Vis spectra for Ag and Au NPs, respectively, indicating the SPR bands located at 402 and 521 nm, respectively, in accordance with the literature for NPs with average size of 5 nm.[32,33] In addition, these metal NPs display negative zeta potentials (Figure 3B), due to the presence of remaining borohydride ions adsorbed to the NPs surface.
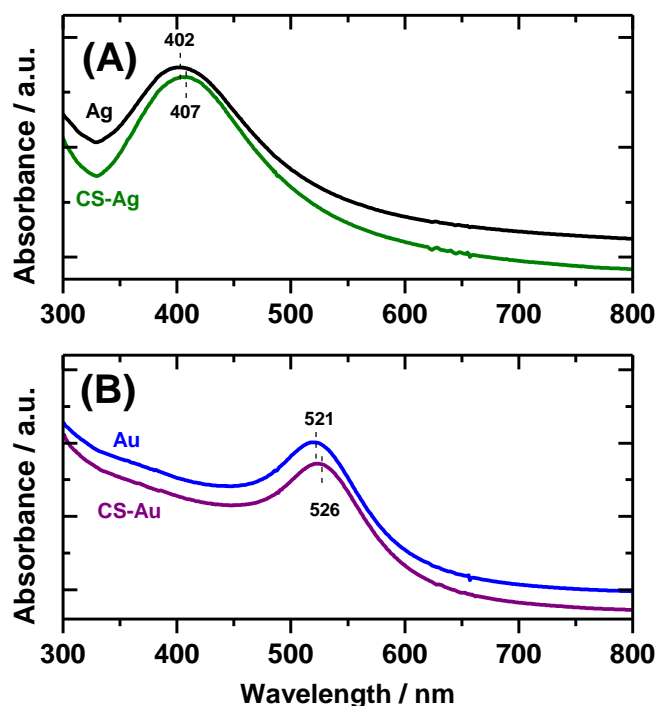
Figure 4. UV-Vis spectra obtained for Ag (A) and Au NPs (B) and their respective conjugates with CS particles. Dashed lines indicate the maxima position of SPR band.

CS-Ag and CS-Au conjugates

To ensure that the metal NPs would be strongly bound to the CS particles, the later were surface-functionalized with thiol groups, taking the advantage of the fact that the PAAm blocks possess, as ending groups, xanthate (from the controlled polymerization reaction), that has been already shown to be converted to thiol groups which interact with metal NPs.[6,29] SAXS (Figure 2) and additional data that will be presented below indicate that the surface functionalization did not alter the nature of the CS particles. The amount of thiol groups on the surface of the particles was 6.6×10^{-21} $\mu mol.nm^{-2}$, indicating that approximately 90% of the initial xanthate groups were converted to SH. Once thiol groups were added to their surface, the CS particles were mixed with the previously prepared Ag and Au NPs, in a mass ratio of 1:1, and the resulting conjugates were further studied.

SAXS data (Figure 2) indicated that, upon attachment of metal NPs to the CS particles surface, their liquid crystalline cores remained $Pm\overline{3}n$ micellar cubic, with no significant variation in the cell parameter, as evidenced by the positions of the scattering peaks that remained essentially the same. These results indicate that the Ag and Au NPs were probably located at the particles surface and displayed no affinity for the liquid crystalline core. This is interesting because it has been shown that the addition of metal-based NPs to liquid crystalline particles usually alter their structure. Examples come from reports on cubosomes (dispersions of reverse bicontinuous lipid cubic phases) functionalized with iron oxide NPs[34] and gold nanorods[35]. In both cases, the addition of metal NPs promoted changes in the cell parameter of the initial liquid crystalline structure or favored the formation of additional structures. However, the liquid crystalline particles in the present study were obtained in such a way that their shell was functionalized to ensure the location of metal NPs at the outermost surface.

DLS data (Figure 3A) show that the resulting conjugates display an average hydrodynamic diameter of ca. 380 nm, indicating an increase of about ~ 50% when compared with the original CS particles. The increase in D_H values most likely not a result of an increase in the CS size due to the conjugation with Ag and Au NPs, but rather a result of the NP greater surface charge, and consequently, increase in hydration layer.

TEM images (Figure 5) confirm this, by showing the dry CS particles, with basically the same average size after surface decoration with metal NPs. An important additional observation is that the Ag and Au NPs were mainly attached to the outer part of the CS particles, and retained their original size and state of aggregation, when compared with the original metal NPs (Figure S6). The DLS and TEM results show that the formation of CS particles surface-decorated with Ag and Au NPs was successfully achieved by using this protocol.
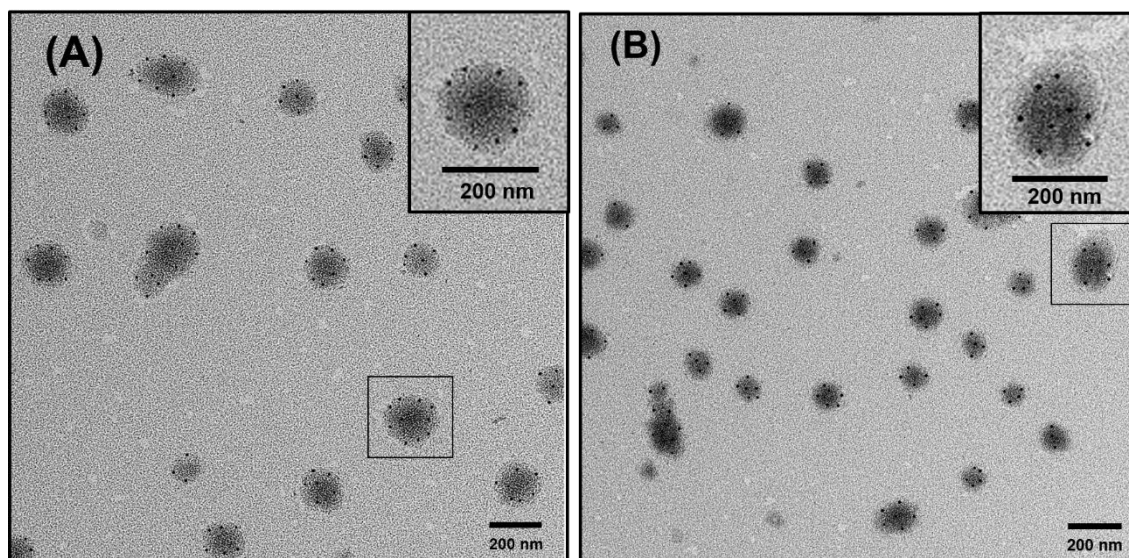
Figure 5. TEM images obtained for CS-Ag (A) and CS-Au (B) conjugates. Samples were negative stained with uranyl acetate solution. Insets show magnification of the squared areas in the respective images.

Zeta potential values (Figure 3B) show that the CS-Ag and CS-Au conjugates possess a high negative surface charge, (ca. -65 mV), probably because both components, the original CS and metal NPs, are also negatively charged (Figure 3B). Such high zeta potential values result in improved colloidal stability, as will be described below.

Conjugating the Ag and Au NPs onto the surface of thiol-modified CS particles, led to no visual change of their appearance as compared to that of the original metal NPs. This was confirmed by UV-Vis spectra (Figure 4) that reveal that the SPR band shows a small red-shift to 407 and 526 nm, for Ag and Au NPs conjugated to CS, respectively, indicating the absence of any noticeable aggregation between the conjugated metal NPs, which is also consistent with the TEM results (Figure 5). According to the literature on similar systems, i.e. colloids surface-decorated with metal NPs, the small red-shift in the SPR band is an indication that local concentration of Ag and Au NPs has increased at the CS particles surface and decreased the

average spatial distance between metal NPs compared to that in the original Ag and Au NPs dispersions.[12]

CP particles (thiol content of 6.9×10^{-21} µmol.nm^{-2}) were also successfully surface-decorated with Ag and Au NPs, as evidenced by the DLS (Figure S5), TEM (Figure S7) and UV-Vis spectroscopy (Figure S8) results. An important information that should be highlighted in this case is that, because the original CP particles display no surface charge (Figure S5), the zeta potential values for CP-Ag and CP-Au conjugates were almost half of those values observed for CS-Ag and CS-Au conjugates, which also impacts on their colloidal stability, as will be discussed in the following topic.

Colloidal stability tests

Depending on the desired application, metal NPs may be exposed to medium with significant variations of ionic strength and pH values, among other environmental variables. Hence, NPs with enhanced stability are highly desired to avoid aggregation and to retain their original properties. Because the SPR band is related to NPs size and state of aggregation[32,33], it can be used as a parameter to monitor the stability of the metal NPs: changes in the position of the band as surrounding conditions are varied may indicate aggregation of NPs. UV-Vis spectroscopy was, therefore, used to monitor the stability of the conjugates and the original metal NPs as a function of salt concentration and pH changes.

Because the original metal NPs displayed low negative surface charge, they are described to be quite sensitive to the addition of salt and will immediately and irreversibly aggregate [32], which is confirmed in Figure S9. At 100 mM of NaCl, the SPR bands vanish because the surface charge of the NPs is shielded, leading Ag and Au NPs to completely aggregate and separate from the solution (confirmed by visual inspection of the samples). The metal NPs also show signs of aggregation at pH = 2, and remain stable at pH = 10.

In remarkable opposition, the CS-Ag and CS-Au conjugates display excellent colloidal stability upon salt addition and pH changes, as evidenced by the SPR bands that remain unchanged (Figure 6). Even at high salt concentrations (500 mM) and low pH (pH = 2), no aggregation was observed. This enhanced stability of the conjugates is ascribed to their high surface charge (ca. -65 mV) and the presence of hydrophilic polymer corona that prevent particle aggregation and phase separation[22]. Because the CP particles display zeta potential values close to zero, their conjugates with metal NPs did not present such an improved colloidal stability (Figure S10), confirming the importance of the surface charge of the CS-Ag and CS-Au conjugates for their stabilization. These results were the first to indicate the advantage of using surfactant-block copolymer particles prepared by the CS method when compared with those prepared by the conventional CP approach.
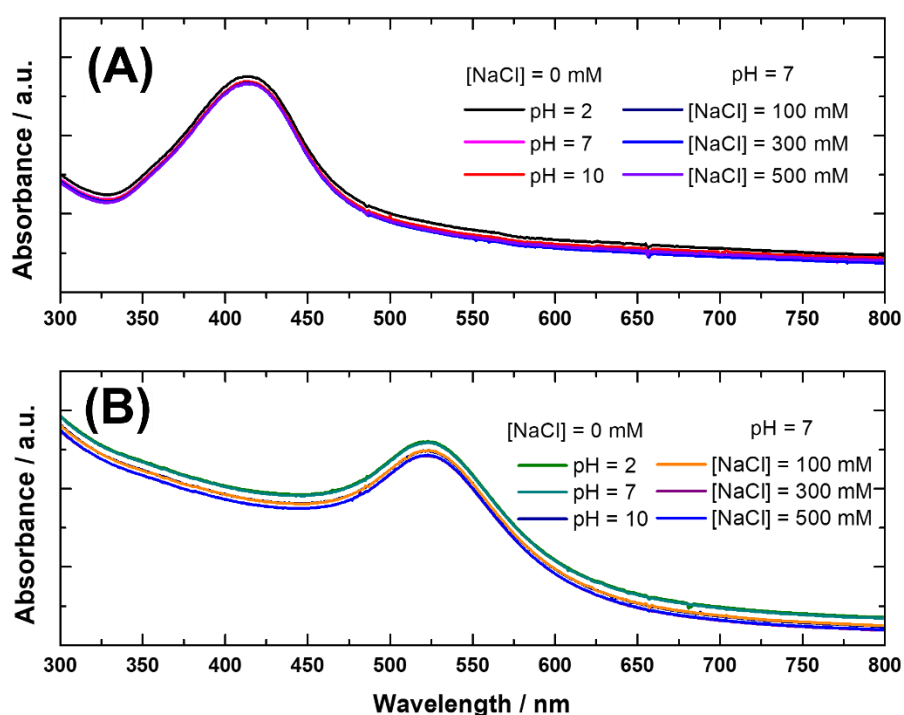

Figure 6. UV-Vis spectra of CS-Ag (A) and CS-Au (B) conjugates as a function of NaCl concentration and solution pH.

Emulsification tests

The ability of the CS and CP particles conjugated to Ag and Au NPs to stabilize oil-in-water emulsions was studied by mixing the aqueous dispersions containing the conjugates with mineral oil in a volume proportion of 8:2. The systems were vortexed for 1 minute and the appearance of the samples was visually monitored. As a control experiment, emulsions stabilized by Ag and Au NPs and CS and CP particles were also prepared. The observations (Table 1) indicated that the best stabilizers were the conjugates with CS particles, with emulsion stability superior to 3 months. The CS particles, solely, could stabilize the emulsions for days before phase separation. All other stabilizers resulted in emulsions with very poor colloidal stability.

Table 1. Stability time of the oil-in-water emulsions stabilized by different particles.

Emulsion Stabilizer	Stability time*
CS	Days
CP	Minutes
Ag	Seconds
Au	Seconds
CS-Ag	Months
CS-Au	Months
CP-Ag	Minutes
CP-Au	Minutes

*Interval at which macroscopic phase separation was observed.

The more stable emulsions were visualized by optical microscopy and the droplets size was monitored over 3 months. The results, shown in Figure 7, confirm the visual observation and showed that the emulsions stabilized by CS-Ag and CS-Au displayed excellent colloidal stability. Their average droplet size remained essentially the same over the investigated time interval. The excellent stability of such emulsions is attributed to the highly negatively-charged conjugates located at the oil-water interface, preventing the droplets aggregation via electrostatic inter-droplet repulsion.
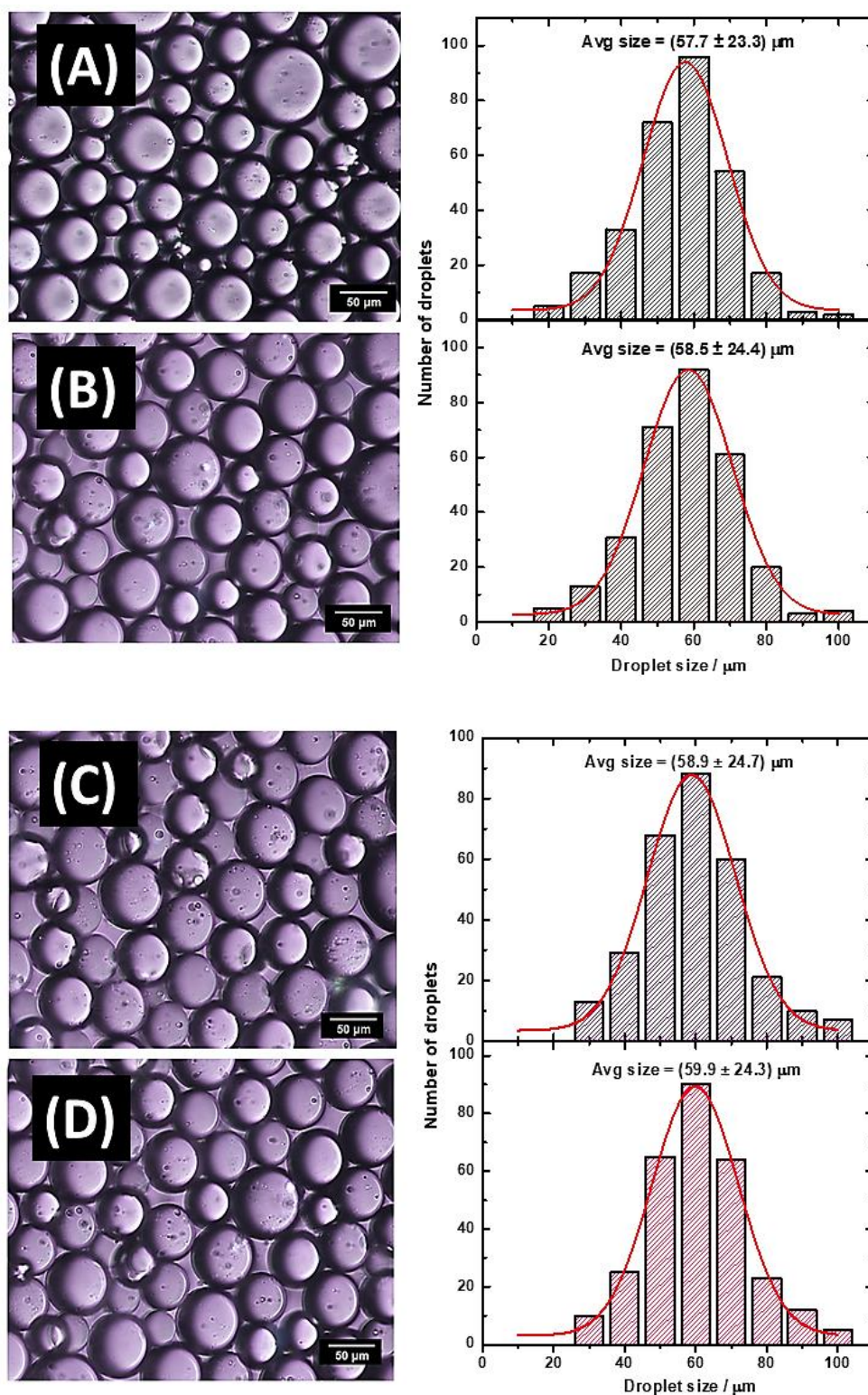
Figure 7. Optical micrographs and respective size distribution histograms (n = 200) with Gaussian fits (red lines) for emulsions stabilized by CS-Ag: freshly prepared (A) and after 3 months (B) and emulsions stabilized by CS-Au: freshly prepared (C) and after 3 months (D).

Pickering emulsions, i.e. emulsions stabilized by particles, are known to display enhanced stability when the stabilizing particles are small in such a way they can form a compact shell surrounding the dispersed droplets in the continuous phase.[26] In the present case, the control experiments indicate that surface charge and the amphiphilic character of the CS-Ag and CS-Au conjugates seems to be equally important for emulsion stabilization. The emulsification tests confirmed the advantage of using metal NPs conjugate to CS instead of CP particles, in agreement with the results obtained in the colloidal stability tests, presented above. Because of these results, CS-Ag and CS-Au were chosen as model systems in the interfacial catalytic experiments, that will be discussed below.

Interfacial catalytic tests

Because metal NPs have been envisaged for catalytic purposes in a variety of chemical reactions in the last years[1,36,37], the CS-Ag and CS-Au conjugates that presented enhanced colloidal stability and emulsification properties were tested as potential catalysts in the biphasic aerobic oxidation of benzyl alcohol to benzoic acid. This model reaction was chosen because it is already known that Au NPs, in aqueous solution, can accelerate the conversion of alcohols to carboxylic acids under mild experimental conditions, i.e. no need of high temperatures, pressure, controlled atmosphere, etc.[28,31,38,39] In addition, a variety of reports have shown the great catalytic efficiency of Au-supported NPs in the aerobic alcohol oxidation.[40-42]

Because the CS-Ag and CS-Au conjugates stabilize oil-water interfaces, a potential use of the emulsions as a medium for interfacial catalysis was seen, with the advantages that the unreacted starting component and the product would concentrate in the oil and aqueous phase, respectively, favoring their separation after the reaction was ended. For this, another reason considered for this choice is the significant difference in aqueous solubility between benzyl alcohol and benzoic acid.

The conjugate dispersions were used as the aqueous phase, after pH adjusting with potassium carbonate, and were mixed with the oil phase, containing the dissolved benzyl alcohol, in the same water-to-oil volume proportion used to prepare the previously investigated emulsions, (8:2 water-to-oil ratio). The resulting emulsion was further stirred at room temperature and the amount of benzoic acid formed was monitored by UV-Vis spectroscopy ($\lambda_{max} = 230$ nm), after separation and acidification of the aqueous phase containing the product in the form of its potassium salt (Figure S11).

Figure 8A shows the yields as a function of reaction time, at the same experimental conditions, by employing the different catalysts. As a reference, the catalytic activity of the pure metal NPs was also studied in aqueous solution, at the same metal content. As described elsewhere, the Au NPs displayed enhanced catalytic efficiency when compared to other metal NPs, Ag, in the present case.[31] Their conjugates with CS particles presented a similar behavior, indicating that the catalytic efficiency of the metal NPs remained essentially the same when they were anchored in the surface of surfactant-block copolymer particles. This seems consistent with the previous results that indicate that the metal NPs are located at the outer surface of the conjugates.

The small yield differences observed when the metal NPs are compared with their respective conjugates with CS particles may be related to higher available surface of the original Ag and Au NPs, differently of the conjugates, in which the metal NPs are covered by PVP and partially-covered by PAAm chains from CS particles. Because side products, such as benzyl benzoate and benzaldehyde, are known to be formed, in all cases,[31] benzyl alcohol is not fully converted to benzoic acid. The linear variation of product concentration with time indicates a first-order reaction (Figure 8B), with rate constants (k) displayed in Table 2, as well as the TOF (turnover frequency) values, which are higher or at least comparable, for Au, to the performance of other polymer-coated metal NPs under similar conditions (Table S1).
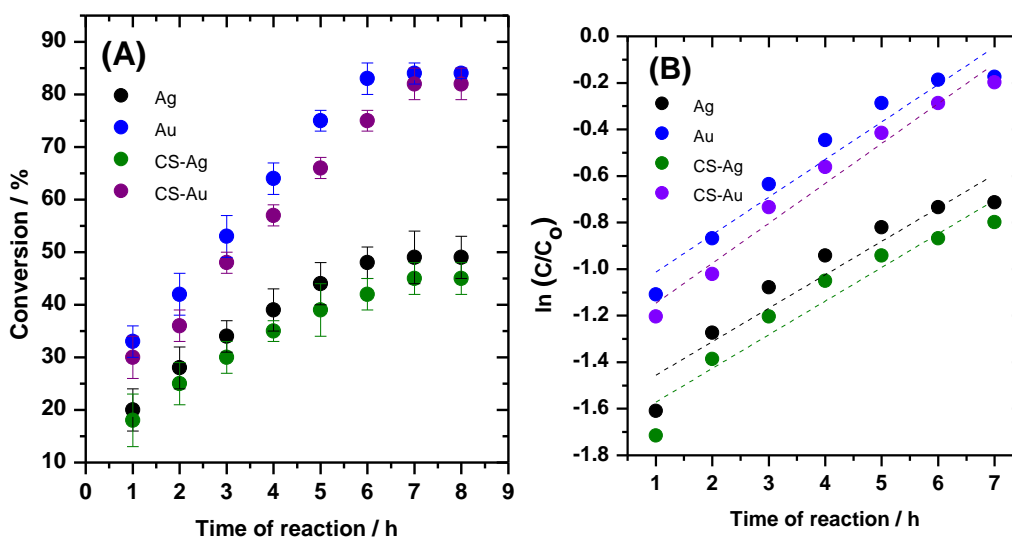
Figure 8. Conversion of benzyl alcohol to benzoic acid as a function of reaction time (A) and the variation of benzoic acid concentration C normalized by the initial concentration C_o as a function of reaction time (B). Data are displayed as the avg $\pm$ SD, from triplicates of independent preparations. In B, the dashed lines represented the linear fit for the data.

Table 2. Maximum conversion, rate constants (k), and turnover frequencies (TOF) for the different catalysts used in the aerobic oxidation of benzyl alcohol to benzoic acid (avg $\pm$ SD, from triplicates of independent preparations).

Catalyst	Conversion / %	k / h^{-1}	TOF / h$^{-1a,b}$
Ag	49$\pm$5	0.144$\pm$0.021	4.0$\pm$0.4
Au	84$\pm$1	0.161$\pm$0.018	7.0$\pm$0.2
CS-Ag	45$\pm$3	0.145$\pm$0.019	3.8$\pm$0.2
CS-Au	82$\pm$2	0.172$\pm$0.013	6.8$\pm$0.2

a. defined as the number of converted moles of benzyl alcohol per metal moles per hour[28]

b. calculated for reaction time in which the product concentration remained unchanged.

After the reaction was finished, the remaining emulsion was centrifuged at 5000 rpm for 1 hour and the conjugates, settled at the bottom of the vessel, were collected, redispersed in water containing potassium carbonate and vortexed with the oil phase containing benzyl alcohol. The resulting emulsion was used again as a medium for a new alcohol oxidation reaction. The recycling tests were performed 5 times for each of the catalysts (CS-Ag and CS-Au). As a control experiment, the recycling of Ag and Au NPs was also studied in aqueous medium. For the five cycles employing CS-Ag and CS-Au as catalysts, the loss of activity was significantly decreased (Figure 9A), while for Ag and Au NPs, there was a significant reduction from the initial catalytic efficiency (Figure 9B).

This decrease could be attributed to the leaching of the original Ag and Au catalysts, as indicated by ICP analysis of the product phase (Figure 9C). In addition, centrifugation and redispersion may induce the metal NPs, with decreased colloidal stability, to form large aggregates that cannot be fully dispersed and possess smaller surface area, which also may greatly impact on their catalytic efficiency.[28] Hence, this compilation of results demonstrates the great efficiency and versatility of the CS-Ag and CS-Au recyclable catalysts for the aerobic oxidation of alcohols in a biphasic system in which the unreacted substance and product are easily separated.

It is important to emphasize that great catalytic results have been found elsewhere for Au-catalyzed aerobic alcohol oxidation. However, all of these reports deal with water-dispersible Au NPs[28,31,38,39] or supported NPs[40-42], making this the first report on the use of metal NPs to perform interfacially-catalyzed oxidation of benzyl alcohol and additionally the nanoconjugates described here could be reused with little loss of their activity.
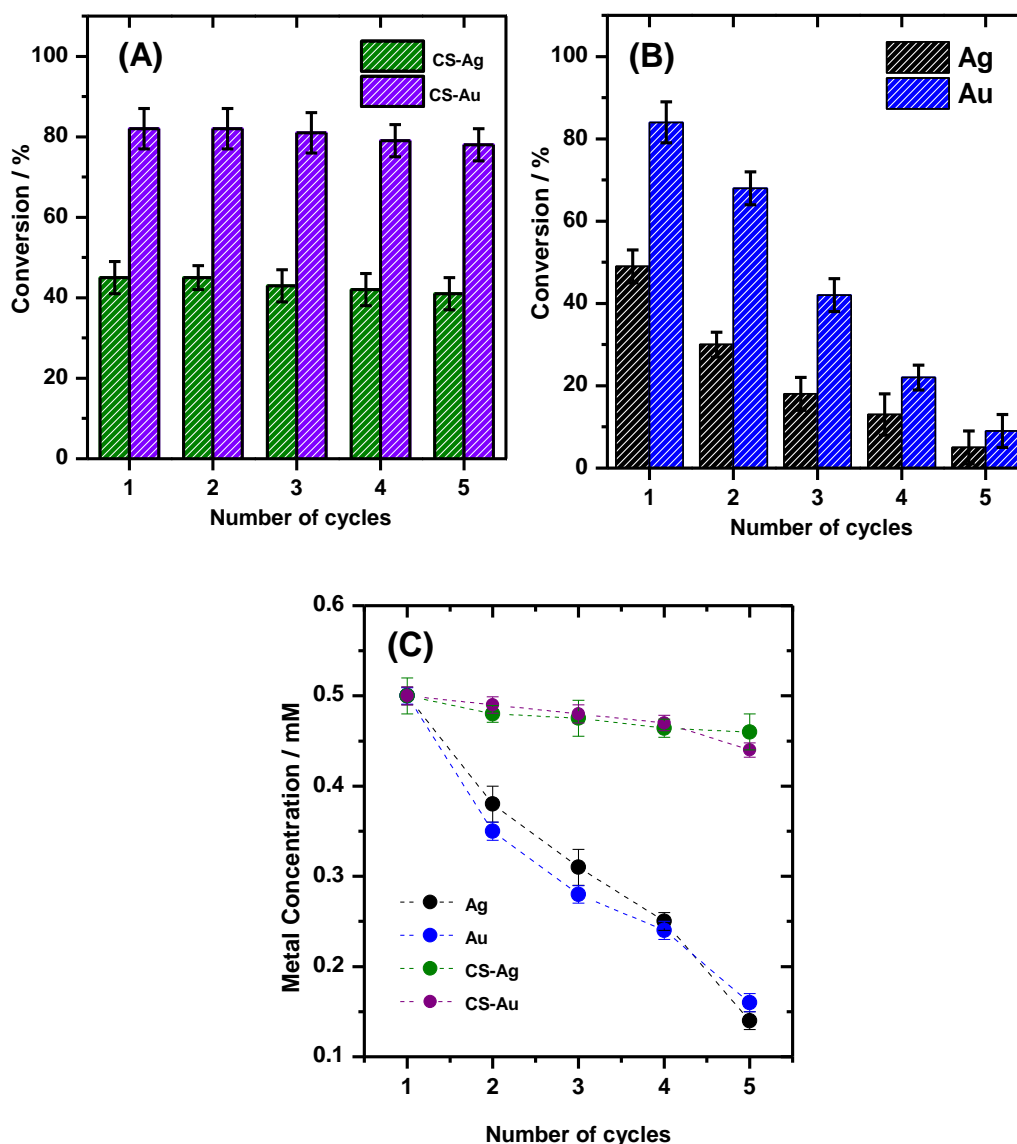
Figure 9. Catalytic efficiency of CS-Ag and CS-Au conjugates (A) and Ag and Au NPs (B) in the aerobic oxidation of benzyl alcohol to benzoic acid. The metal concentration as a function of number of cycles is displayed in (C). The results are displayed as avg $\pm$ SD, from triplicates of independent preparations

CONCLUSIONS

A new approach to the formation of satellite-like nanostructures, based on Ag and Au NPs anchored to the outermost surface of block copolymer-surfactant liquid crystalline particles, is reported. Thanks to the combination of both metal NPs and CS particles, the

conjugates display improved colloidal stability and emulsification properties, while keeping important properties of the individual components, such as the catalytic activity of the metal NPs. These conjugates display great catalytic efficiency towards alcohol aerobic oxidation in biphasic systems that facilitate the product recovery from the reaction mixture.

The present metal-polymer-surfactant conjugates represent a relevant example of using nanotechnology tools by combining advantageous properties of an assembly structure to those of functional materials such as the metal NP catalysts. More than representing a great combination of complex systems, they display properties that could not be reproduced by the individual components. Because colloidally-stable metal NPs are highly desired for multiple purposes and new strategies to obtain such nanomaterials have been widely anticipated, the information reported in the present study is encouraging for future work involving similar novel functional nanomaterials with sophisticated structures and tunable multifunctionalities.

ASSOCIATED CONTENT

Supporting information

The Supporting Information is available free of charge on the ACS Publications website.

AUTHOR INFORMATION

Corresponding Authors

*E-mail: wloh@iqm.unicamp.br (W. L.)

ORCID

Guilherme A. Ferreira: 0000-0002-4932-3666

Watson Loh: 0000-0002-8049-3321

Author Contributions

The manuscript was written through contributions of all authors. All authors have given approval to the final version of the manuscript.

Notes

The authors declare no competing financial interest.

REFERENCES

1 Daniel, M-C.; Astruc, D. Gold Nanoparticles: Assembly, Supramolecular Chemistry, Quantum-Size-Related Properties, and Applications toward Biology, Catalysis, and Nanotechnology. *Chem. Rev.* **2004**, *104*, 293-346.

2 Chen, X.; Zhao, D.; An, Y.; Zhang, Y.; Cheng, J.; Wang, B.; Shi, L. Formation and catalytic activity of spherical composites with surfaces coated with gold nanoparticles. *J. Colloid Interface Sci.* **2008**, *322*, 414-420.

3 Meristoudi, A.; Pispas, S. Polymer mediated formation of corona-embedded gold nanoparticles in block polyelectrolyte micelles. *Polymer* **2009**, *50*, 2743-2751.

4 Xu, J.-P.; Yang, X.; Lv, L.-P.; Wei, Y.; Xu, F. M.; Ji, J. Gold-Nanoparticle-Stabilized Pluronic Micelles Exhibiting Glutathione Triggered Morphology Evolution Properties. *Langmuir* **2010**, *26*, 16841-16847.

5 Tao, Y.; Han, J.; Ye, C.; Thomas, T.; Dou, H. Reduction-responsive gold-nanoparticle-conjugated Pluronic micelles: an effective anti-cancer drug delivery system. *J. Mater. Chem.* **2012**, *22*, 18864-18871.

6 Yin, T.; Liu, X.; Wang, J.; An, Y.; Zhang, Z.; Shi, L. Thermosensitive mixed shell polymeric micelles decorated with gold nanoparticles at the outmost surface: tunable surface plasmon resonance and enhanced catalytic properties with excellent colloidal stability. *RSC Adv*. **2015**, *5*, 47458-47465.

7 Akamatsu, K.; Shimada, M.; Tsuruoka, T.; Nawafune, H.; Fujii, S.; Nakamura, Y. Synthesis of pH-Responsive Nanocomposite Microgels with Size-Controlled Gold Nanoparticles from Ion-Doped, Lightly Cross-Linked Poly(vinylpyridine). *Langmuir* **2010**, *26*, 1254-1259.

8 Wu, T.; Ge, Z.; Liu, S. Fabrication of Thermoresponsive Cross-Linked Poly(N-isopropylacrylamide) Nanocapsules and Silver Nanoparticle-Embedded Hybrid Capsules with Controlled Shell Thickness. *Chem. Mater*. **2011**, *23*, 2370-2380.

9 Xie, M.; Ding, L.; You, Z.; Gao, D.; Yang, G.; Han, H. Robust hybrid nanostructures comprising gold and thiol-functionalized polymer nanoparticles: facile preparation, diverse morphologies and unique properties. *J. Mater. Chem*. **2012**, *22*, 14108-14118.

10 Kirillova, A.; Schliebe, C.; Stoychev, G.; Jacob, A.; Lang, H.; Synytska, A. Hybrid Hairy Janus Particles Decorated with Metallic Nanoparticles for Catalytic Applications. *ACS Appl. Mater. Interfaces* **2015**, *7*, 21218-21225.

11 Jiang, K.; Eitan, A.; Schadler, L. S.; Ajayan, P. M.; Siegel, R. W.; Grobert, N.; Mayne, M.; Reyes-Reyes, M.; Terrones, H.; Terrones, M. Selective Attachment of Gold Nanoparticles to Nitrogen-Doped Carbon Nanotubes. *Nano Letters* **2003**, *3*, 275-277.

12 Xu, H.; Xu,J.; Jiang, X.; Zhu, Z.; Rao, J.; Yin, J.; Wu, T.; Liu, H.; Liu, S. Thermosensitive Unimolecular Micelles Surface-Decorated with Gold Nanoparticles of Tunable Spatial Distribution. *Chem. Mater*. **2007**, *19*, 2489-2494.

13 Lam, E.; Hrapovic, S.; Majid, E.; Chong, J. H.; Luong, J. H. T. Catalysis using gold nanoparticles decorated on nanocrystalline cellulose. *Nanoscale* **2012**, *4*, 997-1002.

14 Perro, A.; Reculusa, S.; Ravaine, S.; Bourgeat-Lami, E.; Duguet, E. Design and synthesis of Janus micro- and nanoparticles. *J. Mat. Chem*. **2005**, *15*, 3745-3760.

15 Rossner, C.; Vana, P. Planet-satellite nanostructures made to order by RAFT star polymers. *Angew. Chem., Int. Ed*. **2014**, *53*, 12639–12642.

16 Rossner, C.; Tang, Q.; Glatter, O.; Muller, N.; Vana, P. Uniform Distance Scaling Behavior of Planet-Satellite Nanostructures Made by Star Polymers. *Langmuir* **2017**, *33*, 2017–2026.

17 Berret, J. F.; Cristobal, G.; Hervé, P.; Grillo, I. Structure of colloidal complexes obtained from neutral/poly-electrolyte copolymers and oppositely charged surfactants. *Eur. Phys. J. E* **2002**, *9*, 301-311.

18 Berret, J. F.; Hervé, P.; Aguerre-Chariol, O.; Oberdisse, J. Colloidal complexes obtained from charged block copolymers and surfactants: A comparison between small-angle

neutron scattering, Cryo-TEM, and simulations. *J. Phys. Chem. B* **2003**, *107*, 8111-8118.

19 Hervé, P.; Destarac, M.; Berret, J.-F.; Lal, J.; Oberdisse, J.; Grillo, I. Novel Core-shell Structure for Colloids Made of Neutral/ Polyelectrolyte Diblock Copolymers and Oppositely Charged Surfactants. *Europhys. Lett*. **2002**, *58*, 912−918.

20 Berret, J.-F.; Vigolo, B.; Eng, R.; Hervé, P.; Grillo, I.; Yang, L. Electrostatic Self-assembly of Oppositely Charged Copolymers and Surfactants: a Light, Neutron, and X-ray Scattering Study. *Macromolecules* **2004**, *37*, 4922−4930.

21 Vitorazi, L.; Berret, J-F.; Loh, W. Self-Assembly of Complex Salts of Cationic Surfactants and Anionic–Neutral Block Copolymers. Dispersions with Liquid-Crystalline Internal Structure. *Langmuir* **2013**, *29*, 14024–14033.

22 Ferreira, G. A.; Loh, W. Addition of n-Alcohols Induces a Variety of Liquid-Crystalline Structures in Surfactant-Rich Cores of Dispersed Block Copolymer/Surfactant Nanoparticles. *ACS Omega* **2016**, *1*, 1104–113.

23 Carneiro, N. M.; Percebom, A. M.; Loh, W. Quest for Thermoresponsive Block Copolymer Nanoparticles with Liquid–Crystalline Surfactant Cores. *ACS Omega* **2017**, 2, 5518–5528.

24 Ferreira, G. A.; Loh, W. Liquid crystalline nanoparticles formed by surfactant-polyelectrolyte complexes. *Curr. Opin. Colloid Int. Sci* **2017**, 32, 11-22.

25 Guo, C.; Wang, J.; Cao, F.; Lee, R. J.; Zhai, G. Lyotropic liquid crystal systems in drug delivery. *Drug Discov. Today* **2010**, *15*, 1032-1040.

26 Pera-Titus, M.; Leclercq, L.; Clacens, J. M.; de Campo, F.; Nardello-Rataj, V. Pickering Interfacial Catalysis for Biphasic Systems: From Emulsion Design to Green Reactions. *Angew. Chem. Int. Ed. Engl*. **2015**, *54*, 2006-2021.

27 Faria, J.; Ruiz, M. P.; Resasco, D. E. Phase-Selective Catalysis in Emulsions Stabilized by Janus Silica-Nanoparticles. *Adv. Synth. Catal*. **2010**, *352*, 2359-2364.

28 Yuan, Y.; Yan, N.; Dyson, P. J. pH-Sensitive Gold Nanoparticle Catalysts for the Aerobic Oxidation of Alcohols. *Inorg. Chem*. **2011**, *50*, 11069-11074.

29 Lowe, A. B.; Sumerlin, B. S.; Donovan, M. S.; McCormick, C. L. Facile Preparation of Transition Metal Nanoparticles Stabilized by Well-Defined (Co)polymers Synthesized via Aqueous Reversible Addition-Fragmentation Chain Transfer Polymerization. *J. Am. Chem. Soc.* **2002**, *124*, 11562-11563.

30 Moser, M.; Schneider, R.; Behnke, T.; Schneider, T.; Falkenhagen, J.; Resch-Genger, U. Ellman's and Aldrithiol Assay as Versatile and Complementary Tools for the

Quantification of Thiol Groups and Ligands on Nanomaterials *Anal. Chem.* **2016**, *88*, 8624–8631.

31 Tsunoyama, H.; Sakurai, H.; Negishi, Y.; Tsukuda, T. Size-Specific Catalytic Activity of Polymer-Stabilized Gold Nanoclusters for Aerobic Alcohol Oxidation in Water. *J. Am. Chem. Soc*. **2005**, *127*, 9374-9375.

32 Pamies, R.; Cifre, J. G. H.; Espín, V. F.; Collado-González, M.; Banos, F. G. D.; de la Torre, J. G. Aggregation behaviour of gold nanoparticles in saline aqueous media. *J. Nanopart. Res*. **2014**, *16*, 2376-2380.

33 Agnihotri, S.; Mukherji, S.; Mukherji, S. Size-controlled silver nanoparticles synthesized over the range 5–100 nm using the same protocol and their antibacterial efficacy. *RSC Adv*. **2014**, *4*, 3974-3983.

34 Szlezak, M.; Nieciecka, D.; Joniec, A.; Pękala, M.; Gorecka, E.; Emo, M.; Stébé, M. J.; Krysínski, P.; Bilewicz, R. Monoolein Cubic Phase Gels and Cubosomes Doped with Magnetic Nanoparticles–Hybrid Materials for Controlled Drug Release. *ACS Appl. Mater. Interfaces* **2017**, *9*, 2796-2805.

35 Fong, W-K.; Hanley, T. L.; Thierry, B.; Kirby, N.; Waddington, L. J.; Boyd, B. J. Controlling the Nanostructure of Gold Nanorod–Lyotropic Liquid-Crystalline Hybrid Materials Using Near-Infrared Laser Irradiation. *Langmuir* **2012**, *28*, 14450-14460.

36 Narayanan, R.; El-Sayed, M. A. Catalysis with Transition Metal Nanoparticles in Colloidal Solution: Nanoparticle Shape Dependence and Stability. *J. Phys. Chem B* **2005**, *109*, 12663-12676.

37 Zahmakiran, M.; Ozkar, S. Metal nanoparticles in liquid phase catalysis; from recent advances to future goals. *Nanoscale* **2011**, *3*, 3462-3481.

38 Han, J.; Liu, Y.; Guo, R. Reactive Template Method to Synthesize Gold Nanoparticles with Controllable Size and Morphology Supported on Shells of Polymer Hollow Microspheres and Their Application for Aerobic Alcohol Oxidation in Water. *Adv. Funct. Mater*. **2009**, *19*, 1112-1117.

39 Tsunoyama, H.; Sakurai, H.; Tsukuda, T. Size effect on the catalysis of gold clusters dispersed in water for aerobic oxidation of alcohol. *Chem. Phys. Lett*. **2006**, *429*, 528-532.

40 Abad, A.; Corma, A.; García, H. Catalyst Parameters Determining Activity and Selectivity of Supported Gold Nanoparticles for the Aerobic Oxidation of Alcohols: The Molecular Reaction Mechanism. *Chem. Eur. J*. **2008**, *14*, 212-222.

41 Su, F-Z.; Liu, Y-M.; Wang, L-C.; Cao, Y.; He, H-Y.; Fan, K-N. Ga-Al mixed-oxide-supported gold nanoparticles with enhanced activity for aerobic alcohol oxidation. *Angew. Chem. Int. Ed*. **2008**, *47*, 334-337.

42 Mitsudome, T.; Noujima, A.; Mizugaki, T.; Jitsukawa, K.; Kaneda, K. Efficient Aerobic Oxidation of Alcohols using a Hydrotalcite-Supported Gold Nanoparticle Catalyst. *Adv. Synth. Catal*. **2009**, *351*, 1890-1896.

Supporting Information

Planet-Satellite Nanostructures Based on Block Copolymer-Surfactant Nanoparticles Surface-Decorated with Gold and Silver: A New Strategy for The Interfacial Aerobic Alcohol Oxidation

Guilherme A. Ferreira, Watson Loh*

Institute of Chemistry, University of Campinas (UNICAMP), P.O. Box 6154, 13083-970 Campinas, São Paulo, Brazil
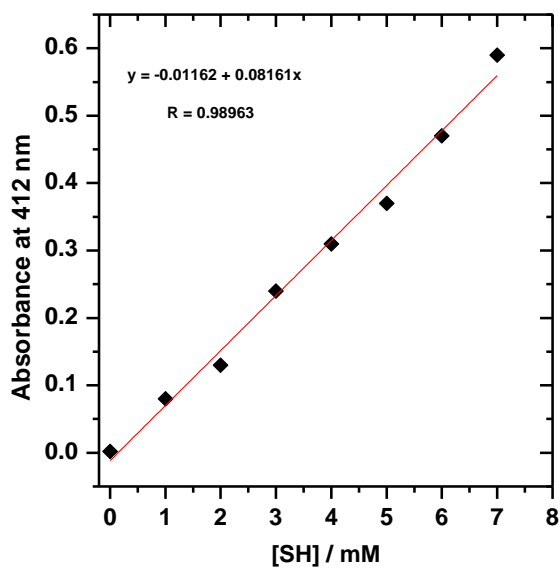
*E-mail: wloh@iqm.unicamp.br.

Figure S1. Variation of absorbance at 412 nm as a function of thiol (SH) concentration in standard L-Glutathione solutions analyzed by UV-Vis spectroscopy.
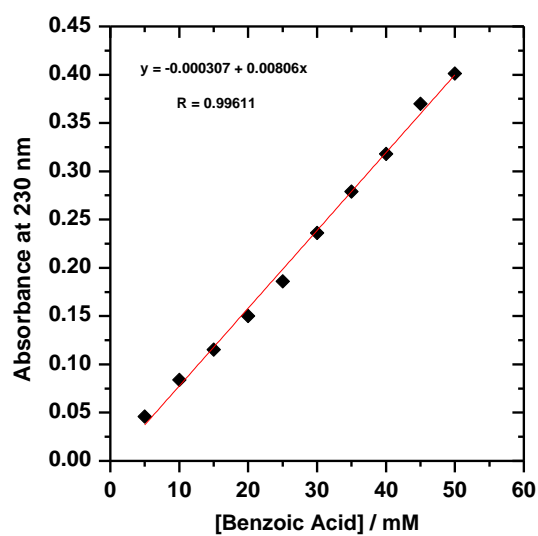

Figure S2. Variation of absorbance at 230 nm as a function of benzoic acid in standard solutions analyzed by UV-Vis spectroscopy.
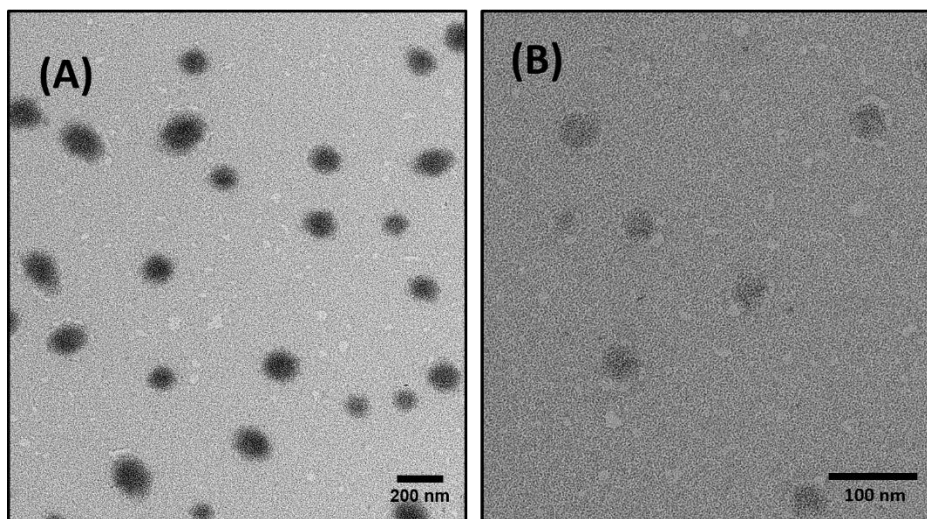
Figure S3. TEM image obtained for (A) CS and (B) CP particles negative stained with uranyl acetate solution.
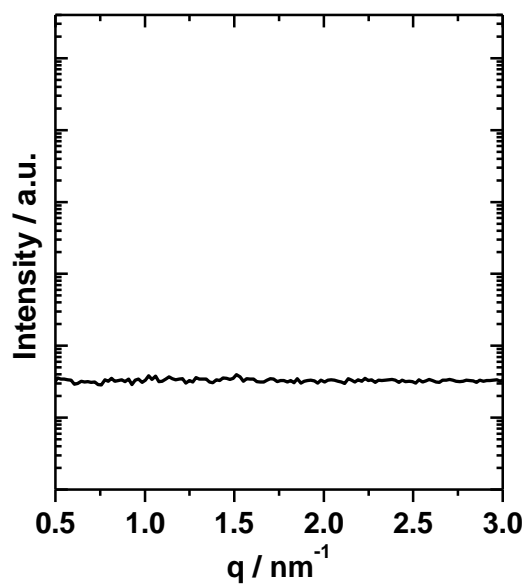

Figure S4. SAXS pattern for CP particles aqueous dispersion at 0.01 wt%.
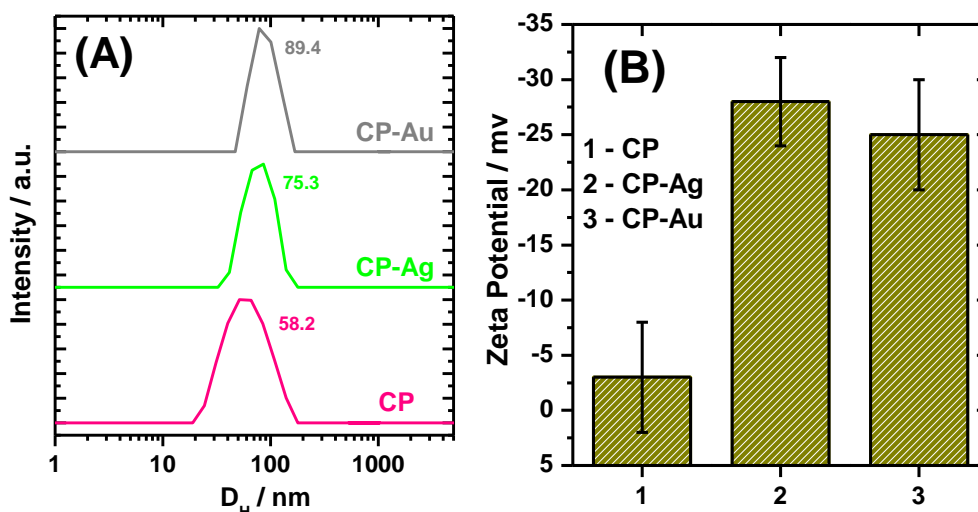
Figure S5. Size distribution obtained by DLS (A) and zeta potential values (B) for CP particles and CP particles conjugated to Ag (CP-Ag) and Au (CP-Au) NPs. In A, the average size is indicated for each of the investigated systems. In B, the mean zeta potential values are displayed as the avg ± SD, triplicate of independent preparations.
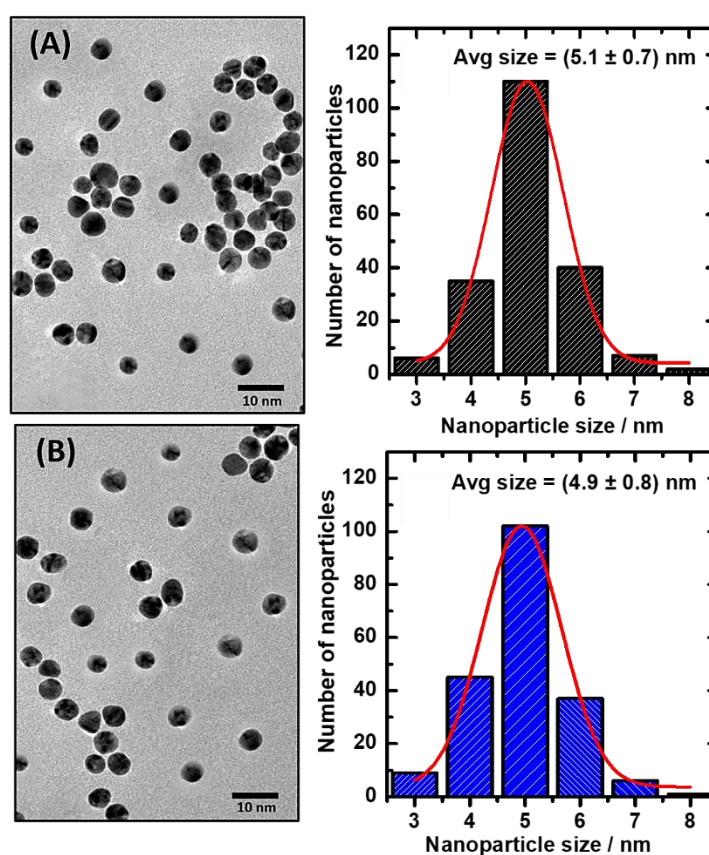
Figure S6. TEM images and size distribution histograms (n = 200) with Gaussian fits for Ag (A) and Au (B) NPs.
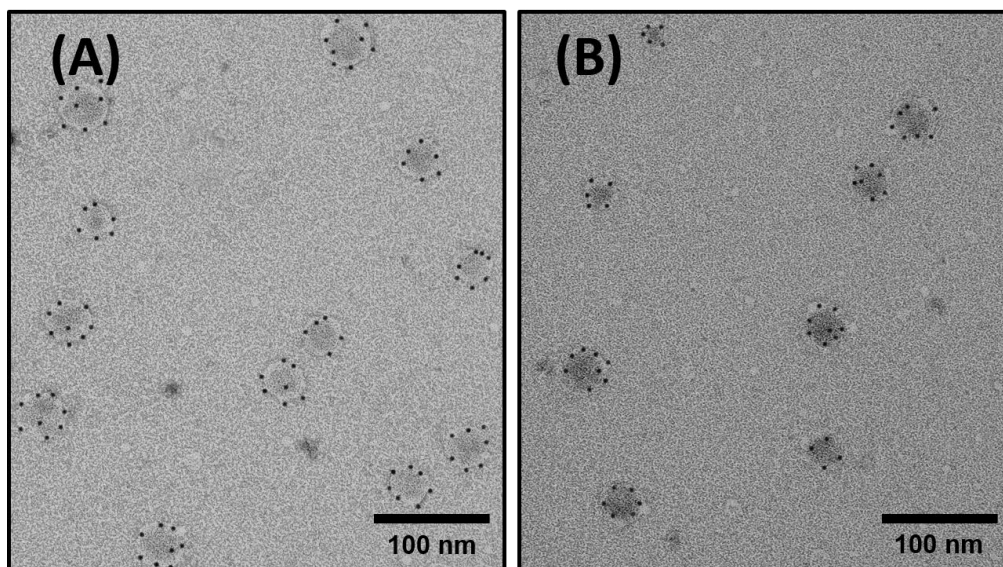
Figure S7. TEM image obtained for (A) CP-Ag and (B) CP-Au conjugates negative stained with uranyl acetate solution.
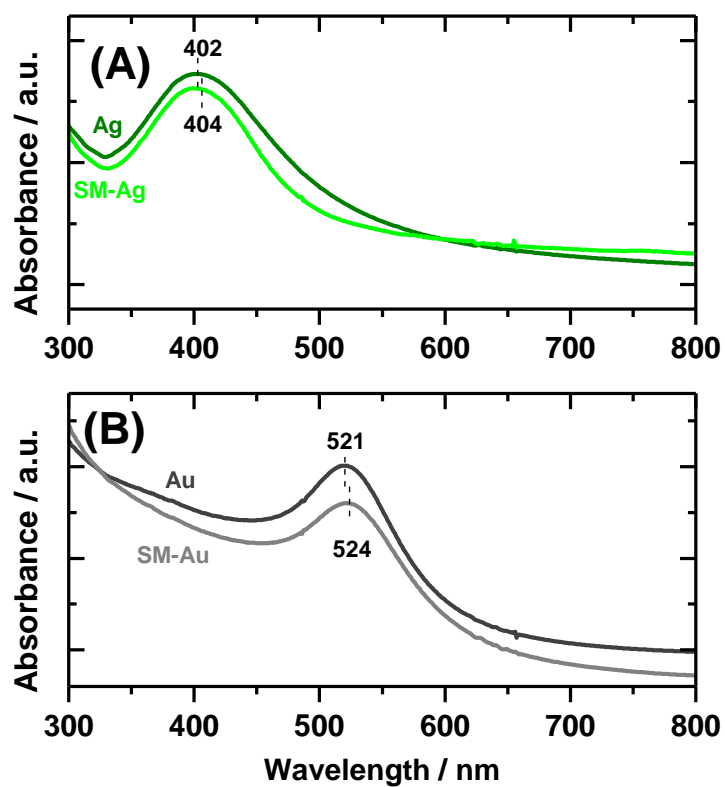
Figure S8. UV-Vis spectra obtained for CP-Ag (A) and CP-Au (B) conjugates. The spectra of Ag (A) and Au (B) NPs are displayed again for comparison purposes. Dashed lines indicate the position of SPR band in all cases.

Figure S9. UV-Vis spectra of (A) Ag and (B) Au NPs as a function of NaCl concentration and solution pH.
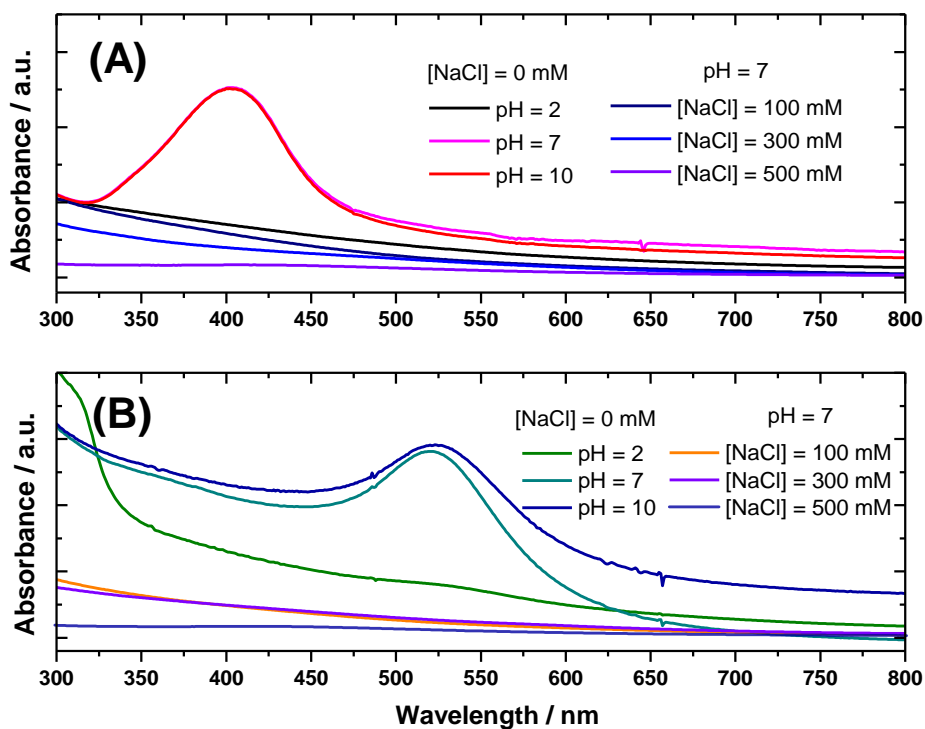
Figure S10. UV-Vis spectra of (A) CP-Ag and (B) CP-Au conjugates as a function of NaCl concentration and solution pH.
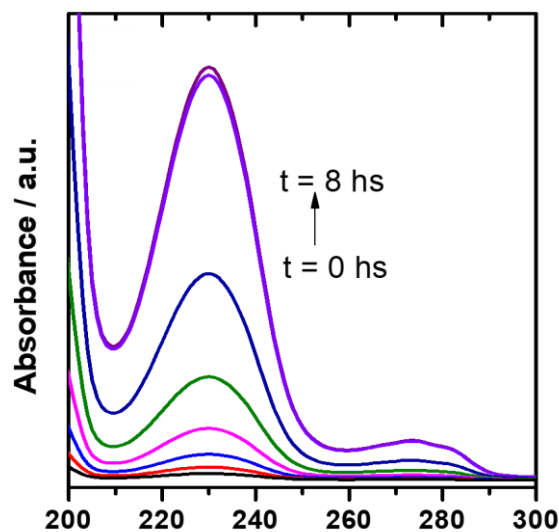
Figure S11. UV-Vis spectra evolution as a function of reaction time in the aqueous phase for interfacial aerobic benzyl alcohol oxidation to benzoic acid catalysed by CS-Au nanoconjugates.

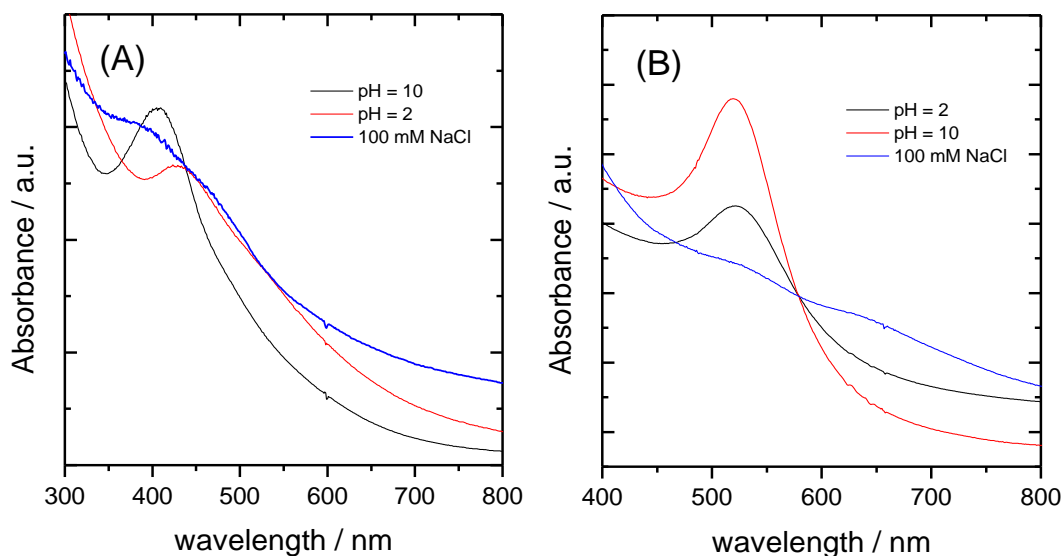**Table S1** Comparison of the catalytic activity[a] of the investigated nanoconjugates with examples from the literature for the Au-catalyzed oxidation of benzyl alcohol.

NP size / nm	Polymer Coating	Alcohol to Au molar ratio	Conv. / %	TOF / h^{-1}	Ref.
3.0	Poly (o-phenylenediamine)	33	95	5.5	1
1.3	Poly(vinylpyrrolidone)	50	99	8	2
2.5	PICB[b]	100	99	4	3
5.0	Poly (o-phenylenediamine)	200	53	18	4
6.7	Poly(1-vinylpirrolidin-2-one-3-carboxylate)	100	83	21	5

a. Reaction in aqueous phase, at room temperature, base: K_2CO_3, oxidant: ambient air.

b. polymer-incarcerated bimetallic nanocluster catalyst

References

1. Han, J.; Liu, Y.; Guo, R. Reactive Template Method to Synthesize Gold Nanoparticles with Controllable Size and Morphology Supported on Shells of Polymer Hollow Microspheres and Their Application for Aerobic Alcohol Oxidation in Water. *Adv. Funct. Mater*. **2009**, *19*, 1112-1117.

2. Tsunoyama, H.; Sakurai, H.; Negishi, Y.; Tsukuda, T. Size-Specific Catalytic Activity of Polymer-Stabilized Gold Nanoclusters for Aerobic Alcohol Oxidation in Water. *J. Am. Chem. Soc*. **2005**, *127*, 9374-9375.

3. Kaizuka, K.; Miyamura, H.; Kobayashi, S. Remarkable Effect of Bimetallic Nanocluster Catalysts for Aerobic Oxidation of Alcohols: Combining Metals Changes the Activities and the Reaction Pathways to Aldehydes/Carboxylic Acids or Esters. *J. Am. Chem. Soc*. **2010**, *132*, 15096-1598.

4. Han, J.; Liu, Y.; Guo, R. Poly(o-phenylenediamine) Submicrosphere-Supported Gold Nanocatalysts: Synthesis, Characterization, and Application in Selective Oxidation of Benzyl Alcohol. *Langmuir* **2009**, **25,** 11054-11060.

5. Yuan, Y.; Yan, N.; Dyson, P. J. pH-Sensitive Gold Nanoparticle Catalysts for the Aerobic Oxidation of Alcohols. *Inorg. Chem*. **2011**, *50*, 11069-11074.

Paper VI

Hydration-Dependent Hierarchical Structures in Block Copolymer–Surfactant Complex Salts

Guilherme A. Ferreira,[†] Lennart Piculell,[‡] and Watson Loh[*,†]

[†]Institute of Chemistry, University of Campinas (UNICAMP), P.O. Box 6154, 13083-970 Campinas, São Paulo, Brazil

[‡]Division of Physical Chemistry, Lund University, P.O. Box 124, S-221 00 Lund, Sweden

Ⓢ *Supporting Information*

ABSTRACT: Block copolymer–surfactant "complex salts" (BCPCS), containing one neutral water-soluble block and one polyion/surfactant-ion block, were prepared from poly-(acrylamide)-*block*-poly(acrylic acid) block copolymers by neutral-izing the acrylate charges with cationic dodecyl- or hexadecyl-trimethylammonium surfactant counterions. The BCPCS were studied in hydrated samples containing 20−99 wt % water (and no additional ions) employing small-angle X-ray scattering (SAXS), dynamic light scattering (DLS), and visual inspection. Selected samples in D_2O were also investigated. The results reveal for the first time, for hydrated samples, the formation of ordered hierarchical structures on both block copolymer and surfactant length scales, analogous to structures that have previously been reported for solvent-free block copolymer–surfactant complexes in the solid or melt. The BCPCS structures do not dissolve but display a finite swelling also in the presence of excess water. The structure on the BCP length scale (lamellar or hexagonal) depends only on the BCP, whereas the structure on the CS length scale (hexagonal or micellar cubic) depends on both the surfactant ion and the water content. The results strongly suggest that the observed concentrated hierarchical structures are the equilibrium states for BCPCS in water, although small aggregates formed reproducibly in the dilute regime have been reported for BCPCS and similar systems, collectively known as complex coacervate core micelles (C3Ms).
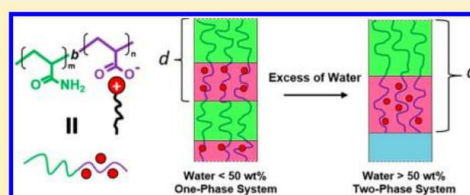
■ INTRODUCTION

A variety of reports on micelles formed through the electrostatic complexation between water-soluble neutral–ionic block copolymers and oppositely charged species in solution have emerged in the past two decades and attracted considerable interest resulting in several investigations on both fundamental and applied aspects of these structures. The studied oppositely charged species include synthetic (co)-polymers with different architectures, biopolymers, such as proteins and DNA, and surfactants.[1−11] The literature contains several terms for such structures, such as polyion complex micelles, PIC micelles,[1,12] complex coacervate core micelles, C3Ms,[2,5] and (inter)polyelectrolyte complexes, PEC.[13,14] For convenience, we will here use the term C3M for the micellar core–shell structures, formed in aqueous solutions, featuring a stabilizer shell consisting of neutral water-soluble units surrounding a water-insoluble (but hydrated) core consisting of complexed oppositely charged units.[5]

Several studies, exclusively limited to dilute systems, have reported C3Ms formed by a charged–neutral diblock copolymer, here abbreviated as BCP, and an oppositely charged polyelectrolyte[15] or an oppositely charged surfactant.[16] There are also C3Ms consisting of two BCP in which the charged blocks are oppositely charged.[17] The commonly encountered history dependence found in some studies[18−23] suggests that C3Ms are not equilibrium structures and that their properties are process-dependent, i.e., depend on their preparation procedure. A variety of works have reported that the average size, micelle shape, colloidal stability, and nature of the core (liquid-, solid-, or crystal-like), among other features, are strongly dependent on experimental conditions such as the mixing protocol, the mixing ratio between the two oppositely charged species, the solution pH, salt concentration, polymer chain length, and so forth.[18−27]

Thus, van der Kooij et al.[18] demonstrated that the polymer chain length and (especially) the salt concentration strongly affect the stability, size, and shape of C3Ms formed from poly(acrylate) (PA) and poly(*N*-methyl-2-vinylpyridinium)-*block*-poly(ethylene oxide) (PM2VP-*b*-PEO). Bronich et al.[19] reported complexes of poly(ethylene oxide)-*block*-poly-(methacrylate) (PEO-*b*-PMA) with single-, double-, and triple-tail surfactants that display a wide range of particle size, shape, and stability upon changes in the block proportions of the copolymer, the surfactant alkyl chain length, mixing ratio, and salt content. Similar results were found for aqueous mixtures of PEO-*b*-PMA copolymer with *N*-alkylpyridinium cations[20] and for poly(*N*-isopropylacrylamide)-*block*-poly-(acrylate), PNIPAM-*b*-PA, C3Ms with dodecyltrimethyl-ammonium bromide (C_{12}TABr).[21]

Voets and co-workers[4] have shown the reversibility of disk-shaped C3Ms formation of aqueous solutions containing poly(acrylamide)-*block*-poly(acrylate) (PAAm-*b*-PA) and poly-(2-methylvinylpyridinium iodide)-*block*-poly(ethylene oxide) (PEO-*b*-P2MVP). Interestingly, long-range order within coacervate domains has been observed in extremely dilute (<1 wt %) triblock copolyelectrolyte complexes with increasing block copolymer concentration although previous studies on similar systems reported the lack of ordered structures in such low concentration range.[22] Recently, Wu et al.[23] discussed the nonequilibrium features of complex formation between poly(ethylene oxide)-*block*-poly(vinylbenzyltrimethyl-ammonium chloride) (PEO-*b*-PVBTMA) and poly(ethylene oxide)-*block*-poly(styrenesulfonate sodium) (PEO-*b*-PSS) in the presence of salt prepared by distinct protocols.

Regardless of the detailed preparation protocol, C3Ms are almost invariably made by mixing two salts; that is, the "original" counterions of the oppositely charged species are included in the resulting mixture. In particular, mixtures containing PAAm-*b*-PA and a cationic surfactant, with their respective counterions, at a charge ratio of 1, have been widely studied in the past decade.[24−27] The aggregates observed displayed an average diameter of 50 nm with cores containing surfactant ion aggregates arranged in a disordered state, showing no long-range order. Our group has recently expanded the studies on PAAm-*b*-PA-cationic surfactant complexes by employing a new methodology based on the complex salt (CS) approach.[28,29] In this case, the acrylate units of the BCP are neutralized by alkyltrimethylammonium cationic surfactant ions using a simple acid−base reaction, resulting in block copolymer complex salts, here abbreviated as BCPCS, free of counterions. Interestingly, the dispersions produced by dispersing such BCPCS in water gave particles with a diameter ca. 300 nm with particle cores displaying a *Pm3n* micellar cubic or hexagonal liquid crystalline structure, depending on the surfactant ion alkyl chain length.

There is a striking absence of studies of *concentrated* mixtures of hydrophilic BCPCS with water. This is surprising since it is well-known that solvent-free melts of analogous block copolymers, that is, block copolymers where one block has amphiphilic molecules associated with the repeat units, typically form hierarchically ordered structures on both the amphiphile and the block copolymer length scales.[30−33]

The first attempts to study polymeric materials with order on multiple length scales were reported by ten Brinke and Ikkala and co-workers, who thoroughly investigated complexes formed by a variety of poly(styrene)-*block*-poly(vinylpyridine) copolymers and different amphiphilic compounds in the melt state. Their work demonstrated that it is possible to obtain several types of hierarchical structures such as lamellar-within-lamellar, lamellar-within-cylindrical, cylindrical-within-lamellar, spherical-within-lamellar, and lamellar-within-spherical ones, depending on the relative sizes of the copolymer blocks and the alkyl chain length of the amphiphile.[34−40]

More recent examples come from complexes of charged−neutral block copolymers and ionic surfactants, where the studied systems are composed of poly(γ-benzyl-L-glutamate)-*block*-poly(L-lysine) with dodecanesulfonic and dodecyl-benzenesulfonic acids,[41] poly(ethylene oxide)-*block*-poly(L-glutamic acid) with primary positively charged alkylamines,[42] and poly(styrene)-*block*-poly(methacrylic acid) with alkyltrimethylammonium surfactants.[43−45] All these systems displayed a structural hierarchy in the solid and melt states,

involving long-range order on the block copolymer length scale and well-defined aggregates on the surfactant length scale within the domains formed by the surfactant-containing blocks.

In view of the structural richness found in the solvent-free BCPCSs or analogous block copolymers, the lack of systematic studies of the structures in the concentrated region of hydrated hydrophilic BCPCS is remarkable. In addition, the finding that the particles obtained by dispersing the BCPCS have properties, like size and core structure, that depend on the method of preparation raises questions about the equilibrium state of the dilute mixtures: are they true solutions or, in fact, nonequilibrium dispersions of an insoluble BCPCS phase? The present report aims to at least partially fill these gaps in our knowledge. One should note that the study of concentrated BCPCS systems is best performed on systems, that as mentioned above, are *free of the "original" counterions*. In mixtures including the latter ions the resulting simple salt would give rise to a screening salt at a concentration that follows the BCPCS concentrations, which would strongly influence the system properties at high concentrations. Therefore, we have here performed structural studies of stoichiometric CS of the block copolymer PAAm-*b*-PA neutralized by dodecyl- or hexadecyltrimethylammonium cationic surfactants over a very wide range of concentrations in water.

Besides the influence of the surfactant chain length, the influence of the (a)symmetry of the block copolymer block lengths has also been investigated. The strategy is based on the previous experiences with systems formed by the corresponding homopolymer CS and water[46,47] and BCPCS in the dilute regime.[28,29] Small-angle X-ray scattering (SAXS) and dynamic light scattering (DLS) together with visual observation of the samples have been used to identify and characterize the phases at different length scales and a full panorama of the block copolymer complex salts behavior in hydrated concentrated systems is presented.

■ EXPERIMENTAL SECTION

Chemicals. The block copolymer PAAm$_{133}$-*b*-PAA$_{49}$, in which the subscript characters refer to the weight-average number of repeating units of each block, was synthesized as described earlier[28] and characterized by proton nuclear magnetic resonance (^{1}H NMR) and gel permeation chromatography (GPC). PAAm$_{422}$-*b*-PAA$_{69}$ was a gift from Rhodia (Cranbury, NJ) and has also been characterized by ^{1}H NMR and GPC. The properties of the block copolymers are presented in Table 1. Dodecyl- and hexadecyltrimethylammonium

Table 1. Weight-Average Molar Mass of the Blocks and Dispersity ($Đ$) of the PAAm-*b*-PAA Block Copolymers Employed in This Work

block copolymer	PAAm (g mol^{-1})	PAA (g mol^{-1})	$Đ^a$
PAAm$_{133}$-*b*-PAA$_{49}$	9415	3500	2.1^b
PAAm$_{432}$-*b*-PAA$_{70}$	30680	5000	1.6^c

^{a}$Đ = M_w/M_n$, as determined by GPC. ^{b}According to this work. ^{c}According to ref 27.

bromide (C$_{12}$TABr and C$_{16}$TABr, respectively), of 99% purity, were purchased from Sigma-Aldrich (USA) as well as the anion-exchange resin Dowex Monosphere 550A (OH) and were used as received. Deionized water with a resistivity greater than 18.2 MΩ cm^{-1}, as obtained by a Milli-Q system, was used in all experiments, unless otherwise stated.

Preparation of BCPCS. All BCPCS were prepared following the general procedure in our laboratories, described earlier.[28,29] Briefly, the hydroxide form of the dodecyl- or hexadecyltrimethylammonium surfactant ion (henceforth abbreviated $C_{12}TA^+$ or $C_{16}TA^+$, respectively) obtained by a previous ion-exchange step, was titrated with 0.5 mol L^{-1}, in acrylate monomer, aqueous solutions of the block copolymers in the acid form until the equivalence point, usually at pH 8.6−8.9. The mixture was then left overnight at 4 °C, and its pH was subsequently adjusted to the equivalence point (when necessary) with the respective block copolymer solution. The BCPCS were freeze-dried to obtain their powders, which were then kept in a desiccator. The final products were named PAAm$_{133}$-b-C$_{12}$TAPA$_{49}$, PAAm$_{133}$-b-C$_{16}$TAPA$_{49}$, PAAm$_{432}$-b-C$_{12}$TAPA$_{70}$, and PAAm$_{432}$-b-C$_{16}$TAPA$_{70}$ according to the surfactant alkyl chain length and the block lengths of the copolymer used in their preparation. The products are henceforth abbreviated as $C_{12}S$, $C_{16}S$, $C_{12}L$, and $C_{16}L$, respectively, where the terms C_{12} and C_{16} denote the surfactant alkyl chain length and S and L refer to the length of the PAAm block in the BCP: S for PAAm$_{133}$ and L for PAAm$_{432}$.

Sample Preparation. Samples in a wide range of concentrations were prepared by weighing the appropriate amounts of BCPCS and water in glass tubes. After mixing with a vortex vibrator, the tubes were flame-sealed. The mixing was continued in a centrifuge at 5000 rpm and 25 °C, where the tubes were turned end over end for 4 weeks. The samples were left to equilibrate at 25 °C for at least one month prior to the measurements. The range of BCPCS concentration varied from 1.0 to 80 wt %. Selected samples were also prepared in D$_2$O (Sigma-Aldrich, USA), following the standard procedure described above.

Techniques. *Small-Angle X-ray Scattering (SAXS).* SAXS measurements were performed to identify the liquid-crystalline structures formed by the BCPCS in water. The measurements were performed at the SAXS1 beamline of the Brazilian Synchrotron Light Laboratory, LNLS, in Campinas, Brazil. The samples were positioned in a cell with two flat mica windows, and a thermal bath connected to the sample holder was used for temperature control. The X-ray wavelength was 1.608 Å, and the sample-to-detector distance was calibrated employing silver behenate. The obtained CCD images were integrated and treated with the software Fit2D[48] to obtain the scattering function $I(q)$, where $q = (4\pi/\lambda) \sin(\Theta/2)$, λ is the wavelength, and Θ is the scattering angle. The relative diffraction peak positions were used to identify the structures formed. The interplanar spacing (d) between two reflecting planes is given by $d = 2\pi/q$, which enables us to calculate the corresponding mean lattice parameter (a).[49] All measurements were performed at 25 °C.

Dynamic Light Scattering (DLS). Dilute phases formed in biphasic systems were analyzed for the presence of nanoparticles by DLS at 25 °C, using a Malvern Nano Zetasizer instrument with a 632.8 nm laser and a detector positioned at 173°. From the apparent diffusion coefficients, the hydrodynamic diameter (D_H) of the nanoparticles were determined using the Stokes−Einstein relationship for translational diffusion.

■ RESULTS

Hydrated BCPCS samples were prepared in the concentration range 1.0−80.0 wt % in H$_2$O. All samples were analyzed by SAXS at different q ranges to cover structures formed at both surfactant and BCP length scales and by visual inspection under normal and crossed polarized light. The SAXS patterns recorded for the various samples are shown in Figures 1−3 for large scattering vectors and in Figure 4 for small scattering vectors. The results indicate that all samples in the concentration range 5−80 wt % featured hierarchically ordered structures on both the BCP and the CS length scales. The most dilute samples (1 wt %) showed liquid-crystalline order on the CS length scale but no long-range order on the BCP length scale.
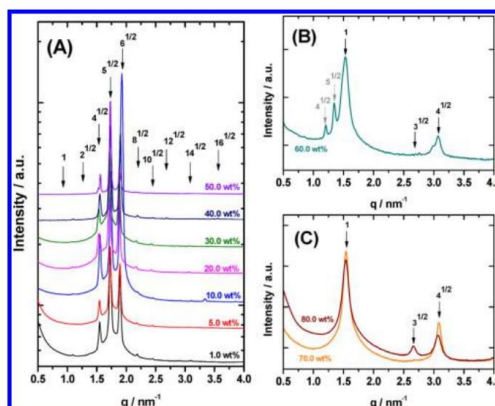

Figure 1. SAXS patterns at high q for $C_{12}S$−H$_2$O mixtures at different $C_{12}S$ concentrations: (A) 1.0−50.0, (B) 60.0, and (C) 70.0−80.0 wt %. In (A) the patterns are shifted along the y-axis for better visualization of the data. In (B) dashed gray arrows or solid black arrows indicate the peak positions of a micellar cubic phase and a hexagonal phase, respectively. In all cases, arrows indicate the expected peak positions, according to the peak ratios (corresponding labels) of the correspondent phase considering the first peak.

Figure 2. SAXS patterns at high q for $C_{12}L$−H$_2$O mixtures at different $C_{12}L$ concentrations: (A) 1.0−40.0, (B) 50.0, and (C) 60.0−80.0 wt %. In (A) the patterns are shifted along the y-axis for better visualization of the data. In (B) dashed gray arrows or solid black arrows indicate the peak positions of a micellar cubic phase and a hexagonal phase, respectively. In all cases, arrows indicate the expected peak positions, according to the peak ratios (corresponding labels) of the correspondent phase considering the first peak.
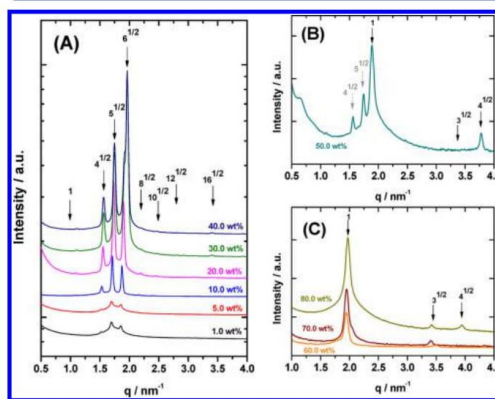
The structures seen on the CS length scale for the C_{12}-based hydrated BCPCS were either micellar cubic $Pm3n$ (for the more dilute samples) with peaks at 1:2$^{1/2}$:4$^{1/2}$: 5$^{1/2}$:8$^{1/2}$, etc., spacing ratios (Figures 1A and 2A) or $p6mm$ hexagonal (at the highest concentrations) with peaks at 1:3$^{1/2}$:4$^{1/2}$ positions (Figures 1C and 2C). A coexistence of the two different structures was observed for both $C_{12}S$ and $C_{12}L$ at intermediate concentrations (Figures 1B and 2B). The results obtained for $C_{16}S$-based BCPCS (Figure 3A and 3B) indicated a hexagonal structure of the long-chain surfactant ions in the entire
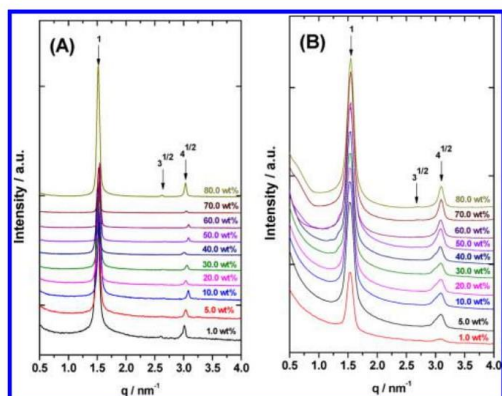
Figure 3. SAXS patterns at high q for (A) $C_{16}S-H_2O$ and (B) $C_{16}L-H_2O$ mixtures at different concentrations. The patterns are shifted along the y-axis for better visualization of the data. In all cases, arrows indicate the expected peak positions, according to the peak ratios (corresponding labels) of the correspondent phase considering the first peak.

concentration range investigated, with the more concentrated samples displaying sharp peaks of a highly ordered liquid-crystalline structure.

Notably, these structures on the CS length scale were the same as those previously found for the corresponding hydrated homopolymer CS[46,47] and dilute BCPCS dispersions.[28,29] The cell parameters calculated for all the surfactant liquid-crystalline structures observed in hydrated BCPCS samples are presented in Table S1. Although there is a slight change with the water content, they fall consistently in a narrow range, as seen before for hydrated homopolymer CS.[50] The only exception is $C_{12}S$ at 60 wt % and above, where the cell parameters displayed slightly higher values, if compared with the correspondent hydrated homopolymer CS.[50] In a previous study, the domain size in the CS length scale was estimated at ca. 100 nm, according to SAXS data, for similar BCPCS in the dispersed state.[28]

The most novel results from this study are the ordered structures on the longer length scale demonstrated for samples in the concentration range 5−80 wt % by the SAXS patterns recorded at small scattering vectors (Figure 4). For the hydrated samples based on the "short" BCP ($C_{12}S$ and $C_{16}S$) peaks at $1:4^{1/2}$ or $1:4^{1/2}:9^{1/2}$ spacing ratios indicate the formation of a lamellar structure. By contrast, the samples containing the "long" BCP ($C_{12}L$ and $C_{16}L$) displayed SAXS patterns at $3^{1/2}:4^{1/2}$ or $1:3^{1/2}:4^{1/2}$ positions, indicating the formation of a hexagonal structure. Their cell parameters are listed in Table S2. Evidently, the long-range structures for the studied systems are independent of water content and surfactant ion chain length but do depend on the (a)symmetry on the BCP length scale. However, the cell parameters (Table S2) decrease with increasing concentration for all BCPCS throughout the range 5−80 wt %.

As a reference, all BCPCS were also studied by SAXS in their freeze-dried state used for preparation of the hydrated samples (see the Experimental Section). The freeze-dried samples were analyzed at small and large scattering vectors in SAXS. Notably, the patterns (Figures S1 and S2) at both

length scales were quite different from those of the hydrated samples displayed above. A set of peaks on the CS length scale were observed for $C_{12}S$ and $C_{16}S$ freeze-dried powders, while for $C_{12}L$ and $C_{16}L$ only one well-defined peak could be seen in the SAXS patterns (Figure S1). On the BCP length scale, no structure was detected (Figure S2).

All hydrated samples were visually observed after the extensive mixing procedure and photographs are presented in Figure S3. Samples prepared in H_2O showed no signs of a separation into two or more phases on a macroscopic length scale, despite the extensive centrifugation cycles. However, the visual observations of several clear samples at high BCPCS concentrations, while samples at lower concentrations were invariably turbid, suggested that the samples at lower concentrations were actually biphasic.

The very similar specific volumes of the BCPCS and H_2O, combined with the high viscosity of the resulting mixtures, may make centrifugation an inefficient method to achieve a macroscopic phase separation. Equilibration could be an issue for such samples and systems out-of-equilibrium may lead to misleading results. This was checked by making selected samples, following the standard procedure of preparation, in D_2O, which has a 10% higher density than H_2O. Indeed, visual observation of the samples in D_2O (Figure S3) revealed macroscopically separated phases at concentrations below ca. 50 wt %.

SAXS patterns obtained at low q on the D_2O samples (Figure S4) confirmed the existence of higher order structures, lamellar for $C_{12}S$ and $C_{16}S$ and hexagonal for $C_{12}L$ and $C_{16}L$, in agreement with the results in H_2O. However, as shown in Figure 5, the cell parameters (listed in Table S3) deviated from those obtained for BCPCS/H_2O, mostly at low concentrations. A series of samples prepared at 5 wt % invariably gave much lower d-spacings in the macroscopically phase-separated samples prepared in D_2O than they did in the uniformly turbid samples in H_2O. Interestingly, the spacings for the phase-separated D_2O samples at 5 wt % were essentially determined solely by the BCP length, following the sequence $C_{12}L \approx C_{16}L > C_{1S}S \approx C_{12}S$. The best agreement between results in D_2O and H_2O was found for $C_{12}S$. The D_2O results for $C_{12}S$ clearly show a plateau of the d-spacing values in the two-phase region below ca. 50 wt % BCPCS, as expected for a biphasic system of only two components at varying mixing ratios. A similar plateau was obtained in H_2O, except for an isolated jump of the d-spacing at 5 wt %. Because the same structures were seen, as evidenced by SAXS, in samples prepared in H_2O and D_2O, we do not assume that changing the solvent would induce significant variation in the behavior of the samples, except for revealing the equilibrium state for some of them (macroscopically separated phases), in this specific study.

Figure 6 shows bar diagrams summarizing the phases and structures in our four BCPCS, as deduced from SAXS results together with the visual appearances (clarity/turbidity, occurrence, or not of macroscopic phase separation in D_2O) of the samples. The upper bar shows the structures on the CS length scale, including regions of phase coexistence for the C_{12}-based systems, whereas the lower bar shows structures on the BCP length scale, together with information about the one- or two-phase regions in mixtures with water. The squared areas at high dilution in the lower bar diagrams reflect the observation that dispersions prepared at 1 wt % in H_2O showed no
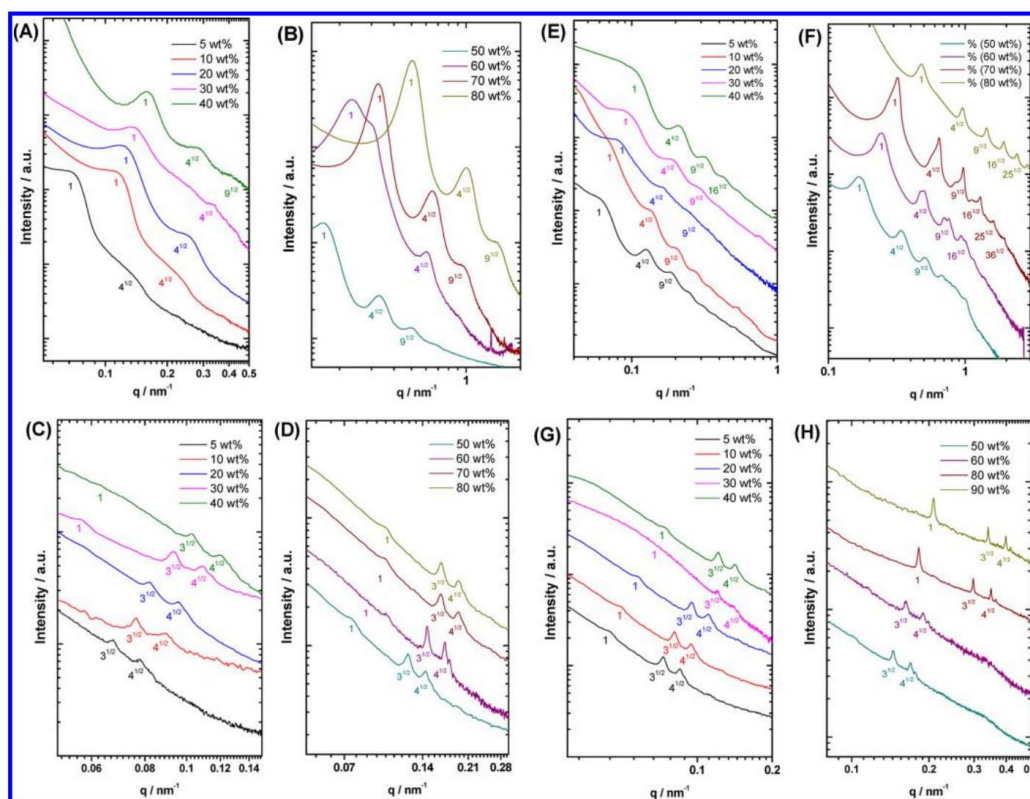
Figure 4. SAXS patterns at low q for BCPCS samples mixed with H_2O: $C_{12}S$ (A, B), $C_{12}L$ (C, D), $C_{16}S$ (E, F), and $C_{16}L$ (G, H). The curves are plotted on a log–log scale and shifted along the y-axis for better visualization of the scattering peaks at small scattering vectors. In all cases, arrows indicate the expected peak positions, according to the peak ratios (corresponding labels) of the correspondent phase considering the first peak.
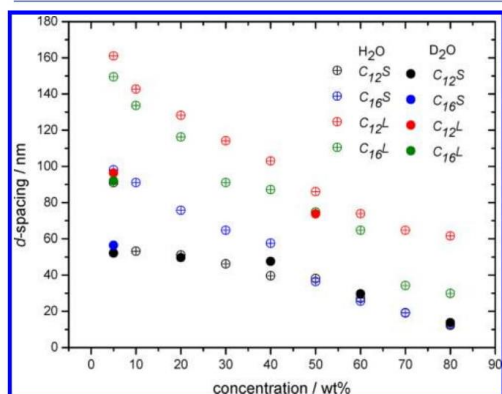

Figure 5. Observed variation of the d-spacing for BCPCS in H_2O and D_2O.

structure on the BCP length scale; note, however, that they did show structure on the CS length scale.

To distinguish nonequilibrium dispersions from thermodynamically stable solutions in dilute mixtures is notoriously difficult. Rather than investigating progressively more dilute mixtures in D_2O for this purpose, we chose to gain additional information about the possible existence of soluble BCPCS aggregates by analyzing by DLS the dilute phases taken out from all macroscopically phase-separated samples in D_2O. These measurements (Table S4) indeed revealed the existence of particles (presumably small aggregates) in the optically clear dilute phases, but these particles had comparatively small hydrodynamic diameter, falling in the ranges 12.2−14.1 nm for the short BCP and 22.3−27.2 nm for the long BCP.

■ DISCUSSION

General Features. In this study, we consistently observed hierarchical ordered structures in hydrated BCPCS. Notably, the structures observed for the freeze-dried precursor materials were very different (Figures S1 and S2). Among the previous studies of solvent-free BCPCS in the literature, those published by Ayoubi and co-workers[43] are the most similar to the present work, in terms of the chemical composition of the BCPCS and the methods by which the complexes were prepared. By a selective complexation between alkyltrimethylammonium
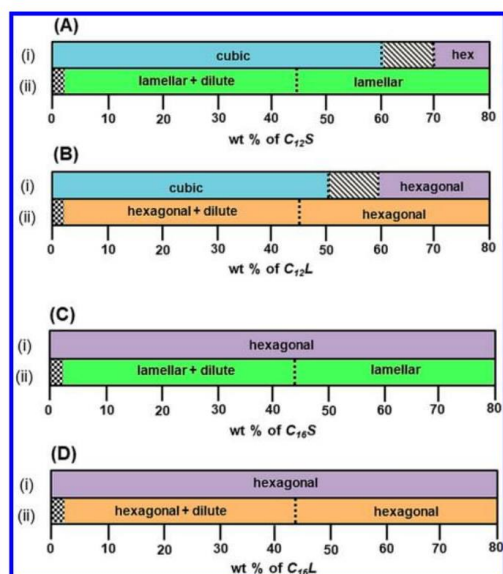
Figure 6. Diagrams of structures observed on CS (i) and BCP (ii) length scales in BCPCS/water mixtures: (A) $C_{12}S$, (B) $C_{12}L$, (C) $C_{16}S$, and (D) $C_{16}L$. The hatched areas in (A) and (B) represent phase coexistences. In all cases, the squared areas represent dispersions in H_2O were no structure was observed at the BCP length scale.

surfactants ions and poly(styrene)-*block*-poly(methacrylic acid) (PS-*b*-PMAA) diblock copolymers, at various grafting densities (number of surfactant ions per carboxylate group of the PMAA block), they prepared complexes consisting of a hydrophobic PS block covalently connected to a strongly amphiphilic CS block.

In the melt state, these complexes displayed simultaneous microphase (between PS and CS blocks) and nanophase (within the CS domains) separation. The authors showed that such separations led to the formation of various structure-within-structure two-scale self-assemblies, similarly to what we have observed for the hydrated samples of this study. The observed structures include spheres-in-spheres in a liquid-like state, spheres-in-spheres in a body-centered-cubic arrangement, spheres-in-hexagonal, spheres-in-lamellar, and hexagonal-in-lamellar structures.[43−45]

Importantly, the structures observed by Ayoubi et al. were achieved by annealing the samples in the melt state at appropriate temperatures and time intervals.[43−45] By contrast, the freeze-drying procedure employed in this study to produce the dry precursor materials, with no subsequent effort made to anneal the samples, cannot be expected to generate equilibrium structures of the respective solvent-free BCPCS. The comparison between our results and those of Ayoubi and co-workers[43−45] therefore strongly suggest that (i) our freeze-dried BCPCS samples do not display equilibrium structures, but (ii) a sufficiently high water content (20 wt % or above) facilitates molecular motion in the BCPCS to the extent that the equilibrium structures at different length scales can develop.

Our study casts new light on the issue of the thermodynamic versus kinetic stability of small BCPCS aggregates or "micelles" in water: At least for the studied combinations of BCP and surfactant ion, and at least in the absence of additional small ions (such as the original counterions emanating from conventional preparation procedures), our studies clearly indicate that dilute mixtures of BCPCS with water are two-phase systems at equilibrium, featuring a water-swollen concentrated phase that is hierarchically ordered on two length scales and a phase of essentially excess water. The latter phase was here found to contain small particles (Table S4), much smaller than the "micelles" typically found by the conventional procedure of mixing polyelectrolyte and surfactant in water, usually in the range 30−200 nm.[16,19−27,51−54] However, the salt-free BCPCS produced and studied here are quite easily dispersed in water by, for example, vortex mixing, as found in this and previous studies from our laboratory.[28,29,55] Thus, more experiments would be required to establish whether the small particles found here in the dilute phase actually represent a true equilibrium solubility.

Structures on the CS Length Scale. BCPCS hydrated samples in the 1.0−80.0 wt % concentration range all displayed liquid crystalline structures on the CS length scale that agree with those previously found for analogous homopolymer CS or BCPCS dispersions.[28,29,46,47,55] The hydrated $C_{16}S$ and $C_{16}L$ systems show a *p6mm* hexagonal structure in the entire studied range of concentrations, whereas hydrated $C_{12}S$ and $C_{12}L$ systems display two structures: a *Pm3n* micellar cubic structure at high water content and a hexagonal *p6mm* structure only at low water contents. The cell parameters of the micellar cubic and hexagonal phases formed in the BCPCS/water mixtures were found to be rather hydration-independent (Table S1). This is again consistent with what has been seen for previously investigated homopolymer CS at varying water contents.[50]

For the C_{12}-based BCPCS/water mixtures, the coexistence of micellar cubic and hexagonal structures was seen to occur at concentrations around 50 or 60 wt % for $C_{12}L$ and $C_{12}S$, respectively. Earlier studies have shown that for hydrated $C_{12}S$-based homopolymer CS, even a very large difference of the polyion length has small effects on the position of cubic/hexagonal phase boundary, which occurs around 60 wt % CS.[47,56]

This observation suggests that the same invariance of the water content at coexistence may hold in the CS domains of our hydrated BCPCS systems. It then follows that the reason that the cubic/hexagonal transition occurs already at 50 wt % $C_{12}L$ is an unequal partitioning of water between the PAAm and the CS domains. In the system with long PAAm chains, the water preferentially partitions to the PAAm domains because of the osmotic stress that the PAAm domains exert on the CS domains. This osmotic stress is lower for the short PAAm chains in $C_{12}S$. As a result, water seems to partition equally between the PAAm and CS domains in the latter system, at least at 60 wt % BCPCS. By increasing the length of the neutral block, one can evidently create CS domains with an enriched surfactant concentration, resulting in phase transitions at lower overall concentrations of the system.

Structures on the BCP Length Scale. Our SAXS results at small scattering vectors (Figure 4 and Figure S4) consistently show a lamellar structure on the BCP length scale for the BCPCS featuring the short PAAm block ($C_{12}S$ and $C_{16}S$), whereas the systems with the long PAAm block ($C_{12}L$ and $C_{16}L$) give hexagonal structures. This variation in

the shape of an amphiphilic aggregate, stabilized by nonionic flexible chains in water, is well documented and understood for classical nonionic surfactants and is explained by the lateral interaction between the neutral "headgroup" chains at the aggregate surfaces which becomes increasingly repulsive with increasing chain length under good solvent conditions.[57] An increasing repulsion between the head groups gives rise to an increasing curvature of the aggregate surface, causing the preferred aggregate shape to switch, in our case from a two-dimensional sheet to a one-dimensional rod. On the next level of organization these aggregates pack into 1-D lamellar and 2D hexagonal structures, respectively.

While consistent structures of our studied BCPCS thus emerge from SAXS patterns, there is overall a considerable scatter in the d-spacings deduced from the patterns (Figure 5) at low q of the samples in H_2O. Such scatter indicates that the systems have not reached their equilibrium states, which could be due to insufficient mixing and/or the fact that the BCPCS are easily dispersed into stable dispersions in the presence of excess water. By contrast, the limited data in D_2O are very consistent (Figure 5), confirming our suspicion that the very small difference in density between H_2O and the BCPCS makes the mixing by centrifugation difficult. This we consider to be the main reason for the scatter in d-spacing observed for all BCPCS at water contents below ca. 50 wt %, where the systems in D_2O revealed a phase separation. For samples at concentrations of 50 wt % and above, a significant scatter was in fact only observed for the $C_{12}L$ and $C_{16}L$ systems; the results for $C_{12}S$ in D_2O and H_2O and for $C_{16}S$ in H_2O all fall on a single smoothly decaying curve. We attribute the difference in behavior for long and short neutral blocks to the difference in structure on the BCP length scale: hexagonal phases are generally much stiffer than lamellar phases and thus more difficult to mix.

From the observed d-spacings in well-equilibrated homogeneous systems we can, in principle, calculate the dimensions of the PAAm and CS domains of the hydrated BCPCS aggregates. A basic assumption in such calculations is that there is a narrow interface between the PAAm and the CS domains ("strong segregation"), which is supported by the observation that the latter domains show the same ordered liquid crystalline phases as the corresponding hydrated homopolymer CS: a significant penetration of PAAm into these ordered structures seems unlikely. However, one also needs additional information about partitioning of water between the two domains. For the CS of the C_{12}-based systems we can actually estimate the water content in the CS domains for the specific compositions where we observe a coexistence between the cubic and hexagonal CS structures; as discussed above, this coexistence suggests that the CS concentration is close to 60 wt %.

The $C_{12}S$ system, where we have consistent SAXS data at concentrations ≥50 wt %, seems most suitable for a detailed analysis. At 60 wt % in H_2O, where we observed cubic/hexagonal coexistence in the CS domain, we found a d-spacing of 27.2 nm (Table S2). From this value and our estimate of 60 wt % CS in the CS domain (see the Supporting Information for calculations) a value of 16.5 nm for the thickness d_{hCS} of a hydrated CS domain in a lamella. This is a quite reasonable thickness as it is comparable to, but shorter than, twice the length of a fully stretched PA_{49} chain, which is 12 nm (the PA chains must necessarily be uniformly distributed in the CS domain; no other counterions are

present to neutralize the surfactant ion aggregates.) The thickness d_{hPAAm} of the hydrated PAAm domain in the structure lamella then becomes 10.7 nm (see the Supporting Information for calculations).

For a lamellar geometry, we can also directly calculate from the composition and the observed d-spacing—without any assumption of the partitioning of the water—the average area A_{chain} taken up by one BCPCS unimer (one block copolymer molecule with its neutralizing surfactant ions) in the lamellar plane (see the Supporting Information for calculations). For 60 wt % $C_{12}S$ in H_2O we obtain A_{chain} = 4.9 nm^2. The numbers A_{chain} = 4.9 nm^2 and d_{hPAAm} = 10.7 nm can be compared with the length of a fully stretched $PAAm_{133}$ chain, which is 33 nm. Clearly, the PAAm chains must be highly coiled and extensively interpenetrating in their domain.

As emphasized above, A_{chain} can be calculated for a homogeneous phase from the known composition and the measured d-spacing without any assumptions of the distributions of the components in the direction perpendicular to the lamellae. To try to estimate also how d_{hCS} varies with water content throughout the lamellar one-phase region, we will make the simple assumption that water partitions equally between the CS and PAAm domains for $C_{12}S$, not only at 60 wt % as concluded above but for *all* investigated concentrations in the range ≥50 wt %. The error introduced by this approximation should not be severe, given that the contribution from water to the total volume decreases with the total concentration. The results from these calculations for $C_{12}S$ in H_2O are shown in Figure 7.
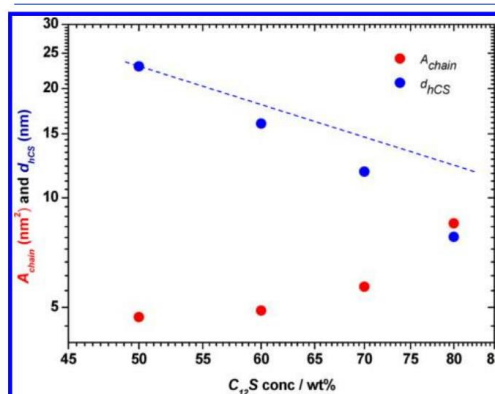

Figure 7. Thickness of a hydrated CS domain in a lamella (d_{hCS}) and the average area (A_{chain}) taken up by one BCPCS unimer as a function of concentration for $C_{12}S$ in H_2O. The dashed line corresponds to the 1/concentration dependence expected for a one-dimensional (constant A_{chain}) deswelling of a lamellar phase (log–log plot).

The results in Figure 7 show that A_{chain} increases significantly as the lamellar structure is compressed on dehydration. The reason, we suggest, is that the PAAm chains respond to the decreasing thickness of their domain by expanding laterally. This in turn results in a decrease of the lamellar spacing d, and the thickness d_{hCS}, which is stronger than the simple 1/concentration dependence that would result from a dehydration at a constant value of A_{chain}.

We will not attempt a similarly detailed analysis of the aggregate dimensions for the $C_{12}L$ and $C_{16}L$ systems because of the significant scatter in the recorded d-spacings. We will restrict ourselves to a single calculation for 50 wt % $C_{12}L$ in D_2O, justified by the overall very consistent results (Figure 7) for samples in this solvent. Recalling that the chosen composition showed a cubic/hexagonal coexistence in the CS domain (Figure 2), we will again assume a concentration of 60 wt % CS in the CS domain. From this assumption and assuming a cylindrical geometry of the hydrated $C_{12}L$ aggregate, we calculate (see the Supporting Information) a value of 26 nm for the radius r_{cyl} of the cylindrical CS domain at the center of the rod-like aggregate. This value is actually quite significantly larger than the length of a fully stretched PA_{69} chain (17 nm). Because the PA chains have to penetrate the entire CS domain, this comparison suggests that the symmetry of the CS aggregate is not strictly cylindrical. Indeed, rods with "flattened" elliptical cross sections have been observed in hexagonal phases of surfactants, especially at high concentrations.[58,59]

The fact that we in our particular systems consistently found the same structure for each of the two BCP, regardless of the water content, should not be taken as evidence that this is always the case. Here we deliberately chose to study BCPCS based on two BCP that differ quite substantially in the PAAm chain length. It seems possible—although this remains to be proven—that one may find some intermediate interval of PAAm chain lengths that would show a structural transition as a result of a changing water content, most likely from a hexagonal phase at high water contents to a lamellar phase at low water contents. One observation above indicates that this would be likely, namely, the flattened noncircular cross-sectional area of the rods in the hexagonal structure suggested by our analysis. In surfactant systems, the latter type of noncylindrical rod-like aggregates are typically found before the structure switches to a lamellar phase at high concentrations.[59]

CONCLUSIONS

Our extensive results on four different salt-free hydrated BCPCS systems over a wide range of compositions show that hierarchical ordered structures on different length scales are formed in such mixtures. The structures found on the BCP length scale were lamellar or hexagonal, depending on the block proportions of the copolymers used to obtain the complexes. On the CS length scale, micellar cubic and hexagonal liquid-crystalline structures were formed. These structures depended not only on the surfactant alkyl chain length but also on the water concentration in CS domain. The latter water concentration could be tuned not only by the overall water content but also by the appropriate choice of the block proportions, since the neutral block absorbs more or less water depending on its length, thereby concentrating the surfactant in the CS domain and so affecting the phase changes. BCPCSs in a solvent thus offer a richer hierarchical phase behavior than analogous BCPCS in the melt. Addition of cosurfactants, such as long-chain alcohols, provides additional tools to vary the structure on the CS length scale, as previously investigated.[29]

Although the formation of small aggregates in the dilute regime has been reported both for BCPCS of the specific chemical composition studied here and for similar systems ("C3Ms" featuring different combinations of oppositely charged macroions in their cores), our detailed analysis of the structures on the BCP level strongly suggests that the hierarchical structures are in fact the equilibrium states for at least salt-free BCPCS in water also in the presence of excess water, where the structures only take up water to a finite swelling limit. However, the true equilibrium repeat distances at the BCP level may be difficult to obtain in practice, due to the mixing issues, as demonstrated in experiments comparing H_2O and D_2O as solvents. The kinetic stability of non-equilibrium states in normal water, which could be either dilute dispersions or ordered structures in concentrated mixtures subjected to extensive mixing, is aided by a typically small difference in density between the BCPCS and H_2O.

■ ASSOCIATED CONTENT

Ⓢ Supporting Information

The Supporting Information is available free of charge on the ACS Publications website at DOI: 10.1021/acs.macro-mol.8b02053.

> Structural parameters for hierarchical structures in BCPCS−H_2O and BCPCS−D_2O systems, SAXS and DLS data for BCPCS−D_2O systems, SAXS data for BCPCS in dry state, and photographs of all investigated samples (PDF)

■ AUTHOR INFORMATION

Corresponding Author
*E-mail: wloh@iqm.unicamp.br (W.L.).

ORCID Ⓞ
Guilherme A. Ferreira: 0000-0002-4932-3666

Notes
The authors declare no competing financial interest.

■ REFERENCES

(1) Harada, H.; Kataoka, K. Formation of Polyion Complex Micelles in an Aqueous Milieu from a Pair of Oppositely Charged Block Copolymers with Poly(ethylene glycol) Segments. *Macromolecules* **1995**, *28*, 5294−5299.

(2) van der Burgh, S.; de Keizer, A.; Cohen Stuart, M. A. Complex Coacervation Core Micelles. Colloidal Stability and Aggregation Mechanism. *Langmuir* **2004**, *20*, 1073−1084.

(3) Cohen Stuart, M. A.; Hofs, B.; Voets, I. K.; de Keizer, A. Assembly of polyelectrolyte-containing block copolymers in aqueous media. *Curr. Opin. Colloid Interface Sci.* **2005**, *10*, 30−36.

(4) Voets, I. K.; de Keizer, A.; de Waard, P.; Frederik, P. M.; Bomans, P. H.H.; Schmalz, H.; Walther, A.; King, S. M.; Leermakers, F. A. M.; Cohen Stuart, M. A. Double-Faced Micelles from Water-Soluble Polymers. *Angew. Chem., Int. Ed.* **2006**, *45*, 6673−6676.

(5) Voets, I. K.; de Keizer, A.; Cohen Stuart, M. A. Complex coacervate core micelles. *Adv. Colloid Interface Sci.* **2009**, *147−148*, 300−318.

(6) Langevin, D. Complexation of oppositely charged polyelectrolytes and surfactants in aqueous solutions. A review. *Adv. Colloid Interface Sci.* **2009**, *147−148*, 170−77.

(7) Kizilay, E.; Kayitmazer, A. B.; Dubin, P. L. Complexation and coacervation of polyelectrolytes with oppositely charged colloids. *Adv. Colloid Interface Sci.* **2011**, *167*, 24−37.

(8) van der Gucht, J.; Spruijt, E.; Lemmers, M.; Cohen Stuart, M. A. Polyelectrolyte complexes: Bulk phases and colloidal systems. *J. Colloid Interface Sci.* **2011**, *361*, 407−422.

(9) Piculell, L. Understanding and Exploiting the Phase Behavior of Mixtures of Oppositely Charged Polymers and Surfactants in Water. *Langmuir* **2013**, *29*, 10313−10329.

(10) Kayitmazer, A. B. Thermodynamics of complex coacervation. *Adv. Colloid Interface Sci.* **2017**, *239*, 169−177.

(11) Ferreira, G. A.; Loh, W. Liquid crystalline nanoparticles formed by surfactant-polyelectrolyte complexes. *Curr. Opin. Colloid Interface Sci.* **2017**, *32*, 11−22.

(12) Harada, H.; Kataoka, K. Polyion complex micelle formation from double-hydrophilic block copolymers composed of charged and non-charged segments in aqueous media. *Polym. J.* **2018**, *50*, 95−100.

(13) Wang, Q.; Schlenoff, J. B. The polyelectrolyte complex/coacervate continuum. *Macromolecules* **2014**, *47*, 3108−3116.

(14) Li, L.; Srivastava, S.; Andreev, M.; Marciel, A. B.; de Pablo, J. J.; Tirrell, M. Phase Behavior and Salt Partitioning in Polyelectrolyte Complex Coacervates. *Macromolecules* **2018**, *51*, 2988−2995.

(15) Gohy, J.-F.; Varshney, S. K.; Antoun, S.; Jérôme, R. Water-Soluble Complexes Formed by Sodium Poly(4-styrenesulfonate) and a Poly(2-vinylpyridinium)-*block*-poly(ethylene oxide) Copolymer. *Macromolecules* **2000**, *33*, 9298−9305.

(16) Uchman, M.; Štěpánek, M.; Prévost, S.; Angelov, B.; Bednár, J.; Appavou, M.-S.; Gradzielski, M.; Procházka, K. Coassembly of Poly(ethylene oxide)-*block*-poly(methacrylic acid) and N-Dodecylpyridinium Chloride in Aqueous Solutions Leading to Ordered Micellar Assemblies within Copolymer Aggregates. *Macromolecules* **2012**, *45*, 6471−6480.

(17) Voets, I. K.; de Keizer, A.; Cohen Stuart, M. A.; de Waard, P. Core and Corona Structure of Mixed Polymeric Micelles. *Macromolecules* **2006**, *39*, 5952−5955.

(18) van der Kooij; Spruijt, E.; Voets, I. K.; Fokkink, R.; Cohen Stuart, M. A.; van der Gucht, J. On the Stability and Morphology of Complex Coacervate Core Micelles: From Spherical to Wormlike Micelles. *Langmuir* **2012**, *28*, 14180−14191.

(19) Bronich, T. K.; Popov, A. M.; Eisenberg, A.; Kabanov, V. A.; Kabanov, A. V. Effects of Block Length and Structure of Surfactant on Self-Assembly and Solution Behavior of Block Ionomer Complexes. *Langmuir* **2000**, *16*, 481−489.

(20) Bronich, T. K.; Kabanov, A. V.; Kabanov, V. A.; Yu, K.; Eisenberg, A. Soluble Complexes from Poly(ethylene oxide)-*block*-poly(methacrylate) Anions and N-Alkylpyridinium Cations. *Macromolecules* **1997**, *30*, 3519−3525.

(21) Annaka, M.; Morishita, K.; Okabe, S. Electrostatic Self-Assembly of Neutral and Polyelectrolyte Block Copolymers and Oppositely Charged Surfactant. *J. Phys. Chem. B* **2007**, *111*, 11700−11707.

(22) Srivastava, S.; Andreev, M.; Levi, A. E.; Goldfeld, D. J.; Heller, W. T.; Prabhu, V. M.; de Pablo, J. J.; Tirrell, M. V. Gel phase formation in dilute triblock copolyelectrolyte complexes. *Nat. Commun.* **2017**, *8*, 14131−14139.

(23) Wu, H.; Ting, J. F.; Werba, O.; Meng, S.; Tirrell, M. V. Non-equilibrium phenomena and kinetic pathways in self-assembled polyelectrolyte complexes. *J. Chem. Phys.* **2018**, *149*, 163330−163340.

(24) Berret, J. F.; Cristobal, G.; Hervé, P.; Grillo, I. Structure of colloidal complexes obtained from neutral/poly-electrolyte copolymers and oppositely charged surfactants. *Eur. Phys. J. E: Soft Matter Biol. Phys.* **2002**, *9*, 301−311.

(25) Berret, J. F.; Hervé, P.; Aguerre-Chariol, O.; Oberdisse, J. Colloidal complexes obtained from charged block copolymers and surfactants: A comparison between small-angle neutron scattering, Cryo-TEM, and simulations. *J. Phys. Chem. B* **2003**, *107*, 8111−8118.

(26) Hervé, P.; Destarac, M.; Berret, J.-F.; Lal, J.; Oberdisse, J.; Grillo, I. Novel Core-shell Structure for Colloids Made of Neutral/Polyelectrolyte Diblock Copolymers and Oppositely Charged Surfactants. *Europhys. Lett.* **2002**, *58*, 912−918.

(27) Berret, J.-F.; Vigolo, B.; Eng, R.; Hervé, P.; Grillo, I.; Yang, L. Electrostatic Self-assembly of Oppositely Charged Copolymers and Surfactants: a Light, Neutron, and X-ray Scattering Study. *Macromolecules* **2004**, *37*, 4922−4930.

(28) Vitorazi, L.; Berret, J.-F.; Loh, W. Self-Assembly of Complex Salts of Cationic Surfactants and Anionic−Neutral Block Copolymers. Dispersions with Liquid-Crystalline Internal Structure. *Langmuir* **2013**, *29*, 14024−14033.

(29) Ferreira, G. A.; Loh, W. Addition of n-Alcohols Induces a Variety of Liquid-Crystalline Structures in Surfactant-Rich Cores of Dispersed Block Copolymer/Surfactant Nanoparticles. *ACS Omega* **2016**, *1*, 1104−1113.

(30) Ruokolainen, J.; Mäkinen, R.; Torkkeli, M.; Mäkelä, T.; Serimaa, R.; ten Brinke, G.; Ikkala, O. Switching Supramolecular Polymeric Materials with Multiple Length Scales. *Science* **1998**, *280*, 557−560.

(31) Ruokolainen, J.; ten Brinke, G.; Ikkala, O. Supramolecular Polymeric Materials with Hierarchical Structure-Within-Structure Morphologies. *Adv. Mater.* **1999**, *11*, 777−780.

(32) Ikkala, O.; ten Brinke, G. Functional Materials Based on Self-Assembly of Polymeric Supramolecules. *Science* **2002**, *295*, 2407−2409.

(33) Ikkala, O.; ten Brinke, G. Hierarchical self-assembly in polymeric complexes: Towards functional materials. *Chem. Commun.* **2004**, *0*, 2131−2137.

(34) Ruokolainen, J.; Saariaho, M.; Ikkala, O.; ten Brinke, G.; Thomas, E.; Torkkeli, M.; Serimaa, R. Supramolecular Routes to Hierarchical Structures: Comb-Coil Diblock Copolymers Organized With Two Length Scales. *Macromolecules* **1999**, *32*, 1152−1158.

(35) Polushkin, E.; Alberda van Ekenstein, G. O. R.; Knaapila, M.; Ruokolainen, J.; Torkkeli, M.; Serimaa, R.; Bras, W.; Dolbnya, I.; Ikkala, O.; ten Brinke, G. Intermediate Segregation Type Chain Length Dependence of the Long Period of Lamellar Microdomain Structures of Supramolecular Comb-Coil Diblocks. *Macromolecules* **2001**, *34*, 4917−4922.

(36) Kosonen, H.; Valkama, S.; Hartikainen, J.; Eerikäinen, H.; Torkkeli, M.; Jokela, K.; Serimaa, R.; Sundholm, F.; ten Brinke, G.; Ikkala, O. Mesomorphic structure of poly(styrene)-*block*-poly(4-vinylpyridine) with oligo(ethylene oxide)sulfonic acid side chains as a model for molecularly reinforced polymer electrolyte. *Macromolecules* **2002**, *35*, 10149−10154.

(37) Valkama, S.; Ruotsalainen, T.; Kosonen, H.; Ruokolainen, J.; Torkkeli, M.; Serimaa, R.; ten Brinke, G.; Ikkala, O. Amphiphiles coordinated to block copolymer as a template for mesoporous materials. *Macromolecules* **2003**, *36*, 3986−3991.

(38) Bondzic, S.; de Wit, J.; Polushkin, E.; Schouten, A. J.; ten Brinke, G.; Ruokolainen, J.; Ikkala, O.; Dolbnya, I.; Bras, W. Self-Assembly of Supramolecules Consisting of Octyl Gallate Hydrogen Bonded to Poly(isoprene)-*block*-poly(vinylpyridine) Diblock Copolymers. *Macromolecules* **2004**, *37*, 9517−9524.

(39) Valkama, S.; Ruotsalainen, T.; Nykänen, A.; Laiho, A.; Kosonen, H.; ten Brinke, G.; Ikkala, O.; Ruokolainen, J. Self-Assembled Structures in Diblock Copolymers with Hydrogen-Bonded Amphiphilic Plasticizing Compounds. *Macromolecules* **2006**, *39*, 9327−9336.

(40) Ruotsalainen, T.; Turku, J.; Hiekkataipale, P.; Vainio, U.; Serimaa, R.; ten Brinke, G.; Harlin, A.; Ruokolainen, J.; Ikkala, O. Tailoring of the hierarchical structure within electrospun fibers due to supramolecular comb-coil block copolymers: polystyrene-*block*-poly-(4-vinylpyridine) plasticized by hydrogen bonded pentadecylphenol. *Soft Matter* **2007**, *3*, 978−985.

(41) Hanski, S.; Houbenov, N.; Ruokolainen, J.; Chondronicola, D.; Iatrou, H.; Hadjichristidis, N.; Ikkala, O. Hierarchical Ionic Self-Assembly of Rod-Comb Block Copolypeptide-Surfactant Complexes. *Biomacromolecules* **2006**, *7*, 3379−3384.

(42) Hammond, M. R.; Klok, H. A.; Mezzenga, R. Self-Organization on Multiple Length Scales in Hairy-Rod−Coil Block Copolymer Supramolecular Complexes. *Macromol. Rapid Commun.* **2008**, *29*, 299−303.

(43) Ayoubi, M. A.; Zhu, K.; Nyström, B.; Almdal, K.; Olsson, U.; Piculell, L. Micro- and nanophase separations in hierarchical self-assembly of strongly amphiphilic block copolymer-based ionic supramolecules. *Soft Matter* **2013**, *9*, 1540−1555.

(44) Ayoubi, M. A.; Almdal, K.; Zhu, K.; Nyström, B.; Olsson, U.; Piculell, L. Lamellar Microdomains of Block Copolymer-Based Ionic Supramolecules Exhibiting a Hierarchical Self-Assembly. *Macromolecules* **2014**, *47*, 3428−3435.

(45) Ayoubi, M. A.; Almdal, K.; Zhu, K.; Nyström, B.; Olsson, U.; Piculell, L. Self-Assembly of Block Copolymer-Based Ionic Supra-molecules Based Upon Multi-Tail Amphiphiles. *RSC Adv.* **2015**, *5*, 31091−31103.

(46) Svensson, A.; Piculell, L.; Cabane, B.; Ilekti, P. A New Approach to the Phase Behavior of Oppositely Charged Polymers and Surfactants. *J. Phys. Chem. B* **2002**, *106*, 1013−1018.

(47) Svensson, A.; Norrman, J.; Piculell, L. Phase Behavior of Polyion-Surfactant Ion Complex Salts: Effects of Surfactant Chain Length and Polyion Length. *J. Phys. Chem. B* **2006**, *110*, 10332−10340.

(48) Hammersley, A. P. *Scientific Software FIT2D*; ESRF Synchrotron: France, 2009.

(49) Glatter, O.; Kratky, O. *Small Angle X-ray Scattering*; Academic Press: 1982.

(50) Li, J.; Gustavsson, C.; Piculell, L. Time- and Space-Resolved SAXS Experiments Inform on Phase Transition Kinetics in Hydrated, Liquid-Crystalline Films of Polyion−Surfactant Ion "Complex Salts. *Langmuir* **2016**, *32*, 5102−5110.

(51) Uchman, M.; Gradzielski, M.; Angelov, B.; Tošner, Z.; Oh, J.; Chang, T.; Štěpánek, M.; Procházka, K. Thermodynamic and Kinetic Aspects of Coassembly of PEO−PMAA Block Copolymer and DPCl Surfactants into Ordered Nanoparticles in Aqueous Solutions Studied by ITC, NMR, and Time-Resolved SAXS Techniques. *Macromolecules* **2013**, *46*, 2172−2181.

(52) Štěpánek, M.; Matějíček, P.; Procházka, K.; Filippov, S. K.; Angelov, B.; Slouf, M.; Mountrichas, G.; Pispas, S. Polyelectrolyte−Surfactant Complexes Formed by Poly[3,5-bis-(trimethylammoniummethyl)4-hydroxystyrene iodide]-*block*-poly-(ethylene oxide) and Sodium Dodecyl Sulfate in Aqueous Solutions. *Langmuir* **2011**, *27*, 5275−5281.

(53) Ram-On, M.; Cohen, Y.; Talmon, Y. Effect of Polyelectrolyte Stiffness and Solution pH on the Nanostructure of Complexes Formed by Cationic Amphiphiles and Negatively Charged Poly-electrolytes. *J. Phys. Chem. B* **2016**, *120*, 5907−915.

(54) Fegyver, E.; Mészáros, R. The impact of nonionic surfactant additives on the nonequilibrium association between oppositely charged polyelectrolytes and ionic surfactants. *Soft Matter* **2014**, *10*, 1953−962.

(55) Carneiro, N. M.; Percebom, A. M.; Loh, W. Quest for Thermoresponsive Block Copolymer Nanoparticles with Liquid−Crystalline Surfactant Cores. *ACS Omega* **2017**, *2*, 5518−5528.

(56) dos Santos, S.; Gustavsson, C.; Gudmundsson, C.; Linse, P.; Piculell, L. When Do Water-Insoluble Polyion−Surfactant Ion Complex Salts "Redissolve" by Added Excess Surfactant? *Langmuir* **2011**, *27*, 592−603.

(57) Shick, M. J. *Nonionic Surfactants: Physical Chemistry*; Surfactant Series; Marcel Dekker: New York, 1967; Vol. *1*.

(58) Hagslätt, H.; Söderman, O.; Jönsson, B. The structure of intermediate ribbon phases in surfactant systems. *Liq. Cryst.* **1992**, *12*, 667−688.

(59) Holmes, M. C. Intermediate phases of surfactant-water mixtures. *Curr. Opin. Colloid Interface Sci.* **1998**, *3*, 485−492.

HYDRATION-DEPENDENT HIERARCHICAL STRUCTURES IN BLOCK COPOLYMER-SURFACTANT COMPLEX SALTS

Supplementary Information

Guilherme A. Ferreira†, Lennart Piculell‡, and Watson Loh*†

† Institute of Chemistry, University of Campinas (UNICAMP), P.O. Box 6154, 13083-970 Campinas, São Paulo, Brazil
‡ Division of Physical Chemistry, Lund University, P.O. Box 124, S-221 00 Lund, Sweden
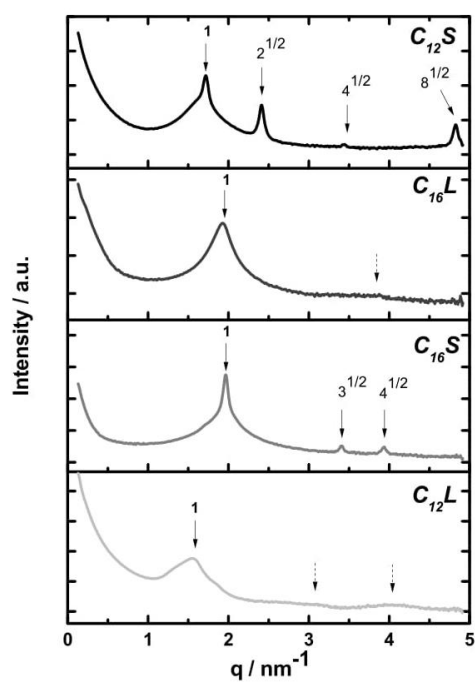
*E-mail: wloh@iqm.unicamp.br (W.L.)

Figure S1. SAXS patterns for the four different BCPCSs in the freeze-dried state. Peaks were assigned as being, probably, for a micellar $Im3m$ cubic phase (a = 3.6 nm) and a hexagonal structure (a = 3.6 nm) for $C_{12}S$ and $C_{16}S$, respectively. For $C_{12}L$ and $C_{16}L$, only a single well-defined peak, marked with solid arrows, could be seen in each of the SAXS patterns. Additional bumps could also be observed (dashed arrows) corresponding to no identified structure
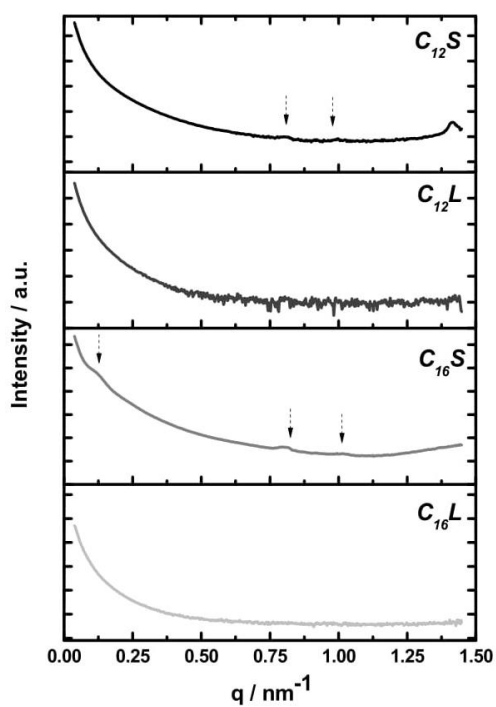
Figure S2. SAXS patterns for the BCPCSs in the freeze-dried state recorded at small scattering vectors. In all cases, no sharp scattering peaks were observed, probably indicating the absence of any highly ordered structure in such a length scale. However, for $C_{12}S$ and $C_{16}S$, some broad peaks (marked with dashed arrows) are apparent. Those peaks could not be assigned to any specific structure.
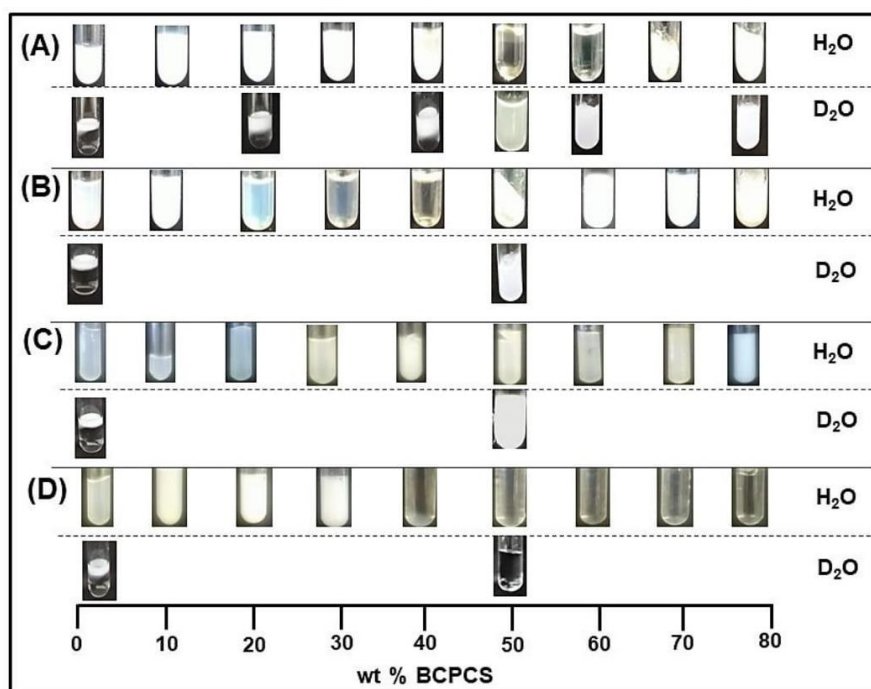
Figure S3. Photographs of the BCPCS/H$_2$O and BCPCS/D$_2$O mixtures at different concentrations for: (A) $C_{12}S$. (B) $C_{12}L$. (C) $C_{16}S$. (D) $C_{16}L$.
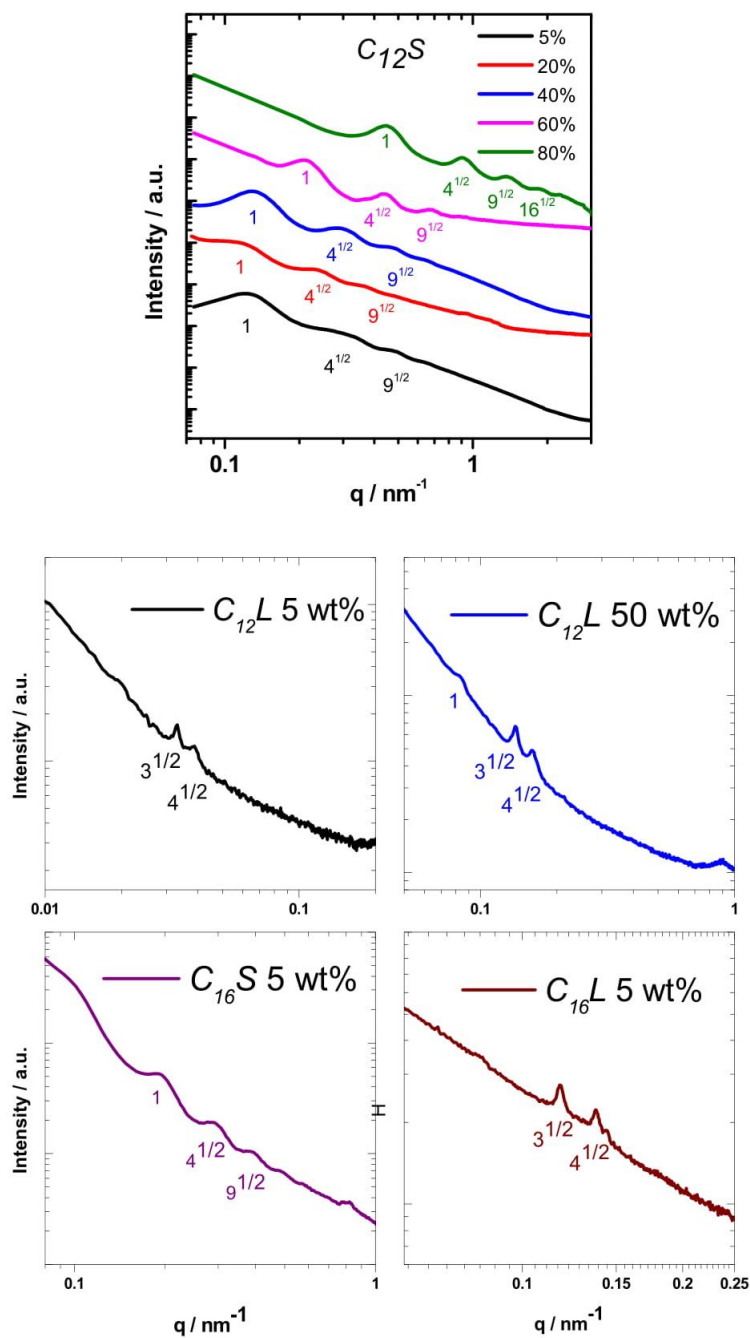
Figure. S4. SAXS patterns for BCPCS/D$_2$O samples at small angle vectors.

Table S1. Cell parameters (a) for the surfactant liquid-crystalline phases formed on the CS length scale in BCPCS/H_2O mixtures.

BCPCS	Concentration / wt%	Surfactant Structure	a / nm
$C_{12}S$	1.0	Cubic	8.40
	5.0	Cubic	8.44
	10.0	Cubic	8.42
	20.0	Cubic	8.41
	30.0	Cubic	8.40
	40.0	Cubic	8.43
	50.0	Cubic	8.44
	60.0	Cubic + Hexagonal	9.80; 4.40
	70.0	Hexagonal	4.40
	80.0	Hexagonal	4.40
$C_{12}L$	1.0	Cubic	8.43
	5.0	Cubic	8.44
	10.0	Cubic	8.44
	20.0	Cubic	8.44
	30.0	Cubic + Hexagonal	8.44; 3.70
	40.0	Cubic + Hexagonal	8.45; 3.70
	50.0	Cubic + Hexagonal	8.40; 3.80
	60.0	Hexagonal	3.80
	70.0	Hexagonal	3.70
	80.0	Hexagonal	3.60
$C_{16}S$	1.0	Hexagonal	4.40
	5.0	Hexagonal	4.42
	10.0	Hexagonal	4.41
	20.0	Hexagonal	4.42
	30.0	Hexagonal	4.39
	40.0	Hexagonal	4.40
	50.0	Hexagonal	4.42
	60.0	Hexagonal	4.40
	70.0	Hexagonal	4.38
	80.0	Hexagonal	4.41
$C_{16}L$	1.0	Hexagonal	4.40
	5.0	Hexagonal	4.40
	10.0	Hexagonal	4.42
	20.0	Hexagonal	4.43
	30.0	Hexagonal	4.42
	40.0	Hexagonal	4.41
	50.0	Hexagonal	4.39
	60.0	Hexagonal	4.38
	70.0	Hexagonal	4.42
	80.0	Hexagonal	4.40

Table S2. Cell parameters for the structures observed on the BCP length scale in BCPCS/H$_2$O mixtures.

BCPCS	Conc. / wt%	BCP Structure	d / nm[a]	a / nm[b]
$C_{12}S$	1.0	Lamellar	-	-
	5.0		91.0	-
	10.0		53.2	-
	20.0		51.1	-
	30.0		46.2	-
	40.0		39.7	-
	50.0		38.1	-
	60.0		27.2	-
	70.0		19.1	-
	80.0		12.3	-
$C_{12}L$	1.0	Hexagonal	-	-
	5.0		161.0	185.9
	10.0		142.7	164.8
	20.0		128.2	148.0
	30.0		114.2	131.8
	40.0		103.0	118.9
	50.0		86.0	99.3
	60.0		73.9	85.3
	70.0		64.7	74.8
	80.0		61.6	71.1
$C_{16}S$	1.0	Lamellar	-	-
	5.0		98.1	-
	10.0		91.0	-
	20.0		75.7	-
	30.0		64.7	-
	40.0		57.6	-
	50.0		36.5	-
	60.0		25.6	-
	70.0		19.3	-
	80.0		12.9	-
$C_{16}L$	1.0	Hexagonal	-	-
	5.0		149.5	172.7
	10.0		133.6	154.3
	20.0		116.3	134.3
	30.0		91.0	105.1
	40.0		87.2	100.7
	50.0		74.8	86.3
	60.0		64.7	74.8
	70.0		34.3	39.6
	80.0		29.9	34.5

a – d is the interplanar spacing for any structure and the characteristic cell parameter of a lamellar structure.   b – a is mean distance between two adjacent cylinders in a hexagonal structure.

Table S3. Cell parameters for the structures observed on the BCP length scale in BCPCS/D$_2$O mixtures.

BCPCS	Conc. / wt%	BCP Structure	d / nm[a]	a / nm[b]
$C_{12}S$	5.0	Lamellar	52.2	-
	20.0		49.7	-
	40.0		47.6	-
	60.0		29.7	-
	80.0		13.7	
$C_{12}L$	5.0	Hexagonal	96.4	111.2
	50.0		73.8	85.3
$C_{16}S$	5.0	Lamellar	56.5	-
$C_{16}L$	5.0	Hexagonal	91.9	106.2

a – d is the interplanar spacing for any structure and the characteristic cell parameter of a lamellar structure. b – a is mean distance between two adjacent cylinders in a hexagonal structure.

Table S4. **Hydrodynamic diameters (D_H) for particles in phase-separated dilute phases in D$_2$O measured by DLS (avg. ± SD).**

BCPCS	Conc. / wt%	D_H / nm
$C_{12}S$	5.0	12.2 ± 5
	20.0	12.9 ± 4
	40.0	13.6 ± 5
	60.0	14.4 ± 7
	80.0	14.1 ± 5
$C_{12}L$	5.0	22.3 ± 8
	50.0	27.2 ± 6
$C_{16}S$	5.0	13.1 ± 5
$C_{16}L$	5.0	23.4 ± 5

Calculations of the BCP lamellar phase dimensions[1,2]

For a uniform lamellar structure, we have that the thickness of the hydrated CS domain, d_{hCS}, is proportional to the d-spacing according to the relation:

$$d_{hCS} = \varphi_{hCS}.d \qquad (1)$$

where φ_{hCS} is the volume fraction of the hydrated CS domain in the structure. The thickness d_{hPAAm} of the hydrated PAAm domain is then obtained as:

$$d_{hPAAm} = d - d_{hCS} \qquad (2)$$

Let A_{chain} be the average area in the plane of a lamella occupied by one BCPCS unimer (one diblock copolymer chain with its associated surfactant counterions), and N be the number of BCPCS unimers per unit volume of the system, which is assumed to be homogeneous and lamellar. The volume element $A_{chain} \times d$ contains on average two BCPCS unimers in the lamellar bilayer, that is,

$$N = 2/A_{chain}d \qquad (3)$$

or

$$A_{chain} = 2/Nd \qquad (4)$$

In the calculations, we have used the molar mass of ca. 21240 for the $C_{12}S$ unimer and a partial specific volume of 1 cm³/g for the BCPCS unimer and for H_2O.

Calculations of the BCP hexagonal phase dimensions[1,2]

The values for cylinder radius (r_{cyl}) for a homogeneous hexagonal phase can be calculated based on the d-values according to:

$$r_{cyl} = \sqrt{\frac{\varphi_{hCS}2d^2}{\sqrt{3}\pi}} \qquad (5)$$

References

1. Bernardes, J. S.; Norrman, J.; Piculell, L.; Loh, W. Complex Polyion-Surfactant Ions Salts in Equilibrium in Water: Changing Aggregate Shape and Size by Adding Oil. *J. Phys. Chem. B* **2006**, *110*, 23433-442.

2. Svensson, A.; Norrman, J.; Piculell, L. Phase Behavior of Polyion-Surfactant Ion Complex Salts: Effects of Surfactant Chain Length and Polyion Length. *J. Phys. Chem. B* **2006**, *110*, 10332-10340.

Copyright Clearance Center

RightsLink®

Home   Account Info   Help   ✉

ACS Publications
Most Trusted. Most Cited. Most Read.

Title: Hydration-Dependent Hierarchical Structures in Block Copolymer–Surfactant Complex Salts

Author: Guilherme A. Ferreira, Lennart Piculell, Watson Loh

Publication: Macromolecules

Publisher: American Chemical Society

Date: Dec 1, 2018

Copyright © 2018, American Chemical Society

Logged in as:
Guilherme Ferreira
Account #:
3001166781

LOGOUT

PERMISSION/LICENSE IS GRANTED FOR YOUR ORDER AT NO CHARGE

BACK   CLOSE WINDOW

Se a Tese ou Dissertação for reproduzida em formato alternativo (com artigos anexados), este documento, preenchido e assinado, deve ser inserido no trabalho como Anexo.
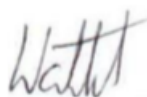
DECLARAÇÃO

As cópias dos documentos de minha autoria ou de minha coautoria, já publicados ou submetidos para publicação em revistas científicas ou anais de congressos sujeitos a arbitragem, que constam da minha Dissertação/Tese de Mestrado/Doutorado, intitulada "Block copolymer-surfactant complex salts: from dilute particle dispersions to concentrated phases and applications" não infringem os dispositivos da Lei nº 9.610/98, nem o direito autoral de qualquer editora.

Campinas, 23 de outubro de 2018.

Autor R.G. nº 5318419 SPTC/GO

Orientador RG nº 4007973219 SSP/RS